ARCTIC ACOUSTIC WORKSHOP PROCEEDINGS

14-15 FEBRUARY

19991227 076

REPORT DOCUMENTATION PAGE

Form Approved
OMB No. 0704-0188

1a. REPORT SECURITY CLASSIFICATION UNCLASSIFIED	1b. RESTRICTIVE MARKINGS NONE
2a. SECURITY CLASSIFICATION AUTHORITY	3. DISTRIBUTION/AVAILABILITY OF REPORT Approved for Public Release; Distribution Unlimited
2b. DECLASSIFICATION/DOWNGRADING SCHEDULE	

4. PERFORMING ORGANIZATION REPORT NUMBER(S) OCNR 112589 - 19	5. MONITORING ORGANIZATION REPORT NUMBER(S)

6a. NAME OF PERFORMING ORGANIZATION Office of Naval Research	6b. OFFICE SYMBOL (If applicable)	7a. NAME OF MONITORING ORGANIZATION APPLIED PHYSICS LABORATORY UNIVERSITY OF WASHINGTON
6c. ADDRESS (City, State, and ZIP Code)		7b. ADDRESS (City, State, and ZIP Code) SEATTLE, WA

8a. NAME OF FUNDING/SPONSORING ORGANIZATION Office of Naval Research	8b. OFFICE SYMBOL (If applicable)	9. PROCUREMENT INSTRUMENT IDENTIFICATION NUMBER

8c. ADDRESS (City, State, and ZIP Code) Code 1125AR 800 N. Quincy Street Arlington, VA 22217	10. SOURCE OF FUNDING NUMBERS			
	PROGRAM ELEMENT NO. 61153N	PROJECT NO.	TASK NO	WORK UNIT ACCESSION NO.

11. TITLE (Include Security Classification)

Arctic Acoustics Workshop Proceedings, 14-15 Feb 1989

12. PERSONAL AUTHOR(S)
Edited by Robert Obrochta, Code 1125AR

13a. TYPE OF REPORT Wksh. Proceedings	13b. TIME COVERED FROM 1985 TO 1989	14. DATE OF REPORT (Year, Month, Day) June, 1989	15. PAGE COUNT 202

16 SUPPLEMENTARY NOTATION

17. COSATI CODES			18 SUBJECT TERMS (Continue on reverse if necessary and identify by block number)
FIELD	GROUP	SUB-GROUP	(U) Arctic Acoustics, (U) Arctic Acoustic Research (U) Arctic Research Accomplishments

19 ABSTRACT (Continue on reverse if necessary and identify by block number)

This report contains summaries of presentations made at the Arctic Acoustic Workshop held at MIT 14-15 Feb 1989. It also contains a few relevant papers and sets of viewgraphs from previously made technical presentations. The editor has written and included a scientific issues paper and an Arctic research plan .

20 DISTRIBUTION/AVAILABILITY OF ABSTRACT ☐ UNCLASSIFIED/UNLIMITED ☒ SAME AS RPT. ☐ DTIC USERS	21. ABSTRACT SECURITY CLASSIFICATION UNCLASSIFIED	
22a. NAME OF RESPONSIBLE INDIVIDUAL Robert Obrochta, Code 1125AR	22b. TELEPHONE (Include Area Code) 202-696-4118	22c. OFFICE SYMBOL

DD Form 1473, JUN 86

Previous editions are obsolete.

S/N 0102-LF-014-6603

FOREWORD

An Arctic Acoustics Workshop was organized by the Office of Naval Research Arctic Programs group(Code 1125AR) at MIT on 14-16 February 1989. The objectives were as follows:

1. To summarize major accomplishments resulting from research efforts over the last five years.

2. To identify and prioritize scientific issues that require further research effort and to create a viable plan to address them.

3. To identify potential scientific efforts that satisfy criteria for becoming viable research option submissions.

4. To provide an interchange of information and ideas between researchers involved in acoustic scattering, propagation, and ambient noise using scale models, computermodels, theoretic models, and field data.

5. To establish a stronger linkage between management and researcher's objectives.

The workshop proceeded as scheduled in Appendix A with only two scheduled presentations being withdrawn. The presentations times scheduled for Dr. S Flatte and Dr. R. Pinkel were used by Dr. Eric Thorsos, APL-UW, to discuss the validity of surface scattering theory as a function of the conditions, i.e. grazing angle, surface kh roughness and Dr. Terry Ewart, APL-UW to present descriptions of instrumentation concepts for developing a pencil beam active 400 Hz sonar that could be deployed through the Arctic ice and steered mechanically and a high tension underwater cable x-y plotter scheme for mapping the underside of the ice.

On the third day, the participants responded to a challenge by Tom Curtin for ideas on possible science issues which could be used as research options for ONR to present for future funding. Summaries of these are included. The attendence to the workshop was limited by invitation to the list of attendees in Appendix B.

The proceedings of the workshop are organized as follows:

1. A general itemized summary of prioritized science issues.

2. Summaries of each science presentation and research issues made were prepared by the workshop sponsor, Robert Obrochta, and chopped through the original presenter.

3. A science plan that addresses the prioritized issues in a coordinated practical way as seen from the author's viewpoint is included.

Table of Contents

Prioritized Arctic Acoustic Science Issues
by Robert Obrochta ONR 1125AR

The following science issues have been prioritized in decreasing value by considering their importance to the operational U.S. Navy.

1. Acoustic Coherence- Acoustic surveillance is based upon maximizing signal-to-noise ratios via higher gain arrays. Knowledge of single path coherence versus frequency is fundamental in establishing array size, shape, and tactical deployment. Single path coherence is dependent on the temporal/spatial 3-D sound velocity structure, the geometric characteristics of the top/bottom boundaries, and the visco-elastic properties of the boundaries. In other words, a propagation model with real ocean and boundary conditions treated correctly(fully elastic) is required to support the understanding and full utilization of acoustic coherence.

2. Ambient Acoustic Noise Characteristics and Causes- Knowledge and predictability of spatial/temporal occurrences and variations, and the characteristics of individual events are extremely important. Acoustic system design and signal processing are based upon an understanding of the ambient noise characteristics with performance being degraded by ambient noise increases in amplitude and spatial and temporal coherence. The scientific goal is to predict ambient noise characteristics accurately from knowledge of forcing functions, i.e. wind, water currents, Coreolis forces, inertial forces, tidal motion and heat flux, which produce ice canopy motion, stress buildup, deformation, ice cracking and floe breakup, and acoustic radiation into both the ice floes and the water.

3. Acoustic/ice Interaction with Known Ice Morphology- This issue is a subset of both 1 & 2 and is highlighted separately because it is totally unique to the Arctic Ocean. Operationally, the ice is known to be the cause of high attenuation of acoustic signals above 30 Hz and a major reverberant boundary at higher frequencies. Scientifically, the ice is a complex visco-elastic rough flawed congregation of irregularly sized plates. In order to understand acoustic/ice interaction, it is necessary to know what the effects of ice thickness, plate size and shape, underice roughness, cracks, and variations in ice material properties do to acoustic scattering, energy coupling, mode conversion, atttenuation, and reradiation. This knowledge is required to properly address forward propagation, reverberation, and discrimination between ice keels and submarines.

4. Acoustic Bottom Interaction- This issue is also a subset of 1 & 2 and is important in water depths less than 1000 meters. Operationally, this subject is of high interest due to the geographic occurrence of shallow water between the USSR and the Central Arctic basins. Scientifically, bottom interaction in the Arctic, i.e. Barents Sea, presents different problems than the temperate shallow water areas,i.e. the existance of permafrost, frozen gas hydrates, extremely heterogeneous glacial morraine deposits, salt diapirs, and ice gouging of sediments are all probable depending on location and past history. The scientific acoustic issue is to quantify the effects of these anomalous conditions, including bottom roughness, such that operational systems and tactics can minimize adverse effects since it is impractical to survey the bottom/sub-bottom geoacoustics properties over the vast shallow water regions of the Arctic. This quantification may aid the transformation of already available geological information into geoacoustic information that improves shallow water modeling predictions. It should also be noted that scientifically, sedimentation processes now occurring provide no useful knowledge relative to

underlying glacial sediment distribution or rough boundary conditions.

5. ULF/VLF Noise in the Arctic- This issue has more scientific value at the present than operational value since target signatures at ULF can be poorly quantified at best. However, the Arctic offers an ideal laboratory to reduce the number of mechanisms thought to produce the noise,i.e. wave/wave interaction, and surf pounding. The ice canopy decouples atmospheric systems from the water eliminating waves and surf while still allowing the differential pressure. Measurements of ULF noise should produce correlations with conditions that provide new insight into cause mechanisms.

6. Arctic Oceanography- The research issues in oceanography that couple directly to acoustic research are the 3-D sound velocity field, its fluctuations, i.e. internal waves, eddies, tidal depth changes, and strong boundary currents. The Central Arctic is thought to be the most stable 3-d sound velocity region in the world due to the presence of ice continually keeping the surface at the same temperature and decoupling the winds from the water. Upper ocean mixing is done primarily by ice keels during high wind events that set the ice canopy in motion. This mixes the upper water column above the strong thermocline/halocline
(upper 50 meters). Internal waves are a factor of 10 smaller than temperate oceans. In the marginal ice zone where ice/open water processes combine, the picture is extemely compicated with upwelling, boundary currents, eddies, and much deeper mixing. In the MIZ, it unclear how to obtain sufficient oceanographic sampling to resolve the dynamics and delineate the fluctuating sound velocity unless one resorts to high density acoustic tomography transceiver deployment and inverts the data collected. In the shallow water, Barents Sea, very little is known about the water column sound velocity or oceanographic properties. It is complicated by bottom interaction, warm and cold water (also fresh and salt water) mixing, brine rejection from rapidly freezing open water, and diurnal tidal current actions. This region is just as difficult to measure oceanographically as the MIZ and possible more difficult to model due to the stronger coupling of the forcing functions.

CEAREX ACOUSTIC CAMP PLANS
Presented by: Dr. Art Baggeroer, MIT

In mid-March 1989, two Arctic ice camps will be established north of FRAM STRAIT. An Oceanographic camp will be located at 84.0 deg.N 25.0 deg.E and an Acoustics camp at 82.7 deg.N 07.0 deg.E. The acoustic research issues that will be addressed are: (1) Acoustic Coherence, (2) Ambient Noise, (3) Acoustic Back-scattering, (4) and Greenland Sea Project Tomography.

The acoustic coherence effort is a continuation of previous work done in Fram II and IV which showed that single path acoustic coherence was spatially longer than the arrays being used to measure it, i.e. 2000 meters horizontal and temporally longer than 30 minutes. The temporal/spatial coherence of acoustic signals and noise determine effective array sizes, shapes, and integration time. When coupled with propagation loss information and ambient noise characteristics, optimal frequencies and signal processing to use in various environmental conditions to produce maximum detection ranges can be determined.

The spatial layout of the Oceanography and Acoustics camp with all of the supporting ARGOS drifters , ARAMPS buoys, 30 km horizontal array, and oceanography stations is shown in Figure 1. Figures 2-4 show an aerial view of the 30 km hydophone array, a top view of the crossed hardwired 2X2 km center portion of the 30 km array with connected x-x showing the location of vertical arrays, and side view showing hydrophone locations of the vertical arrays with respect to the hardwired horizontal array.

Temporal coherence will be examined by projecting a line spectrum of tonal signals from a periodic airgun source located at the O-Camp. This will measure the temporal coherence across frequency, i.e. the two frequency correlation function, as well as the Doppler spread of individual tones. Signals will be transmitted for three day durations in order to include tidal and inertial scales in the fluctuations.

The low frequency spatial coherence will be measured across the 30 km aperture using the STS(sensor tracking system) for positioning the sensor locations. The STS uses active acoustic pingers 8-13 KHz distributed spatially to give good range-range localization of + or - 2m. The acoustic source for the spatial coherence will be the airgun at the O-Camp operated during 11-24 April, 1989.

Environmental correlates of coherence will be achieved by installing three oceanography stations equally spaced between the O-Camp and the A-Camp. Each station will have a thermistor string and current meter. This will be supplemented with CTD lines between the two camps at the beginning and end of the experiment. The objective is to correlate the spectral variability of the oceanographic measurements with the temporal and spatial spreading observed at the receiving array.

The second major research issue is acoustic ambient noise. Two scales of ambient noise processes will be investigated. Mesoscale variability of the noise will be observed along the path between the two ice camps and in a region of 100 to 200 km from the A-Camp. This will be done using five ARAMP(Arctic Remote Autonomous Measurement Platform) buoys which will record ambient noise, environmental processes , and position. The objective is to correlate the ambient noise with the environmental forcing including the mesoscale stress of the ice dynamics.

1

This will be done using meteorological observations, current meter data at two depths and three component accelerometers. The ARAMP positions will be supplemented by 10 ARGOS position drifters and the ice dynamics observations supplemented by remote sensing sythetic aperture radar flights. Microscale process phenomena will be observed using the 30 km array. This will include compiling event statistics, classification, and localization as well as continuous spectral observations. These will be correlated with the local environmental stresses including meteorological, current meter, and precise ice dynamics obserced at the A-Camp as well as remote sensing observation over the array.

Events and spectra in the ULF/VLF bands will be recorded on both hydrophones and geophones . The propagation effects in these bands will be removed using the CTD data and ice observations to determine the effective source level of noise in this low frequency regime during different periods of environmental stress.
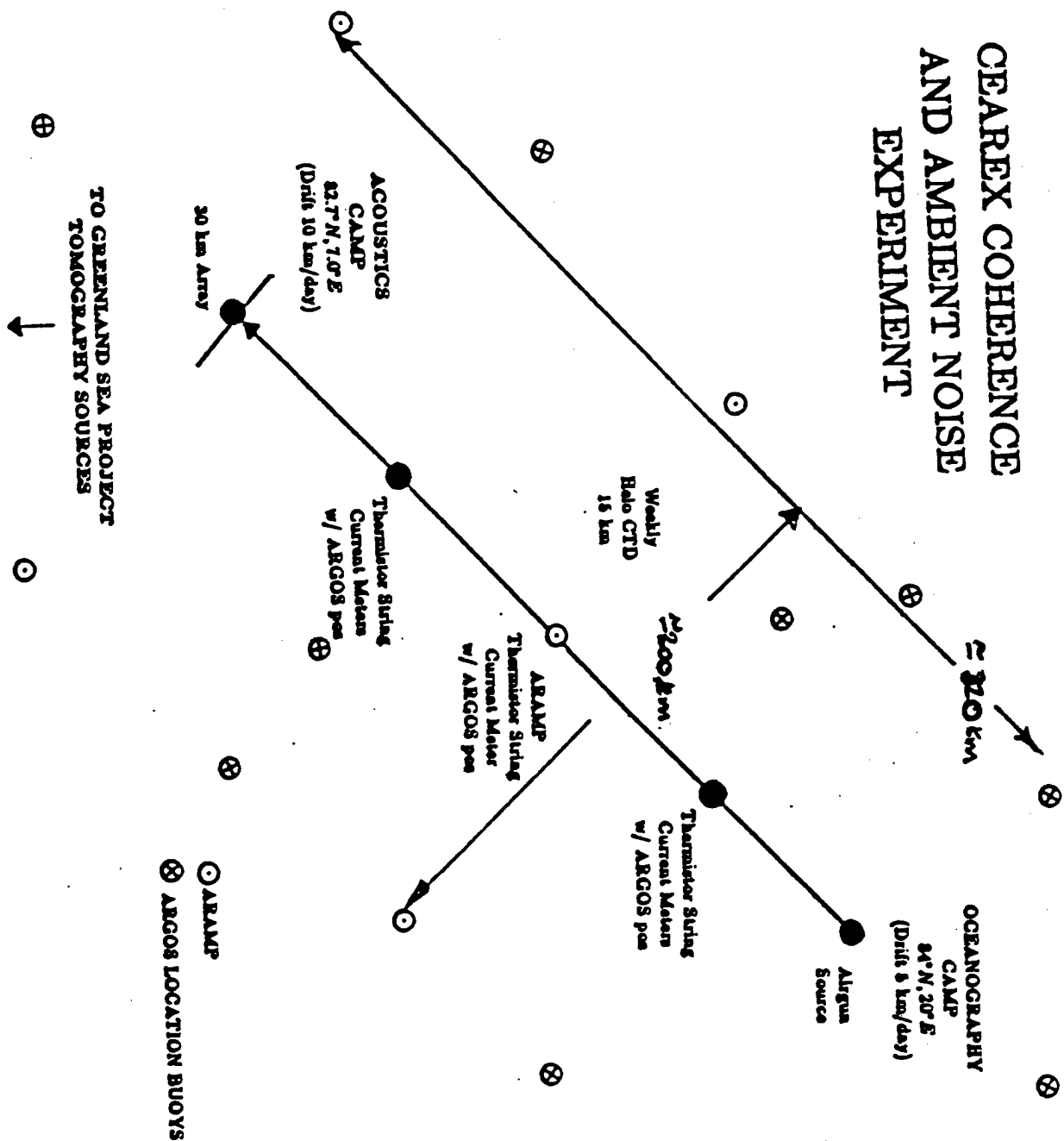
The third major objective at the A-Camp is to acquire high resolution acoustic backscatter information from both the ice/water and the water/bottom interfaces. The airgun will be colocated with the long vertical array from 22 MAR- 9 APR 1989 for this purpose. The data collected on the vertical arrays will be used to determine the backscattering that returns from ice and bottom features as a function of both angle and frequency. The temporal stability will be monitored over the duration of the experiment.More details of this effort are described in the presentation summary entitled " NRL CEAREX Plans", pages 7-9. At least one seismic refraction line with large explosives i.e. 20 kg or more per shot, will be shot towards the A-Camp to identify the sound speed vs. depth profile and tectonic structure at the base of the Yermak Plateau. Bottom interacting explosions will be shot to the horizontal and vertical arrays to determine the sediment profile and the partitioning of energy propagating through the the seabed.

The operational value of the reverberation effort is to determine the characteristics and repeatability of reverberation responses such that signal processing techniques can produce improvements in signal to reverberation ratios. In most cases where operation sonars are in the vicinity of rough elastic boundaries, active sonars are reverbation limited.

The fourth research issue is the Greenland Sea tomography measurements. These measurements will provide a measure of the arrival structure of the acoustic signals transmitted from the Greenland Sea, the signal path stability versus time, the energy partitioning into the paths received, thus quantifying the variability possible and potentially some relationships with oceanographic causes.

The CEAREX A-Camp experiment has now been completed . Accomplishments that were actually achieved will be summarized and published by October, 1989.

CEAREX COHERENCE
AND AMBIENT NOISE
EXPERIMENT

ACOUSTICS
CAMP
82.7°N, 7.0°E
(Drift 10 km/day)

30 km Array

TO GREENLAND SEA PROJECT
TOMOGRAPHY SOURCES

Weekly
Halo CTD
16 km

Thermistor String
Current Meters
w/ ARGOS pos

ARAMP
Thermistor String
Current Meters
w/ ARGOS pos

Thermistor String
Current Meters
w/ ARGOS pos

Airgun
Source

OCEANOGRAPHY
CAMP
84°N, 20°E
(Drift 8 km/day)

≈ 200 km.

≈ 110 km

⊙ ARAMP
⊗ ARGOS LOCATION BUOYS

3

30 km APERTURE FOR DRIFTING & VERTICAL ARRAYS

U VERTICAL ARRAY
● DRIFTING RECEIVER
T TRACKING RECEIVER

2 km CENTRAL ICE FLOE

±1km CROSS WIRED ARRAY

≃ 30 km
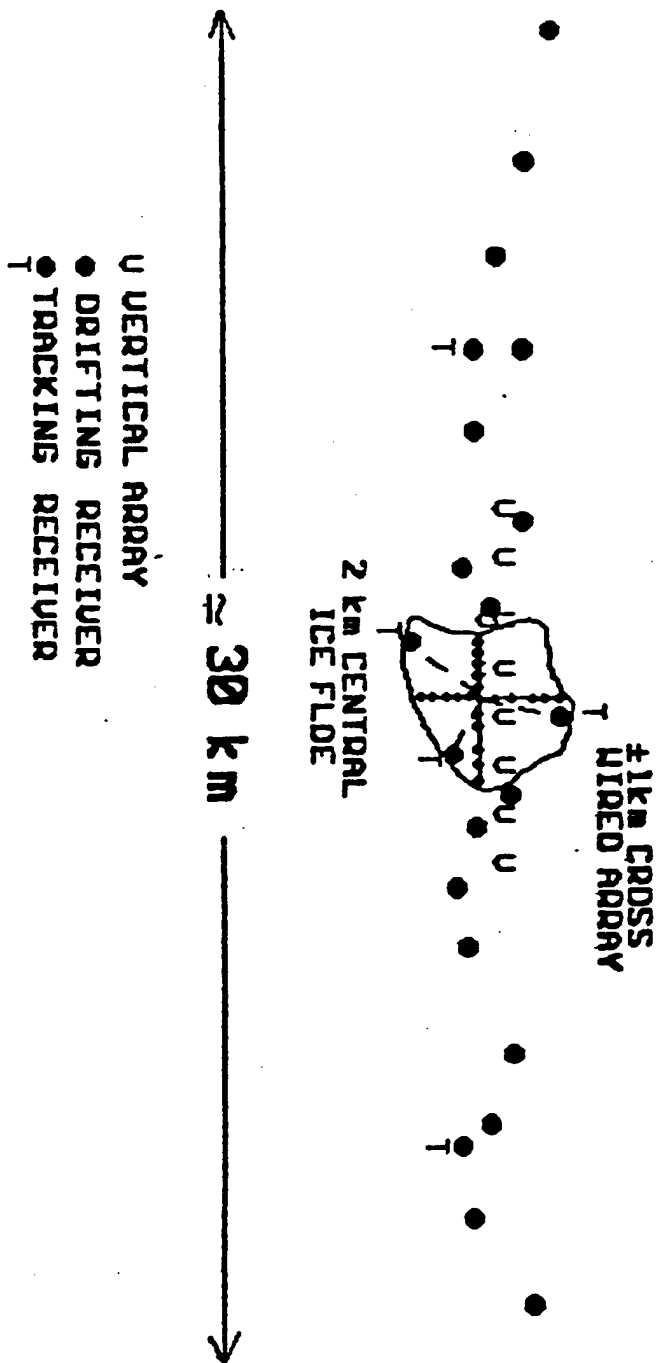
D.B.

CEAREX 89
ACOUSTIC ARRAYS
TOP VIEW
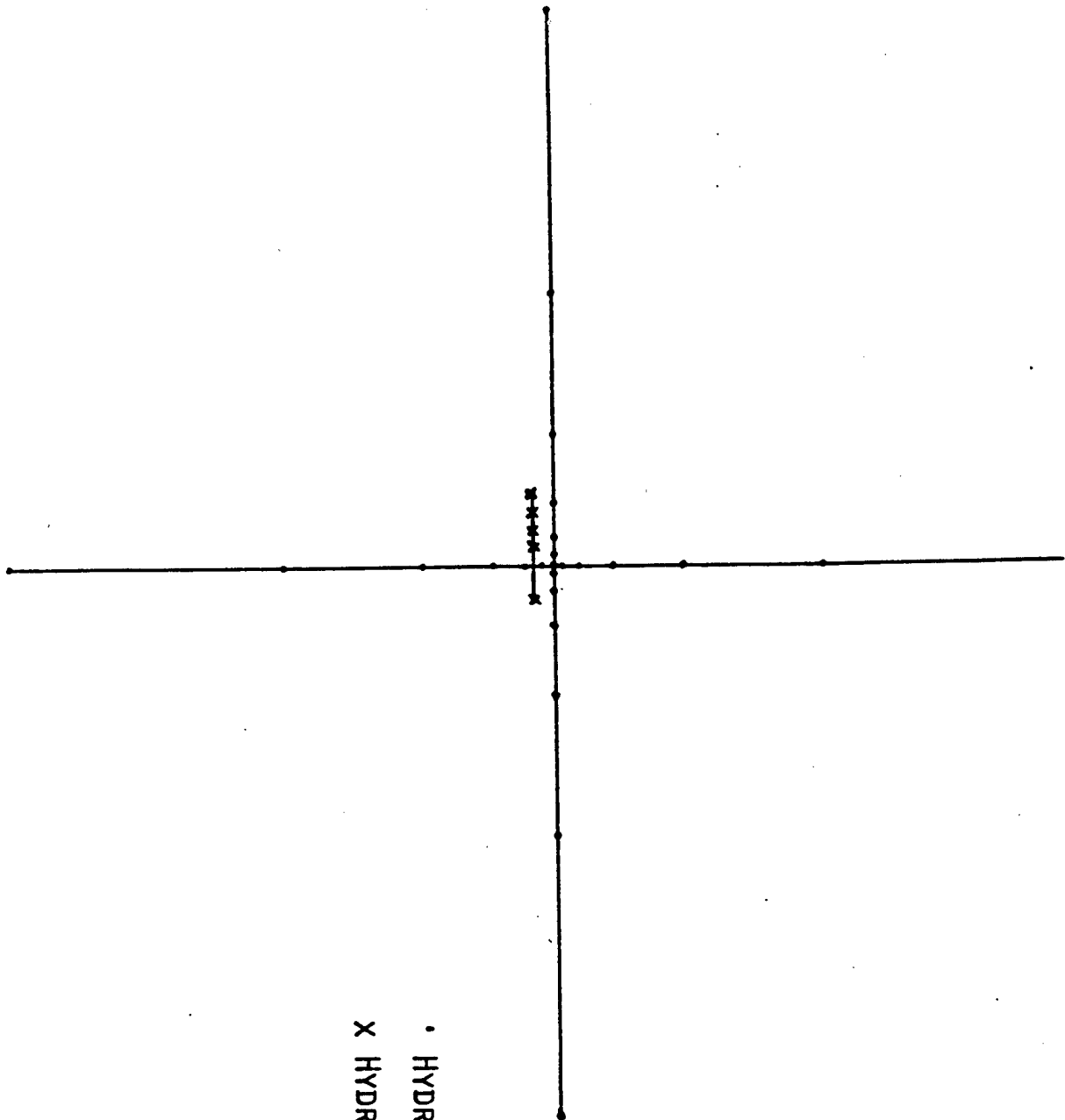
• HYDROPHONE
X HYDROPHONE ARRAY

5

CEAREX 89
ACOUSTIC ARRAYS
SIDE VIEW

NRL Research and CEAREX Plans
Presented by T. C. Yang

This presentation describes NRL's research objectives, key technical issues, experimental design, measurement methodology, remaining issues, and analytical approach in the characterization of low-frequency under-ice scattering and reverberation in an Arctic environment.

The NRL objectives are: (1) To conduct measurements of low-frequency (5 to 50 Hz) under-ice forward scattering and backscattering in both mono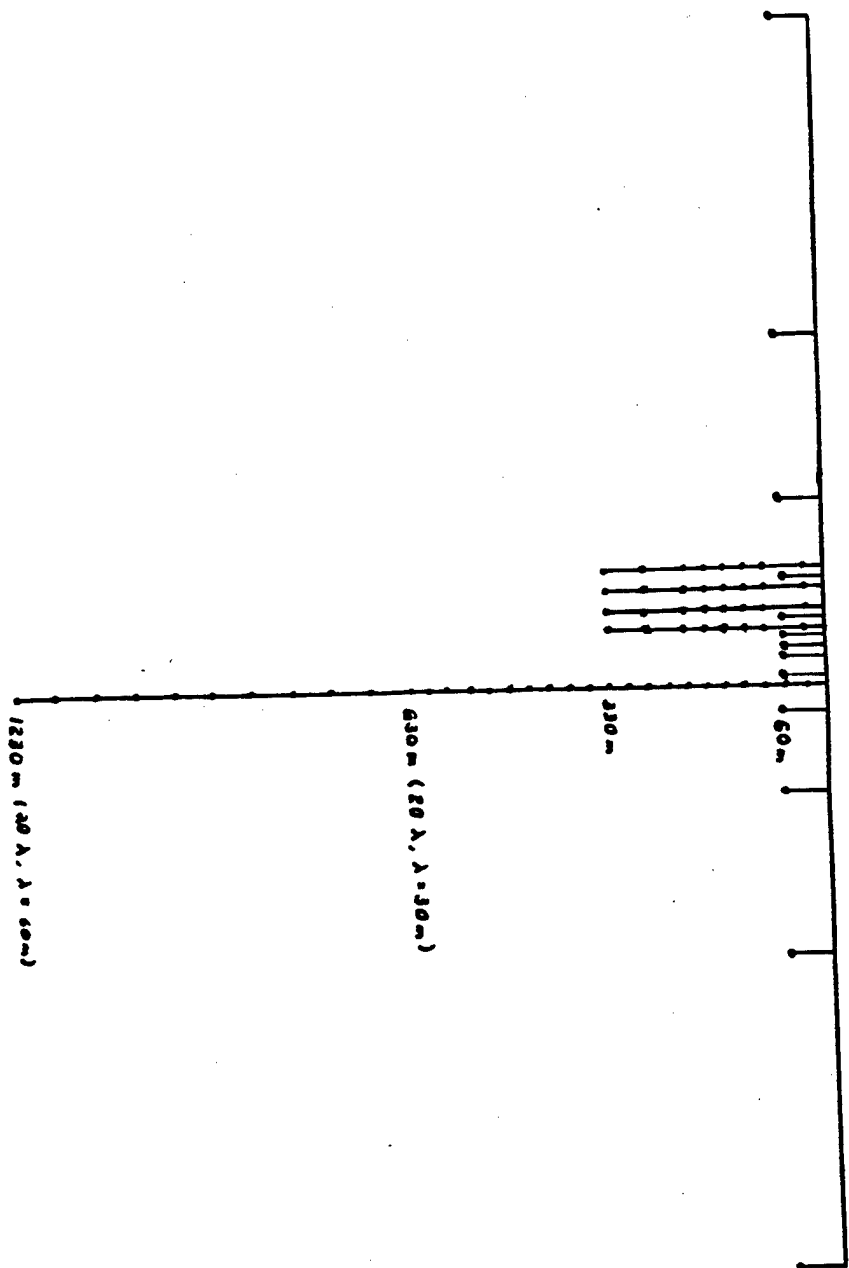static and bistatic modes; (2) to characterize the time-azimuth decay of measured reverberation in an Arctic environment; and (3) to apply advanced signal processing (e.g., matched-field/matched-mode processing) techniques to separate the surface and bottom components of the reverbera- tion, estimate the depth of scatterers, and measure the scattering strength of both ice and bottom as a function of frequency and of vertical and azimuthal angles.

Present data on scattering strengths at low frequencies are very limited. Previous results from MIT indicate that the bottom is the dominant scatterer at very low frequencies (approximately 7 Hz). At higher frequencies (50 Hz and above), the ice dominates the reverberation return. At intermediate frequencies (10-50 Hz), returns from under-ice features such as the larger ice keels and ice islands could be significant and need to be measured.

A key technical issue to be investigated in this research is, "What is the frequency and angular dependence (the re-radiation pattern) of under-ice scattering?" The angular and frequency dependencies of ice and bottom scattering are needed for the characterization and prediction of under-ice propagation and reverberation.

A second key issue is the depth discrimination of long-range scatterers. Because of the upward-refracting sound-speed profile in an Arctic environment, surface reverberation levels can be comparable to bottom reverberation levels at all ranges (in contrast to the case of a deep sound channel environment), so that advanced processing techniques are required to discriminate surface and bottom reverberation.

In the CEAREX 89 experiment, acoustic sources include 2- to 40-lb explosives at ranges up to 150 km and a 2000-psi air gun both in camp and at a range of 250 km. Sensor arrays include one NRL 1230-m and four 330-m vertical arrays, the MIT 2x2-km cross horizontal array, an NRL 11-element telemetered geophone array approximately 20 km long, and an MIT telemetered hydrophone array approximately 30 km long. Results of matched-field simulations have been considered along with practical

constraints to arrive at a configuration for the combined cross and
multi-vertical array that provides simultaneous vertical and 360-deg
azimuthal resolution of the monostatic reverberation measurements as
well as a higher-resolution capability for measuring the vertical/azimuth
distribution of forward-scattered energy. The array elements are
localized using a 16-kHz pinger for the vertical arrays and five 8-13 kHz
pingers for the horizontal hydrophone and geophone arrays.

During bistatic measurements, the air gun will be located at the
CEAREX O-Camp nominally 250 km from the A-Camp arrays. Supplementing the
air gun, explosives will be dropped in a series of runs from the A-Camp.
The charges will vary in size from 2 to 40 lbs of TNT. Requirements for a
successful experiment include proper gain settings to avoid overload,
monitoring of hydrophone positions, and a sufficiently low ambient noise
level to permit the recording of reverberation. On the basis of previous
reverberation experiments, the maximum permissible noise level has been
set at 86 dB//uPa**2/Hz @ 20 Hz.

An issue currently under study is the question of how to achieve
the depth resolution necessary to resolve surface features at low
frequencies. To improve depth resolution, a high-resolution modal-
beamforming technique based on the minimum-variance (MV) principle
has been developed. The MV beamformer has been shown in simulations to
improve resolution significantly over conventional modal beamforming for
high signal-to-noise ratios. For low signal-to-noise ratios, depth
resolution approximates that of the conventional modal beamformer.
Results of the matched field/matched mode studies are documented in two
papers by Dr. T. C. Yang: "Modal Shading Coefficients for High-Resolution
Source Depth Localization" and "Effectiveness of Mode Filtering: A
Comparison of Matched-Field and Matched-Mode Processing".

A further requirement is the development of wave-theoretic
descriptions of scattering and reverberation appropriate for the
frequencies (5 to 50 Hz) of interest in this research. A coupled-mode
description extending the formulation of Boyles is under development and
will include the representation of scattering functions in the basis of
local modes, providing the description of forward and backward propagation
and scattering necessary both for the simulation/prediction of rever-
beration and for the extraction of scattering functions from the measured
CEAREX data.

The processing methods currently being investigated include:
(1) a method combining modeling results with matched-field and/or matched-
mode processing and short-time spectral analysis of reverberation time
histories; and (2) an alternative method based on applying control-
theoretic techniques to the coupled-mode equations. These methods will be
developed and applied to the estimation of backscattering strengths from
reverberation data. An additional outcome of the development of these
processing techniques will be a potential method to map bottom contours and
sea ice ridge parameters over vast areas.

SOURCES

- 2 - 40 lb TNT Explosions at ranges up to 150 km
- Air Gun (2000 psi) in camp and 250 Km away

SENSOR ARRAYS

- NRL Vertical Arrays: 1 1230 m Long and 4 330 m Long
- MIT Cross (2 Km x 2 Km) Horizontal Array
- NRL Telemetered Geophone Array (~20 Km)
- MIT Telemetered Hydrophone Array (~32 Km)

Data Recording

High Rate Recording (0 - 1.2 KHz)
- Long Vertical Array (32 Channels)
Low Rate Recording (0 - 100 Hz)
- Short Vertical Arrays (32 Channels)
  MIT Cross Array (25 Channels)
  MIT Telemetered Hydrophone Array (15 Channels)
  NRL Telemetered Geophone Array (11 Channels)

Fundamental Arctic Acoustics Ultrasonic Modeling Studies
Presented by Jacques R. Chamuel/Sonoquest

The presentation started with a short summary of past scaled ultrasonic modeling studies on (1) the effect of topography on Rayleigh and Scholte wave propagation and attenuation; examples from Nevada, Tibet, and the Canadian Arctic were demonstrated. (2) waveguide properties using an air-suspended water layer to isolate acoustic from seismic phenomena in presence of scatterers or boundary roughness. After this background review, a long series of viewgraphs on seismo-acoustic wave phenomena beyond the current state-of-the-art of theoretical analysis were explained utilizing laboratory results obtained under controlled conditions. The following 31 figures highlight the new ultrasonic modeling findings (previously presented at the Acoustical Society of America Meetings as referenced). The figures are nearly self-explanatory. These ultrasonic modeling results illustrate the importance of cracks, keels, floe edges and thickness on seismo-acoustic waves. The results provide a good basis for both theorists and experimentalists to follow when addressing the difficult Arctic ice canopy problem. The research succeeded in demonstrating the existence of several hidden fundamental seismo-acoustic wave phenomena and provided physical insight into Arctic acoustics. The research is jointly sponsored by DREP and ONR. Numerical computer analysis support provided by Dr. Gary H. Brooke/DREP was acknowledged.
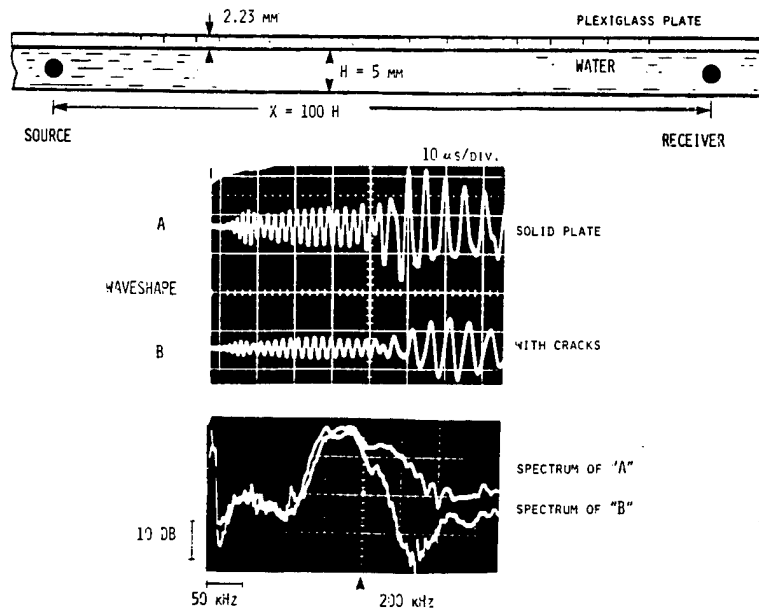
FIG. 1. Attenuation of low frequency acoustic waves in
a shallow water waveguide by cracks in floating
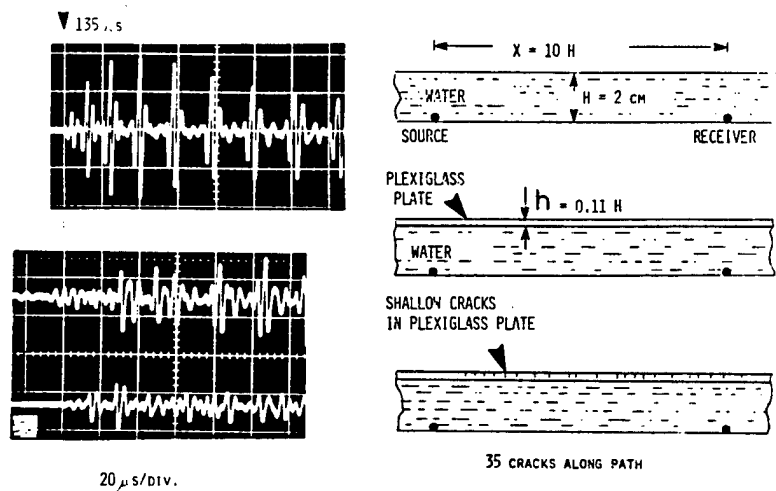plate. (J. Acoust. Soc. Am. 80,S1,S115,BBB6,1986).

FIG. 2. Effects of floating plate on water waveguide waves.
Top: air/water/air "perfect" waveguide. Middle:
Solid plate in contact with water. Bottom: cracked
plate in contact with water. (JASA 80,S1,S115,BBB6,1986).

FIG. 3 area labels:

7 CM

A B

S/R

PLEXI PLATE
2 45mm

H = 3 cm
X = 88.5 cm

B > A

200 μs

A B
EDGES
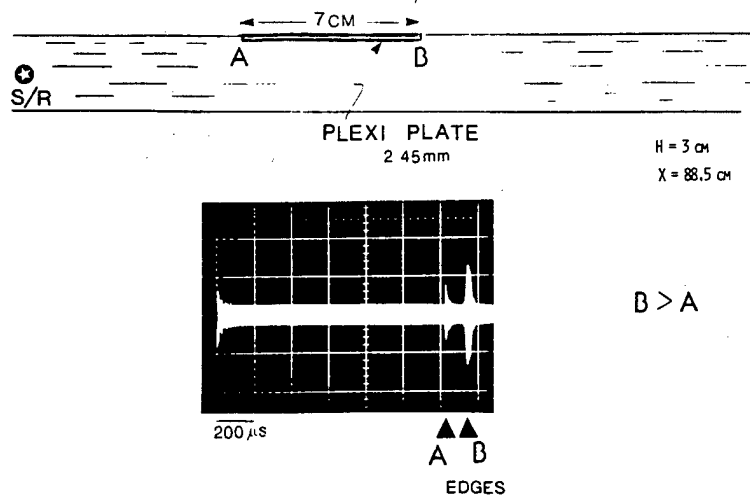
FIG. 3. Relative backscatter from edges of floating plate. Notice dominant backscatter from lagging edge "B". (J. Acoust. Soc. Am.82,S1,S31,M17,1987).

SOURCE/RECEIVER

A B AIR

H = 3 CM h = 2.41 MM — WATER

X = 90 CM W = 7 CM AIR

BROADBAND
SINGLE PULSE

WAVESHAPE

SPECTRUM OF **B**

A B

f

20 μs

10 DB

$t_A = \dfrac{2X}{C_W} = 1.2$ ms

$t_B = \dfrac{2(X+W)}{C_W}$

250 300 350 KHz

RINGING ASSOCIATED WITH ACOUSTIC WAVE TRAVELING WITH C_W IN PLATE AND IN WATER

$C_W = 1480$ M/s
$C_P = 2540$ M/s
$C_S = 1360$ M/s

ARBITRARY

h_1 h_2 h_3

10 DB

0 50 100 150 200 250 300 350 KHz

		f MEAS.	$f = \dfrac{C_S}{2h}$ CALC.
h mm	h_1 5.74	115	118 KHz
	h_2 2.84	242	239.4 KHz
	h_3 2.41	282	282 KHz

PLEXIGLASS
$C_P = 2450$ M/s
$C_S = 1360$ M/s

SPECTRA OF BACKSCATTERED WAVES FROM FLOATING PLATE EDGE "B"

A B

S/R

FIG. 4. Waveshape and spectra of backscatter from trailing edge "B" of floating plate. Notice ringing frequency decreases as plate thickness is decreased. (J. Acoust. Soc. Am. 83, S1,S47,U3,1988).
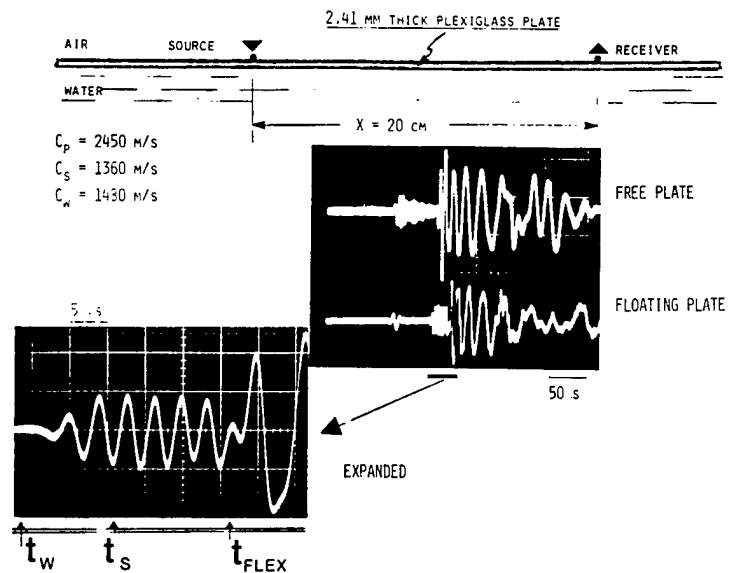
FIG. 5.   Ringing in "infinite" floating plate associated
with acoustic mode in water. (J. Acoust. Soc.
Am. 83,S1,S47,U3,1988).
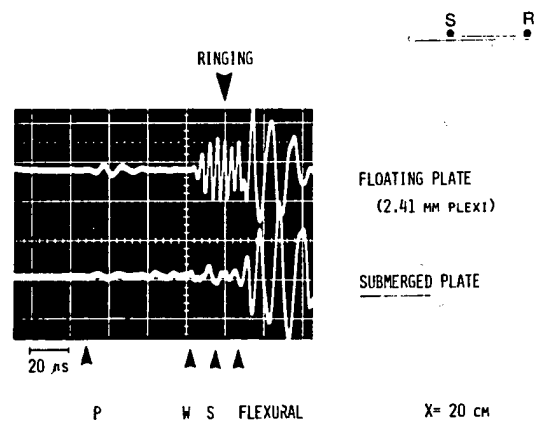
FIG. 6.   Absence of ringing associated with acoustic wave for
submerged plate case. (J. Acoust. Soc. Am. 83,S1,S47,
U3,1988).
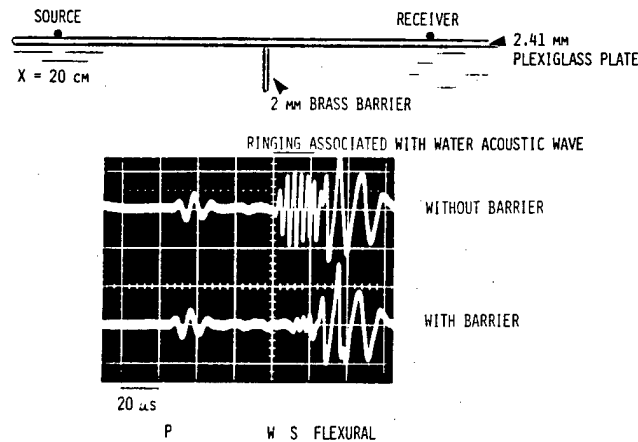
FIG. 7. Use of barrier in water to demonstrate that ringing is associated with acoustic wave in water and is not an independent shear wave in the plate. (J. Acoust. Soc. Am. 83,S1,S47,U3,1988).
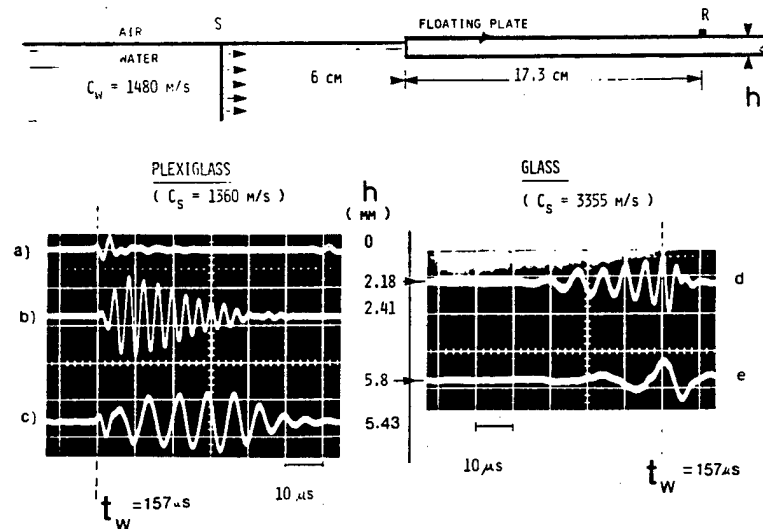
FIG. 8. Plate waves generated by underwater acoustic waves incident at grazing angle on finite plate for two cases: a) Plexiglass/water and b) glass/water. Notice ringing follows the water direct arrival for case "a". Dispersive wavetrain of case "b" ends at water wave arrival. (J. Acoust. Soc. Am. 83,S1,S47,U3,1988).
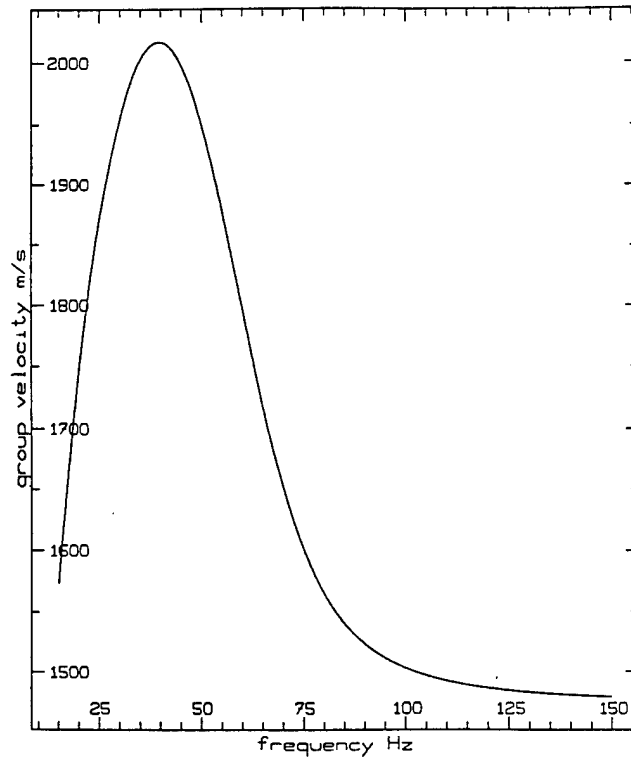
FIG. 9.   Flexural wave group velocity for floating glass plate
5.8 mm thick on water. (G.H. Brooke/DREP 1988).

Fig. 6-7. Theoretical phase- and group-velocity curves for a floating ice sheet; α = 12,400 ft/sec, β = 6,040 ft/sec, σ = 0.345 for ice, α = 4,800 ft/sec for water. (*After Crary.*)
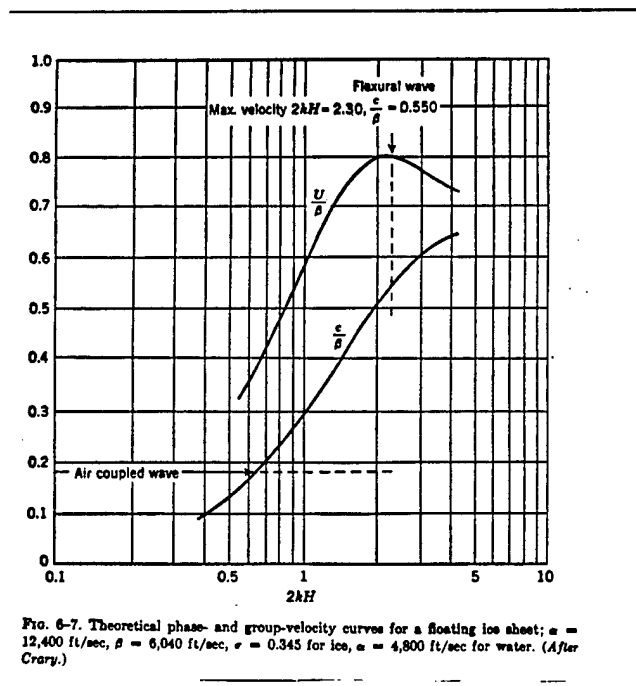
FIG. 10.   Theoretical phase and group velocity curves for a floating
ice sheet. (After Crary, from Ewing, Jardetsky, and Press,
1957, p.298). One flexural wave branch is presented.
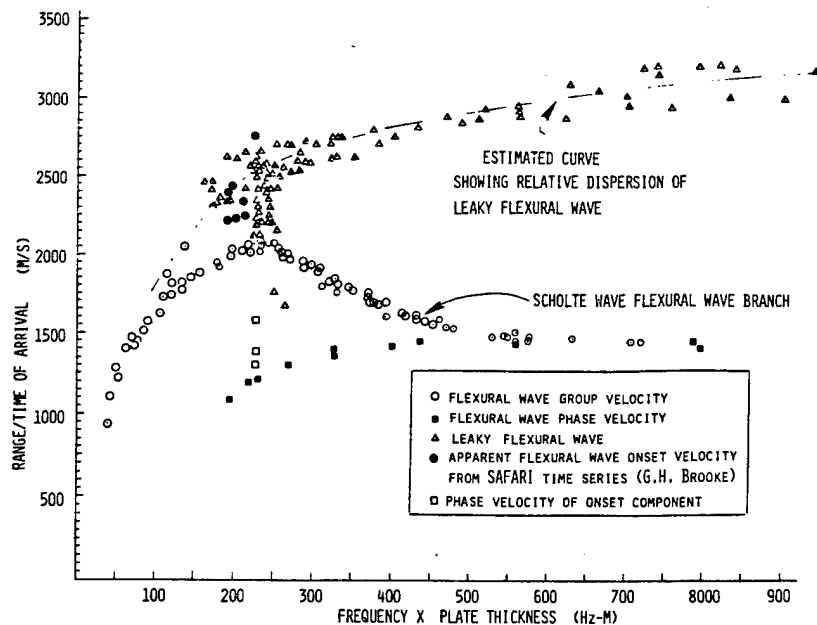
FIG. 11. Experimental ultrasonic results demonstrating existence of two flexural wave branches for floating glass plate. The top curve is the leaky flexural wave branch. (Chamuel, ONR/DREP Progress report No. Sonoquest JRC-44-88, July 1988).
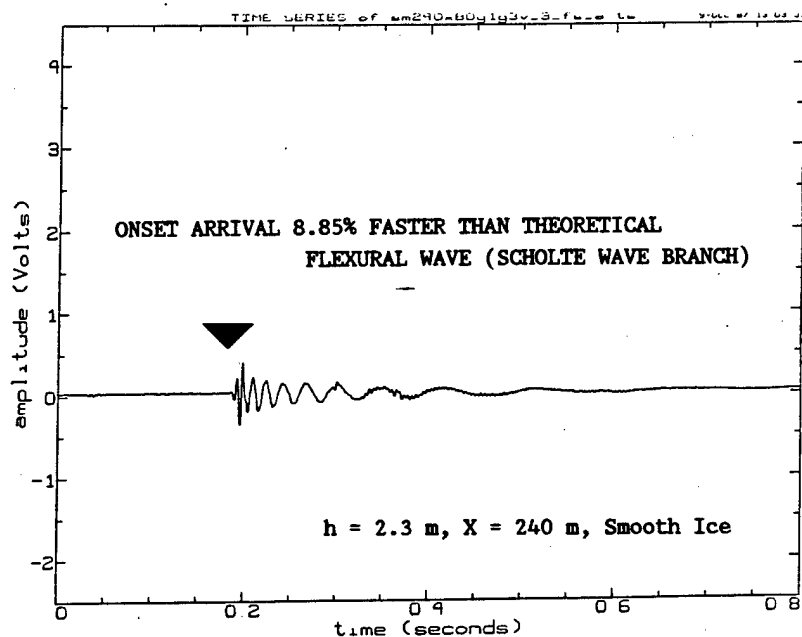
FIG. 12. Arctic field data obtained by G.H. Brooke/DREP indicating arrival of wave components ahead of flexural wave Scholte branch observed at close range.

(x = 5 cm)

20 us/DIV.   FLEXURAL WAVE

▼ DIRECT WATER WAVE

▲ FLEXURAL WAVE
CONVERTED BY TOPOGRAPHY

RECEIVER
AIR
STEEL PLATE
WATER
SOURCE
VERTICAL

SOURCE
HORIZONTAL

RIDGE IN PLATE
(SELECTED MODEL TO ENHANCE
CONVERSION TO FLEXURAL WAVE)
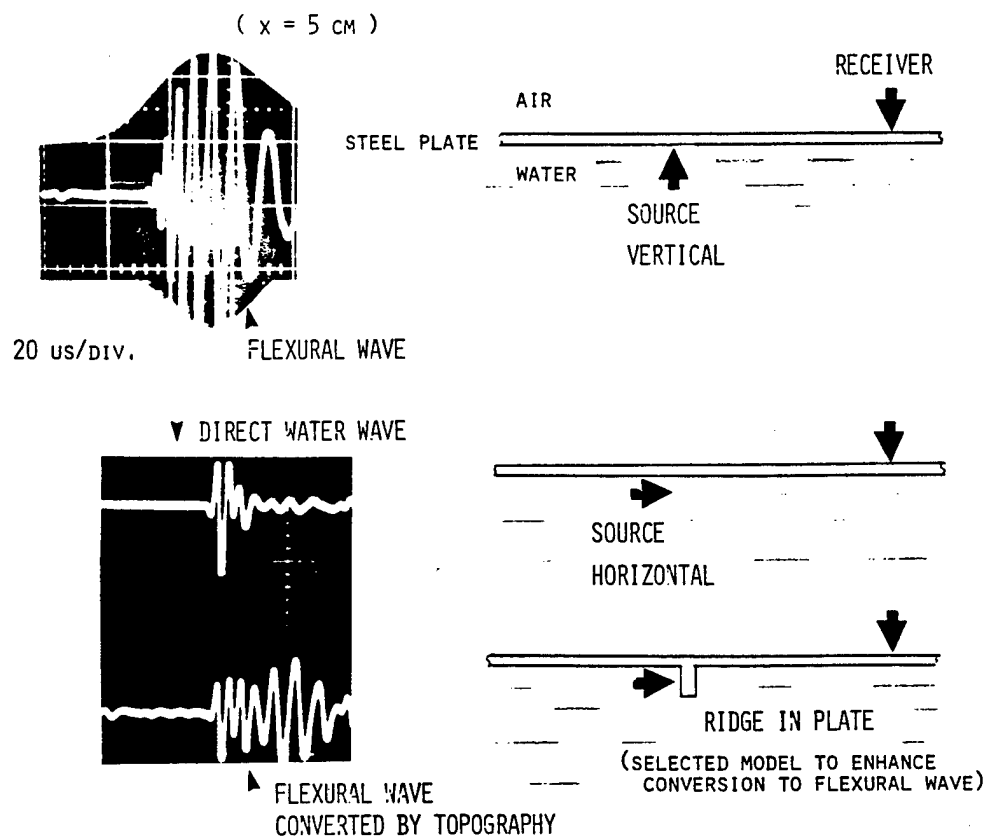
FIG. 13. Preliminary laboratory experimental results showing
effect of ridge keel on converting underwater acoustic
waves into plate waves. (J. Acoust. Soc. Am. 79,S1,S57,
Z14, Spring 1986).
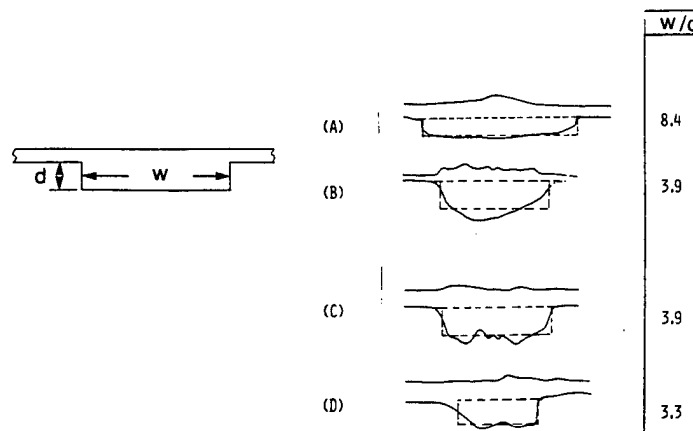
FIG. 14.   Representing ice keels with approximate rectangular
           ridges. Ridge profiles "a" and "b" by Kovaks, and
           "c" and "d" by Francois as referenced by Diachok 1976.
           (J. Acoust. Soc. Am. 82,S1,S31,M17,1987).

PARAMETERS: W = 15.28mm, h = d = 2.4 mm, H = 3 cm, X = 53.4 cm, C_p = 2650 m/s, C_w = 1500 m/s)
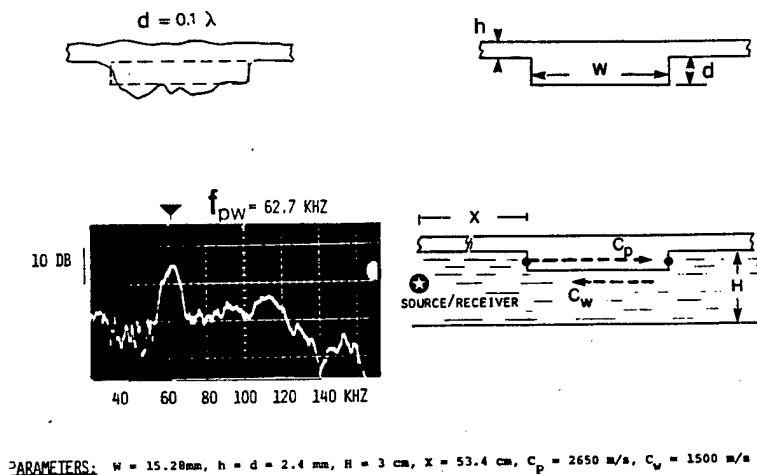
FIG. 15.   Low-frequency backscatter from ridge width resonances.
           (J. Acoust. Soc. Am. 82,S1,S31,M17,1987).

NUMBER OF RIDGES N
W   15.28mm
H - 3 cm
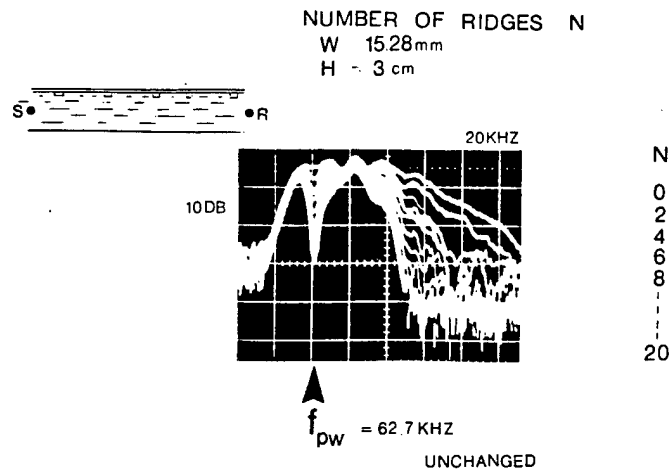
FIG. 16.   Effects of number of identical ridges along path on
           attenuating low-frequency underwater acoustic waves.
           (J. Acoust. Soc. Am.82,S1,S31,M17,1987).
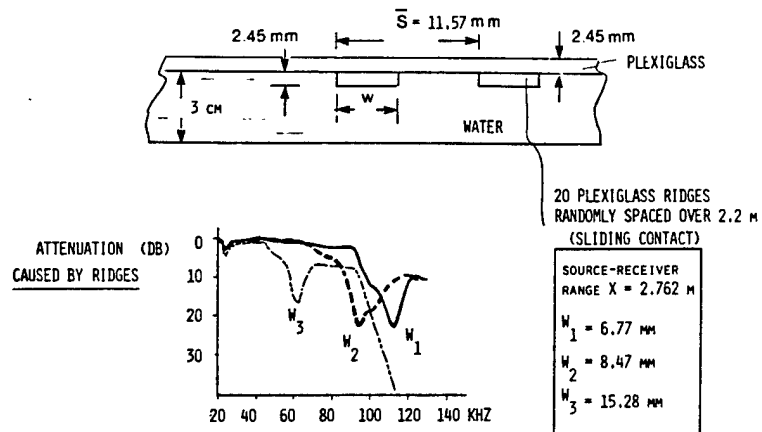
FIG. 17.   Transmission loss affected by ridge width.
           The attenuation peak shifts to lower frequencies
           as ridge width is increased. Notice all ridges are
           shallow and have the same depth. (J. Acoust. Soc. Am.
           82,S1,S31,M17,1987).

W₃ W₁

MIXTURE OF 20 RIDGES 6.77 MM WIDE AND 10 RIDGES 15.28 MM WIDE

f_1 62.68 KHZ f_3 110.78 KHZ

ATTENUATION (DB) CAUSED BY RIDGES

0
10
20
30

20 40 60 80 100 120 KHZ

$H = 3$ CM
$d = h = 2.23$ MM
$X = 2.76$ M
$\overline{S} = 7.58$ CM

$C_{WATER} = 1500$ M/s
$C_{PLEXI} = 2650$ M/s
$C_{SHEAR} = 1388$ M/s

$$f_3 = \frac{1500 \text{ KHZ}}{6.77 \times 2}$$

$$f_1 = \frac{1 \text{ KHZ}}{\frac{15.28}{1500} + \frac{15.28}{2650}}$$
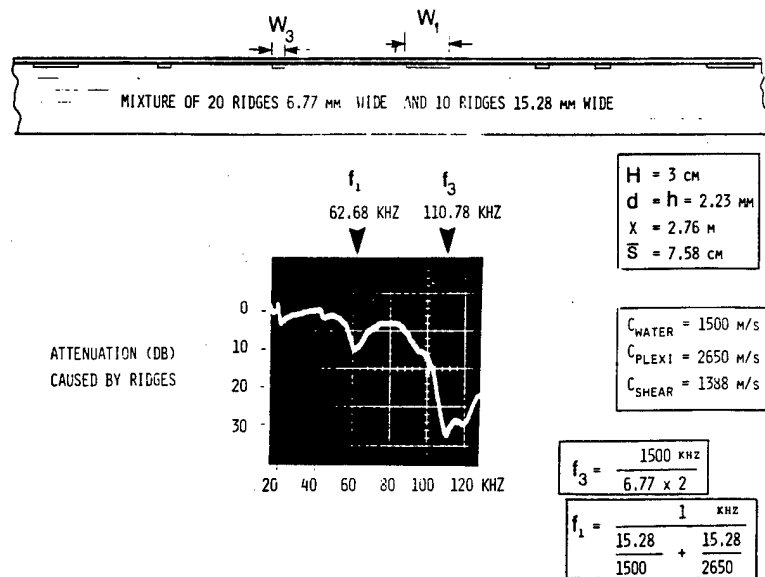
FIG. 18. Mixture of two types of ridges creating corresponding transmission loss peaks. (J. Acoust. Soc. Am.82,S1,S31, M17,1987).

PLEXI
W   SEMI-CYLINDERS

12.9 mm

5 cm

$F_0 = 100$ KHZ

10 DB

← FLAT

← 20 RIDGES

20 KHZ

77 KHZ $> \{ \begin{array}{c} \\ c_p c_w \end{array}$ → 74 KHZ
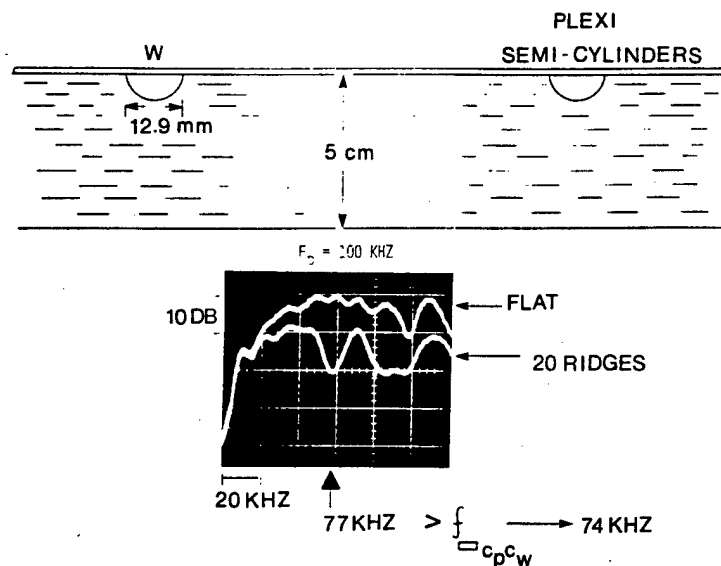
FIG. 19. Same effects observed in cylindrical ridges at a slightly higher frequency as expected. Top trace corresponds to spectrum of transmitted waves for the flat-plate boundary case. (J. Acoust. Soc. Am. 82,S1,S31,M17,1987).

W = 10mm

PLEXI

3 cm

20KHZ

X = 2.3M
N = 20 RIDGES

10DB

C_p = 2650 m/s

C_{p_L} = 2333 m/s

f_{ww} f_{pw} f_{pp}

75KHZ   133 KHZ

95.8 KHZ
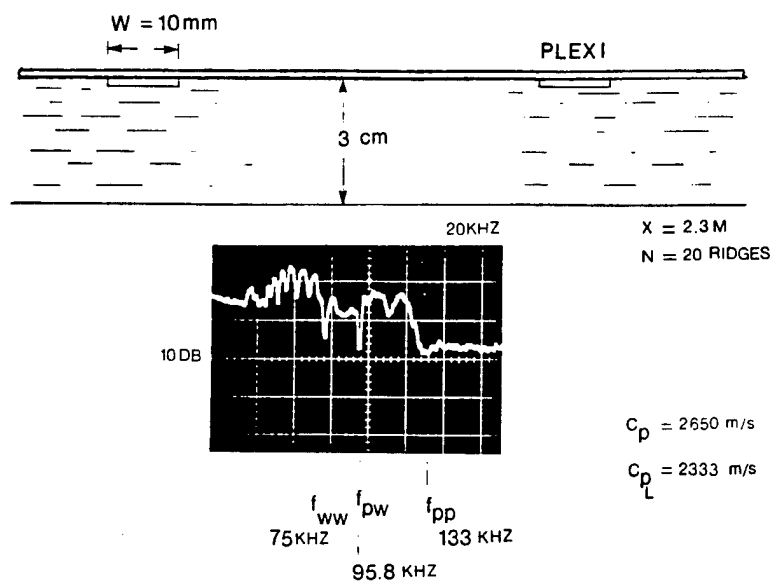
FIG. 20.   Multiple ridge width resonances observed in some
           models. (J. Acoust. Soc. Am.82,S1,S31,M17,1987).

EDGE "A"   CRACK "C"   EDGE "B"   AIR

SOURCE/RECEIVER

●——— 100 CM ———|←— 10 CM —→|←— 12 CM —→| H = 3 CM   WATER

                                                            AIR

FLOATING PLEXIGLASS PLATE
(2.45 MM THICK)

BACKSCATTER   A   C   B

CRACK ON TOP
(0.1 MM WIDE CRACK)

CRACK ON BOTTOM (DRY CRACK)

CRACK ON BOTTOM (WET CRACK)

50 μs
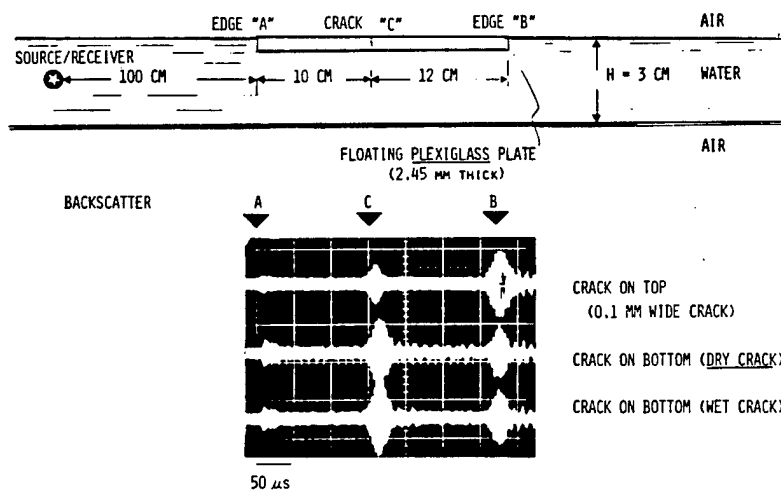
FIG. 21.   Relative backscatter from cracks and edges of
           floating plate. (J. Acoust. Soc. Am.83,S1,S47,
           U3,1988).

21
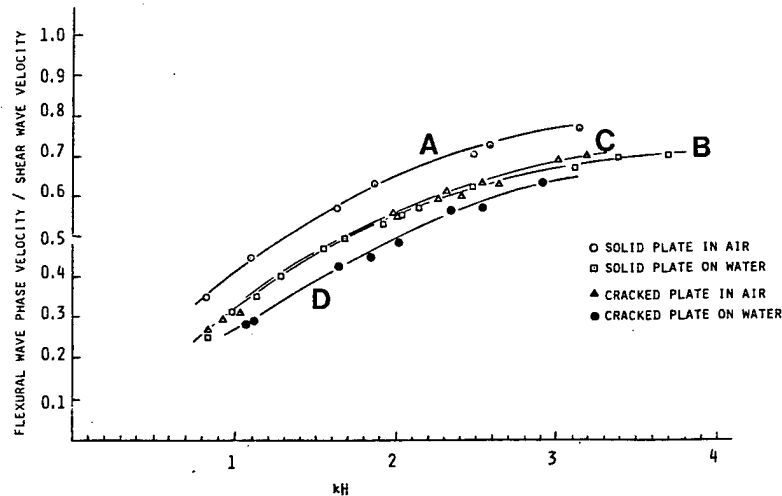
FIG. 22. Effects of water loading and shallow cracks in solid smooth plate on decreasing the flexural wave velocity. Model consists of a 2.6 mm thick plexiglass plate, average crack spacing 5mm and crack depth h/3. (J. Acoust. Soc. Am. 79,S1,S57,Z14,1986).
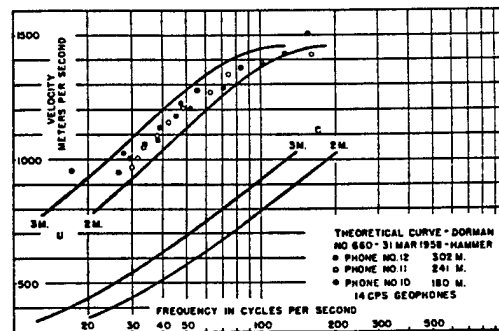
Fig. 11b. Comparison of observed and theoretical dispersion for record 660. $\alpha = 3.31$ km/sec, $\beta = 1.83$ km/sec.
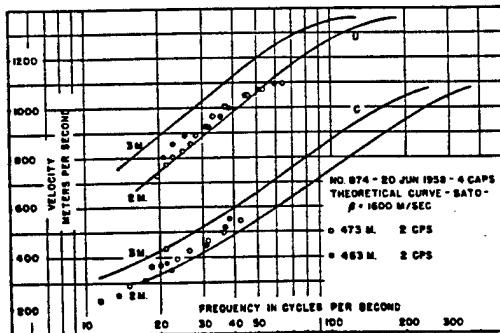
Fig. 13. Comparison of observed and theoretical dispersion for record 874, June 20, 1958.
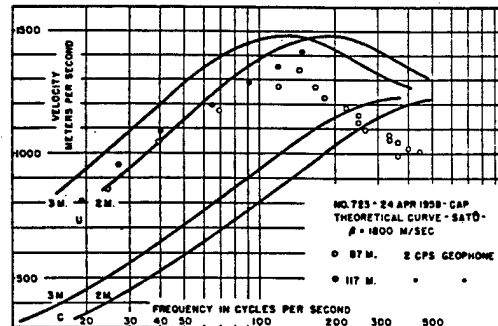
Fig. 12. Comparison of observed and theoretical dispersion for record 723, April 24, 1958.

FIG. 23. Sea ice thicknesses determined from flexural wave dispersion are generally lower than actual thicknesses. (K. Hunkins, J. Geophys. Res. 65(10)3459-3472,1960).
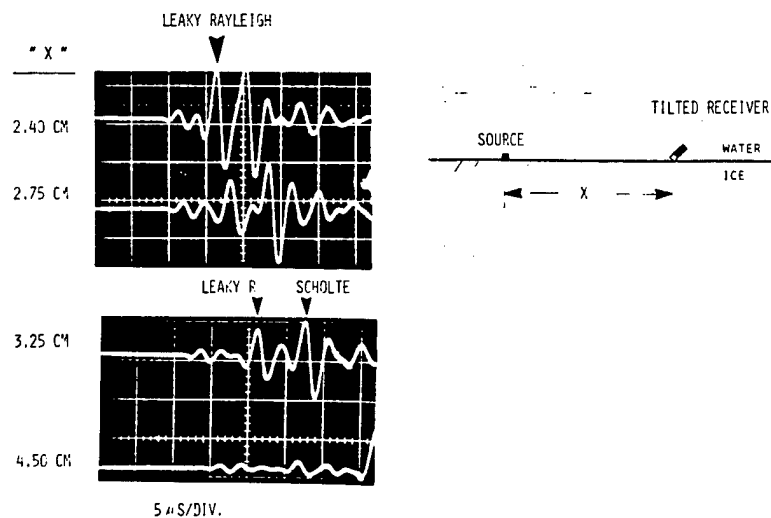
FIG. 24. Attenuation of leaky Rayleigh wave at water/ice
interface with range. (J. Acoust. Soc. Am. 80,S1,
S54,Y8,1986).
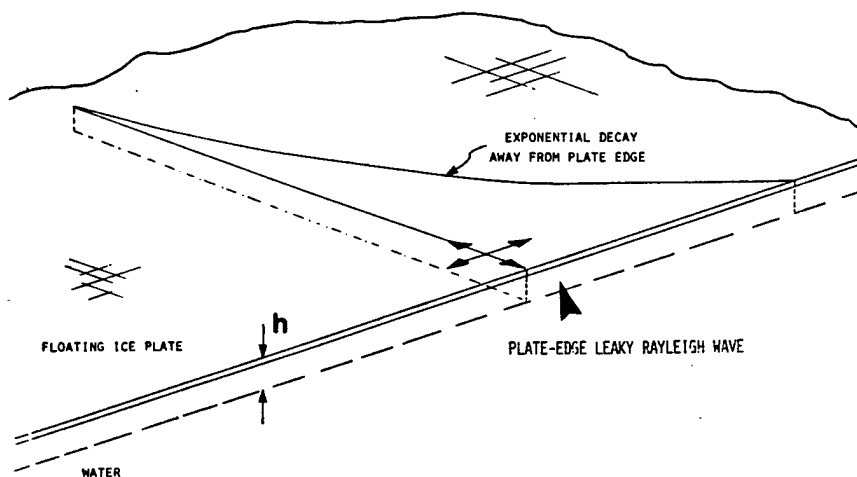
FIG. 25. Plate-edge leaky Rayleigh wave.
(J. Acoust. Soc. Am.81,S1,S10,D4,1987).
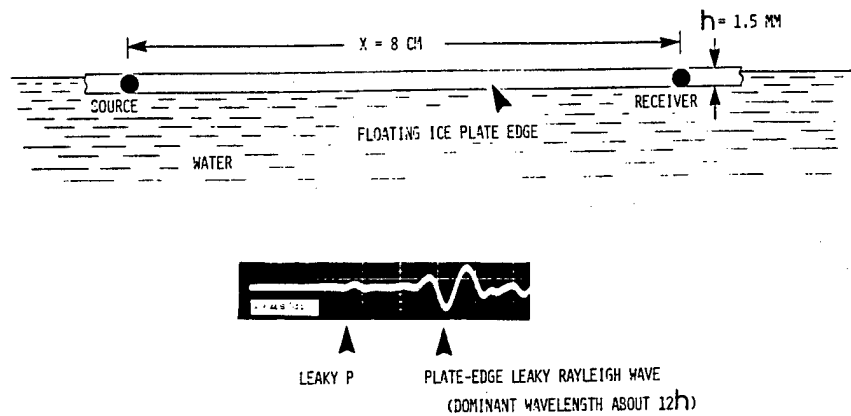
FIG. 26. Low-frequency plate-edge leaky Rayleigh wave in ice plate. (J. Acoust. Soc. Am.81,S1,S10,D4,1987).
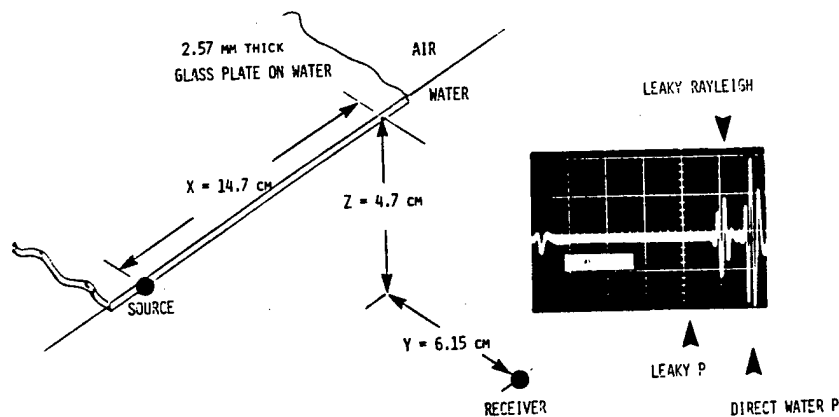
FIG. 27. Underwater remote detection of low-frequency plate-edge leaky Rayleigh wave. Glass plate model on water to enhance the leaky Rayleigh wave. (J. Acoust. Soc. Am. 81, S1,S10,D4,1987).
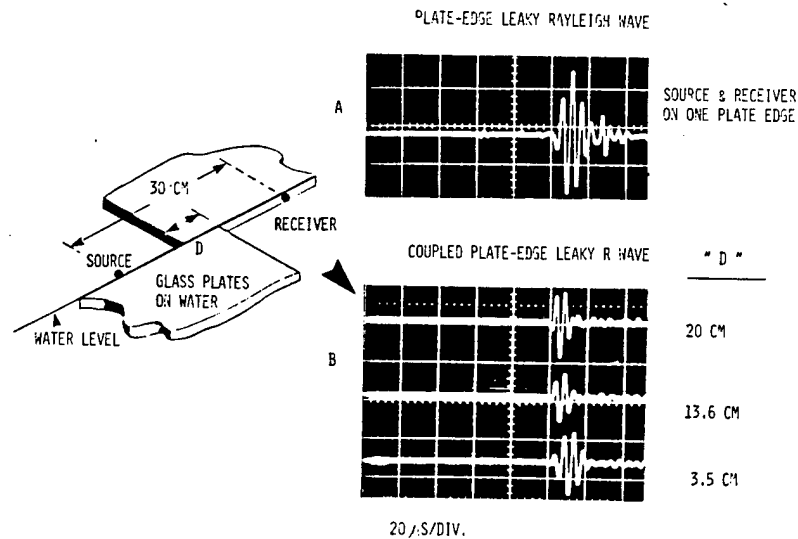
FIG. 28. Plate-to-Plate coupling between floating plates
dominated by plate-edge leaky Rayleigh wave.
Glass plates model. (J. Acoust. Soc. Am. 81,S1,
S10,D4,1987).

FIG. 29. Restrictions on the existence of the leaky Rayleigh wave.
(Brower et al., IEEE Trans. Sonics Ultrasonics SU 26(4),
306-308, 1979).

FREON 113 |← X = 3.25 CM →|

SOURCE   ICE   RECEIVER

5 μS/DIV.

LEAKY P   LEAKY RAYLEIGH

$$C_{FREON} = 671 \text{ M/S}$$

$$\frac{\rho_{FREON}}{\rho_{ICE}} = 1.7$$
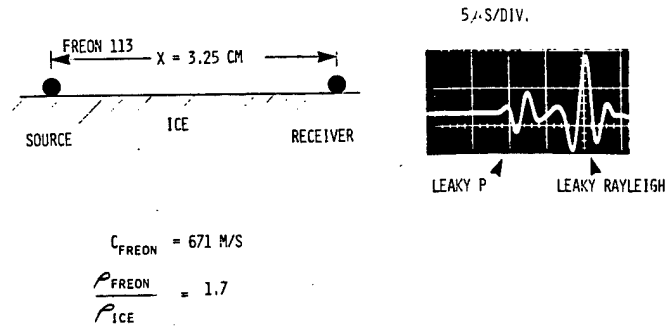
FIG. 30. Leaky Rayleigh wave at Freon 113/ice interface
demonstrating the effect of a dense liquid.
(J. Acoust. Soc. Am. 81,S1,S10,D4,1987).

X = 7.1 cm

water
receiver
source
ice

edge   source   water
receiver
ice

10 μs/div.

Half-space
Quarter-space

Leaky Rayleigh
wave

leaky R   scholte
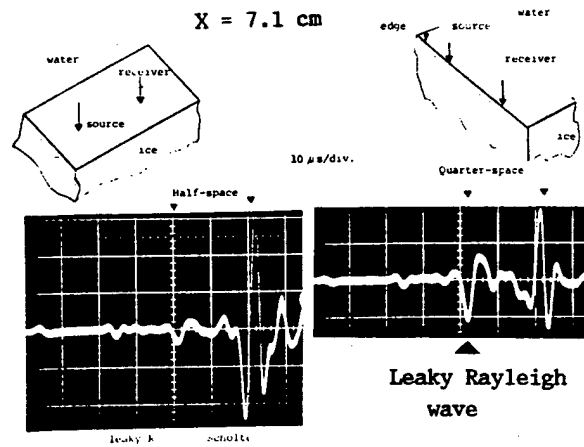
FIG. 31. Leaky Rayleigh wave along edge of ice quarter-space
in water. (Acoust. Soc. Am. Meeting, Syracuse, May
1989).

Arctic Ocean Acoustics at APL-UW
Presented by Terry Ewart, APL-UW

The Arctic Ocean Acoustics research effort at APL-UW was initiated with the AIWEX Acoustics Transmission Experiment (AATE). This field experiment was part of the Arctic Internal Wave Experiment (AIWEX) that took place during the Spring of 1985. The AATE field measurements continue in the tradition of earlier acoustic measurements made at Cobb Seamount during 1971 and 1977. Pulses were recorded at AATE both in depth and time, thus extending the earlier measurements to include dense spatial sampling in the vertical as well as in time. As part of the AIWEX effort, the overall focus of the combined environmental and acoustic measurements was to sample an environment where internal wave energy was low compared with that found in the open ocean. In relation to AATE, the environmental measurements supply a simultaneous environmental data set, determining the statistics of the sound speed fluctuations that scatter acoustic energy.

The scientific objective of the program is to understand how internal waves and other arctic environmental processes affect acoustic propagation. The specific problems addressed by this research include: (1) predict in a forward sense, the acoustic fluctuations at a receiver due to arctic internal wave and finestructure variability; (2) study the periodic and stochastic nature of arctic environmental processes by using the "integral memory" retained by the propagating acoustic field to infer the medium statistics; (3) study how internal wave motions and oceanic finestructure limit our ability to locate sources using acoustic receiving arrays; (4) study the influence that surface scattering from the ice canopy has on the spatial fluctuations in the acoustic field; and (5) develop methods to measure the 3-dimensional sound field using vertical arrays and ice suspended sources.

To advance our understanding of arctic scattering processes, this program, like its predecessors at Cobb Seamount, takes a coordinated approach between experimental, numerical , and theoretical methods. The field measurements taken during AATE will be used to validate and test our ability to make numerical and theoretical predictions of acoustic scattering statistics in the vertical and time. The environmental statistics measured during AIWEX are determined and are used as input to both theory and numerical simulation. Evaluations of theory are done in close collaboration with the group at Cambridge University, headed by Dr. Barry Uscinski.

The accomplishments are as follows.

(1) AATE data collection yielded 10 Gigabytes of stored, digitized 2, 4, 8, and 16 kHz pulses. These data are now reduced to travel times and amplitudes. The reduction stage was accomplished using a constrained multi-dimensional matched filter. This method evolved from the algorithm described in Bell and Ewart (IEEE Trans. Acoust. Speech and Sig. Proc., 34(5), 1986). Figure 1 shows an example of the AATE travel times and intensities. Statistical quantities are obtained from the reduced data for comparison with theoretical predictions. Preliminary estimates of the 2-dimensional travel time spectra are shown in Figure 2 obtained from periods before and after an arctic wind event.

(2) Uscinski has extended earlier work to include effects of linear, quadratic and cubic

background sound speed profiles in fourth moment theory. An equivalent quadratic profile has been calculated for AATE for use when evaluation software development is completed.

(3) Both geometric and full-wave equation backpropagation algorithms have been studied for use in determining how internal wave and finestructure limit our ability to locate the AATE source position. The AATE data from the receiving array is used.

(4) A wide-band numerical solution to the wide-angle parabolic wave equation is also being studied for its applicability to the AATE source localization problem. Figure 3 shows the received pulses and their focused source obtained using the wide-angle, wide-band PE. The focused source exemplifies two effects: the Rayliegh limit to the focus and the effect of internal wave and finestructure variability.

(5) A parabolic equation marching method has been developed to study scattering from rough ocean surfaces. The resulting 2-dimensional cross-section amplitude distributions provide a means of examining the effect that the rough boundary has on a scattered beam. Figure 4 is an example from the method displaying scattering from a rough air/water interface.
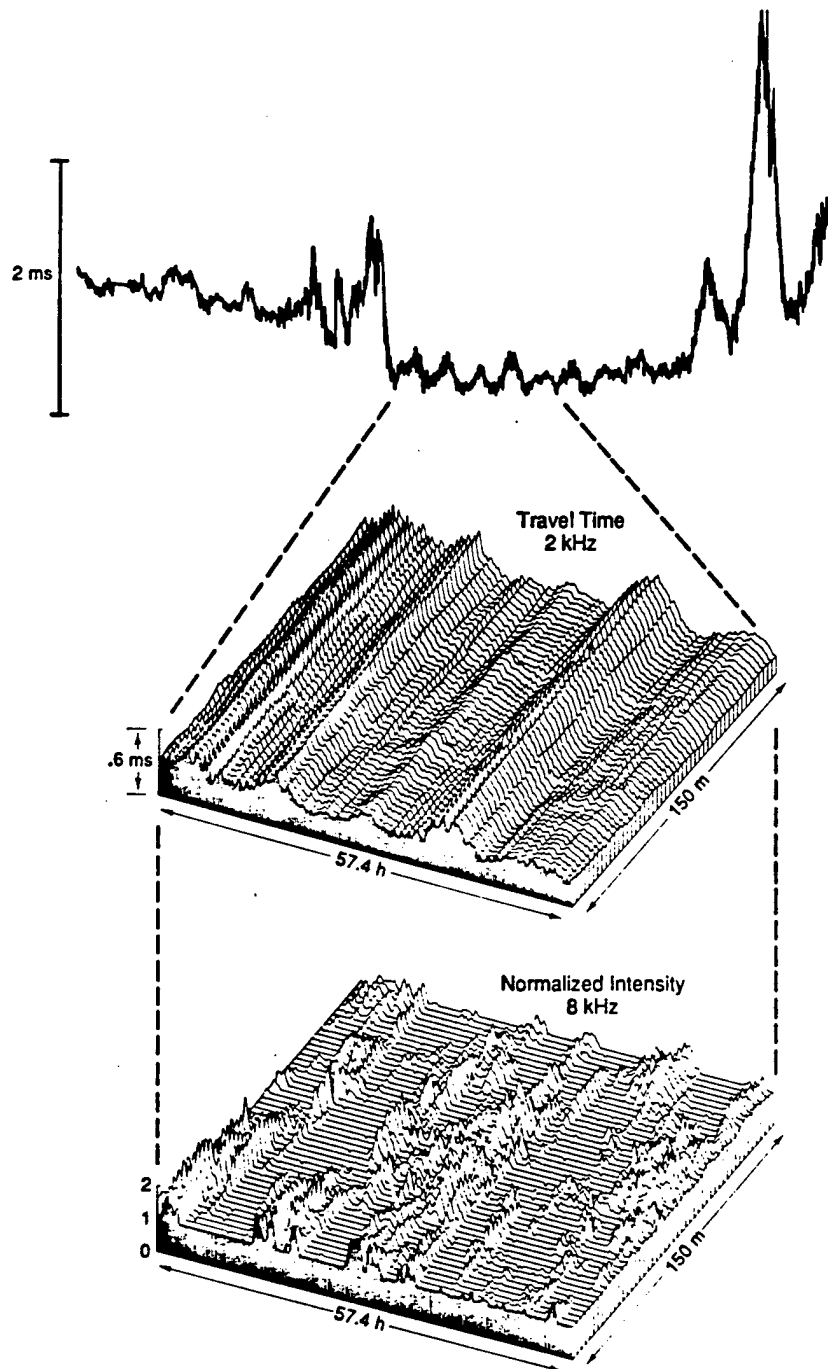
Figure 1. Results from AATE displaying the 2kHz travel times and the 8 kHz intensities. The travel times from a fixed position at the top of the array are shown to compare the two-dimensional data with the data obtained from a single receiver.
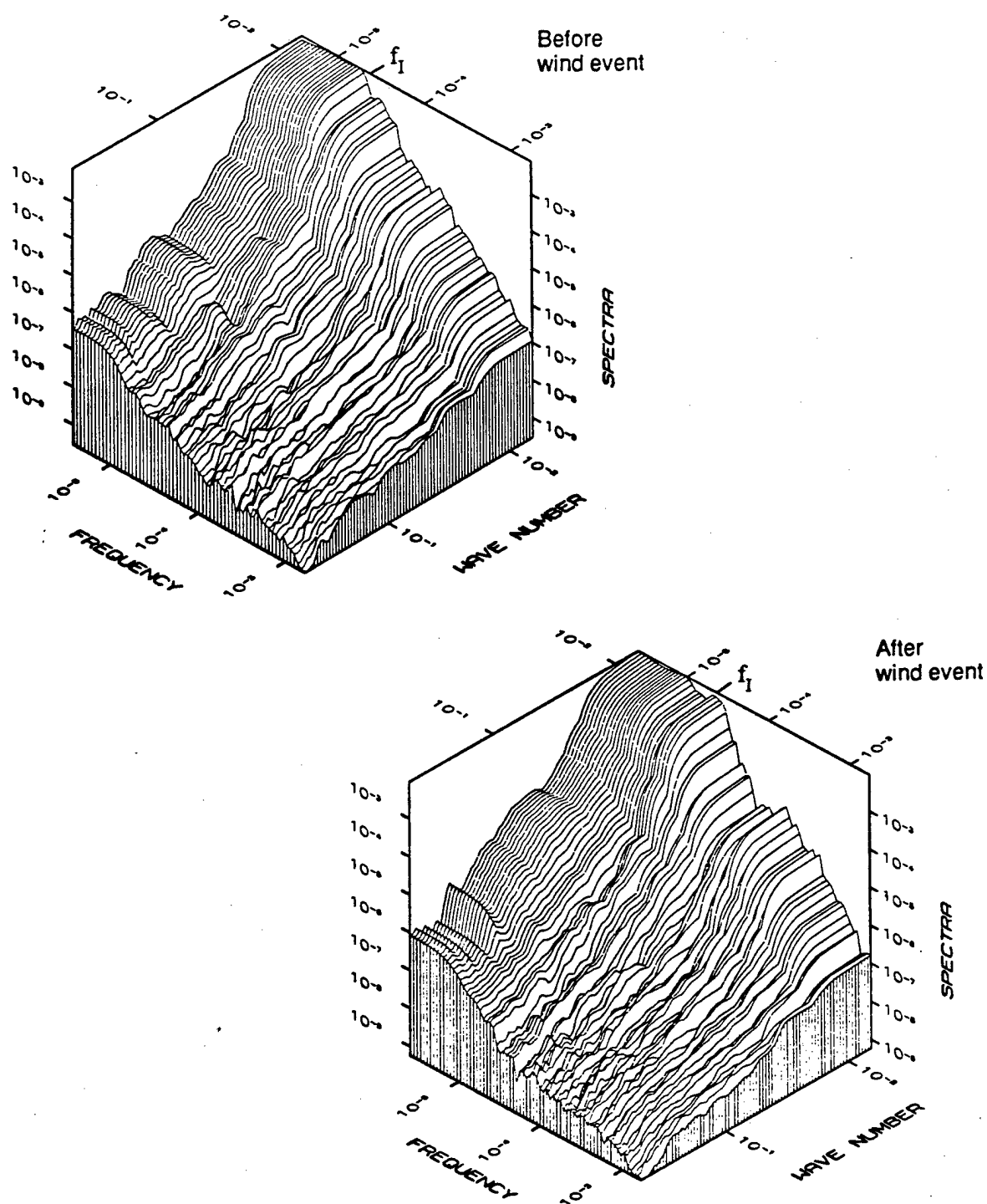
Figure 2. Estimates from AATE of the two-dimensional travel time spectrum as a function of frequency (in Hz) and vertical wavenumber (in cpm). Estimates from before and after a wind event are shown. A peak is observed near the the inertial frequency, f_I, in the spectrum after the wind event.
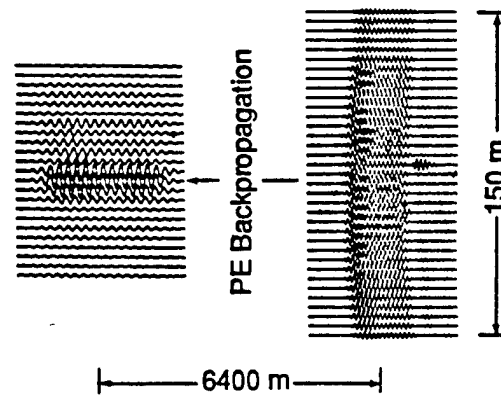
Figure 3. Results from backpropagation studies using the AATE 4 kHz pulses. The pulses received over the 150 m synthetic aperture were backpropagated to 4600 m using a wide-band, wide-angle PE algorithm.

Figure 4. A split-step PE solution for the incoming and outgoing intensity field scattered from a randomly rough surface having a Pierson-Moskowitz spectrum (20 m/s wind speed).

Instrumentation for Acoustic Monitoring of
Arctic Internal Waves in Depth and Time

TERRY E. EWART* AND STEPHEN A. REYNOLDS

Applied Physics Laboratory, College of Ocean and Fishery Sciences
University of Washington, Seattle, WA 98105-6698

*Also associated with the School of Oceanography, University of Washington

ABSTRACT

Instrumentation for measuring the evolution of volume scattered acoustic signals in both depth and time is described. Measurements were taken for twelve days during the spring of 1985 with transmitters and receivers suspended beneath arctic pack ice in the Beaufort Sea. These acoustic measurements were made simultaneously with extensive oceanographic measurements taken by other investigators during the Arctic Internal Wave Experiment (AIWEX). A depth cycling vertical array of three receivers and a single fixed horizontal receiver 100 m transverse to the propagation path were deployed over 6.4 km from moored transmitters. A vertical depth cycle of 51 m produced a synthetic vertical aperture of 153 m. Pulses spanning three octaves in acoustic frequency (2, 4, 8, 16 kHz) were used. The scattered field was sampled more often at 8 and 16 kHz to assure sufficient sampling (better than Nyquist) of the space/time fluctuations. Ten Gbytes of acoustic pulse receptions were recorded on optical disk storage for later processing. The measurements provide a unique two-dimensional (space/time) data set for testing acoustic volume scattering theories.

1. Introduction

Over time and space scales of hours to days and meters to kilometers, oceanic internal waves are the dominant scattering mechanism of acoustic energy transmitted in the broad frequency range of 100 Hz to 20 kHz. Moreover, internal waves and the steppy nonwavelike variability often called "finestructure" are ubiquitous in the ocean. Over the past two decades, several measurements have been made of acoustic variability in pulses transmitted over kilometer ranges in the ocean. (See, for example, Ewart (1976), Worcester et al. (1981), Ewart and Reynolds (1984), and Reynolds et al. (1985).) These measurements tested propagation theories where internal wave and finestructure statistics characterize the scattering medium. Usually fixed or relatively fixed experimental geometries were employed, the theoretical assumption being that each pulse transmission encounters a fixed snapshot of the intervening oceanic environment. Repeated acoustic transmissions then measure the temporal variability in the acoustic fluctuation statistics. The spatial variability of the medium is the actual scattering mechanism, and the evolution of the spatial index of refraction field in time is the observation. Because it is the spatial variability that scatters each pulse, a measurement in both depth and time is required to fully test acoustic volume scattering theories. In this paper, we describe instrumentation used to make such a measurement beneath the arctic pack ice.

In the open ocean, the observation of acoustic travel times and amplitudes over a large depth span is difficult. For example, observations during the Mid-Ocean Acoustic Transmission Experiment, MATE (Ewart and Reynolds, 1984) and the Cobb71 Experiment (Ewart, 1976) were made at a few spatially separated points (four during MATE and three during Cobb71). In both experiments, towers were placed on seamounts to provide the rigidity required to measure the acoustic phase to a small fraction of a wave period. These measurements, however, did not provide sufficient spatial fluctuation measurements.

In the experiment described here, measurements of the two-dimensional (time and depth) variability of acoustic signals were made using a depth cycling set of transducers receiving pulses from a multifrequency transmitter 6.43 km away. The transmitter and

receivers were suspended beneath arctic pack ice in the Beaufort Sea. These measurements were made during the AIWEX Acoustic Transmission Experiment (AATE) in the spring of 1985 as part of the Arctic Internal Wave Experiment (AIWEX). The latter was conducted by investigators from several institutions, the goal being the observation of oceanic internal waves in a low energy environment—under arctic pack ice.

AIWEX provided the opportunity, given the stable ice platform from which transmitters and receivers could be suspended, to measure the acoustic variability in both depth and time. The environmental measurements made by the AIWEX investigators provide the model statistics needed for input to acoustic fluctuation theory. The statistics predicted by theory are compared with the observed acoustic fluctuation statistics (this is known as the forward or direct problem). Eventually we hope to fully invert the acoustic measurements and obtain the statistics of the ocean sound speed field.

2. Experiment Overview

The measurement goal of AATE was to obtain acoustic amplitude and travel time fluctuation statistics in both depth and time for testing predictions from wave propagation theories. The specific scientific goals addressed by this research include the following:

- in a forward sense, compare the acoustic fluctuations at a receiver due to arctic internal wave and finestructure variability with predictions;

- in an inverse sense, study the periodic and stochastic nature of arctic environmental processes by using the "integral memory" retained by the propagating acoustic field to infer the medium statistics;

- study how internal wave motions and oceanic finestructure limit our ability to locate sources using acoustic receiving arrays; and

- study the influence that surface scattering from the ice canopy has on the spatial

35

fluctuations in the acoustic field.

Studies of ocean acoustic fluctuations differ from other problems in wave propagation in random media in that the statistics of the fluctuating medium are measurable. AATE took place during the environmental[†] sampling program conducted at the AIWEX ice camp. The environmental variability was well sampled in space and time. Because the expected fluctuations dictated the design of AATE, we briefly review AIWEX, provide an overview of the AATE component, and conclude the section with a summary of some of the environmental results relevant to the acoustics measurements.

AIWEX was conducted in the spring of 1985 in the Beaufort Sea north of Prudoe Bay, Alaska. The AIWEX environmental sampling program began on 20 March and was concluded on 3 May with camp evacuation. The camp layout is shown in Figure 1a, and the drift track of the camp during the data taking phase of AATE is shown in Figure 1b. The camp included investigators from several institutions making measurements over a broad range of temporal and spatial scales (e.g., Levine et al. (1987) and Padman and Dillon (1987)).

To predict the acoustic propagation statistics, the statistics of the environmental field must be known. In general, stochastic models are employed (e.g., for internal waves the Garrett and Munk model or a variant is traditionally used (Munk, 1981; Levine, 1983). Parameters in the model are obtained from the local measurements and require spatial and temporal series. Ideally several types of measurements are made so that model statistics can be checked for consistency between the measurements. This is the case with AIWEX. Both moored time series and vertical series of sound speed and current velocity were obtained by the AIWEX investigators (Levine et al., 1987).

---

†The word environmental is used to distinguish the measurements made by the AIWEX environmental program from the acoustics propagation measurements made in AATE.

AATE
AIWEX Acoustic Transmission Experiment
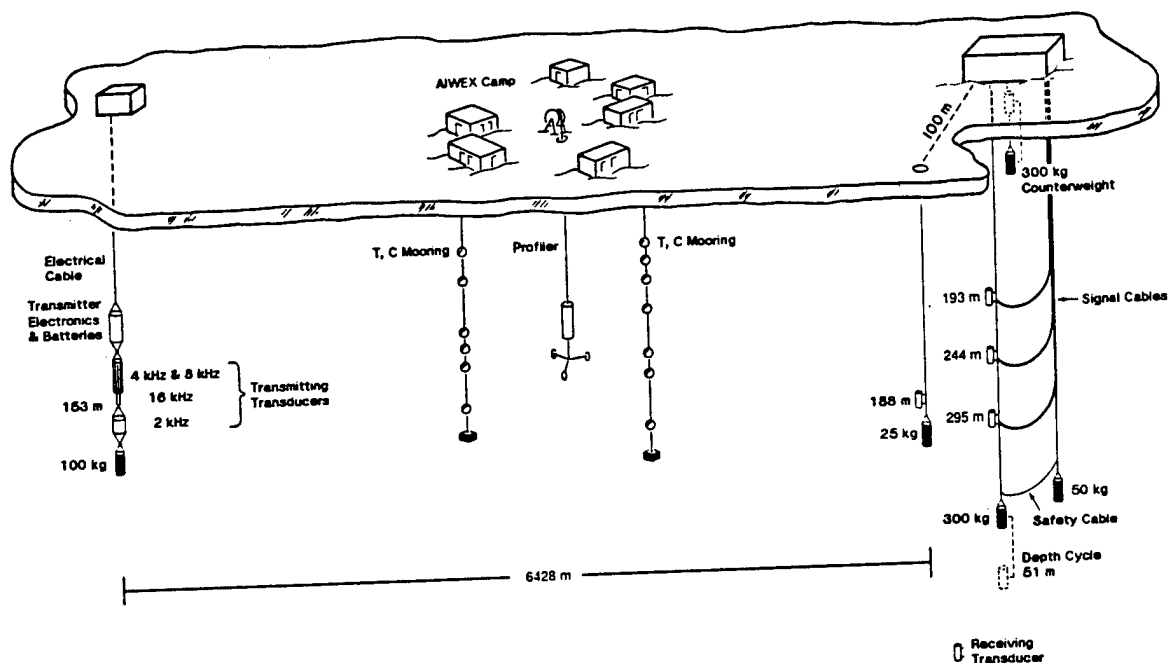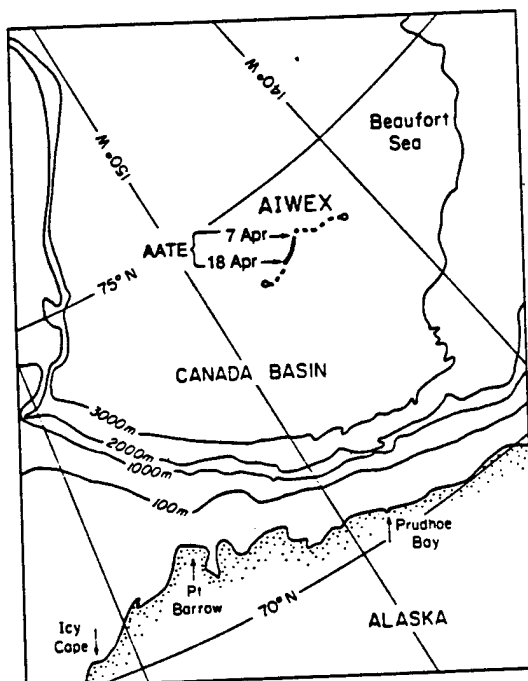
AIWEX Camp

300 kg
Counterweight

0—100 m

Electrical
Cable

T, C Mooring

Profiler

T, C Mooring

Transmitter
Electronics
& Batteries

193 m — Signal Cables

244 m

4 kHz & 8 kHz
16 kHz   Transmitting
                Transducers
2 kHz

153 m

188 m

295 m

25 kg

100 kg

50 kg

300 kg   Safety Cable

6428 m

Depth Cycle
51 m

Receiving
Transducer

(b)

140° W

150° W

Beaufort
Sea

AIWEX

AATE { 7 Apr—
        18 Apr—

75° N

CANADA BASIN

3000 m
2000 m
1000 m

100 m

Prudhoe
Bay

Pt
Barrow

70° N

ALASKA

Icy
Cape

FIG. 1.   A diagrammatic view of AATE is shown in (a). Note that the receiver hut at the right in (a) was actually about 0.3 km NNW of the AIWEX main camp. The remote transmitter hut, depicted at left, was about 6 km SSE of the main camp. The location of the ice camp during AIWEX is shown dashed in (b) (from Padman and Dillon, 1987). The location of the camp during the AATE data taking phase is shown as a solid line.

The AATE acoustic measurements began on 7 April and concluded 18 April. The AATE components of AIWEX (Figure 1a) consisted of a hut near the AIWEX main camp that housed the receiving hardware and computer, and a remote transmitter site located over 6.4 km to the southeast. The receiver hut, about 0.3 km from the AIWEX main camp, also served to house the AATE personnel.

The ice deployment is both a constraint and an asset. Physical constraints in an ice camp environment require that equipment be portable and easily deployed using man power. On the positive side, the ice acts as a stable platform for suspending equipment. In AATE, our equipment consisted of a set of transmitting transducers with associated electronics; a set of receiving transducers and receiving electronics, with digitizing and data storage; and accurate, stable clocking. In addition to these components for making temporal acoustic measurements, we used a low-noise winch in taking measurements of the vertical acoustic field. A vertical array of receivers was cycled in depth to make the spatial measurement. The winch/cable combination was designed to generate little if any acoustic noise during the data taking (down) phase of the cycle. The winch was provided by Marconi Underwater Systems of Cambridge, England.

At the remote site, the transmitter consisted of an electronics bottle suspended at depth just above four transducers. Four acoustic frequencies coherent with pulse repetition and pulse sampling rates were used (2.083, 4.166, 8.333, and 16.666 kHz— nominally 2, 4, 8, and 16 kHz). These three octaves sampled a broad range of scattering parameters. With the available power, 16 kHz was the highest frequency we could use that would overcome chemical absorption over the AATE range. The details of the transmitter and receiver equipment are given in the next section.

The vertical receiving array consisted of three transducers spaced on a cable driven over repeated depth cycles using the winch. The deployed configuration consisted of four vertically spaced transducers. The bottom transducer, however, failed during launch, so the fourth data channel was used to record pulses at a fixed transducer placed 100 m transverse to the vertical array. This fixed transducer was suspended at 188 m depth and allowed a single sampling of the transverse acoustic field.

The sampling of the acoustic field was established during the planning stages of the experiment by anticipating the scattering regime from earlier measurements in the Arctic (Levine et al., 1985). These measurements demonstrated that the internal wave energy levels would be lower than those observed under open ocean conditions. Measurements made at Cobb Seamount during the Mid-Ocean Acoustic Transmission Experiment (MATE) (Ewart and Reynolds, 1984) served as a guide to estimate the coherence times and spatial scales for sampling. An internal wave energy level a factor of 10 lower than MATE was used. Because AATE was planned for a shallower deployment where the buoyancy frequency is higher, the effect of the lower internal wave energy was canceled by the increase in the local buoyancy frequency. Hence the index of refraction fluctuation levels due to internal waves were expected to be similar to those observed at the MATE site.

Given the estimated fluctuation level, the temporal and spatial decorrelation scales could be calculated from theory (Uscinski, 1985). For the large end of the spatial scale, the spatial sampling needed to be at least a vertical correlation length of internal waves (about 100 m) and temporally sampled for as long as practical. The internal wave decorrelation time and space scales for 16 kHz were estimated to be 10 minutes and 2.5 m, respectively. (Finestructure scales are expected to be similar.) For 2 kHz, the vertical decorrelation scale estimate was 20 m.

With the sampling scale a function of acoustic frequency, the equipment needed to sample at a rate equal to half or one-fourth the smallest estimated scale for each acoustic frequency. Because this rate is a function of acoustic frequency, the pulses were transmitted in the sequence 4, 16, 8, 16, 2, 16, 8, 16. The vertical array needed to be driven at a relatively slow speed during the data taking cycles in order to keep generated acoustic noise to a minimum. The temporal constraints meant the winch needed to return the 16 kHz transducers to their starting place at least every 5 minutes to avoid the temporal decorrelation limit. With a transducer separation of 51 m, the full depth span was sampled with the winch driven at a speed of 0.26 m/s during down cycles. To sample the 16 kHz at vertical scales at least half the decorrelation scale of 2.5 m, a basic

transmission period of $\Delta t = 0.49152$ s was established. Thus the 16 kHz was sampled every $2 \cdot \Delta t \cdot 0.26$ m/s $= 0.2556$ m. Over a full down cycle, 400 pulse samples were recorded from each transducer for a total time of 3.28 minutes. This allowed over a minute and a half to return the winch to its rest position and start it down so the receivers would be moving at the proper speed at the starting time and position of the next sampling cycle. These rates satisfied the anticipated Nyquist criteria in space and time.

All the receiver electronics, time windowing, pulse digitization, and winch operation were under the control of a single computer, a Masscomp MC5500 with an integral data acquisition system, control hardware, and software. Each of the four channels of pulse data were received and digitized every 15 µs; 1024 digitized samples were then recorded from each channel. With 3.2 Mbytes of data recorded for each cast, the total equaled nearly 10 Gbytes over the 12 day period. To store the data for post-experiment analysis, the received data were written to an Optimem optical disk drive having 1 Gbyte of storage per removable cartridge.

Before turning to a detailed hardware description, we briefly review results from the internal wave measurements. The measurements reported by Levine et al. (1987) were taken from current and temperature sensors moored in two triangular grids. The internal triangle carried a relatively dense suite of instruments. Simultaneously with the moored measurements, Morison and Andersen sampled the vertical variability with repeated casts of the Advanced Profiling System (Morison, 1989). AIWEX temperature observations indicate an energy level of the internal wave field a factor of 0.03 to 0.07 of lower latitude, open ocean measurements (Levine et al., 1987). In addition, the temporal frequency dependence is quite different from the traditional GM model. The consequences for the acoustic observations will be treated in future publications; here we only note that the energy level is around a factor of 20 lower than open ocean values. The additional environmental variables needed to characterize the propagation environment are the "background" average sound speed and buoyancy frequency profiles. These were obtained from the vertical measurements of Morison and Andersen. From the background sound speed profile, a ray trace was calculated and is shown in Figure 2. The ray
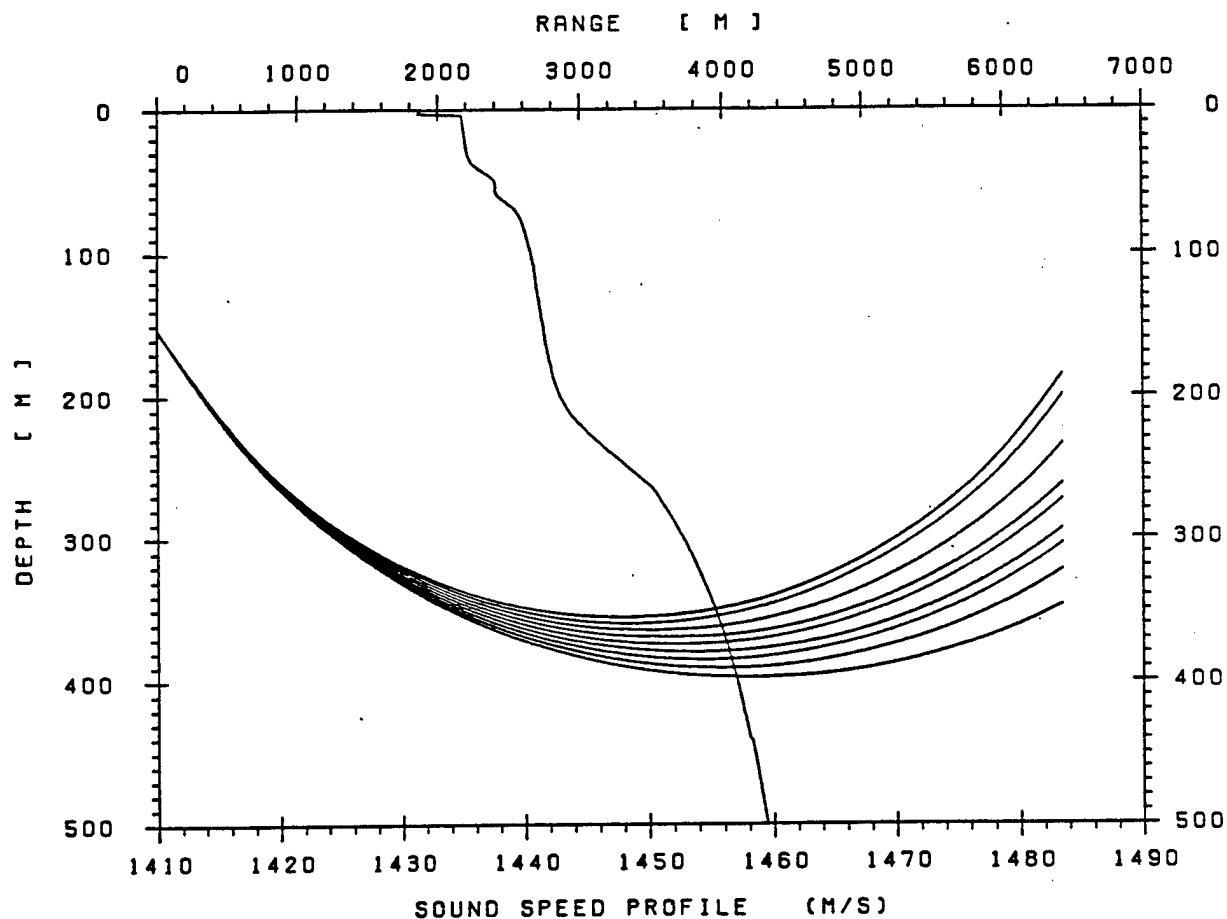
RANGE [M]

FIG. 2. Raytrace of the sound field over the 6.428 km AATE range. The transmit ray angles are from 7.95° to 8.35° with a uniform spacing of 0.05°. The sound speed profile used to calculate the raytrace is overplotted, with the scale shown along the bottom axis. The profile is from a 3 day average of casts taken during the middle of AATE with the Advanced Profiling System of Jamie Morison at the University of Washington.

angles near the transmitter and receiver are relatively steep (around 8°). There is no apparent multipathing. Note that even though the rays are shot at equal angular increments, the rays are not equally spaced at the receiver plane, indicating that the background average intensity profile varies over the depth spanned by the receivers.

3. Equipment

The AATE hardware elements consisted of the transmitter assembly, receiving array, winch, computer that controlled the receiving elements, and accurate clocks to ensure phase coherence between the transmitter and receiver. Because accurate measurement using acoustic techniques relies on stable clocking, we begin with the clocks. This is followed by a discussion of the transmitter and receiver/winch hardware. The section ends with a description of the computer data acquisition, storage, and control system. Much of the transmitter and receiver hardware had been used in 1977 during MATE (Ewart and Reynolds, 1984; Reynolds, 1982).

3.1 Clocks

Phase stability between the transmitter and receiver was maintained with 5 MHz Austron Digiquartz® clocks. The clock housed in the receiver hut was termed the master, and the transmitter clock the slave. The clocks had not been run-in long enough to achieve the lowest possible drift rates, so the drift was measured during AATE. A radio link between the transmitter and receiver hut was used to monitor the drift between the two clocks. Figure 3 shows the relative drift between the clocks during the 12 day experiment. A cubic spline fit is shown as dashed.

In both the slave and master clocks the 5 MHz oscillator frequency was divided down, first by 75 and then by 2^{15}, to get the basic sampling rate. The first division was the 15 microsecond pulse digitization rate and the second the 0.49152 s pulse repetition rate. The computer data acquisition and control clocking frequencies were obtained from the master clock. The timing is discussed further in the computer hardware section below.

FIG. 3. Measurements of the relative drift during AATE. Two Digiquartz oscillators maintained the phase accuracy between the transmitter and receiver. Sync information was telemetered between the remote transmitter hut and the master clock at the receiver. (The two clocks could be resynchronized over this link.) The base 5 MHz signal was divided down to the required digitization and pulse transmission rates. At the beginning of the experiment, the two clocks were synchronized and then their relative drift was monitored through the radio link. The relative drift measured between the two clocks is shown with asterisks in the diagram (the transmitter clock is ahead). A cubic spline fit to the drift data is shown as a dashed line.

3.2 Transmitter

A block diagram of the transmitter hardware is shown in Figure 4. There were three items at the surface: the deployment winch; a power generator that recharged the batteries in the electronics bottle through a control box at the surface; and the radio transmitter for monitoring the signal transmissions and clocking at the main hut. The transmitting transducers and electronics bottle were all suspended below the ice, with the 16 kHz transducer deployed at a depth of 153 m.

Transmit/receive angles were a major concern in designing the arrays at AATE. The sources and receivers needed relatively wide beam patterns because the transmission angles were near 8°. The 4 and 8 kHz transducers consisted of five and three elements, respectively, with a spacing of 9.94 cm between elements. The 16 kHz transducer is a two-element array with a spacing of 8.26 cm. The 4, 8, and 16 kHz transducers are lead titanate zirconate cylinders encapsulated in polyurethane [EDO Western 249-5 (4 and 8 kHz) and 249-17 (16 kHz)]. The 2 kHz transducer is a single oil-filled ring consisting of a neoprene boot covering two active cylindrical elements [EDO Western 415-1.5]. The 4, 8, and 16 kHz elements were arranged in an axial array suspended with the electronics housing on an armored coaxial cable.

In the transmitter, pulse selection and generation was under digital control. Once the frequency was selected, a pulse was downloaded from PROM (Programmable Read-Only Memory), passed through a D/A converter, and sent to a driver and power amplifier for transmission from the appropriate transducer.

Several options for pulse shape and length were recorded in the PROM and available through the control box at the surface. The final pulses selected during AATE were 2 ms pulsed tones. With our pulse analysis technique, it was necessary to record the pulses at short range and "propagate" these ideal (unscattered) pulses out to the final range by modifying the pulses for the effects of geometric spreading and chemical absorption. (The equation of Francois and Garrison (1982) was used.) These single path, ideal pulse "replicas" are shown in Figure 5.
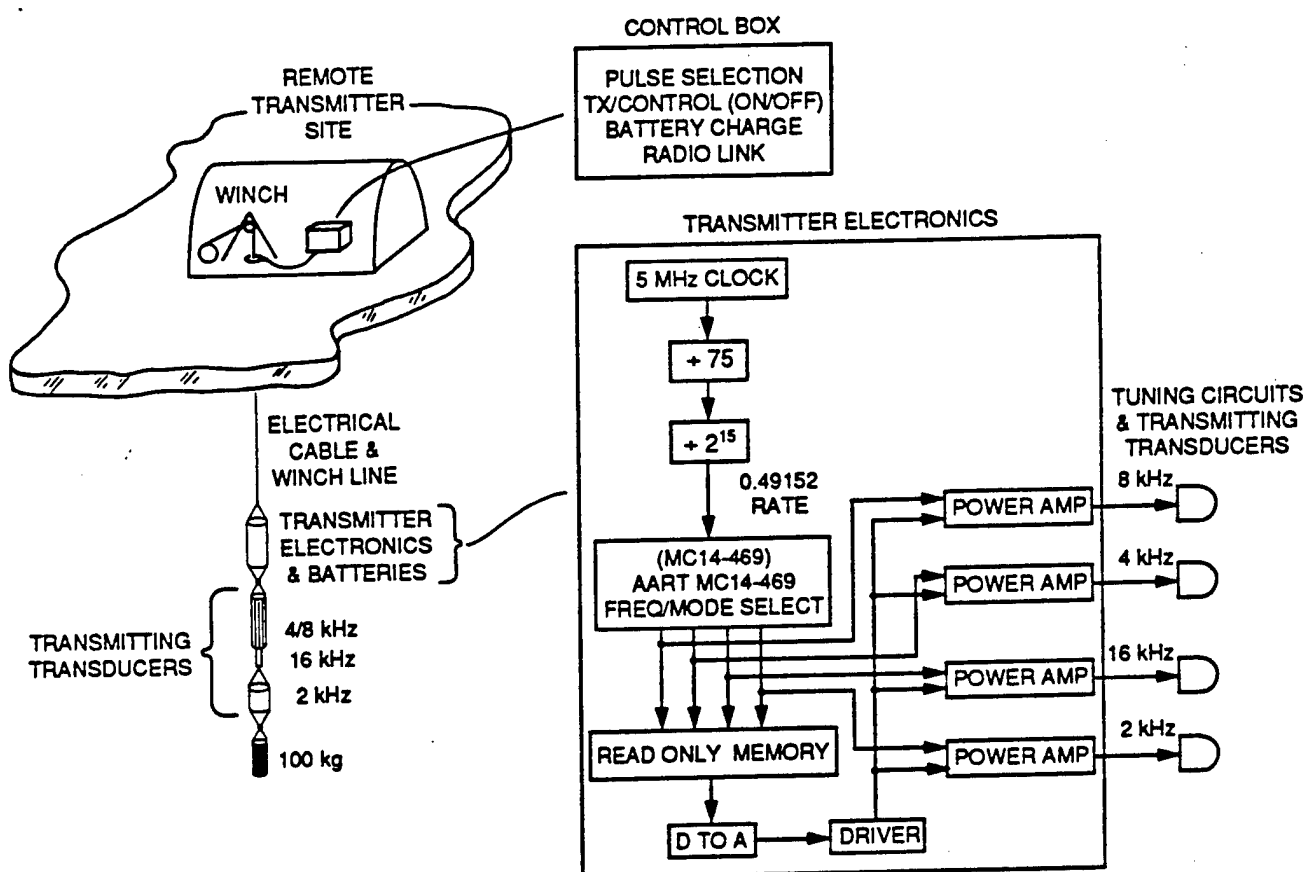
FIG. 4. Diagram of the transmitter showing the remote site and block diagrams of the electronics. The control box inside the remote hut allowed selection of eight pulse programs for four frequencies that control pulse length, ramp-up, and ramp-down. The selection used an addressable asynchronous receiver/transmitter (AART) to control programmable memory in the transmitter electronics.

FIG. 5. The AATE replica pulses used in the multidimensional matched filter. The pulses were recorded 100 m from the transmitter, then numerically propagated to 6.428 km by correcting for geometric spreading and chemical absorption (the formula of Francois and Garrison (1982) was used).

3.3 Winch and Receiving Array

The receiving array was suspended from a winch cable that was driven over the element separation distance of 51 m by the Marconi low-vibration, counterbalanced winch system. The counterbalance consisted of a free and a motorized pulley, cabling, and weights. The entire assembly was designed to provide a stable, low acoustic noise system that could be driven up and down under computer control. The receiving transducers were supported on a Kevlar line attached via rubber vibration isolators to a plastic coated steel cable that ran over the pulleys. The steel cable came up through a 36" hole in the ice, ran over the free pulley, across to the motorized pulley, and down through a second 16" hole through the ice for the counterbalance. The two pulleys were separated by nearly 3 m. Suspended at the ends of the cables were 311 kg weights. The weights were carefully balanced so that the motor needed only to overcome the inertia, the drag, and the differential length of cable in the system. The winch, as described in the previous section, was under computer control. The winch position was monitored using an incremental shaft encoder mounted on the free pulley. An optical switch sensed a mark on the cable on each cast. The computer algorithm used the sense information to eliminate creep in the "zero" position of the transducer. The total time between casts was about 5 minutes.

The pulses were received by the three vertically spaced transducers suspended on the winch cable and the single horizontally spaced transducer. A diagram of the received signal hardware is shown in Figure 6. Each receiving transducer on the winch cable consisted of four elements separated by 4.8 cm. The beam patterns of these transducers were broad enough to allow no more than 2 dB of loss for the 16 kHz pulses at angles less than 10° and still have some directivity at 2 kHz. The horizontal transducer was a spare and differed somewhat from the other three. This transducer consisted of three elements with element spacing of 5.8 cm. The loss was less than 3 dB for angles less than 10°.

Each receiver contained a 40 dB preamp stage. From the preamps, the connection to the surface receiving electronics and computer was made through twisted pairs of Belden 8412 conductors. The signal cables from the transducers were suspended between the
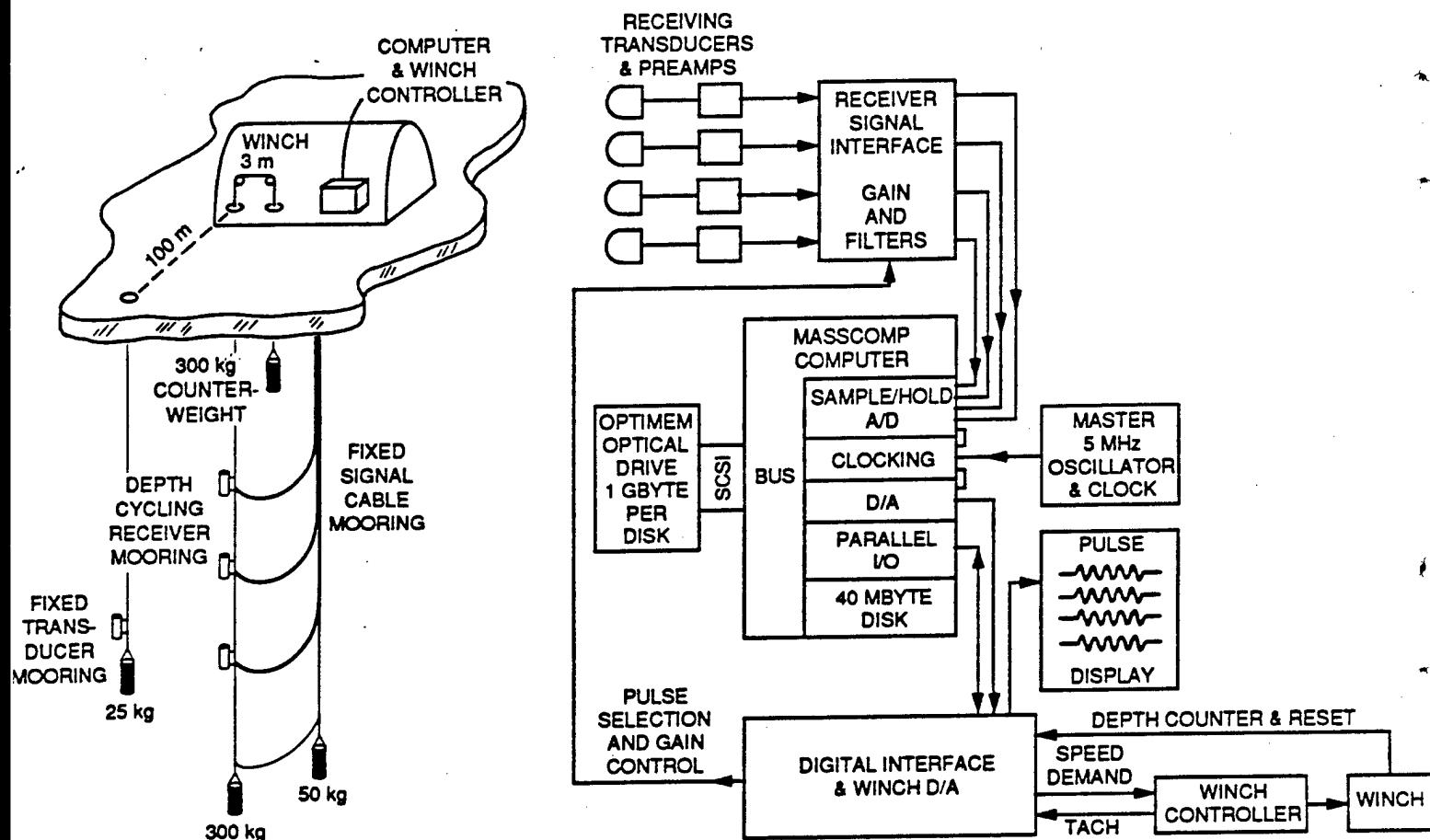
FIG. 6. Diagram of the receiver array, winch, receiver electronics, and computer system.

receivers and a secondary mooring 25 m behind and to the right of the receiver winch cable (see Figure 1). Small weights were hung from the signal cables to prevent the cables from streaming and to reduce the effects of current drag. From the stationary transverse receiver, the cable simply ran up its mooring line.

The signal conductors were connected to the receiver electronics inside the hut. These electronics provided frequency bandpass filters and attenuation control of the analog signals from the receiver transducers. The signals passed through two gain stages and then into an acoustic-frequency-dependent bandpass filter. The frequency selection and gain in the receiver were controlled by the Masscomp computer to be in lock-step with the transmitter sequence. From these electronics, the signals were connected to sample-and-hold and A/D converters on the host computer.

3.4 Computer Control and Data Storage

In addition to the winch controller and receiving electronics, three other pieces of electronics hardware were housed in the receiver hut: the clocking hardware described above; a Tektronix 611 display tube for real-time display of the received pulses; and the Masscomp MC5500 computer that monitored the clocks, controlled the receiving electronics, drove the winch, and digitized and stored the received pulses with intermediate display (see Figure 6). The computer contained a data acquisition and control processor (DACP®). The software interface to the DACP allows the entire data acquisition and control software to be written in high level languages (FORTRAN and C). All of the receiving data acquisition and storage, real time display, monitoring of the external clocks, and winch control was carried out using the single Masscomp. Five DACP modules were used for the experiment: a clocking module containing eight counters; a 12 bit sample-and-hold; an A/D board for digitizing the four input channels of received pulses; a D/A module for real-time output of the received pulses to the display scope; and a 16 line parallel interface module that was used to control the winch and send the frequency select and attenuation settings to the receiving electronics. The parallel interface was also used to monitor the shaft encoder and the winch controller output. Without this

system, the experiment would have been impossible under our budgetary and time constraints. (The entire experiment was put together in less than 6 months and was conducted by a party of two scientists and four part-time support engineers.)

The winch cycles were controlled as follows. From rest at the top of each data cast, the software commanded the winch to cycle down so that it was at the selected speed at the correct time and depth for sampling the first pulse in the sequence. After the 400 samples were acquired and stored, the winch was reversed and returned to its rest position. A modified position feedback algorithm was used to control the speed and position of the winch during the data taking phase. From the upper sampling depth, only the depth separations were maintained; i.e., sampling positions were not adapted during the cast. This approach avoided over-driving the winch. The upper sampling depth was modified cast-to-cast by "learning" a starting time that would get the top receiver closer to the desired starting depth. The upper sampling position then stabilized as the experiment progressed. A plot of depth counter output in Figure 7 shows nearly constant positions over time, indicating that this scheme worked well. More than a day of depth counts are shown.

Over the 12 day experiment, nearly 10 Gbytes of data were acquired and stored. Because of our inexperience with both the optical drive and the computer acquisition system, a problem occurred at intervals of about an hour that required restarting the data acquisition. After the experiment we learned that the optical disk drive automatically refocuses its optical module at hourly intervals. This problem resulted in some loss of data; however, the amount of data returned was nearly 90% of the possible total, and we feel that the overall system performance was exceptional.

4. Pulse Reduction and Preliminary Results

The equipment used during AATE recorded pulses in depth and time that traversed the 6.43 km range between the transmitter and four receivers. In order to compare the received pulses with acoustic fluctuation theory, the pulses are reduced to sets of amplitudes and travel times. We model the received pulses in the standard way, by assuming
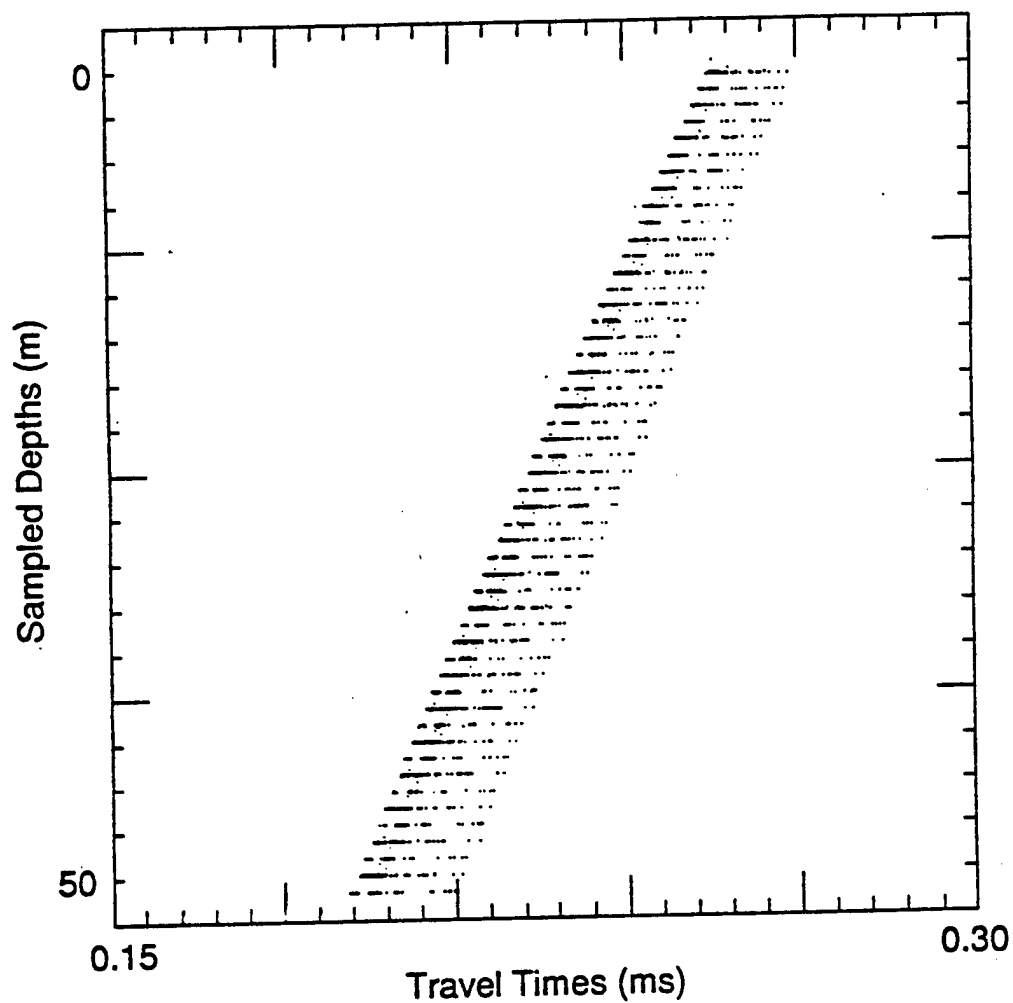
FIG. 7. Representative output of the depth counter during 4 kHz pulse receptions as a function of travel time, for more than a day during the experiment. The fact that the depth counts are at discrete counts implies that the position feedback algorithm controlling the winch worked well.

that the pulse receptions $r(t)$ consist of time shifted, amplitude scaled replicas $s(t)$ contaminated by additive noise $\varepsilon(t)$:

$$r(t) = \sum_{j=1}^{N} a_j \cdot s(t - \tau_j) + \varepsilon(t) . \tag{1}$$

We call the method used for finding the amplitudes a_j and travel times τ_j a multidimensional matched filter (MDMF). The algorithm as originally implemented is described by Bell and Ewart (1986). Several modifications to the MDMF were made during the processing of the AATE data; a publication describing the use of the algorithm is in preparation. Here we outline the MDMF algorithm used for the AATE pulse reduction.

Following the notation of Bell and Ewart (1986), the algorithm solves for the sets of $\{a_j\}$ and $\{\tau_j\}, j=1,...,N$ that minimize the difference between the modeled pulse $\sum_{j=1}^{N} a_j \cdot s(t - \tau_j)$ and the received pulse $r(t)$; i.e.,

$$\underset{(t)}{\text{minimize}} \, \| r(t) - \sum_{j=1}^{N} a_j \cdot s(t - \tau_j) \|^2 . \tag{2}$$

This least squares approach is equivalent to a maximum likelihood method when the noise $\varepsilon(t)$ is white over the bandwidth of $s(t)$. The travel time solution reduces to maximizing the objective function

$$\tfrac{1}{2} \bar{\Phi}(\tau)^T \bar{\Lambda}(\tau)^{-1} \bar{\Phi}(\tau) \text{ over } \tau , \tag{3}$$

where $\bar{\Lambda}(\tau)$ is a matrix of approximate replica autocorrelation functions and $\bar{\Phi}(\tau)$ represents the approximate single pulse matched filters. The approximation arises from the method chosen to remodulate the demodulated correlation functions (see Bell and Ewart (1986) for further discussion). The travel time problem is solved first; the amplitudes are obtained from the travel times using the relation

$$a(\tau) = \bar{\Lambda}(\tau)^{-1} \bar{\Phi}(\tau) .$$

Each AATE pulse frequency has a replica as shown in Figure 5. The number of paths, N, is left as a parameter. For each pulse, the algorithm solves the $N = 1$ problem first, then progresses to two paths, and so on. The maximum number of paths solved for AATE was two. For the one-path solution, an initial estimate for the travel time search is taken from the maximum of the demodulated matched filter. The function in Eq. (3) is searched for its maximum. For the two-path solution, τ_2 is initialized to the maximum in the output of the remainder function

$$\tilde{C}(t) - a_1 \cdot \tilde{A}(t - \tau_1).$$

The two-path objective function is then solved for τ_2.

Two paths were used in the analysis. With two paths the remainder function was reduced to a value nearly equal to the noise energy in the bandwidth of the replica. Using two paths also ensured that when multipaths were present the solution would be obtained in an optimal way. In fact, the pulse receptions were usually fit by a single path as anticipated from the ray traces. In tests using more than two paths, additional path amplitudes were much less than the main path amplitude and represented a fitting of noise present during the pulse reception.

The MDMF algorithm is efficient, a requirement because the AATE data set is large. Nominal analysis times were from 1 to 2 s per pulse, only a factor of 2 to 4 of real time. An initial pass through the data set revealed occasional 2π jumps in phase. A constrained algorithm was developed to remove the jumps. A search was made limited to a wavelength of the unconstrained path. Using a simple differential detector, jumps were detected and displaced back to be less than 2; the jumps usually occurred where the signal-to-noise ratio was low. The method used for pulse analysis was checked for accuracy using a network-based matched filter (Bell and Reynolds, 1989). All pulse reduction has been completed.

Preliminary results from the experiment are shown in Figure 8. The single path travel times from the top position of the array are shown in the upper part of the figure. The pulse travel times are the measurements one would obtain from a single moored
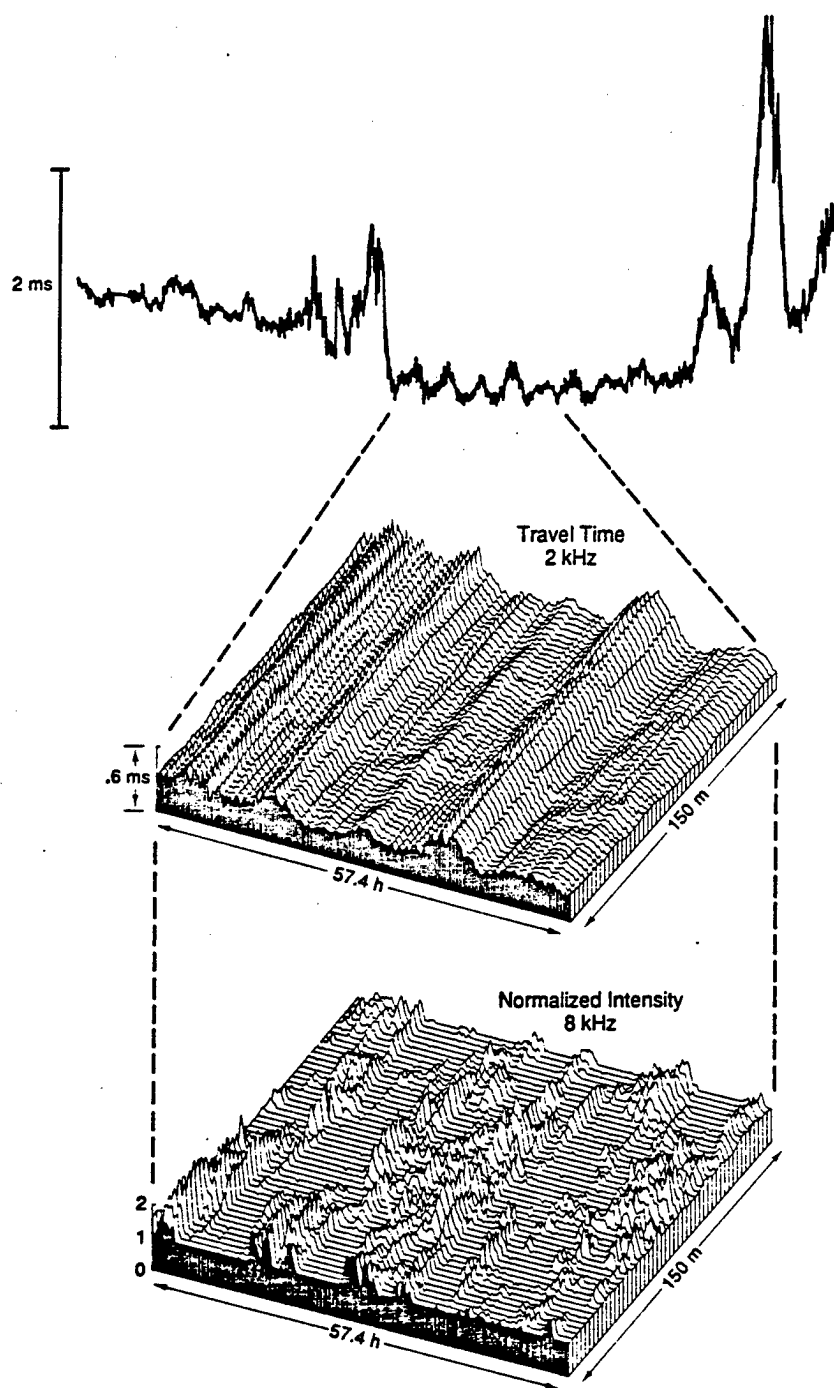
FIG. 8. An example of data from AATE. The top curve shows a one-dimensional record-
ing of the 2 kHz travel times taken at a fixed depth. The large travel time excursions occurred
during wind events when ice motion increased. Data sets of this type are recorded in traditional
fixed receiver experiments. The depth-time segment taken from the middle of the top data set is
shown in the middle graph. The depth-time intensity series from the 8 kHz pulses is shown at bot-
tom.

transducer. The information in two dimensions, in the middle and lower part of Figure 8, was measured from the three depth-cycled receiving transducers. The 2 kHz travel times are shown, with the 8 kHz intensities below.

5. Discussion and Summary

The depth sampling algorithm used during AATE requires a resampling of the data series on a uniform depth-time grid. Statistics calculated from the resampled series will be used to test numerical and theoretical solutions for volume scattering by internal waves and finestructure. This is the direct or forward problem. This approach has guided much of our progress toward predicting acoustic travel time and intensity fluctuation statistics. The inversion of the observed acoustic results to infer the statistics of the medium is also planned. The results from AATE are currently being used in studies of source localization and backpropagation methods.

In summary, novel instrumentation was used in the Beaufort Sea during 1985 to make two-dimensional measurements of acoustic travel times and amplitudes. The experiment, AATE, took place as a part of AIWEX, the Arctic Internal Wave Experiment. The measurements were made by suspending a three-receiver array from the ice platform and using a low noise electric winch to cycle 51 m, resulting in a receiving aperture that spanned 188 to 341 m. The received pulses propagated over a 6.4 km path from remote 2, 4, 8, and 16 kHz transmitters suspended at 153 m depth. The recorded pulses represent a data return of nearly 90% and will be useful in testing volume fluctuation theory for travel time and intensity fluctuations produced by arctic internal waves and finestructure. Eventually the measurements themselves will be used to obtain the statistics of the intervening medium.

REFERENCES

Bell, B.M., and T.E. Ewart, 1986: Separating multipaths by global optimization of a multidimensional matched filter. *IEEE Trans. Acoust. Speech and Sig. Proc.,* **34,** 1029–1037.

Bell, B.M., and S.A. Reynolds, 1989: A matched filter network for estimating pulse arrival times. *IEEE Trans. Acoust. Speech and Sig. Proc.* (submitted).

Ewart, T.E., 1976: Acoustic fluctuations in the open ocean—A measurement using a fixed refracted path. *J. Acoust. Soc. Am.,* **60,** 46–59.

Ewart, T.E., and S.A. Reynolds, 1984: The Mid-Ocean Acoustic Transmission Experiment, MATE. *J. Acoust. Soc. Am.,* **75,** 785–802.

Francois, R.E., and G.R. Garrison, 1982: Sound absorption based on ocean measurements. Part II: Boric acid contribution and equation for total absorption. *J. Acoust. Soc. Am.,* **72,** 1879–1890.

Levine, M.D., 1983: Internal waves in the ocean: a review. *Rev. Geophys. and Space Phys.* **21,** 1206–1216.

Levine, M.D., C.A. Paulson, and J.H. Morison, 1985: Internal waves in the Arctic Ocean: Comparison with lower-latitude observations. *J. Phys. Oceanogr.,* **15,** 800–809.

Levine, M.D., C.A. Paulson, and J.H. Morison, 1987: Observations of internal gravity waves under the arctic pack ice. *J. Geophys. Res.,* **92,** 779–782.

Morison, J.H., 1989: Physical oceanography instrumentation for the polar regions: A

review. *IEEE J. Ocean. Eng.,* **14,** 173–185.

Munk, W. H., 1981: Internal waves and small-scale processes. *Evolution of Physical Oceanography.* B. A. Warren and C. Wunsch, Eds., MIT Press, 264–291.

Padman L., and T. M. Dillon, 1987: Vertical heat fluxes through the Beaufort Sea thermohaline staircase. *J. Geophys. Res.,* **92,** 10799–10806.

Reynolds, S. A., 1982: The Relation of Acoustic Fluctuations to Environmental Variability at Cobb Seamount: the Direct Approach. Ph.D. dissertation, University of Washington, Seattle, 183 pp. (available from University Microfilms, Ann Arbor, MI).

Reynolds, S. A., S. M. Flatfe, R. Dashen, B. Buehler, and P. Maciejewski, 1985: AFAR measurements of acoustic mutual coherence functions of time and frequency. *J. Acoust. Soc. Am..* **77,** 1723–1731.

Uscinski, B. J., 1985: Range and time dependence of acoustic intensity fluctuations. *Proceedings from NATO Conference on Seismo-Acoustics* (preprint).

Worcester, P. F., G. O. Williams, and S. M. Flatfe, 1981: Fluctuations of resolved acoustic multipaths at short range in the ocean. *J. Acoust. Soc. Am.,* **70,** 825–840.

Figure Captions

FIG. 1.   A diagrammatic view of AATE is shown in (a). Note that the receiver hut at the right in (a) was actually about 0.3 km NNW of the AIWEX main camp. The remote transmitter hut, depicted at left, was about 6 km SSE of the main camp. The location of the ice camp during AIWEX is shown dashed in (b) (from Padman and Dillon, 1987). The location of the camp during the AATE data taking phase is shown as a solid line.

FIG. 2.   Raytrace of the sound field over the 6.428 km AATE range. The transmit ray angles are from 7.95° to 8.35° with a uniform spacing of 0.05°. The sound speed profile used to calculate the raytrace is overplotted, with the scale shown along the bottom axis. The profile is from a 3 day average of casts taken during the middle of AATE with the Advanced Profiling System of Jamie Morison at the University of Washington.

FIG. 3.   Measurements of the relative drift during AATE. Two Digiquartz oscillators maintained the phase accuracy between the transmitter and receiver. Sync information was telemetered between the remote transmitter hut and the master clock at the receiver. (The two clocks could be resynchronized over this link.) The base 5 MHz signal was divided down to the required digitization and pulse transmission rates. At the beginning of the experiment, the two clocks were synchronized and then their relative drift was monitored through the radio link. The relative drift measured between the two clocks is shown with asterisks in the diagram (the transmitter clock is ahead). A cubic spline fit to the drift data is shown as a dashed line.

FIG. 4.   Diagram of the transmitter showing the remote site and block diagrams of the electronics. The control box inside the remote hut allowed selection of eight pulse programs for four frequencies that control pulse length, ramp-up, and ramp-down. The selection used an addressable asynchronous receiver/transmitter (AART) to control

programmable memory in the transmitter electronics.

FIG. 5.   The AATE replica pulses used in the multidimensional matched filter. The pulses were recorded 100 m from the transmitter, then numerically propagated to 6.428 km by correcting for geometric spreading and chemical absorption (the formula of Francois and Garrison (1982) was used).

FIG. 6.   Diagram of the receiver array, winch, receiver electronics, and computer system.

FIG. 7.   Representative output of the depth counter during 4 kHz pulse receptions as a function of travel time, for more than a day during the experiment. The fact that the depth counts are at discrete counts implies that the position feedback algorithm controlling the winch worked well.

FIG. 8.   An example of data from AATE. The top curve shows a one-dimensional recording of the 2 kHz travel times taken at a fixed depth. The large travel time excursions occurred during wind events when ice motion increased. Data sets of this type are recorded in traditional fixed receiver experiments. The depth-time segment taken from the middle of the top data set is shown in the middle graph. The depth-time intensity series from the 8 kHz pulses is shown at bottom.

Greenland Sea Tomography
Presented by Jim Lynch, WHOI

The Greenland Sea Tomography Project has many acoustic and oceanographic scientific objectives. Some of the main ones are as follows: (1) to examine the 3-D sound velocity structure and its variability in the central Greenland basin over a full year; (2) to identify and quantify the physical oceanographic processes occurring in the Greenland Sea, e.g. deep water formation, gyre vorticity, surface and internal wave strengths, etc.; (3) to investigate the feasibility of doing acoustic tomography with a moored array of transmitters and a ship that moves from station to station, making a drifting reception at each; (4) to explore the long range deep water path structure from the Greenland Sea through the Fram Straits, and its spatial and temporal coherence and variability.

The Greenland Sea Tomography Project is a joint ONR/NSF program initiated in 1986. During its initial years, the effort was focussed on computer simulation of anticipated oceanographic responses and transceiver development. The simulation efforts addressed: (1) the deployment pattern, i.e. a pentagon with a center buoy to provide the most coverage in case of buoy failures; (2) the transmission sequence coding; and (3) the resolution achievable over the pattern and the long path to the A-Camp north of the Fram straits. On the instrumental side, a competitive procurement resulted in the purchase of HLF-5 Hydroacoustic Sound Sources operating at 250 Hz ($\pm$50 Hz) with 193 dB source level. The first three transceivers built were deployed in the Megameter Pacific Gyre Tomography Experiment. Problems with water leakage occurred requiring retrieval, repair, and redeployment. Smooth operation occurred after redeployment for the three months before scheduled recovery. This performance lay the groundwork for the deployment of the six transceivers in the Greenland Sea during September 1988.

Operation to date has been nominal (to the best of our knowledge), with all active transmissions occurring as scheduled. Receptions made by single hydrophone sonobuoys (as part of the routine deployment procedure) showed very clear arrival structures with high signal to noise ratio (see Fig. 1). Indeed, up to 40 dB SNR and eight bottom reflections were seen in these receptions when the seas were calm, an excellent indication that the recorded data should be of high quality.

During the final half of the Greenland Sea Tomography Project deployment cruise, moving ship tomography was implemented, using the six moorings as sources and circling around the array as shown in Fig. 2. Using onboard Appolo workstations, B. Cornuelle of SIO was able to produce a preliminary inverse of the gyre from the data collected, and will be following this up with a more complete and careful shoreside analysis. At the very end of the deployment cruise, a sonobuoy was deployed enroute to Spitzbergen in order to test the feasibility of the long range transmissions to the MIT acoustics ice camp in CEAREX. Encouragingly, 25 dB SNR was obtained at 456 km from the furthest source (see Fig. 3), a good indicator

that the GSP to CEAREX transmissions should be viable. (At the time of this writing, there are positive indications that the transmissions were in fact successful.)

Pickup of the Greenland Sea tomography sources is slated for August 1989, with a week of moving ship tomography preceeding it. In the meantime, we are collecting meteorology, satellite remote sensing, hydrography, and other data from various sources to make the Greenland Sea Project Tomography a scientifically complete data set, and one of great value.

FIF Magnitude (Lin) and Phase: sono4.s5

beam angle: 0.0 degrees
doppler: 0.050 knots
r max:4159723
at loc:11591
median:70957
plot max:4159723
skipped scans:8176

law:1553
angle:87.467040
periods:3
cyc/dig:4
sam/cyc:8
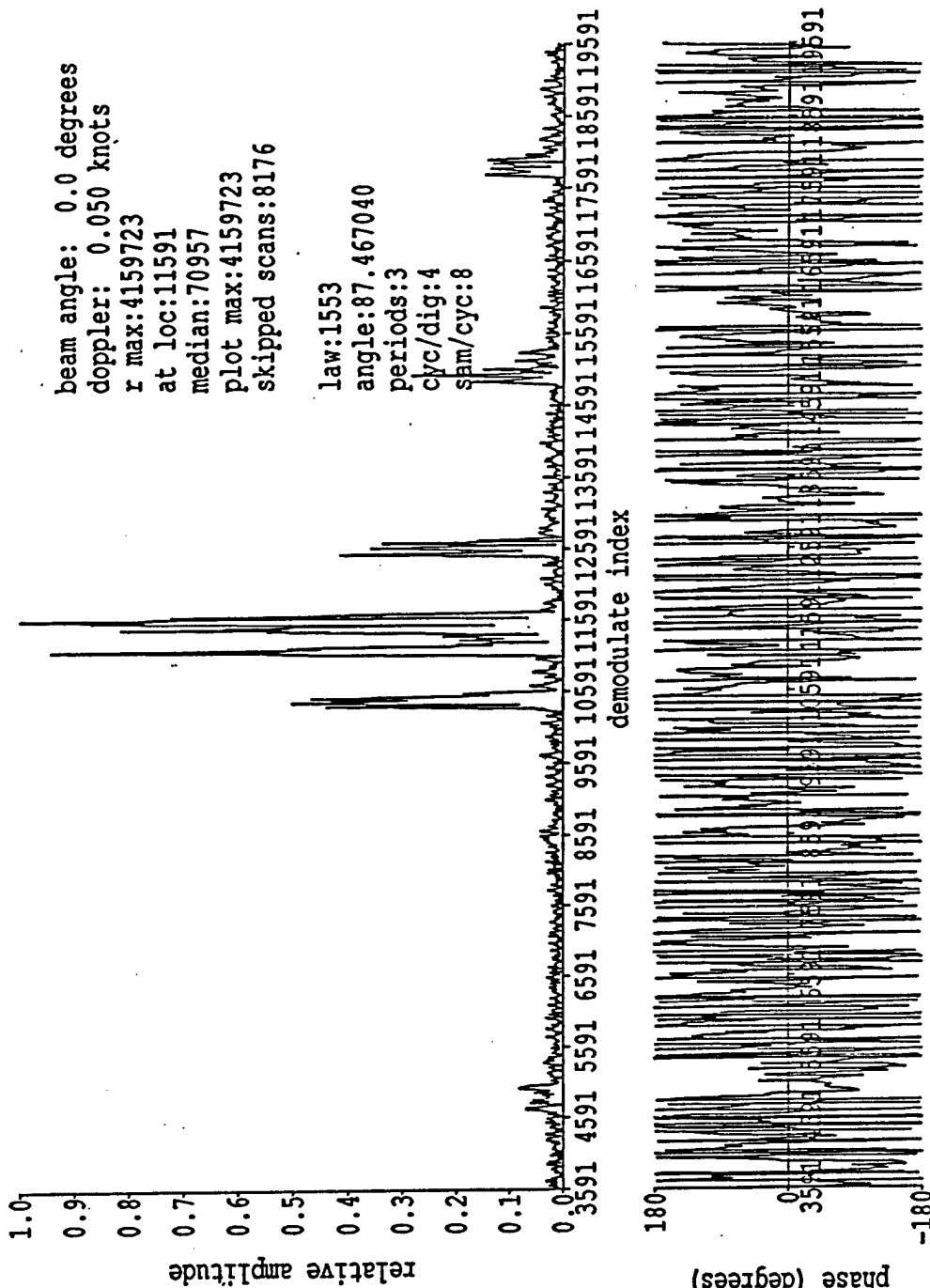
Fig 1. Arrival pattern structure seen from source at mooring 5 transmitting to a sonobuoy hydrophone near mooring 1 (z_r = 400 ft, z_s = 90 m, R = 124km). Paths with up to eight bottom reflections have been identified in this eight second long sequence, which starts near the "9591" mark. Signal-to-noise ratio is up to 35 dB for largest peaks. The data is of very good quality, but the moored array data should be even better.

63
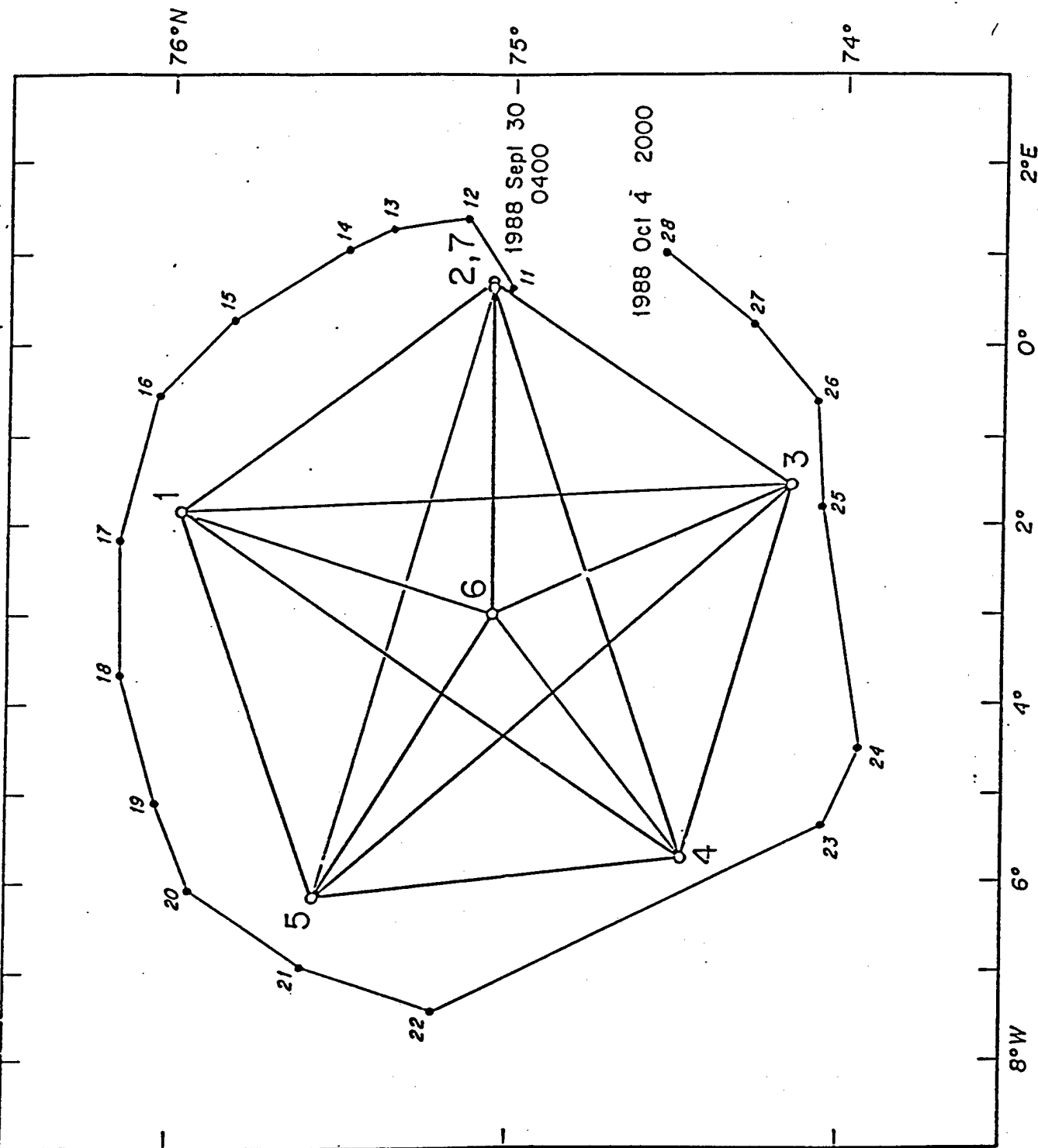
Fig 2. Greenland Sea Tomography array and the path taken around it during the Moving Ship Tomography phase of the deployment cruise.

64

FIF Magnitude (Lin): sono.jl.d4

relative amplitude

1.0 0.9 0.8 0.7 0.6 0.5 0.4 0.3 0.2 0.1 0.0

277 1277 2277 3277 4277 5277 6277 7277 8277 9277 10277 11277 12277 13277 14277 15277 16277

demodulate index
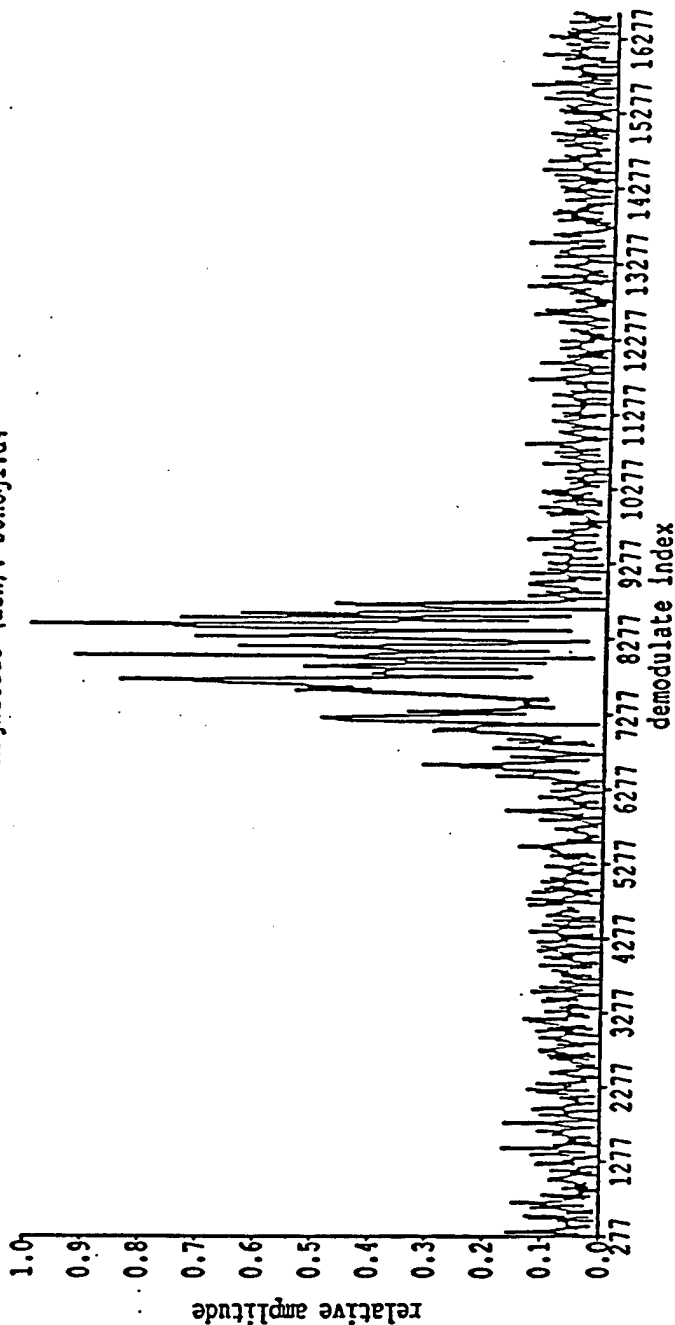
source: 4 day: 279 hour: 16
source lat: 74.481670 lon: 5.791670 (degrees)
recvr lat: 76.816667 lon: -7.809833 (degrees)
rough travel time: 315.5907 sec

law:1617
angle:87.467000
periods:3
cyc/dig:4
sam/cyc:8

plot span: 8.1760 sec
beam angle: 0.0 degrees
doppler: -0.150 knots
max snr: 24.5 dB
r max:3117658
at loc:8453
median:186746
plot max:3117658.
skipped scans:8176

Fig 3. Arrival pattern seen at 456 km from mooring number 4, showing up to 24.5 dB
SNR. This transmission has crossed both the ridge between the Greenland Sea
and Boreas Abyssal Plains and the front between the Greenland Sea and the
West Spitzbergen Current. The main purpose of this transmission was to act
as a test of expected signal strength for the Greenland Sea Tomography to
CEAREX acoustic camp transmissions in Spring 1989.

65

1 Ambient Noise at Low Frequencies in the MIZ

One can recognize in the MIZ, patterns of change in measured ambient noise that are relatively long term evolutions and relatively short term episodic behaviors. The rms pressure in a low frequency band over many days will have an autocorrelation time on the order of 4 hr, which shows a degree of persistence much shorter than its counterpart in the central Arctic (about 24 hr). Further, a weak periodic pattern is evident between about 13-14 hr in MIZ data. Neither the 4 hr autocorrelation time, nor the 13-14 hr weak periodic pattern is as yet connected with known MIZ oceanic or atmospheric properties, but is perhaps more likely connected with ice dynamical properties. (See Figures 1-3 for the ambient noise observations.)

A curious briefer episode in time has been observed that persists for about 1-2 hr. These "bursts" have been observed to propagate through the sensor field at a speed with a direction consistent with an internal wave. Presumably the internal wave affects the concentration of ice as it propagates through the MIZ, with wave banding of the ice relating to bursts or the local increase of noise. (Figures 4-7 are the data giving rise to these conclusions.)

MIT's research therefore concentrates on long term evolution within which there are various time scales such as the 13 hr or so weak periodic pattern, the 4 hr or so autocorrelation, and the 1 hr or so burst. The spatial scales of these phenomena can range from something on the order of 1 km or less, and at times from 10 km or more. Candidate environmental correlations being studied are ice concentration over large areas for long term evolution, ice concentration on a local basis that may help explain the 4 hr autocorrelation and/or the 1 hr burst, ice strain over all scales, since basically ice must be in shear and normal stress to cause noise, and finally, the role of incoming sea and/or swell in causing noise.

2 Event Physics of the MIZ

As has previously been accomplished in the central Arctic, detailed studies are underway on ambient noise at the microscopic event scale, i.e, by study of radiation caused by an individual ice fracture process. We have been able to observe MIZ events over our sensor array for frequencies from about 25 to 2000 Hz. The most important conclusion is that such events bear striking resemblance in both a qualitative and quantative sense to those studied in the central Arctic.

One can localize MIZ events, and we have shown in detail that such events occur in groups lasting perhaps for a few tens of seconds within which there might be on the order of ten separate ice fractures. Upon plotting the locations within an individual group, the ten or so fractures do not follow a unidirectional trajectory; rather fracture takes place in a hop-scotch pattern. The totality of the hop-scotch pattern is to define a shape within which the fractures have taken place, so that one can conclude, for example, that along a boundary of one floe adjacent to another, ice action in the form of fractures has caused noise.

Upon localization of each fracture, one can fit a radiation model, the most successful of which is the dipole. This result, while consistent with the central Arctic research, was surprising to us in that we expected that vertical or horizontal floe/floe shearing action under compressive stress would give rise to octupole radiation. While the basic ice action is likely as expected, what must also be happening is that small ice protruberances deform in the shearing action, causing local volume changes. The dipole radiation associated with the volume changes, although small, can nonetheless dominate octupole radiation.

Dipole forces extracted from the MIZ fracture events appear to agree well with data for the central Arctic dipole forces. (See Figures 8-14 for data leading to the foregoing descriptions and conclusions.)

Research on MIZ event physics is aimed towards better understanding of the data and extraction of dipole forces, event densities, and event patterns. Further, we are studying fracture radiation models that include edge-loaded deformation, ridge moment loading, and flexural fracture as may be due to the incoming sea and/or swell.

3 Event Physics during Ridge Building in the Central Arctic

We have returned to the 1980 Fram 2 data during which a pressure ridge was built very close to our array. The noise created locally was many tens of dBs higher than normal, and we wish to understand such pathological occurrences in the overall scheme of Arctic ambient noise. The conclusion, at least tentatively, is that ridge-building creates fracture events very much like those observed during benign central Arctic conditions and benign MIZ conditions.

The forces obtained by inversion of the dipole model for pathological ridge-building are consistent, with forces observed under benign conditions. Apparently, we are presented with an important simplification in physical thinking on the nature and interpretation of ambient noise: Ice does not care where or how it's broken. When broken, it has universal event properties. (Figures 15-17 give the supporting data.)

Our studies continue on Fram 2 ridge-building to expand the degree of overlap in the frequency domain between pathological and benign conditions. We are also pursuing research on radiation from cracks in the central Arctic that may be quite long and which would open at supersonic speeds, the latter giving rise potentially to horizontal directivity effects.

4 Event Density as a Measure of Noise Level

If all events are created equal, what then in this democratic physics would account for the aristocracy of low noise at some times and places, and the serfdom of high noise in others? The most plausible hypothesis at this stage is that the number of fractures per unit area, per unit time (i.e. the event density) is the measure of total strength of noise radiation.

By comparing the benign event densities from the central Arctic, the benign event densities from the MIZ, and the pathological event densities from Fram 2 ridge-building, we can conclude that event density is indeed the most likely metric for the overall noise. Our preliminary results, for example, show that MIZEX 84 event densities are about 6 dB higher than the Fram 4 event densities, which in turn, are about 35 dB quieter than

the Fram 2 ridge-building densities, and these values are consistent with the overall noise data. (Figures 18-20 show these comparisons.)

MIZEX 84

25-50 Hz band
3-5 min average
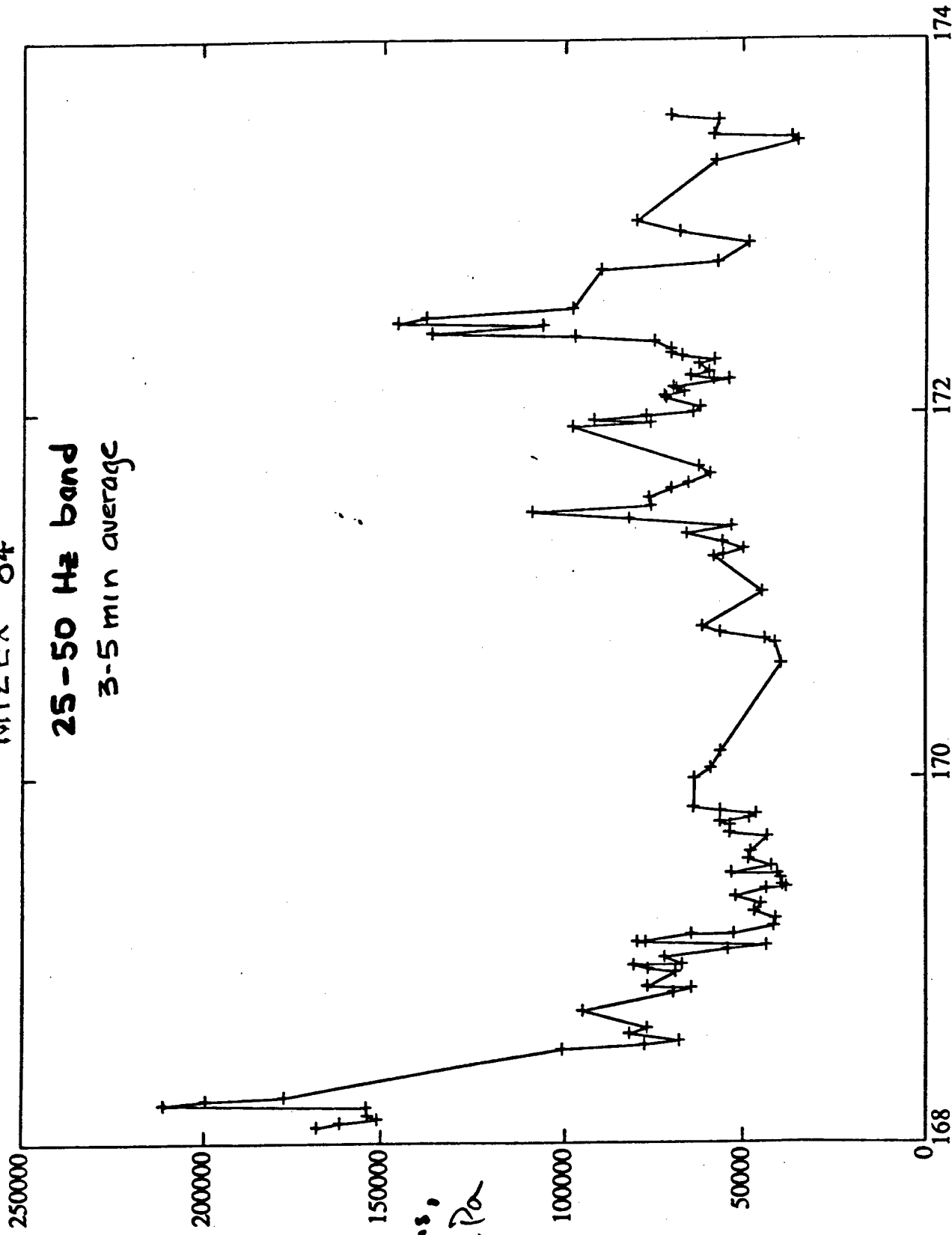
Wed Oct 19 12:27:58 1988

J day

antilog-d6.short.edit3

P_rms,
micro Pa

$T(1/e) \sim .18 \text{days} = 4.3 \text{ hours}$
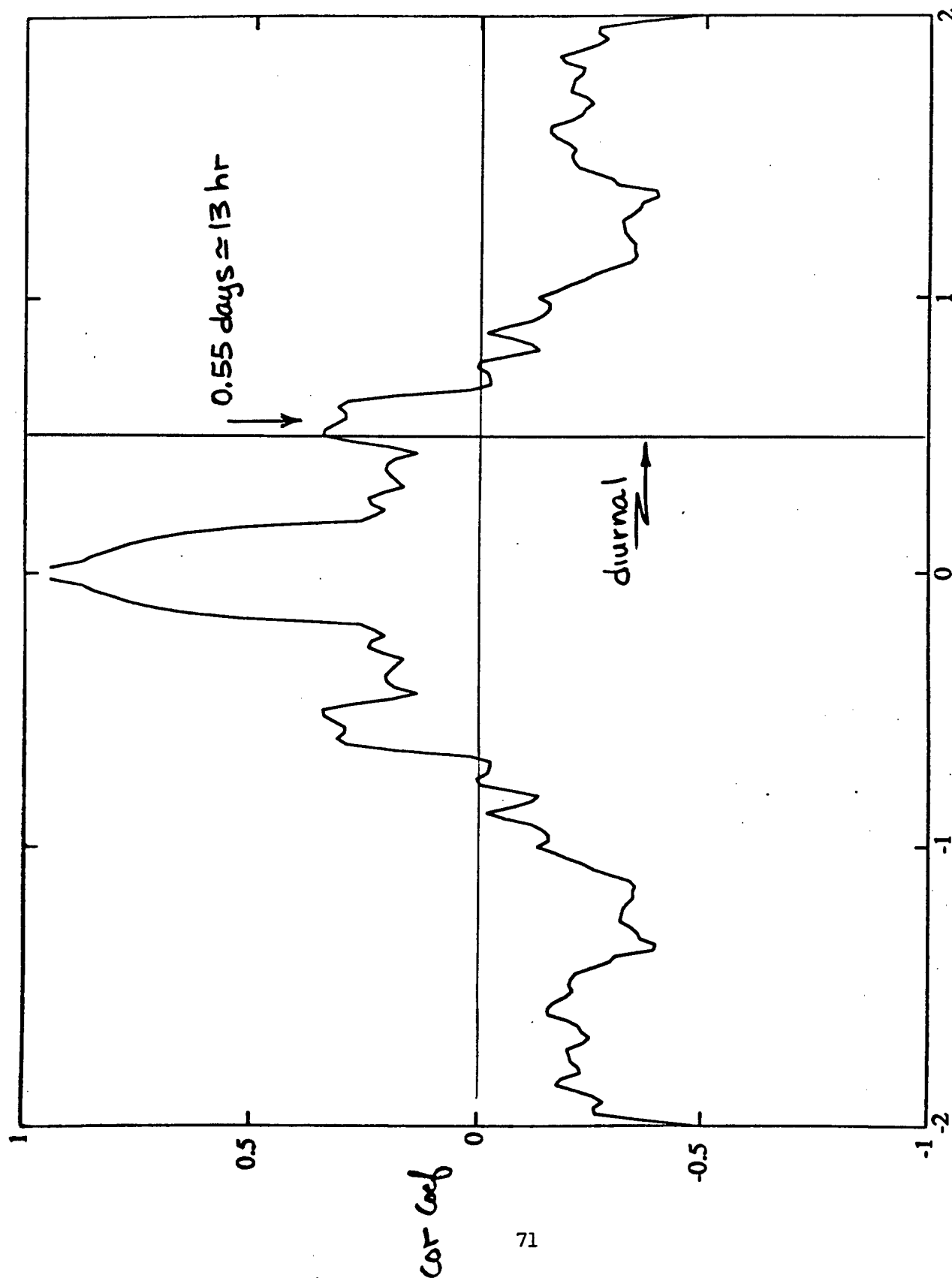
$0.55 \text{ days} \simeq 13 \text{ hr}$

diurnal

Cor Coef

Cros1:antilog-d6.short.edit3.int.0-antilog-d6XhartCedit3Xia800:43 1988

71

diurnal

1.73 cyc/day
≈ 0.58 day
period
(14 hr)

dB re
1 unit Po
72
cycle/day

Wed Oct 19 12:57:45 1988

Cycles/i)

antilog-d6.short.edit3.int.spec
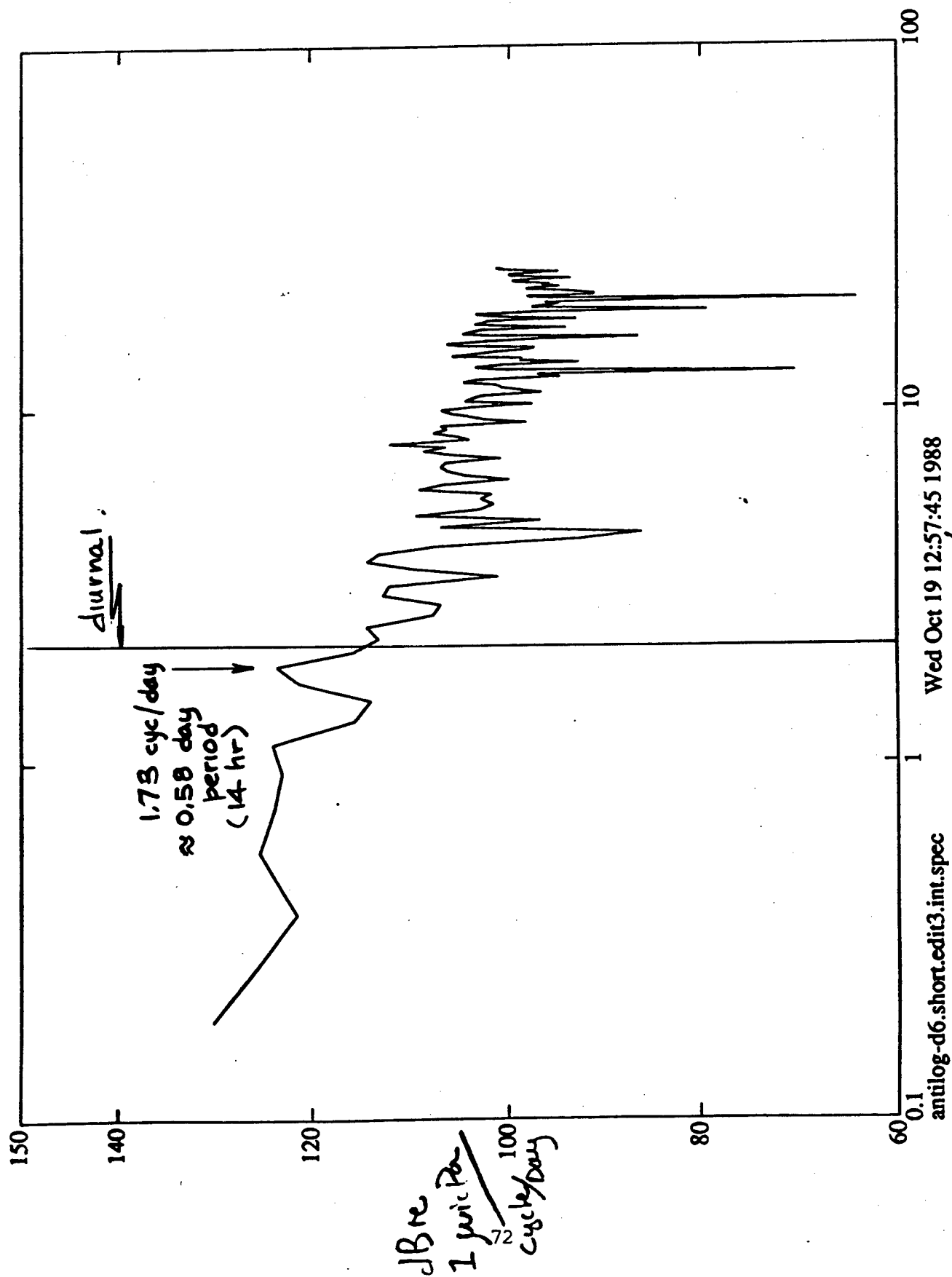
$\Delta T \sim .06 \, day \sim 1.4 \, hr$
($\tau_{autocorrelation} \sim 4.3 \, hr$, for 6 day record)

Prms, μPa

300000

200000

100000

0

171.2 171.3 171.4 171.5 171.6 171.7
Wed Oct 19 13:31:49 1988

Julia, day

rms pressure

p_{rms}, Pascal

D19

D8

D4

.2

.1

.0

D24

D10

D6

D5

171.2   171.3   171.4   171.5   171.6   171.7

Julian Day

74
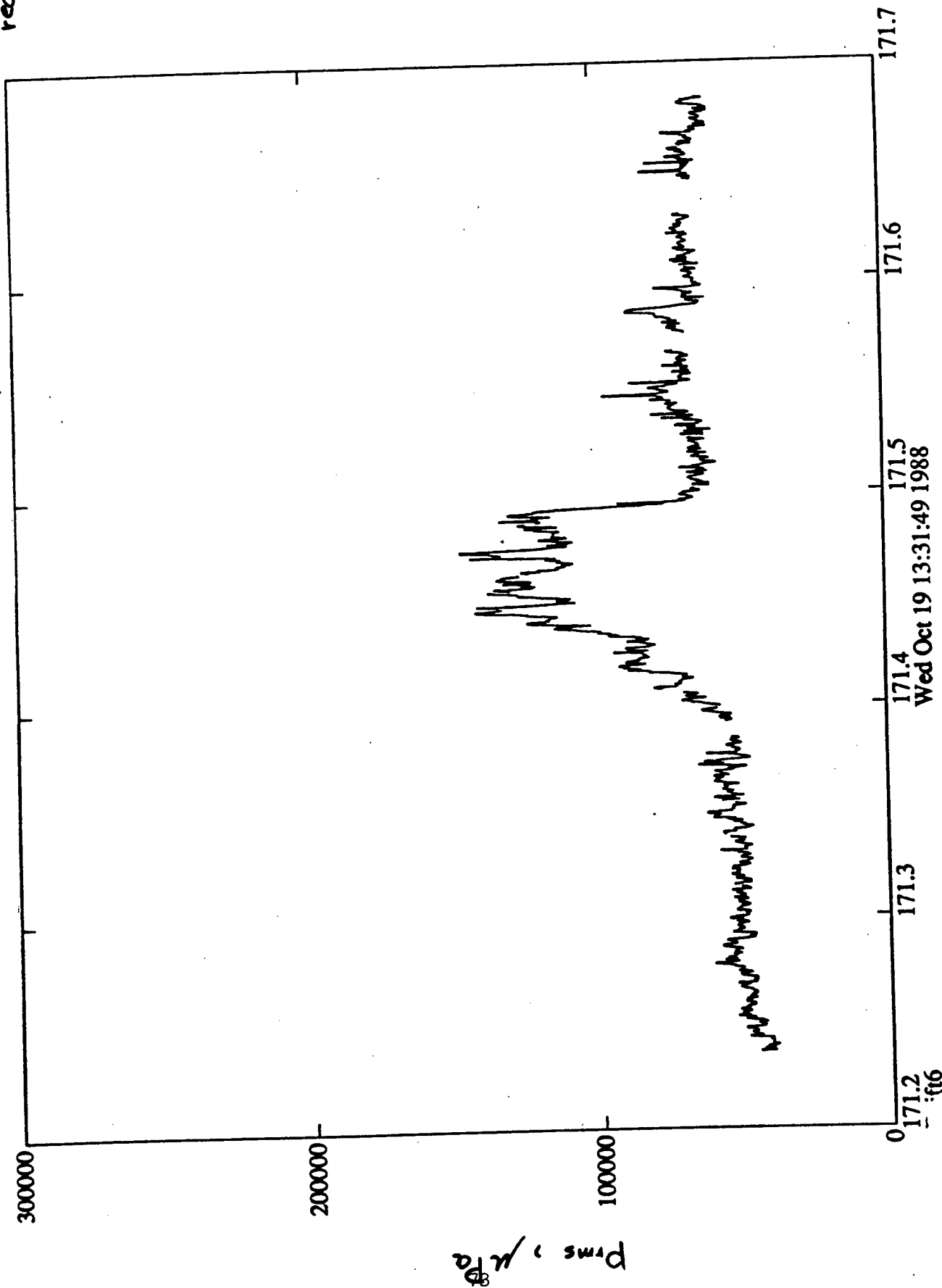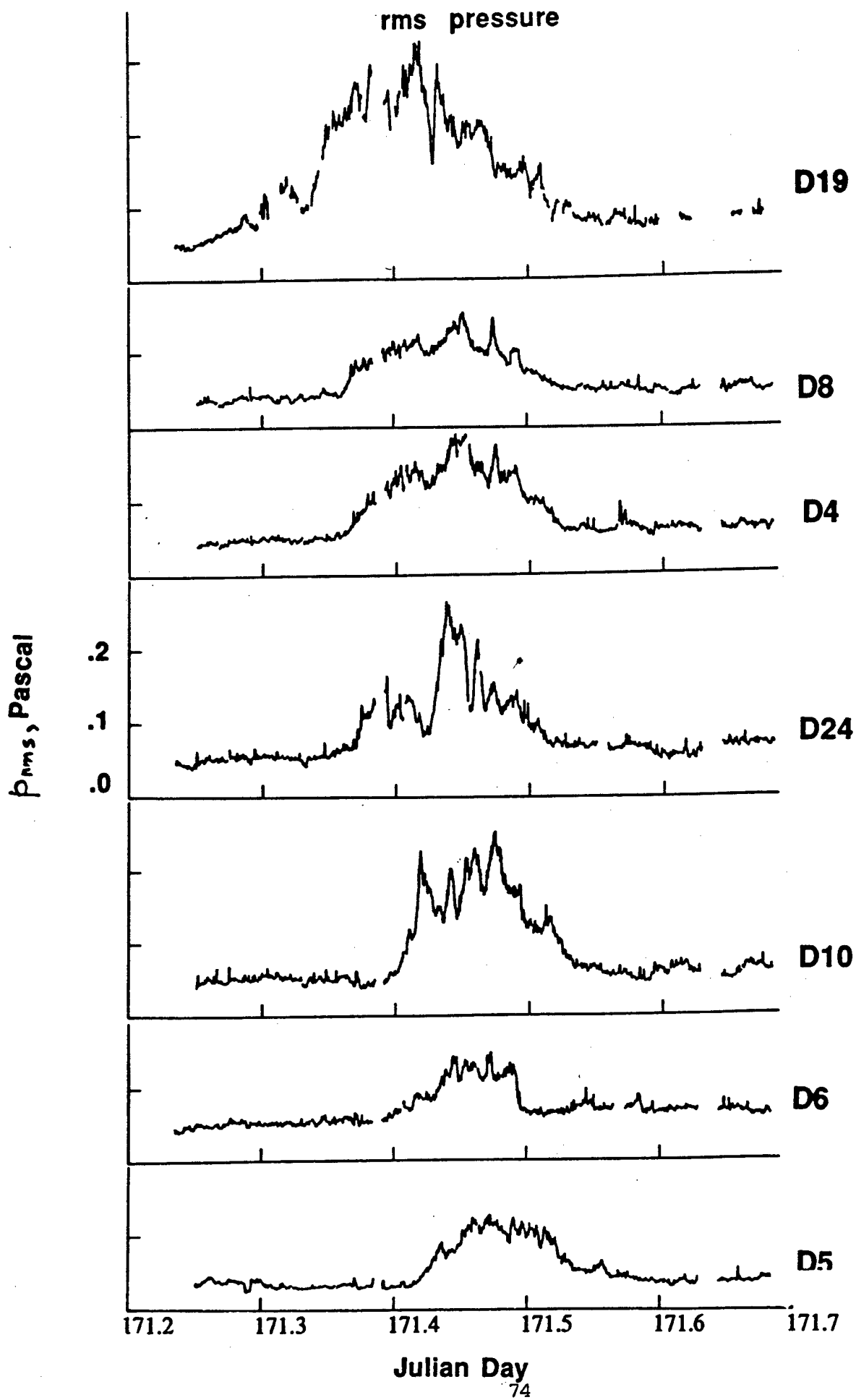
Cross with D19 fixed

(cor. coef. , time lag)
(MIN)

ship

km

50
(.5,+50)
D5

25

D6 (.6,+29)

N

$C_g \sim 3.2$ km/hr

(.6,+51)
D10

(.7,+26)

D24 D4
D8
(.8,+37)

D19

(.6,+27)

(1,0)

6

5

4

3

2

1

1   2   3   4   km
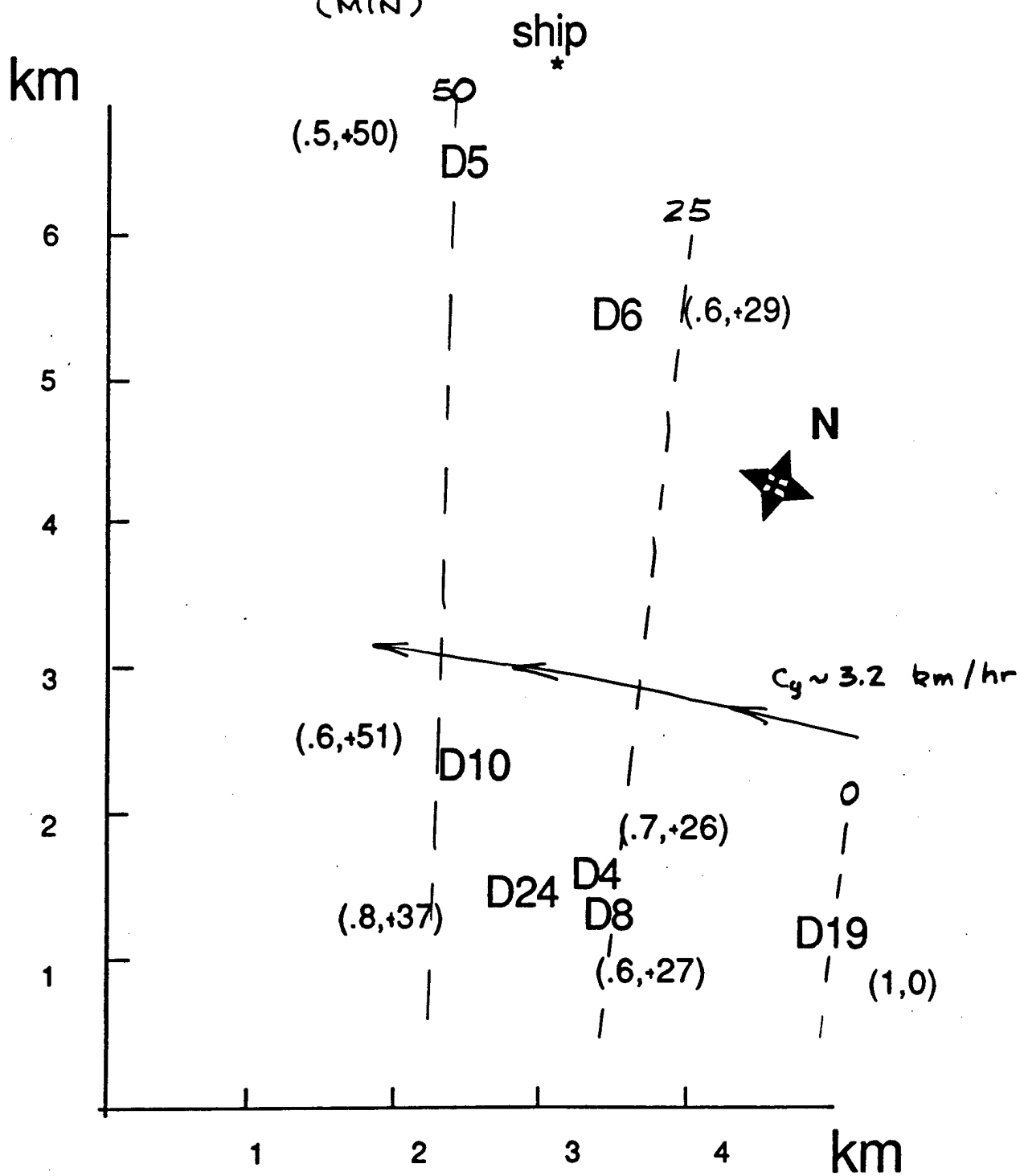
SPATIAL VARIABILITY OF STRAIN RATES
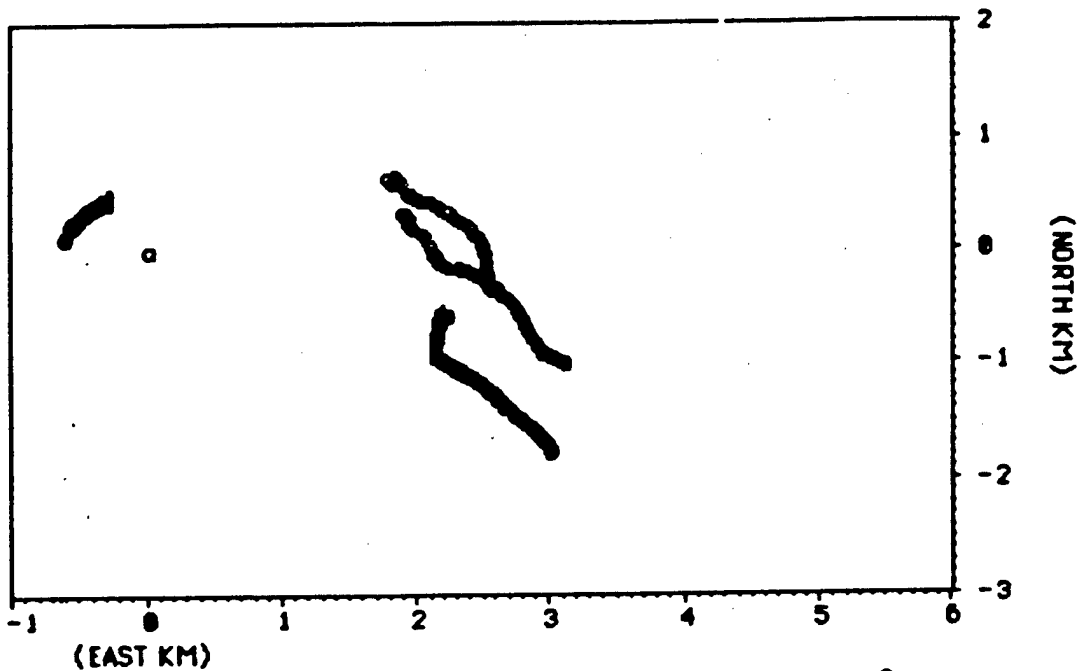
%/HOUR
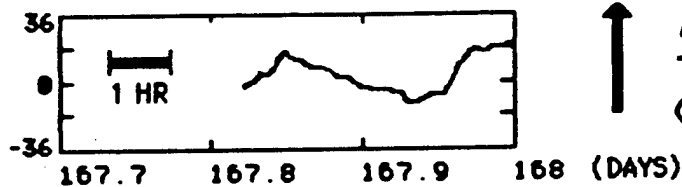
Period:
T ≳ 3.6 hr
(T/3 ~ 1.2 hr)

DIVERGENCE
RATE
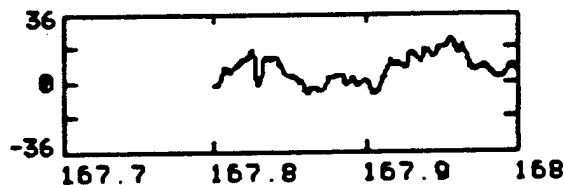
Period:
T ~ 3.0 hr
(T/3 ~ 1.0 hr)

FILE: gevent.3.6   DATE: Thu Dec 8 16:16:17 1988   ZERO= 0   GAIN= 0.8   VRED= 0   XFILE= ./array6
MAXF= 0.449939   MINF= -1.20146   FL=100   FU= 0   DEC= 1

t, SEC
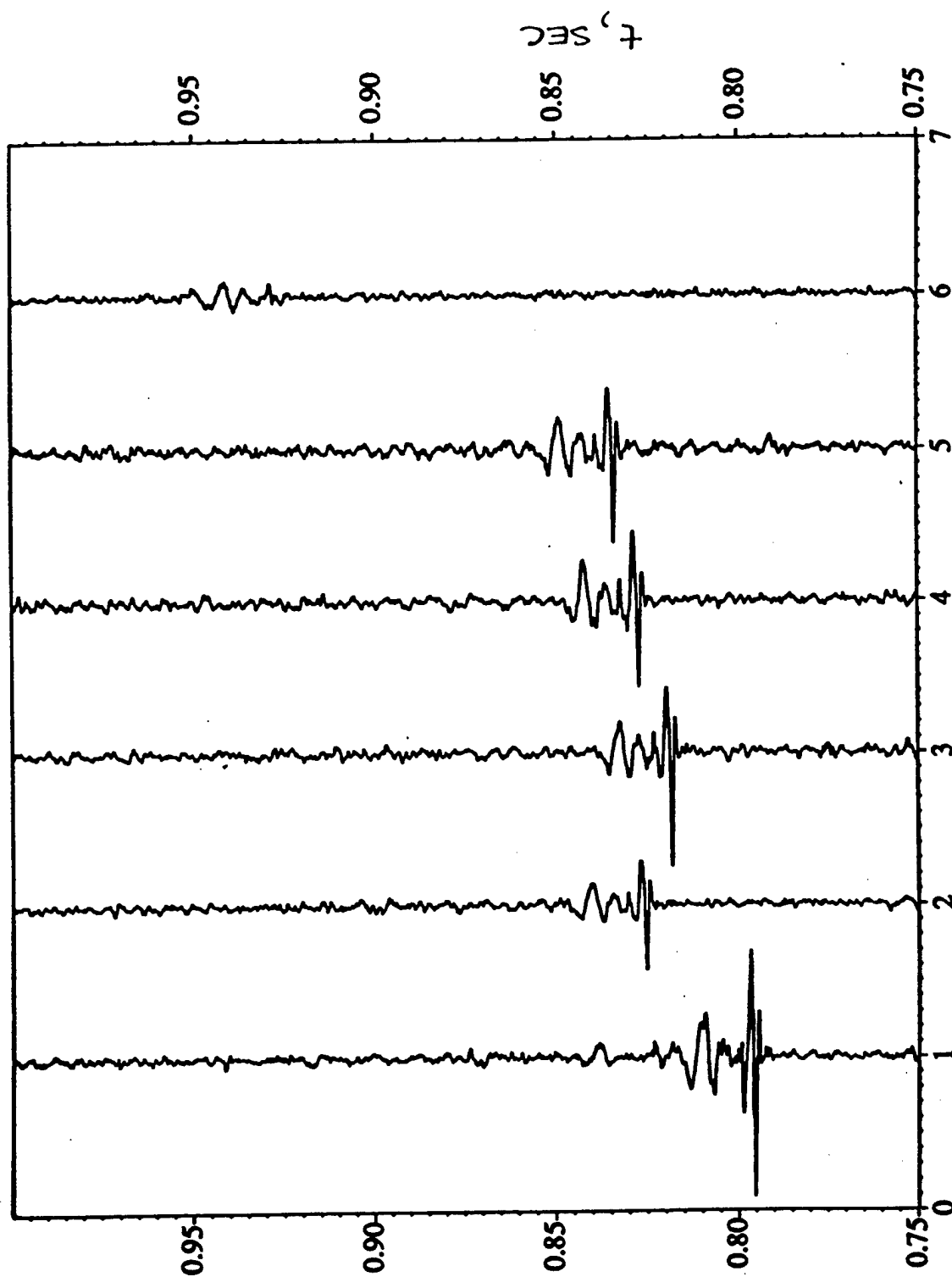
MIZREAD nskip=88 nseg= 4
manip -gain pts 0-1399 rows

77

FILE: gevent8.3.6   DATE: Thu Dec 8 16:26:10 1988   ZERO= 0   GAIN= 0.8   VRED= 0   XFILE= ./array6
MAXF= 0.449939   MINF= -1.20146 FL=15 FU= 100 DEC=1
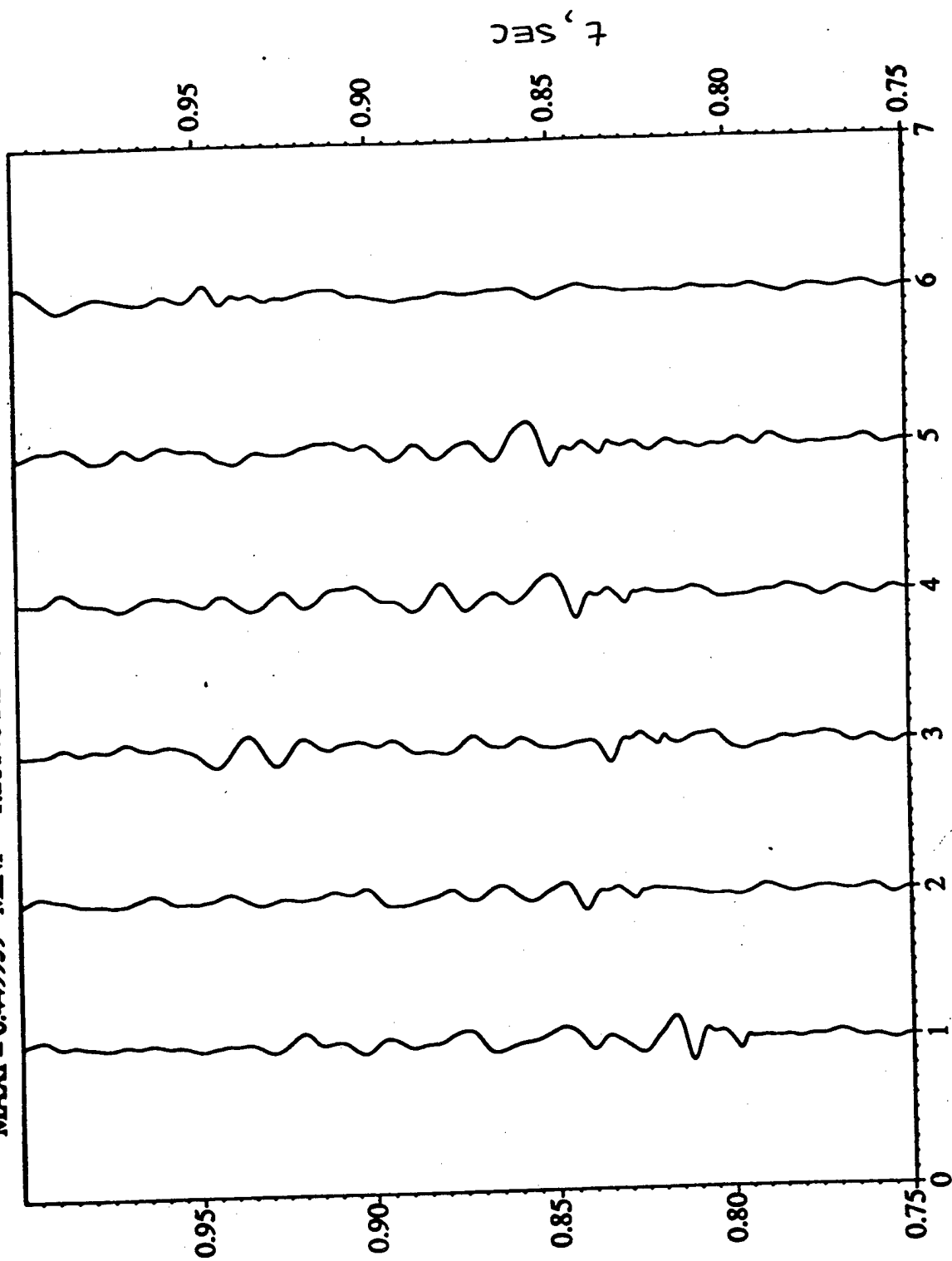
t, sec

MIZREAD nskip= 4
manip -gain pts 0-11399 rows

event8.3.g 1 to 49.907 by 2 fmin= 0 fmax= 49.907 zero= 0
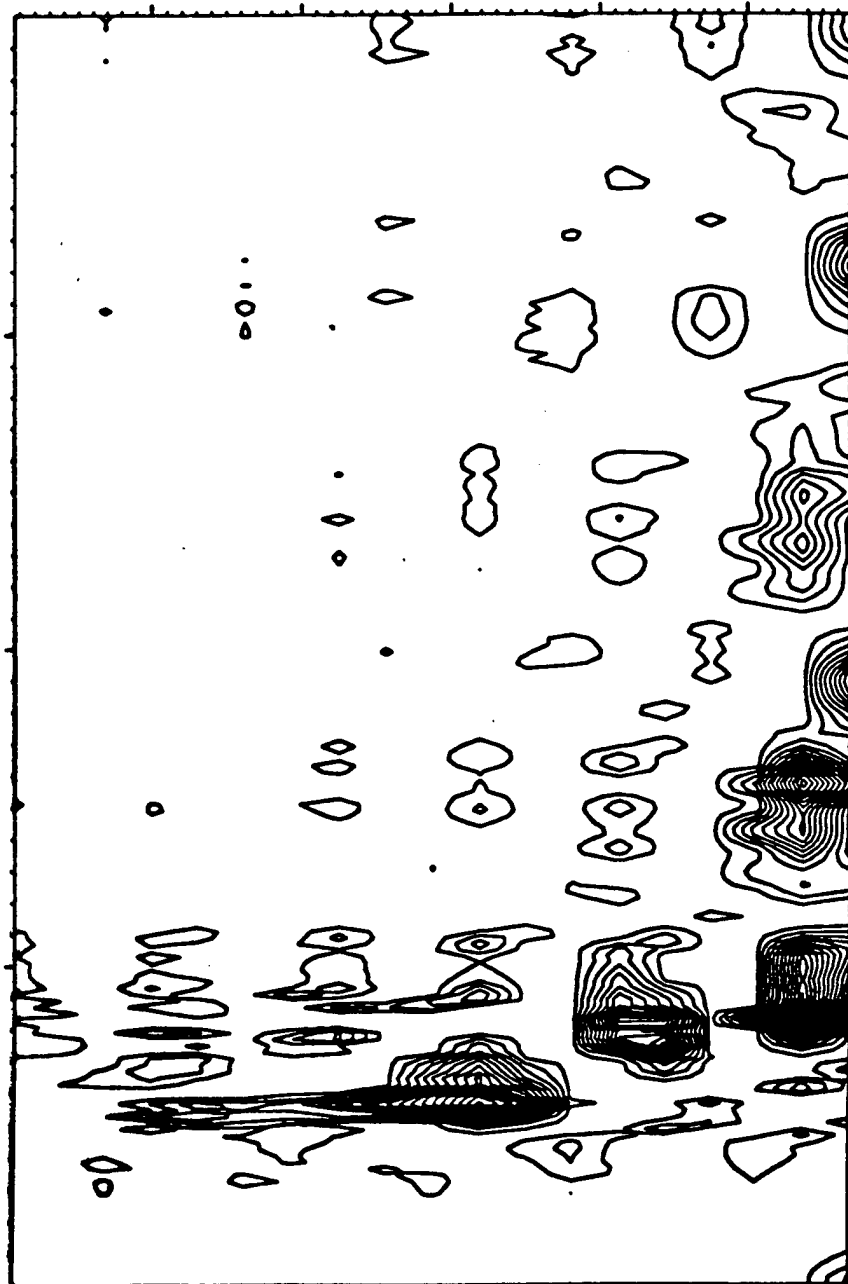
gtfrf -dhead -gld 3 start 0.0000 t 0.70-1.00,T 0.0100,T 0.0100 nT1 81 adv 0.0010 fft 128 f 31.25-2000.00

MIZ
200-1400 Hz

Duration (sec) vs **Cluster Number**

Values: 38.6, 38.6, 32.5, 72.2, 37.3, 13.1, 27.1, 16.7, 15.7, 55.3, 18.8, 21.2, 12, 16.2, 43.4, 42.9, 1, 22.3, 44.3
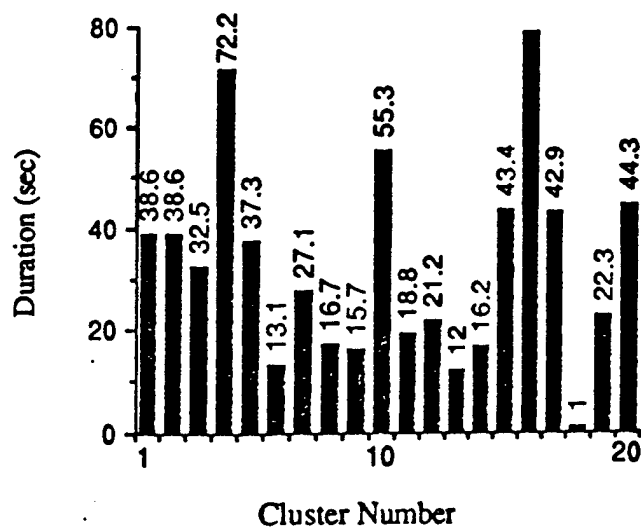
mean = 32.4 seconds ~ 0.54 min

stddev = 19.7 seconds

Inter-arrival Time (sec) vs **Cluster Number**

Values: 68.9, 157.4, 53.9, 96.7, 36.8, 137.5, 30.8, 31.6, 38.4, 31.8, 60, 48.1, 186.6, 138.2, 65.3, 39.4, 28.1, 29.9, 45.8, 62.1
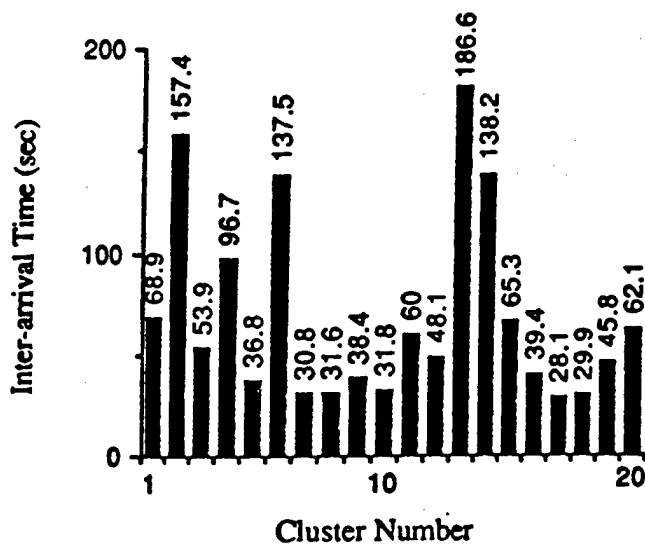
mean = 69.37 seconds ~ 1.2 min

stddev = 46.7 seconds

80

phones

Y-axis: DIST, m (values 90, 92, 94, 96, 98, 100)
X-axis: DIST, m (values 5, 6, 8, 10, 12, 14, 15)

Points:
2 △ (~8.9, 97.2)
3 △△ 6 (~9.6, 97)
△5 (~10.6, 95.5)
△11 (~9.2, 94)
△8 (~11, 93.5)
△9 (~10.7, 92.8)
△4 (~12.1, 91.1)
△12 (~13.5, 90.3)

cluster3
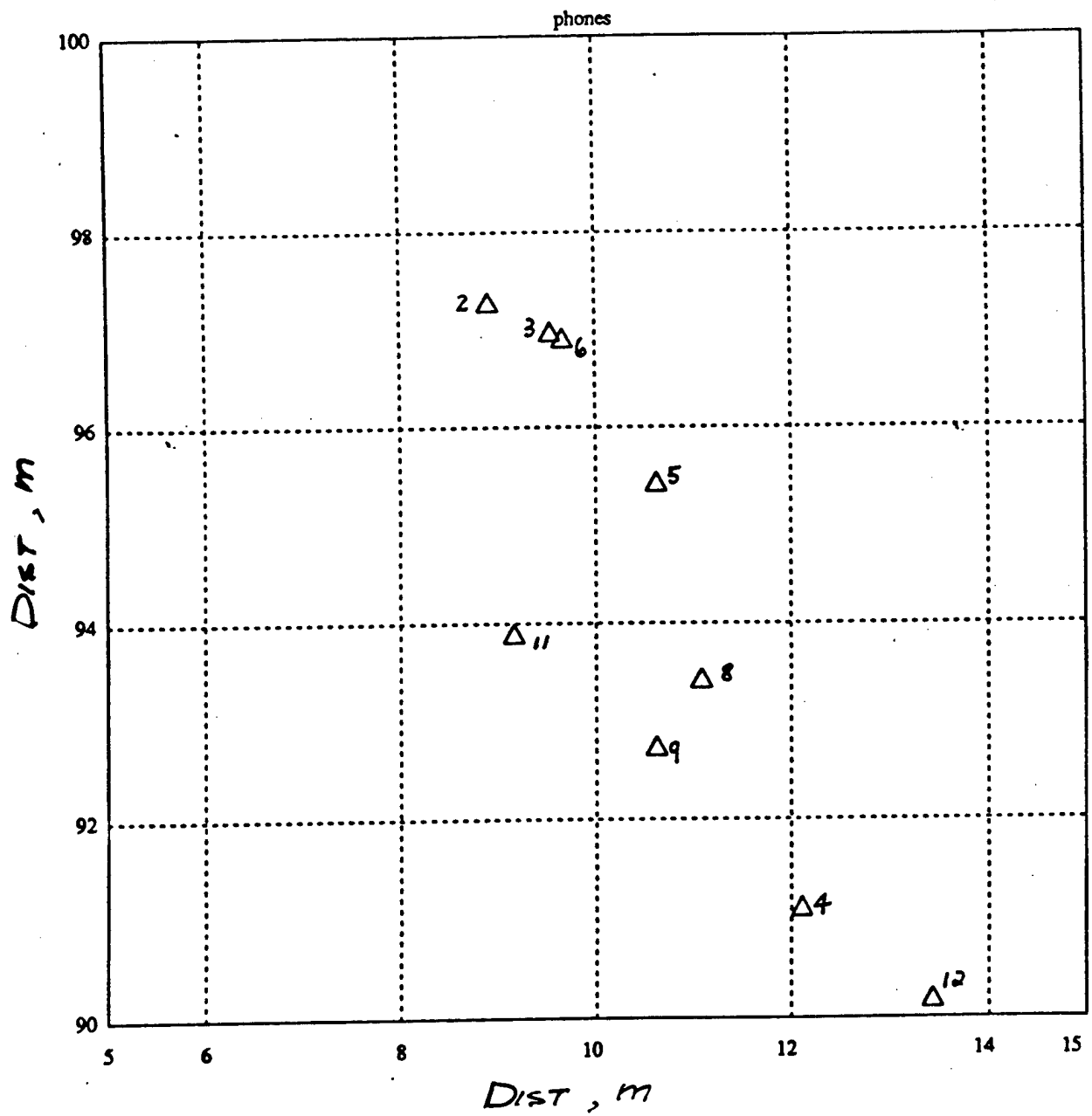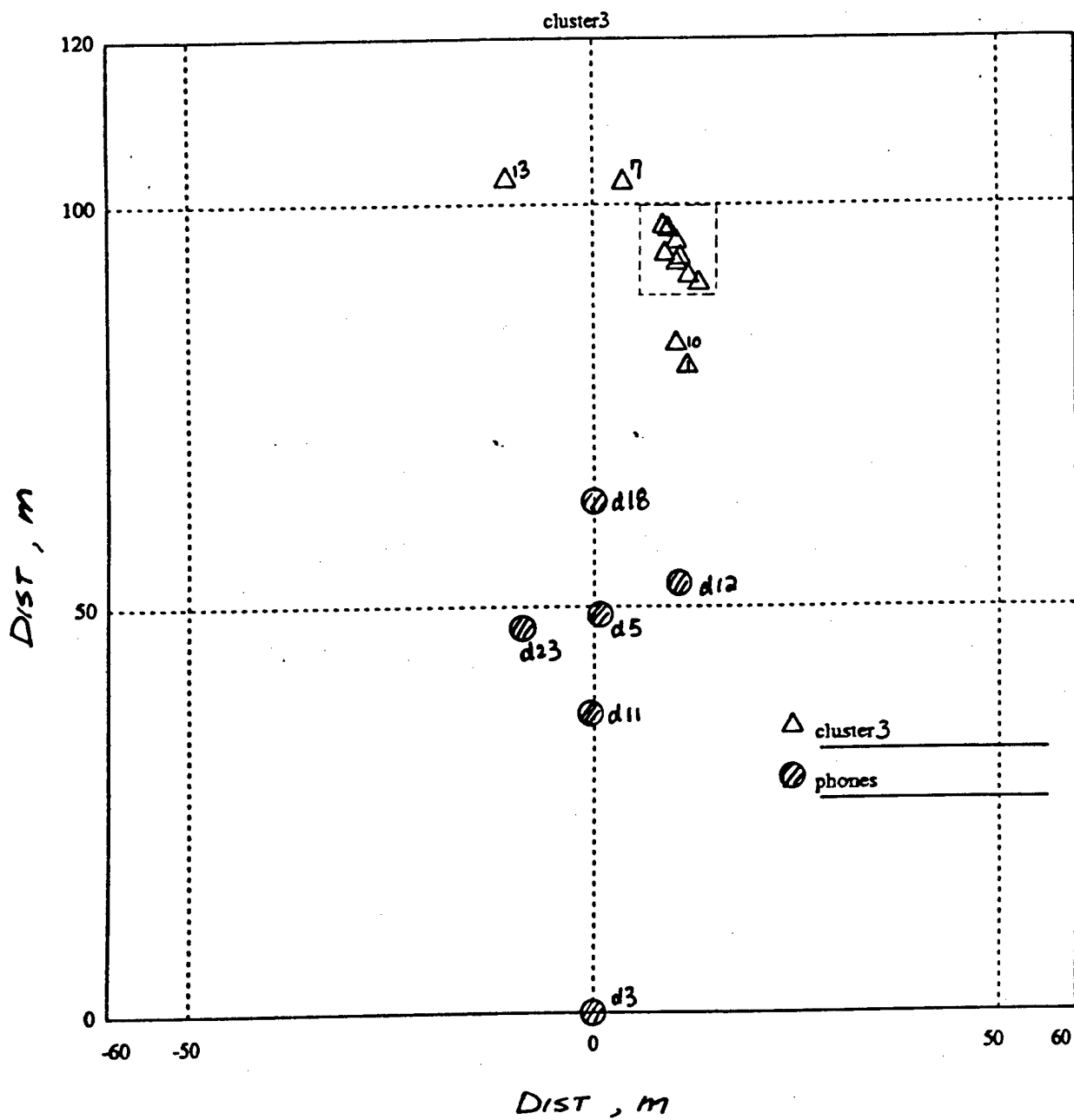
log10(dipole force [N]) = -1.38917 * log10(peak freq [Hz]) + 7.17999

linefitting coeff r = 0.594844

total number of events = 114

DIPOLE_FORCE
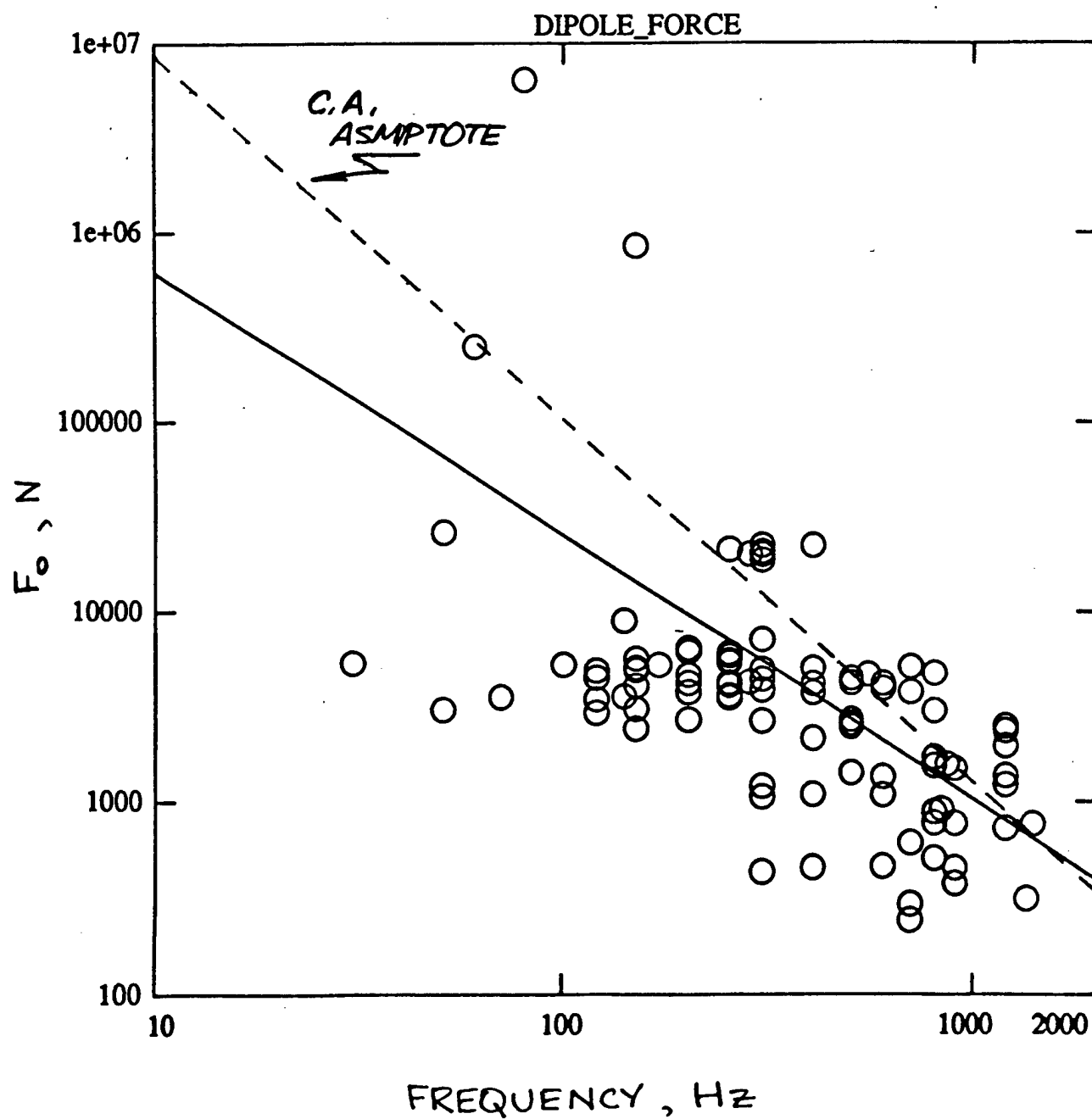
FIGURE III 'Ridge Building'

LOCATION OF EVENTS

$N \sim 80/km^2/hr$
from 10 to 15 Hz
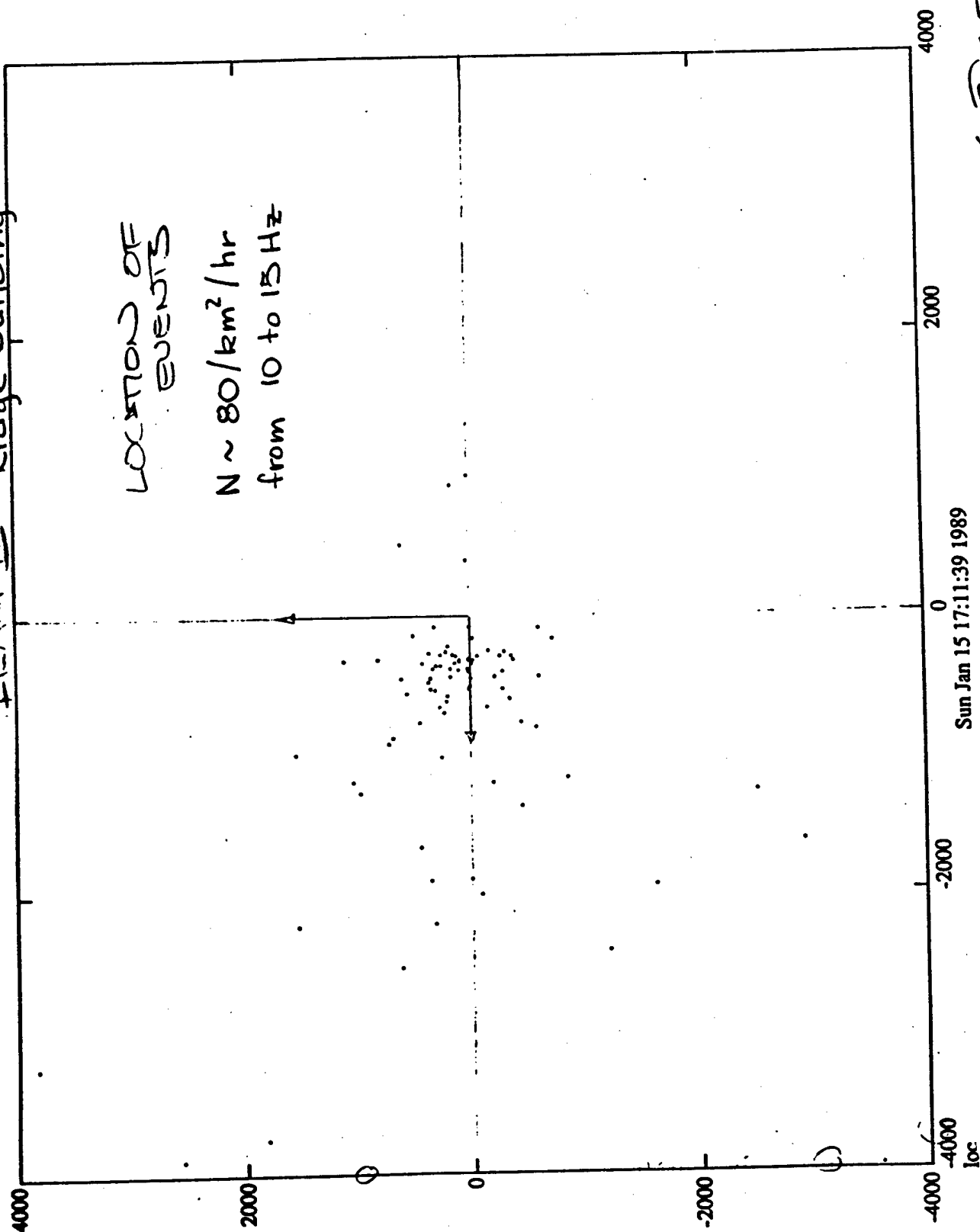
Sun Jan 15 17:11:39 1989

loc

K LARGE 160/3

FRAM II Ridge Building

DIPOLE FORCE, N

FREQUENCY, Hz
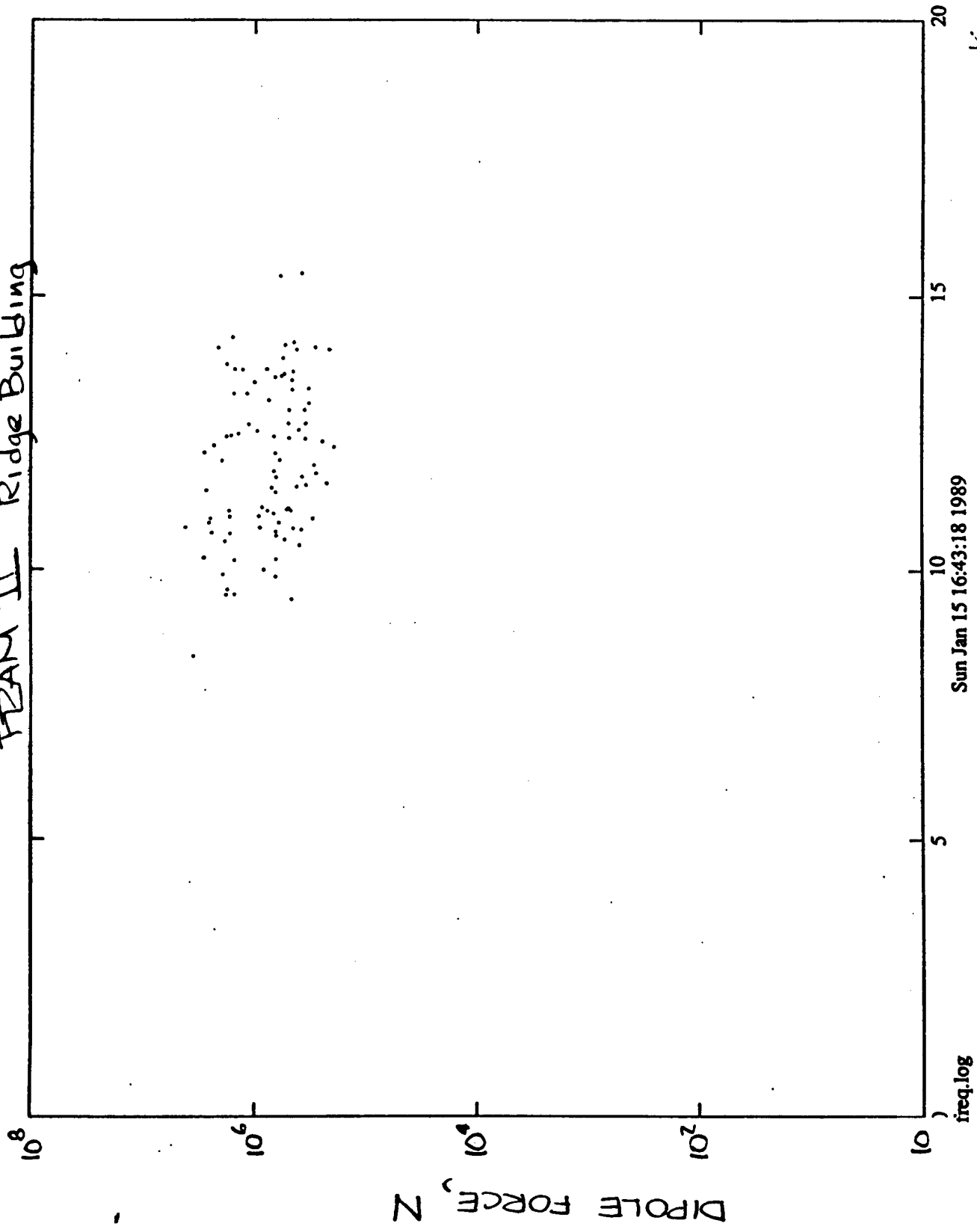
Sun Jan 15 16:43:18 1989

freq.log

85
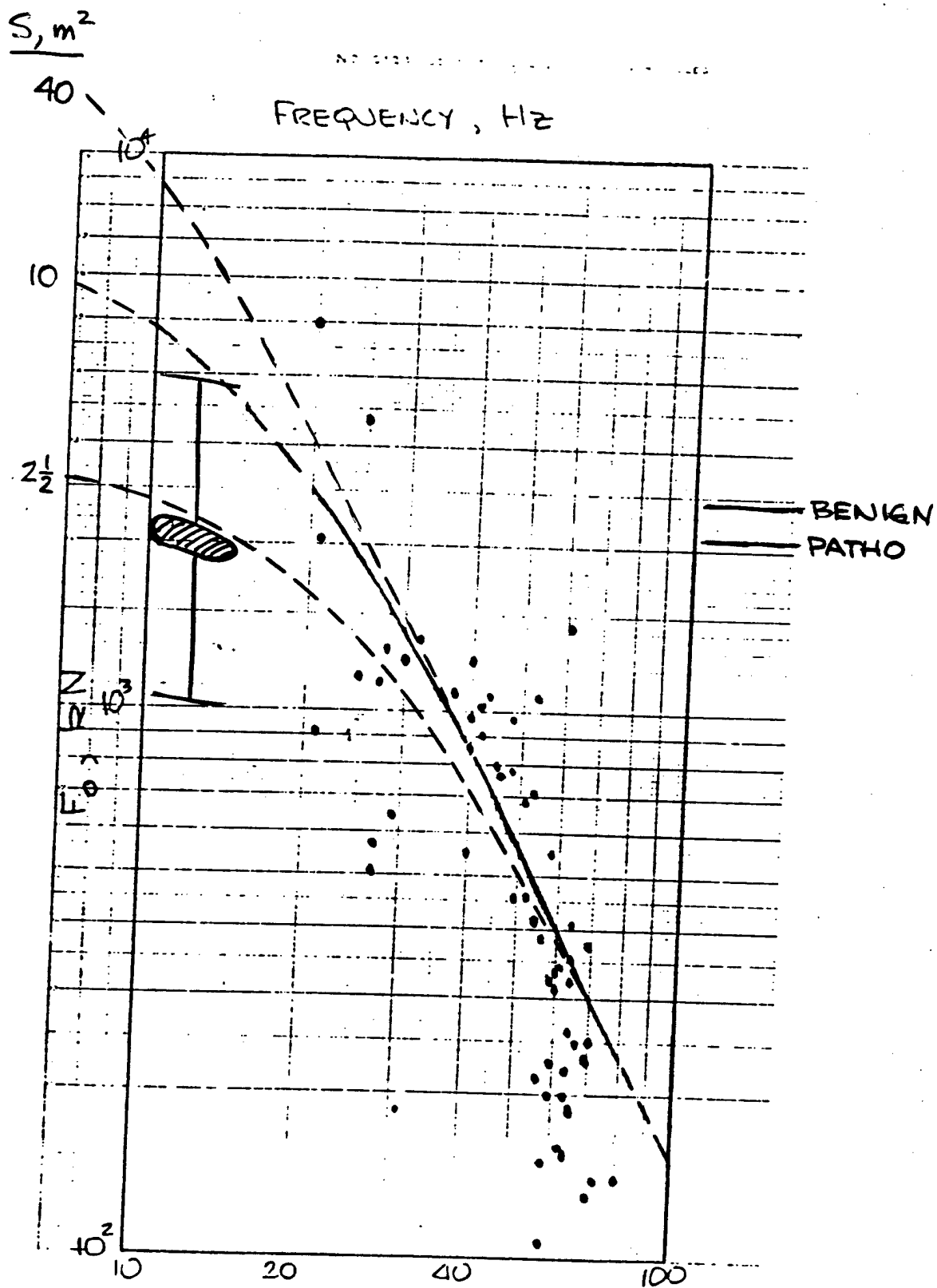
$F_o(f \to 0)$ LIMITED BY 1 MPa SHEAR
STRENGTH THRU SECTION AREA S.

FRAM IV BENIGN

10 log η, dB re 1 Hz

FREQUENCY, Hz
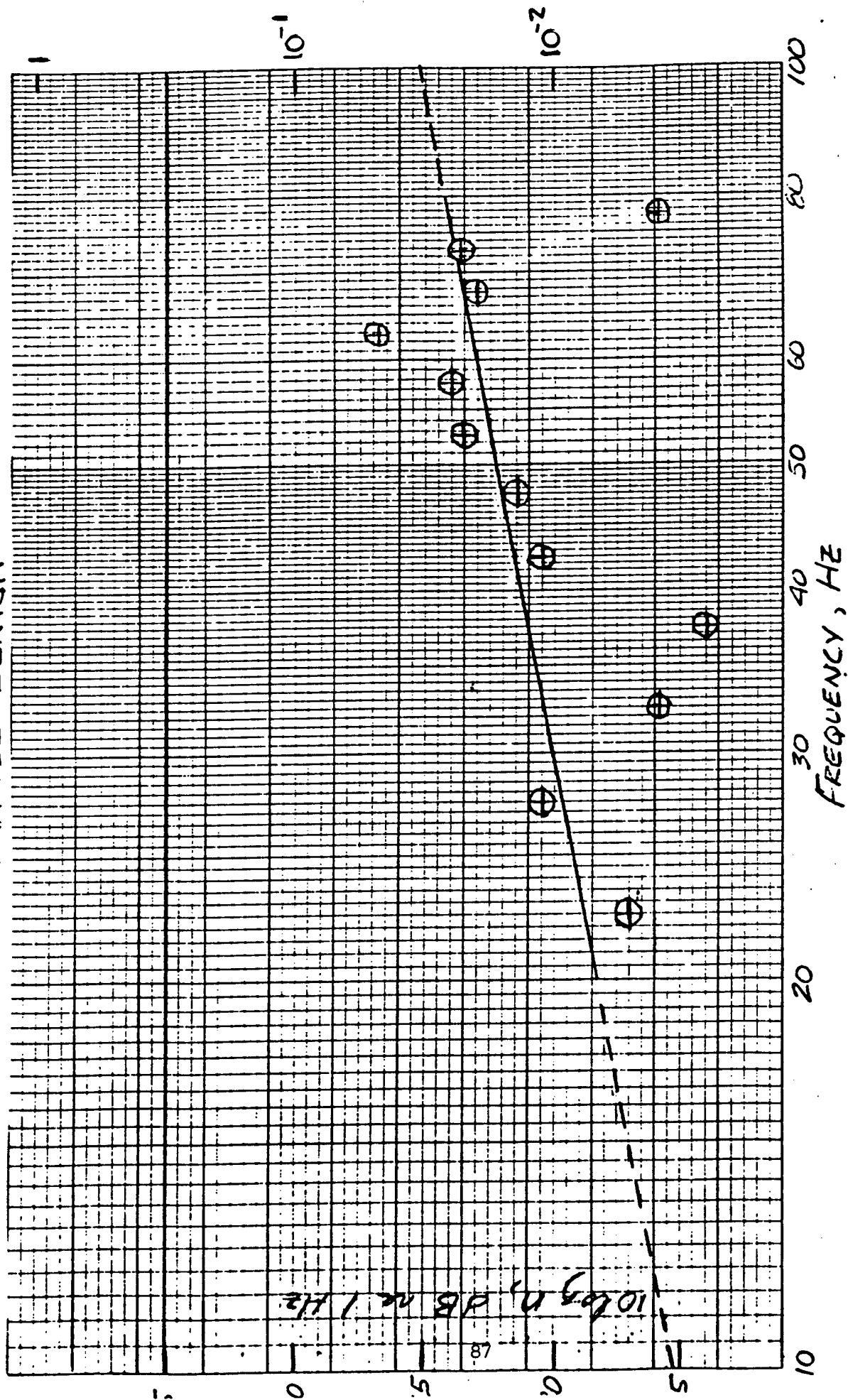
log10(event.den) = 1.37019 * log10(peak freq) + -1.63, for 100<peak freq<300

log10(event.den)= -1.33459 * log10(peak freq) + 4.79, for 300<peak freq<2000

EVENT_DENSITY
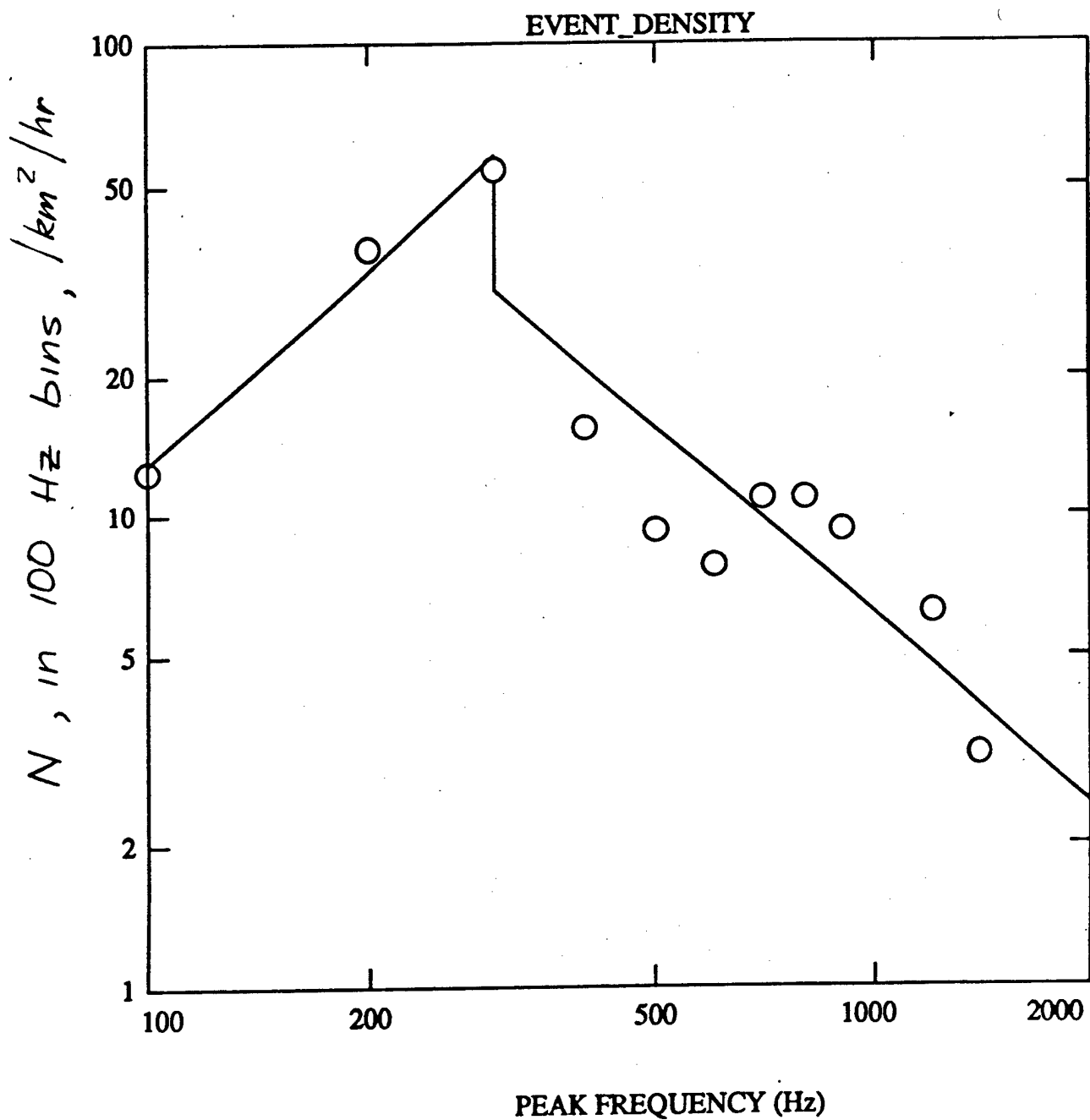
PEAK FREQUENCY (Hz)
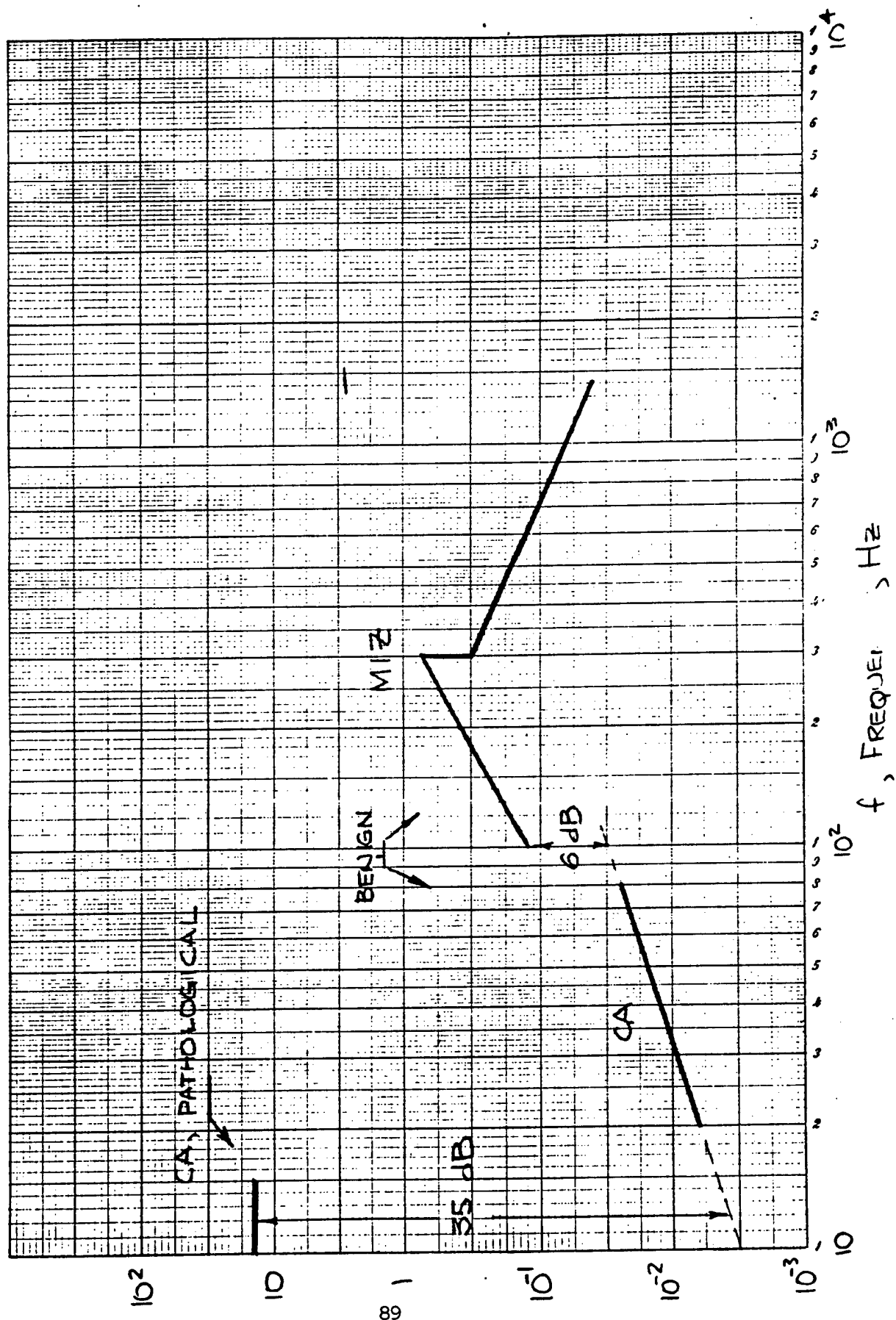
Arctic Ambient Acoustic Noise Relationships
to Ice kinematics and Heat Flux
Presented by James Lewis, SAIC

Ambient noise in ice-infested waters is significantly different from that in open oceans. The reason for this is the presence of the thin veneer of sea ice, an often highly brittle, wind driven substance that can cover large areas. One may ask what specific mechanisms within sea ice result in under-ice noise. This is a difficult question to answer for a number of reasons. First, the extent, thickness, and rigidity of sea ice varies with season and region thus introducing temporal and spatial variations in the cause/effect relationships. Also, identification of all mechanisms within an ice cover which could possibly cause acoustic noise is still hypothetical. Moreover, one mechanism could cause noise across a broad band of frequencies, with the result being the masking of other noise variations induced by a different mechanism. Finally, the difficulty of working in the remote and cold regions of the poles has resulted in a relatively limited collection of noise and environmental data to study.

Despite these problems, some progress has been made in relating under-ice noise levels to sea ice phenomena. Milne(1972 JGR 77 pg 2177-2192) found that higher frequency noise(kHz) variations could be related to the thermal cracking of sea ice, in an area of landfast ice. The noise occurred only when the air temperature dropped. Greene and Buck(Navy J of Underwater Acoustics,28(4) 1977) correlated atmospheric pressure gradients with ambient noise levels in the Beaufort Sea, obtaining correlations of the order of 0.6. This was a reasonable result , seeing that wind is the primary force on sea ice. Pritchard(1984 JASA 75(2) pg 419-427) used a ridging model to calculate energy dissipation, and he then correlated the energy levels with noise intensity at 10 and 32 Hz noise variations for several 20 day periods during the 1975-76 winter in the Beaufort Sea achieving correlations of 64%. Makris and Dyer(1985 JASA 79(5) pg 1434-1440) used current, wind, Coriolis force, and ice motion data to compute internal ice stresses and bending moments from steady-state equations for ice motion. Although the data consisted of a nine day time series, the correlations of the magnitudes of stress and moment variations with ambient noise at low frequency (10-20 Hz) produced correlations of 0.81 and 0.87 respectively.

SAIC has worked with noise data collected during the Arctic Ice Dynamics Joint Experiment(AIDJEX) in 1975-76. The characteristics of the noise are discussed in Lewis and Denner (1988, JASA 83(2), pg 549-565). In this paper, a statistical model is used to investigate ice/noise relationships. Ice motion was determine by satellite-tracked drifters on the ice and this motion was decomposed into its five components; translation , vorticity, divergence, normal deformation and shear deformation. Figure 1 shows the locations of the buoys examined and Figure 2 illustrates the five basic components of ice motion. Correlations between ice motion components and ambient noise intensity showed different components correlated for different seasons but correlations varying from 0.6 to 0.84 could be achieved(Lewis and Denner 1988, Sea surface Sound pg 565-581). During the summer, observations indicate that most under-ice noise is generated by the ice rushing through the water. Differential motion appears insignificant. This situation changes by fall when the total deformation of the pack ice becomes important in producing lower frequency noise(10-20 Hz). Ice convergence(could be ridging, shearing during reorientation and fracturing due to high internal stress) becomes important in the winter as

open water disappears. At higher frequencies(1000 Hz), fall and winter data appear to be a combination of both stress/motion induced and thermal cracking. A heat flux model has been developed by Lewis that indicates that long wave radiational cooling of the ice should produce stress levels that fracture the ice but the process is very dependent upon the snow covering of the ice and cloud cover that interrupts radiation. Ice rheology has been incorporated into the model and sound radiation versus crack location in the ice column have been consider theoetically(Lewis and Denner, 1988 JASA 84(4) pg 1444-1455). This most recent work indicates that higher frequency Arctic ambient noise is highly variable due to the ice rheology. The rheology, a function of the most recent history of stress levels as well as temperature, often results in inconsistant noise patterns at higher frequencies under the ice.
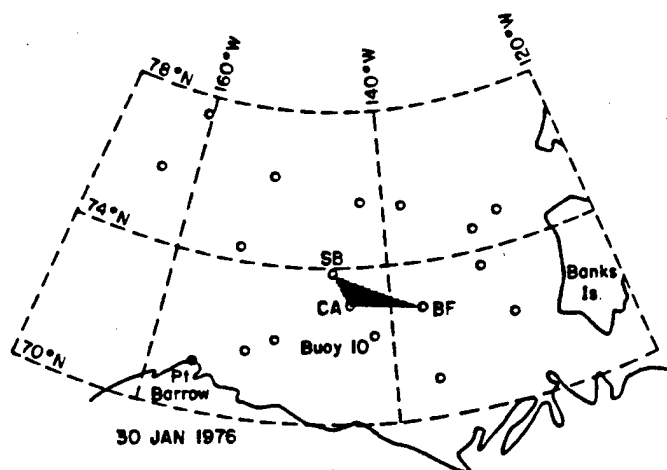
Fig. 1. Locations of a number of AIDJEX data buoys and manned camps (SB, CA, and BF) for 30 January 1976. Station 10 acoustic data discussed in this paper were collected at Buoy 10.
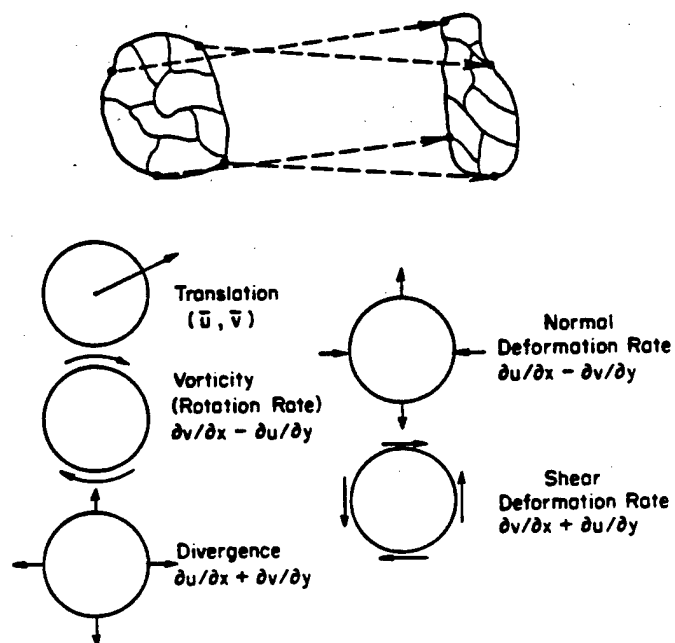
Fig. 2. Mathematical and physical definitions of the five basic components of the motion of a parcel of ice.

92

Acoustical Scattering From Undeformed Saline Ice
Presented by Dr. Ken Jezek

This effort has been conducted by Drs. Timothy K. Stanton and Ken Jezek with support from Anthony Gow. The objective of the effort has been to identify and quantify the important scattering and absorption mechanisms in undeformed saline ice and the relationships between changing ice morphologies and ice acoustic properties. The approach is illustrated in Figure 1.

A large number of normal incidence angle reflection experiments were conducted in a controlled manner on saline ice at Cold Regions Research and Engineering Laboratory in Hanover, NH. The experiments covered an acoustic bandwidth of 5-800 KHz and a number of ice types were examined. As ice starts growing, the crystals are randomly orieted both horizontally and vertically. In a short time, the crystals start alligning their C-axis vertically such that large thin ice crystals are formed. Figure 2 illustrates both a horizontal and a vertical cross section. During the freezing process, saline brine is rejected and it accumulates at the crystalline boundaries. This brine drains downward vertically under the influence of gravity. Drainage during cycles when the ice column is warmed produce dramatic changes. Figure 3 shows the difference between ice cross sections taken before and after a thermal event. At the ice/water interface during freezing conditions, the new ice crystals form a skeletal layer with thin platy crystals protruding into the water. The composition of the ice changes gradually vertically over ten centimeters where the composition is essentially hard ice. The freezing process starts with sea water at 30-35 ppm but the ice formed has only about 10 ppm in the skeletal layer and 4 ppm in multiyear floes. Figure 4 illustrates the changes in reflection coeficient as ice grows (120 KHz acoustic frequency). Figure 5 provides probability density functions of reflection coefficients for a variety of ice types measured in NH while Figure 6 shows similar data measured in the Arctic. Figure 7 quantifies both the effects of ice thickness and incidence angle using an acoustic frequency of 190 KHz. This data indicates that a critical angle for reflection of incident energy occurs between 35 and 40 degrees.

Considerable effort was spent on quantifying the attenuation of sea ice as a function of frequency for acoustic waves traveling through the ice in a vertical direction. Figure 8 summarizes the findings on growing sea ice that has a skeletal layer. The findings of Langleben have been added to the figure to show the effects of the skeletal layer. Langleben measured old solid sea ice correctly but the addition of the effects of the growing skeletal layer changes the picture dramatically. The presence of this layer in the Arctic has been confirmed .

A number of issues remain that are linked directly to the effects of the environment on the ice. These are : (1) the magnitudes of vertical gradients in velocity and attenuation as ice grows and environment changes, (2) diffraction from ice-edge(elastic waves in lossy ice), and (3) Morphologic controls on backscatter strength.

APPROACH

Perform high-frequency (8-800 kHz) monostatic and bistatic experiments on laboratory grown saline ice

Monitor ice morphology (thin section, salinity, temperature)

Validate key laboratory work by performing similar experiments in the field

Congelation Ice

A
Vertical

9.1 cm

B
Horizontal
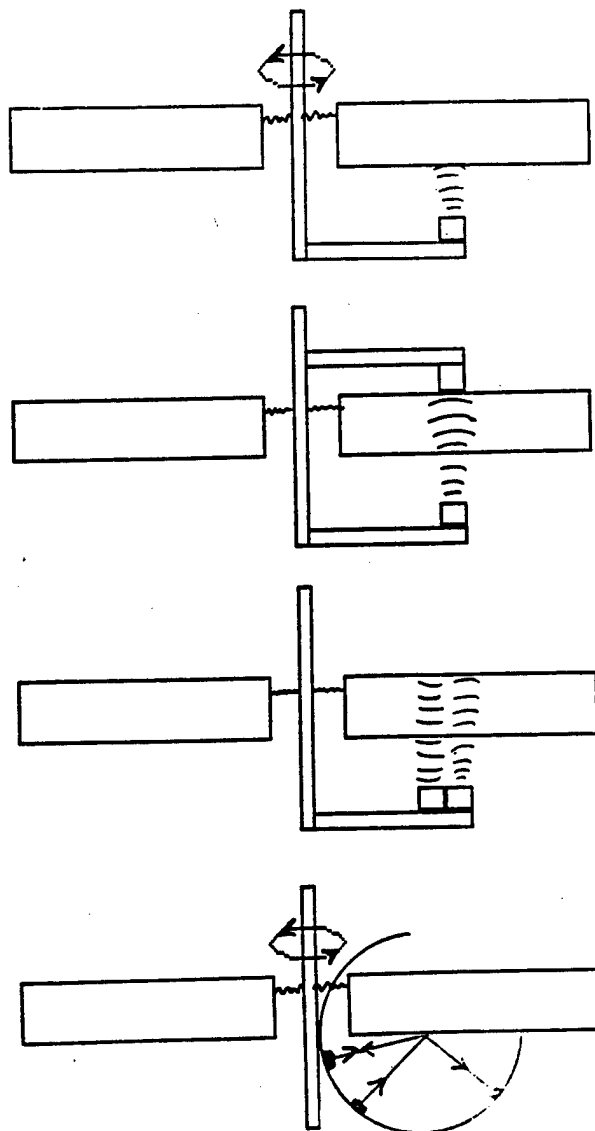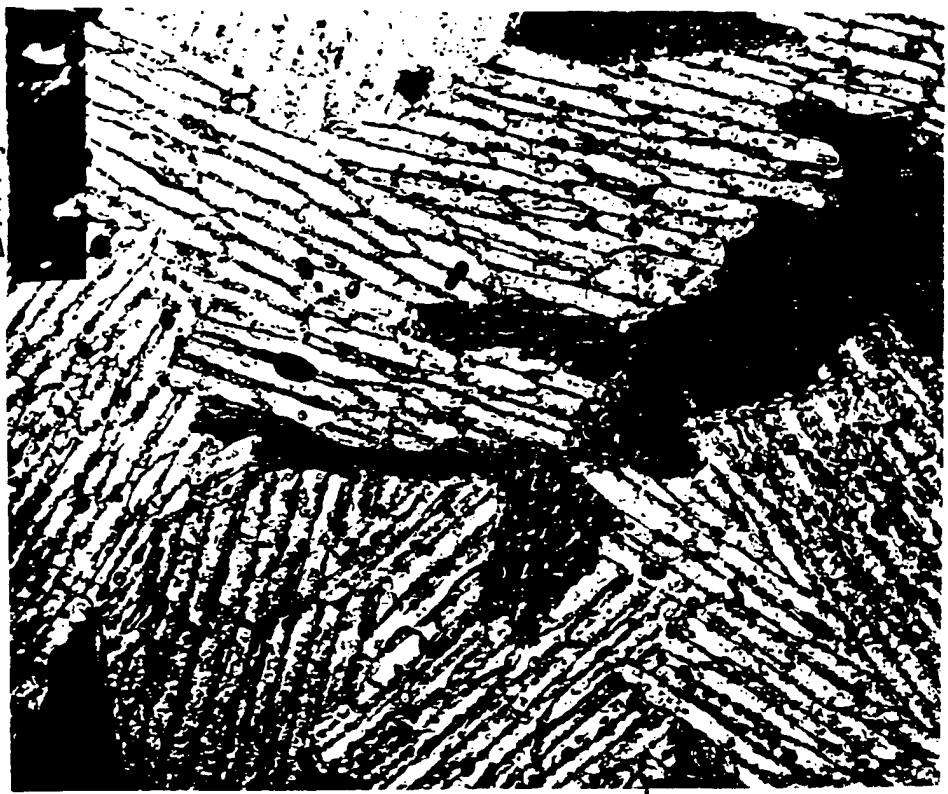
C Horizontal
Enlarged

Ice Growth - 120 kHz
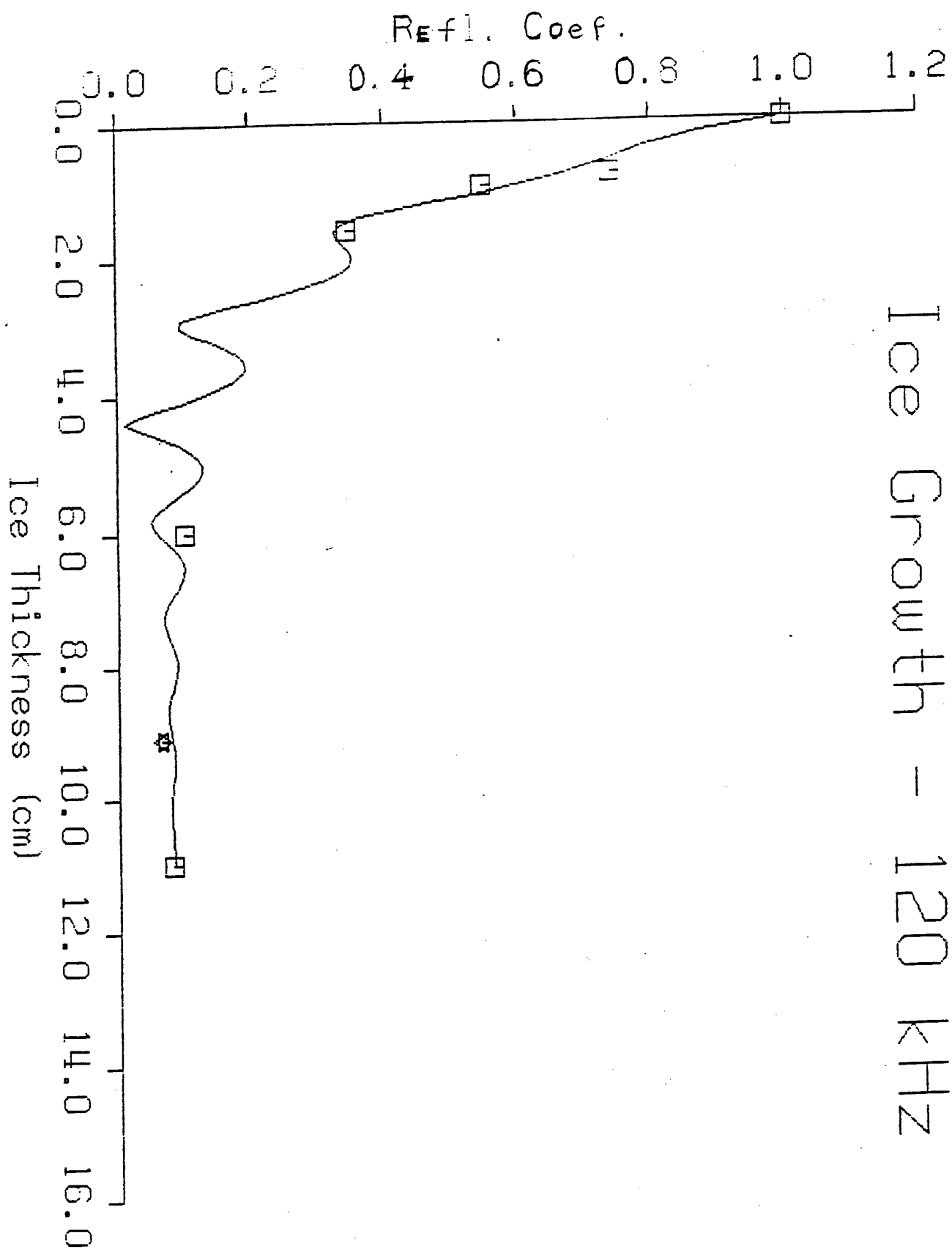
Normal Congelation Ice

After thermal cycling

ICE TYPES

188 KHZ

P.D.F.

Refl. Coef.

NEW

CELL

LAKE

SLUSH

98

ICE TYPES - FIELD

188 KHZ

P.D.F.

NEW ICE

CELL

ALTERED

Refl. Coef.

GROWTH (190 kHz)

Reflection Coef.

4 mm

6 mm

9 mm

15 mm

ATTENUATION VS FREQUENCY
18CM THICK CONGELATION ICE

..... J-S-G

——— LANGLEBEN

$A = 2.9*F^{1/2}+(7.9E-10)*F^4$

ATTENUATION (DB)
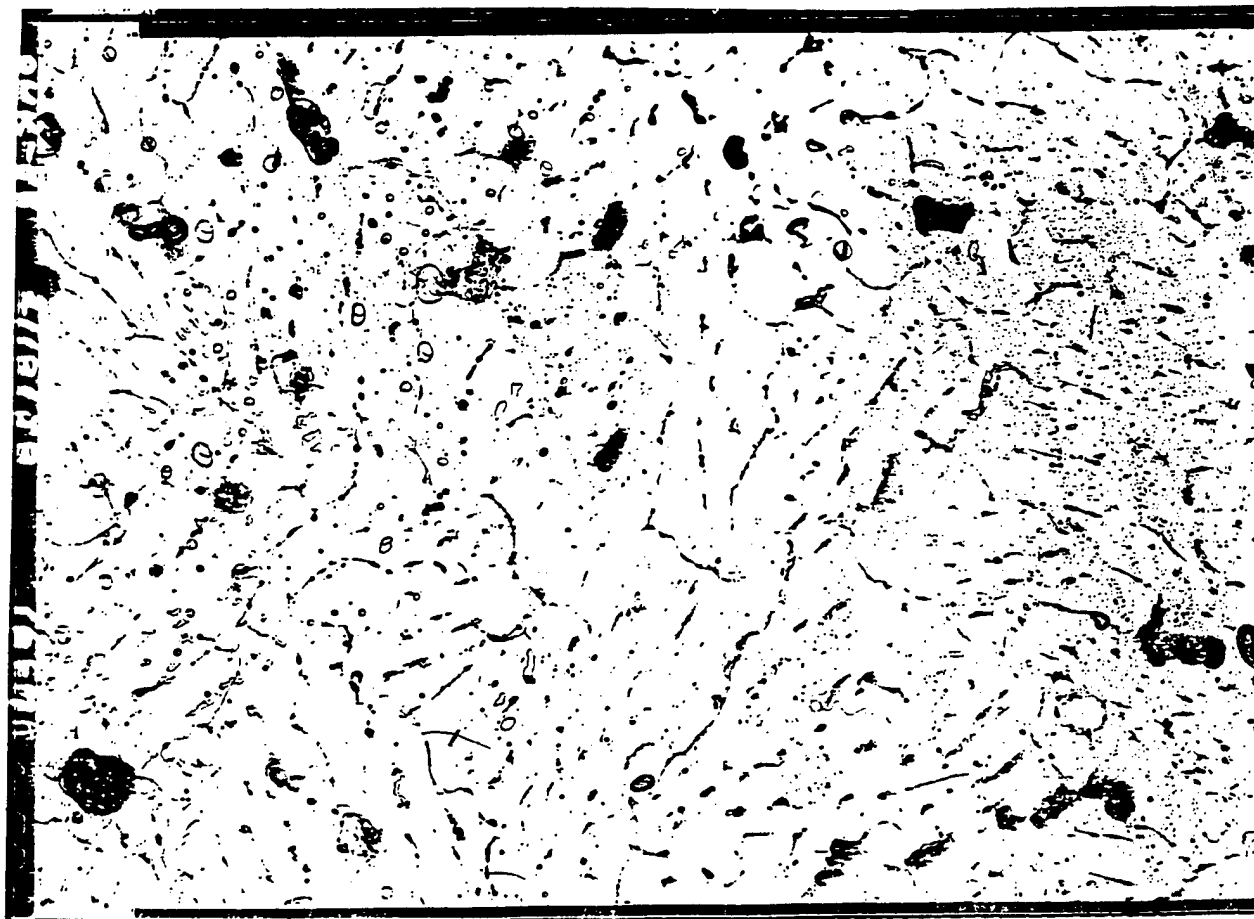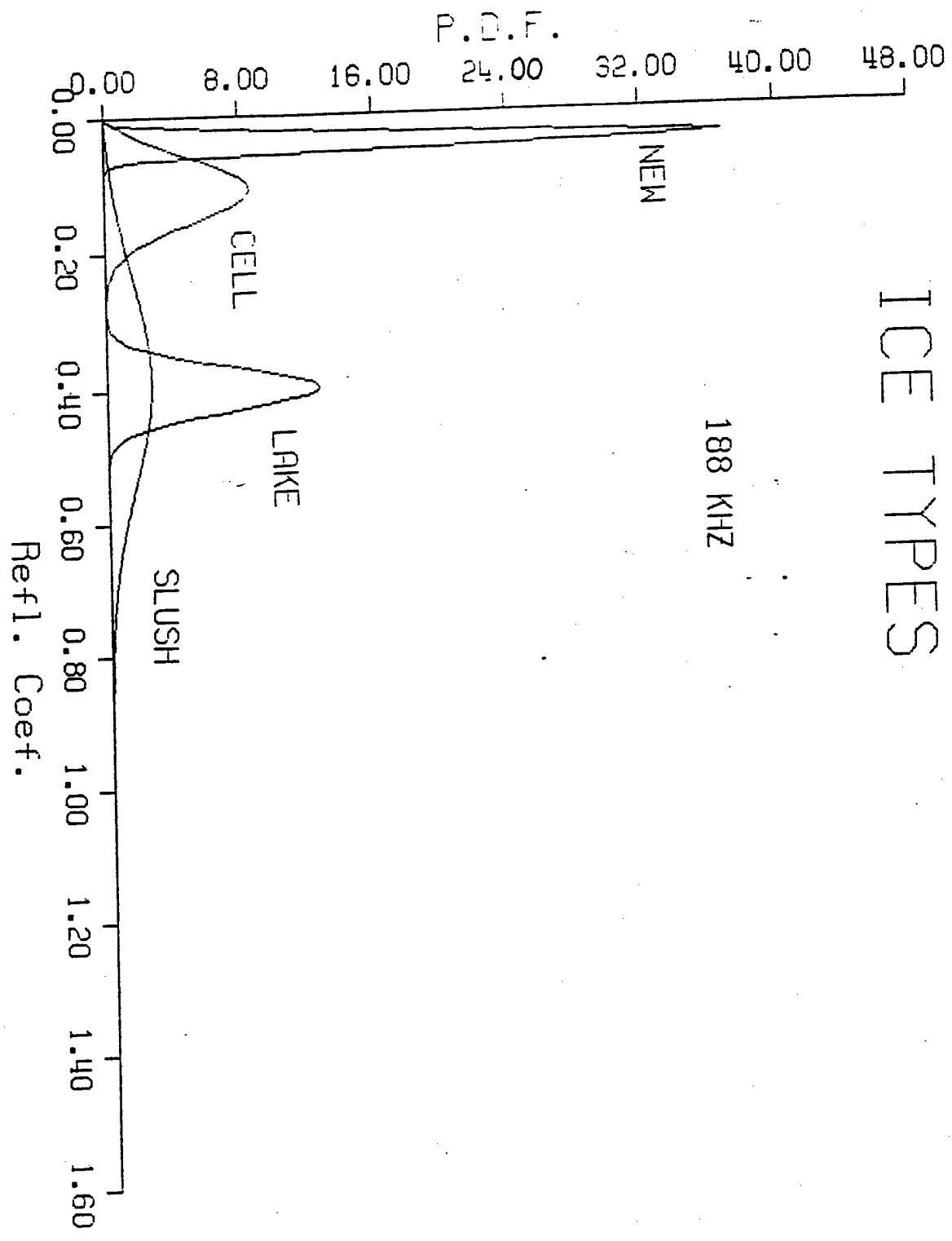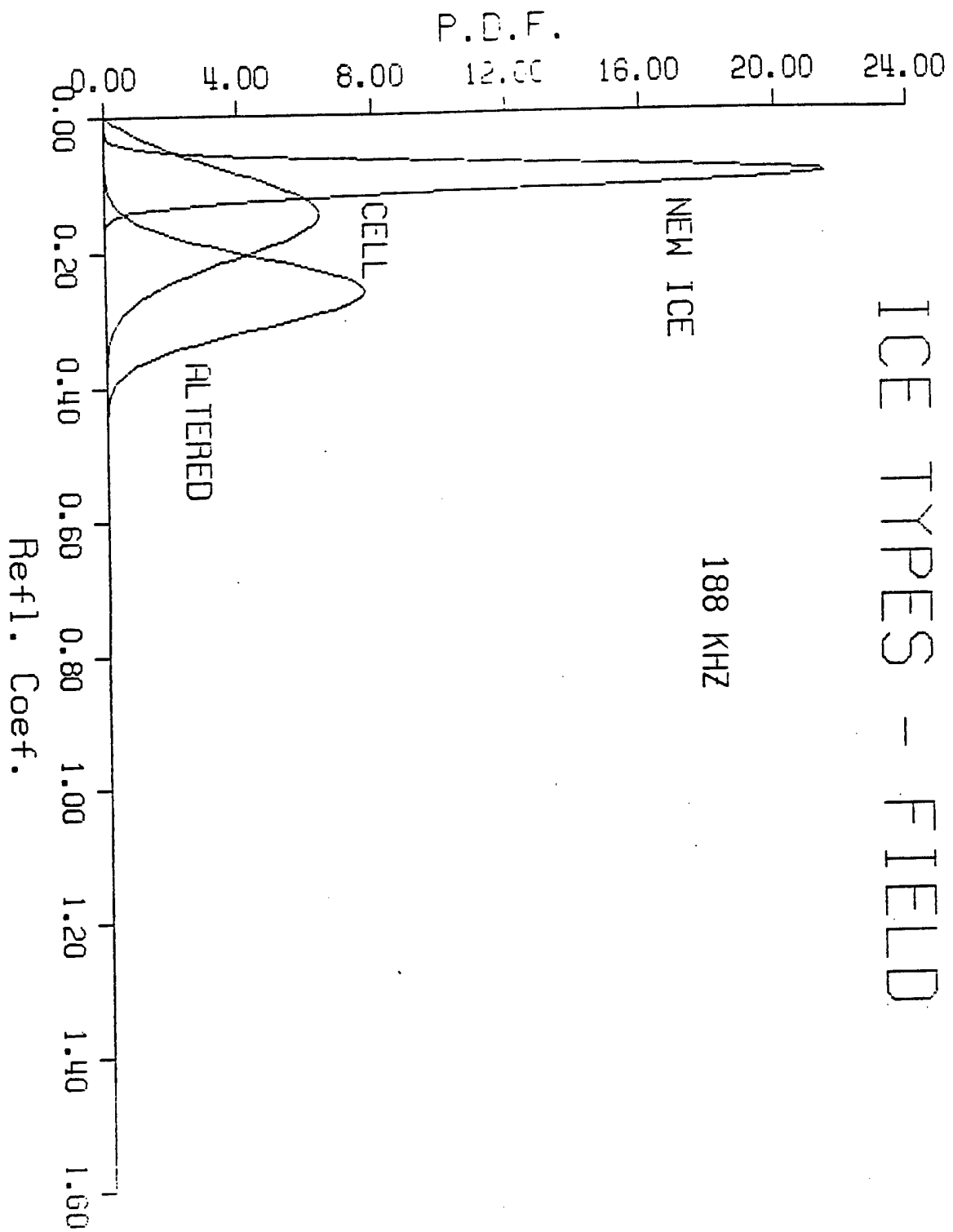
Frequency (Khz)
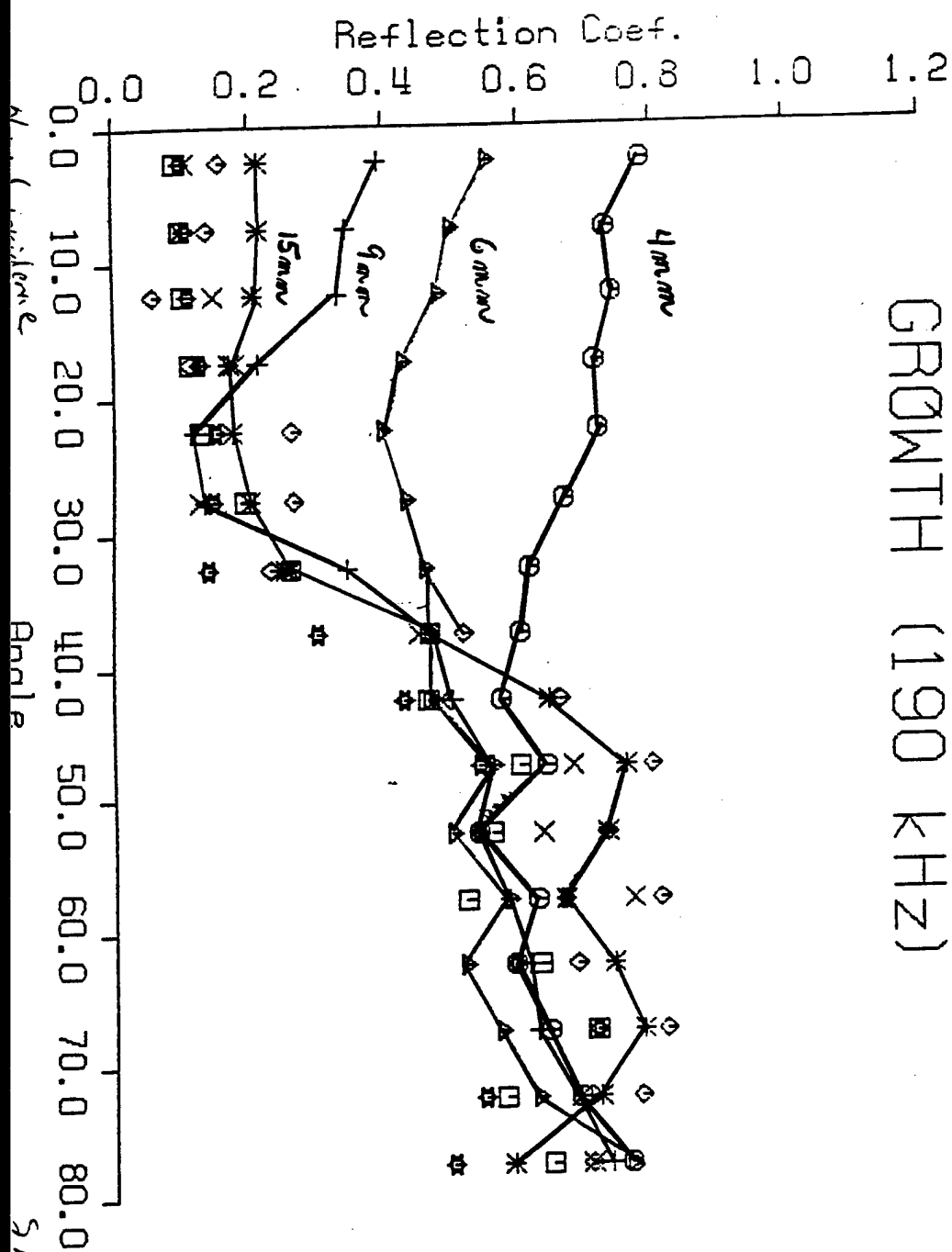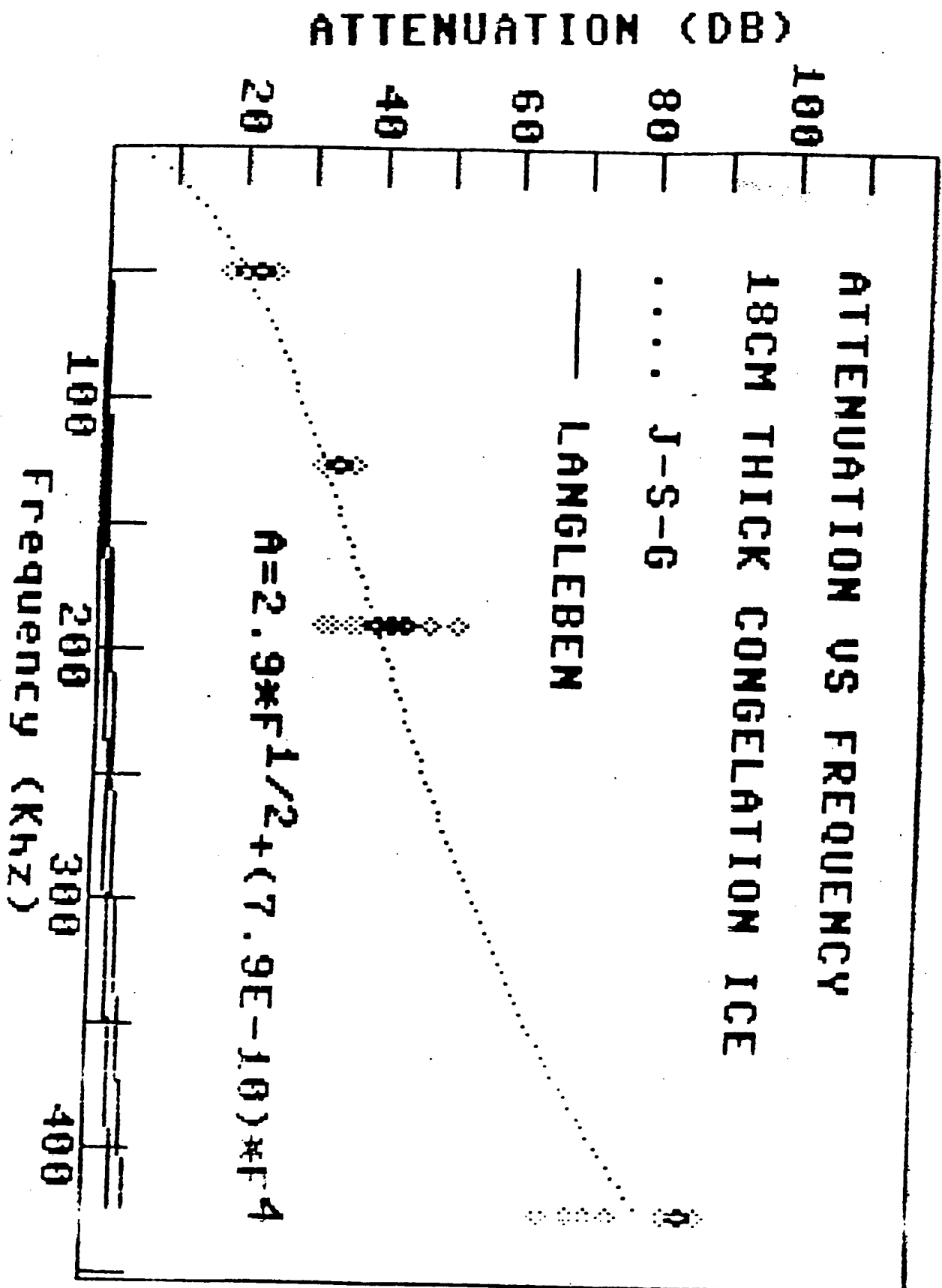
Arctic Tomography Experiment

S. D. Rajan
Woods Hole Oceanographic Institution
Woods Hole, MA 02543

A number of acoustic propagation experiments have been conducted in the ice covered Arctic ocean. Efforts to predict the experimentally measured field by theoretical approaches have met with limited success. One of the causes suspected is the lack of adequate environmental information. Due to such limitations, theorists have treated the ice surface as either pressure release or as a rigid reflector when it is knoown that ice is elastic with variable properties as conditions change. Figure 1 is taken from a Russian paper shows a model that has been proposed for the compressional wave speed profilein sea ice. Table 1, also from a Russian paper, is the compressional wave speed profile in sea ice based on field measurements. This appears to be the only effort to date to measure the compressional wave of the ice with depth.

Sea ice is a complicated material, a schematic drawing is shown in Figure 2. Extensive work has been performed on the properties of ice and snow without consideration of acoustic properties. the problem lies in the fact that the snow/ice plate is very heterogeneous with brine drainage channels, layers of varying density and crystal size material, and a porous skeletal layer on the ice/water interface that could lead to very complex acoustic scattering as function of acoustic wavelength. As the acoustic wavelength increases the properties will be integrated and the plate characteristics will dominate but this too has complications because the plate is rough (thickness not uniform), it has cracks and it is really a composite of pieces (floes) with the pieces sometimes piled to form ridge/keel or rubble field composites (some refrozen solidly while the others are unconsolidated).

Acoustic tomography offers many advantages for examining complex elastic structure if the interest is to find out how the the structure responds to acoustic energy. With the proper placement of transmitters and receivers, it is possible to directly measure the compressional, shear and surface wave velocities, determine the attenuation versus frequency for all types of waves, determine the energy partitioning at the boundaries, and the scattering that occurs at cracks and floe edges.

An acoustic tomography experiment is scheduled to take place in the Arctic during the month of May 1989. The primary objective of this experiment is to measure the 3-D structure of compressional wave speed and attenuation in Arctic sea ice. The experiment is also designed to measure the compressional wave speed and attenuation over a range of frequencies which will give some insight into dispersion characteristics of sea ice. Figure 3 shows the source/receiver geometry for such an experiment which should produce the ray diagram in Figure 4.

To investigate whether the array geometry in Figure 3 is viable and to understand the problems that may encountered in engineering a large tomographic array for deployment in the Arctic, an experiment was performed in lake ice during February 1989. An array of 10 sources/receivers was deployed in the ice. The array geometry is shown in Figure 5 with the corresponding ray diagram in Figure 6. The number of measurements taken during the experiment were limited as the ice cover cracked during the course of the experiment resulting

in loss of acoustic link between sources/receivers. With the limited data set obtained (a total of only 23 ray paths) inversion for the compressional wave speed was carried out and the estimate obtained is shown in Figure 7. The average value of the compressional wave speed (average over range) is tabulated in Table 2 together with the measured temperature profile. As expected the compressional wave speed is a maximum where the temperature is a minimum. Further the gradients in compressional wave speed is large at depths where there is strong temperature gradient. The values of compressional wave speed obtained is consistent with the only results published in the literature for fresh water ice , nemely the results published by Bogorodskii(Soviet Physics - Acoustics, 15-17,1957) which is shown in Figure 8. Resolution studies indicate that for the results obtained with this limited data set the maximum resolution is 2 meters in the horizontal and 0.25 meter in the vertical.

To estimate an average value of the compressional wave attenuation, the amplitude of the received and transmitted signal for the path connecting (elements 1 and 9 in Figure 5) were compared. This yielded a value 0.043 dB/m/kHz as compared to 0.075 dB/m/kHz given by Westphal (Journal of Geophysical Research, 70(8),1849-1853,1965) for glacial ice.

In addition to confirming the ability to obtain meaningful results using a tomographic array, the experiment also established the following:
 1) No distortion of received signal due to tube waves was noticed.

 2) Stable transmission between the elements in the ice and the hyrophone placed in the water column under the ice were obtained. The ice/water interface did not exhibit any of the known characteristics of a skeletal layer.

The reflection coefficient of the ice underside obtained from transmission between two phones placed in the water column indicate that under the conditions prevailing at the time of the experiment the interface acted as a definitive reflective boundary.

Figure 1. Layered model of compressional wave speed for Arctic pack ice (based on data in
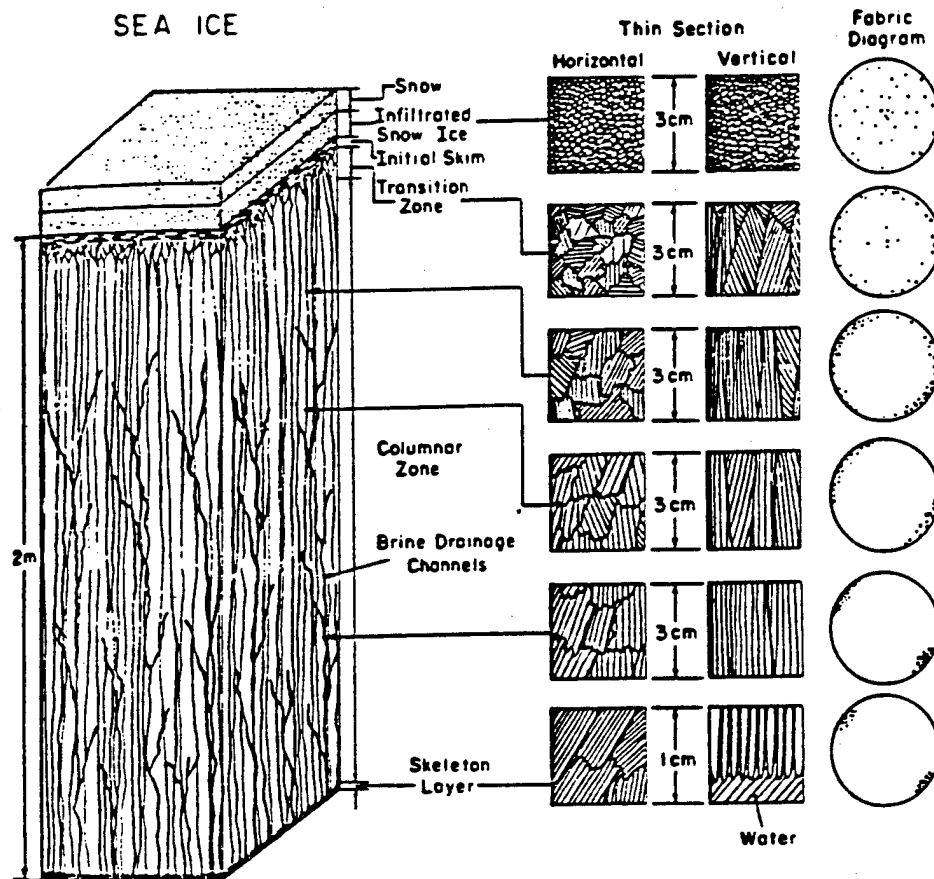
Figure 2. Structure of sea ice

POSITION OF SOURCES

ICE

RECEIVERS

BOREHOLES

WATER

HYDROPHONES

Figure 3.

RAY DIAGRAM

DEPTH (m)

RANGE
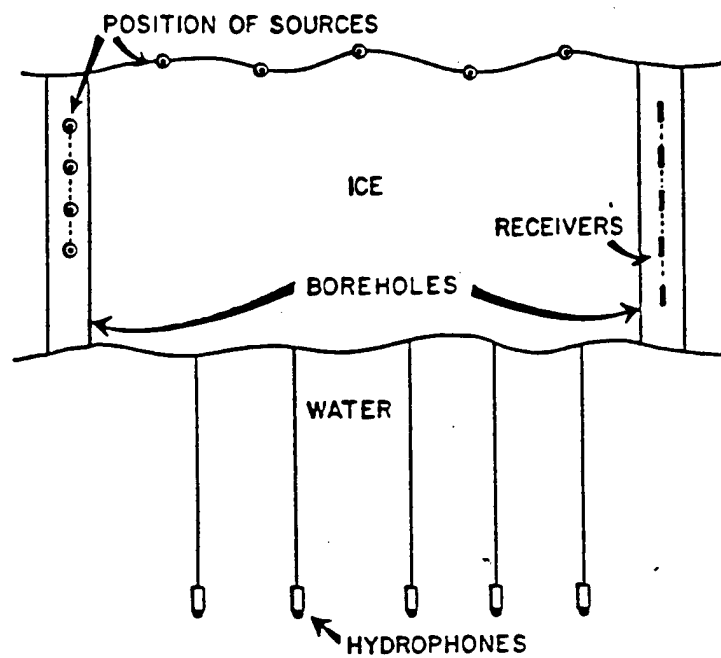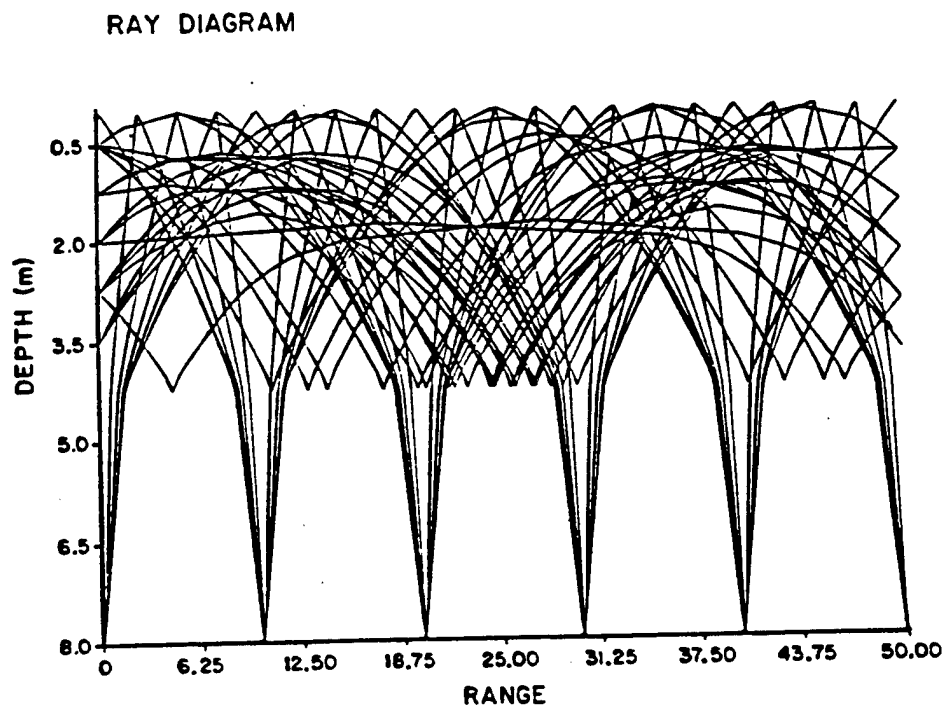
Figure 4. Ray diagram for revised configuration

105

Acoustic Scattering from
Elastic Ice

J. Robt. Fricke

MIT/WHOI Joint Program

Cambridge, MA 02139

The following is a list of captions for figures from presentation O8 at the 115th meeting of the ASA in Seattle, Washington held May 17-20, 1988.

This is the first report on new work dealing with rough surface scattering from the Arctic ice. Approximate methods like the Kirchhoff approximation and perturbation methods fail in the 10-100 Hz band since the length scale of the rough surface scatterers is approximately the same as the insonifying wavelength. This presentation is based upon a finite difference solution of the full wave elastic wave equation. Controlled numerical experiments were performed to gain insight into the local (i.e., short range) details of acoustic/elastic interaction for the air/ice/water system.

Figure 1: Introduction – The presentation covers three topics: (1) an overview of the finite difference modeling geometry, (2) results from a flat ice experiment, and (3) results showing scattering from an isolated keel.

Figure 2: 2-D Modeling Geometry – The model is based on a 2-D Cartesian grid with an axis of symmetry on the left. A pulsed line source is constrained to lie on the axis of symmetry. Lines of receivers may be placed horizontally anywhere in the computational grid. The field parameters, $\underline{u}$, are horizontal and vertical displacement. The finite difference model is formulated as a 2nd order spatial and temporal approximation to the elastic wave equation. In the heterogeneous region the *heterogeneous* isotropic elastic wave equation is discretized for the finite difference formulation. In this region the Lamè parameters, λ and μ, and density, ρ, may vary over x and z. In the homogeneous regions, it is assumed that the Lamè parameters and the density are all constant in x and z, hence the spatial derivatives of λ and μ are zero. In these regions the *homogeneous* isotropic elastic wave equation is discretized. Absorbing boundaries are implemented on the bottom and right side of the grid and a dissipative region using the "telegraph" equation (which adds a term $\alpha \underline{u}_t$ to the wave equation) is used on the top. The physical parameters used for the model are as follows. For the air $c_p = 340$ m/s and $\rho = 0.0012$ Kg/m^3. For the ice $c_p = 3500$ m/s, $c_s = 1600$ m/s, and $\rho = 0.91$ Kg/m^3. For the water $c_p = 1500$ m/s and $\rho = 1.0$ Kg/m^3.

Figure 3: Flat ice model – This experiment was run with a center fre-

quency of 50 *Hz*. The ice is modeled as being flat with a thickness of 3 *m*. The line source is placed 100 *m* below the bottom of the ice and a line of receivers is placed 50 *m* below the ice. We expect to see the reflection from the ice/air complex with a reflection coefficient near -1. In addition, there is the possibility of exciting the longitudinal plate wave in the ice. For the parameters chosen this wave has a phase velocity of about 2713 *m/s* which is supersonic with respect to the water and can thus be excited by incident acoustic energy at a grazing angle of about 56°. The other plate mode that can exist at this low frequency is the flexural wave but we do not expect it to be excited since is has a phase velocity of about 860 *m/s* at 50 *Hz* which is subsonic with respect to the water.

Figure 4: x-t Plot for Flat Ice Experiment – In this plot positive values cause a right going deflection of the trace and negative values cause a left going deflection. Range in meters across the figure and time in seconds runs vertically. The trace spacing is 2.5 *m*. As expected we see the direct arrival from the source to each of the receivers. We also see the reflection from the ice/air complex. Measurements verify that the reflection coefficient is nearly -1. (Remember this is 2-D geometry so the spreading loss is $1/r^{1/2}$ not $1/r$.) We do not, however, see any evidence of the longitudinal plate wave. Experiments with SAFARI revealed why. First, the longitudinal plate wave energy is very small compared to the direct arrival and the reflection. Second, the longitudinal wave arrival does not break out ahead of the direct arrival until a range of 300 *m* is reached. Thus, in retrospect, we should *not* have expected to see the longitudinal wave arrival in this experiment since the maximum modeled range is 300 *m*.

Figure 5: Snapshot at 0.15 *s* from Flat Ice Experiment – In this figure the red colors are negative values and the blue colors are positive values. This is a snapshot of the horizontal displacement component of the field at a time of 0.15 *s* after the shot is fired. The gray zone extending across the figure at at depth of 0 *m* is the 3 *m* ice sheet. The incident field is seen propagating to the right at a range of about 175 *m*. The reflected field is identified as the semi-circular feature in the range from 50 to 150 *m*. Of particular interest is the discontinuity in the horizontal component of the field at the lower surface of the ice sheet. The vertical component (not shown) is continuous across the same interface. No boundary conditions for the ice/water interface are explicitly incorporated into the model but, rather, are incorporated implicitly by virtue of the definition of the heterogeneous wave equation. Nevertheless, the results satisfy the physical requirement of continuity in the vertical component with no constraint on the horizontal component. There is a line of receivers at a depth of 50 *m* which produced the x-t plot of the previous figure.

Figure 6: Isolated Keel Model – The geometry for this experiment is identical to that of the flat ice experiment except that a single isolated triangular keel has been added to the otherwise flat ice sheet. The keel is 40 *m* wide and 20 *m* deep. The source is again centered at 50 *Hz* and thus has a wavelength of 30 *m* which is of the same order as the dimensions of the keel. This is a case in which neither the Kirchhoff nor the perturbation approximations are valid. We

expect to see the direct arrival and the reflection as for the flat ice case with the addition of diffractions from the keel. In this case we will also see flexural waves excited in the ice.

Figure 7: x-t Plot for Isolated Keel Experiment – As expected we see the direct arrival along the line of receivers, the reflection from the ice/air complex prior to the keel location at 150 m and then the diffractions from the keel starting at a time of about 0.17 s.

Figure 8: Snapshot at 0.15 s from the Isolated Keel Experiment – This is a snapshot of the vertical displacement component of the field at a time of 0.15 s after the shot was fired. The gray area across the figure indicates the location of the flat ice sheet and the keel structure located at a range of 150 m. Just as with the flat ice experiment, the incident and reflected wave fronts are identified. The matching of the keel dimensions and the insonifying wavelength is graphically illustrated here. Note that the right side of the keel is being dispaced (infinitesimally) down while the left side is being displace up. As the incident and reflected wave pass the keel is it alternately torqued clockwise and counter-clockwise. This is the mechanism by which flexural waves are excited in the ice even though they are subsonic with respect to the water and the usual matching of trace speeds is impossible.

Figure 9: Snapshot at 0.25 s from the Isolated Keel Experiment – This is a snapshot of the vertical displacement component of the field at a time of 0.25 s. There are several features to note: (1) the ice roughness has provided a mechanism by which flexural waves may be excited, (2) since the flexural waves are subsonic they are evanescent and are thus trapped in the ice, (3) the polarity of the vertical component of the flexural wave is opposite on either side of the keel which is what one would expect from the "keel torquing" injection mechanism, and finally (4) the forward and back scattered field propagate away from the keel.

Figure 10: Conclusions – The finite difference results are verified in comparisons with SAFARI for the flat ice experiment. Based upon results from the isolated keel experiment it appears that consideration of the elastic nature of the ice is essential in properly identifying how the incident acoustic energy interacts with elastic energy in the ice. There apparently is a loss mechanism by which acoustic energy is removed from the coherent propagating field and trapped in the ice as flexural waves. This is only possible when the ice is rough and when the elastic nature of the ice is included. If either of these features are ignored then flexural waves can not be excited. Furthermore, it appears that a tuning phenomenon exists. That is, if the size of a keel is matched to the insonifying wavelength, then injection of the flexural wave into the ice will be efficient. If the keel size is not matched then the injection efficiency will be reduced.

Acoustic Scattering from Elastic Ice

- Modeling geometry

- Flat ice

- Single keel scattering

Fig. 1

2-D Modeling Geometry

Telegraph region

- -

Homogeneous region

Air

Heterogeneous region

Ice

Homogeneous region

H_2O

Axis of symmetry

∇ ∇ ∇ .... ∇ ∇ ∇

↑

* Source

↓

Absorbing B.C.

Line of receivers
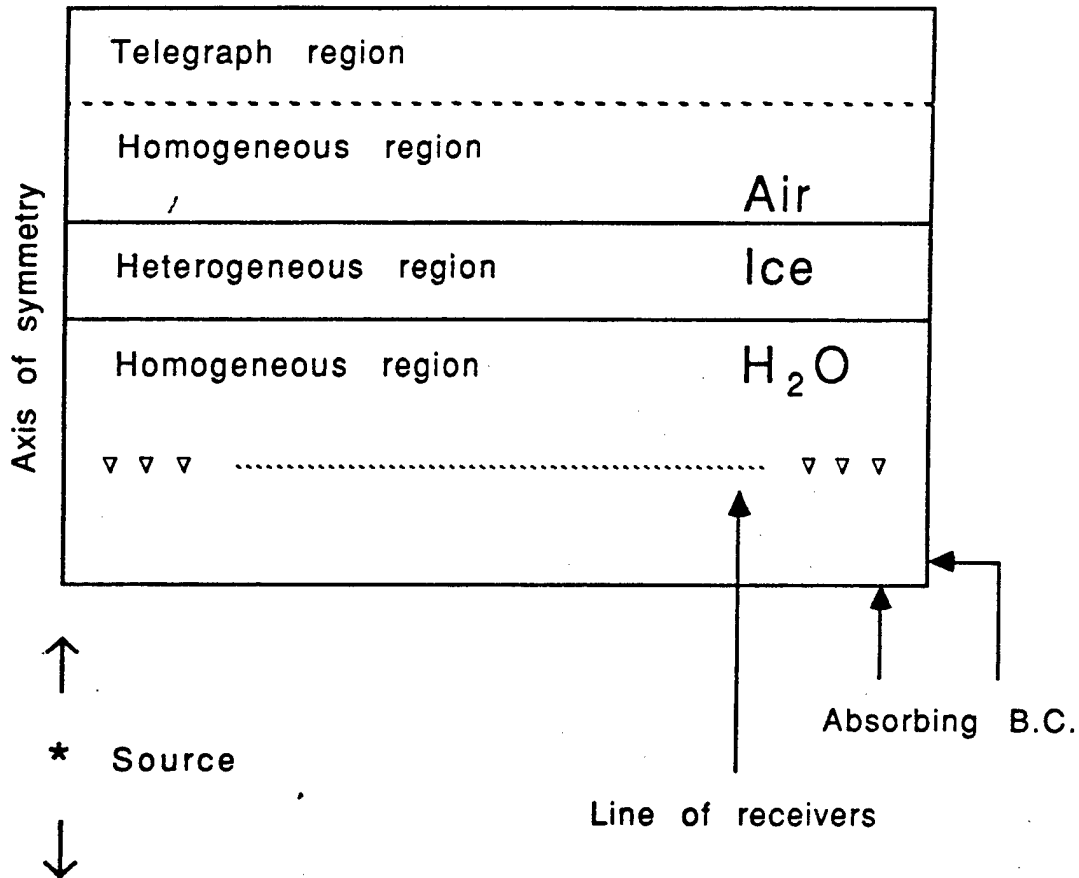
Homogeneous Elastic Wave Equation

$$\rho \underline{u}_{tt} = (\lambda + 2\mu)\nabla(\nabla \cdot \underline{u}) - \mu\nabla \times \nabla \times \underline{u}$$

Heterogeneous Elastic Wave Equation

$$\rho \underline{u}_{tt} = (\lambda + \mu)\nabla(\nabla \cdot \underline{u}) + \mu\nabla^2\underline{u}$$
$$+\nabla\lambda(\nabla \cdot \underline{u}) + \nabla\mu \times (\nabla \times \underline{u})$$
$$+2(\nabla\mu \cdot \nabla)\underline{u}$$

Fig. 2

110

Flat Ice Model

Fig. 3

3m Flat Ice

Time(s)

Range(m)

Fig. 4

F= 50.0Hz SD= 100.0m   CONDR,FIP

Depth (m)

Range (m)
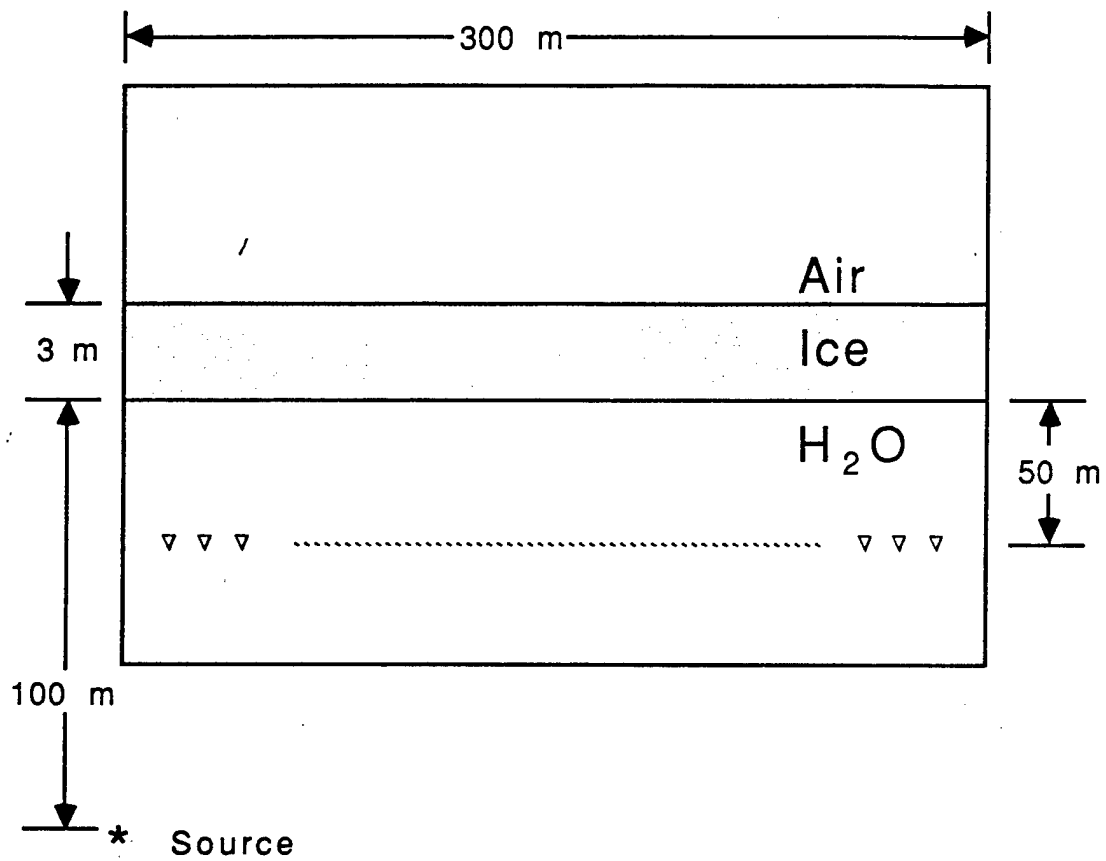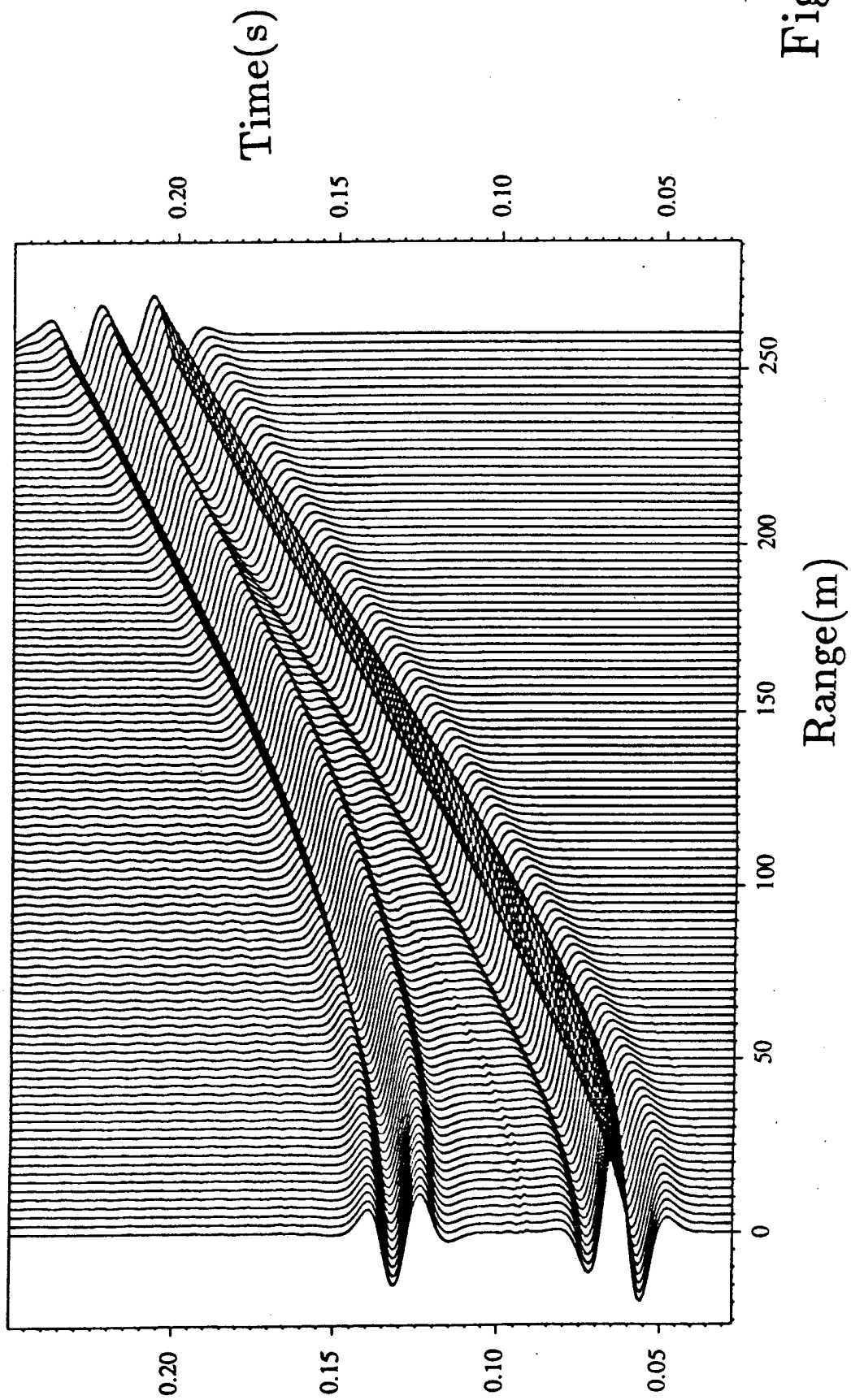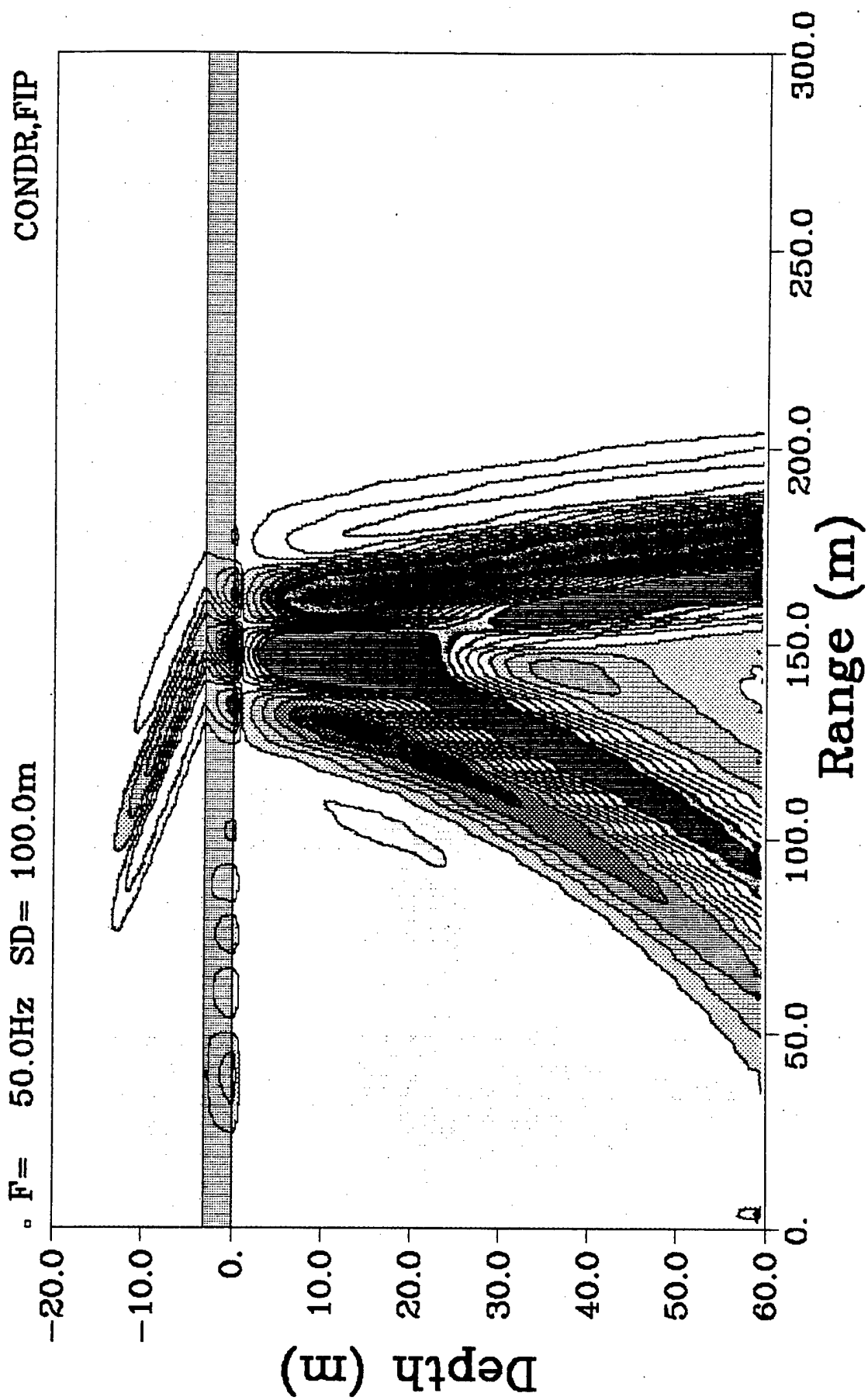
3m Flat Ice, 0.15s, Horiz

Fig. 5

113

Keel Model

Fig. 6

3m Ice with Keel

Time(s)

Range(m)

Fig. 7

3m Ice with Keel, 0.15s, Vert

Fig. 8

F= 50.0Hz SD= 100.0m

CONDR,FIP

Depth (m)

Range (m)
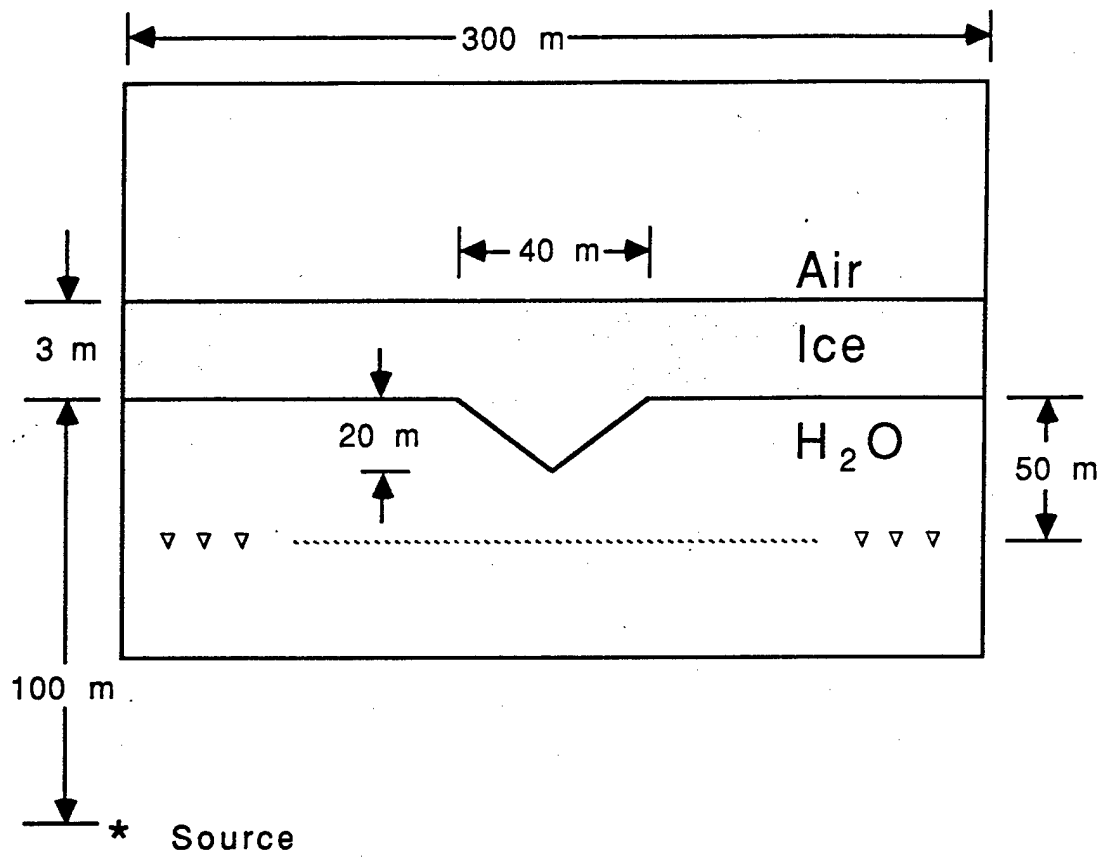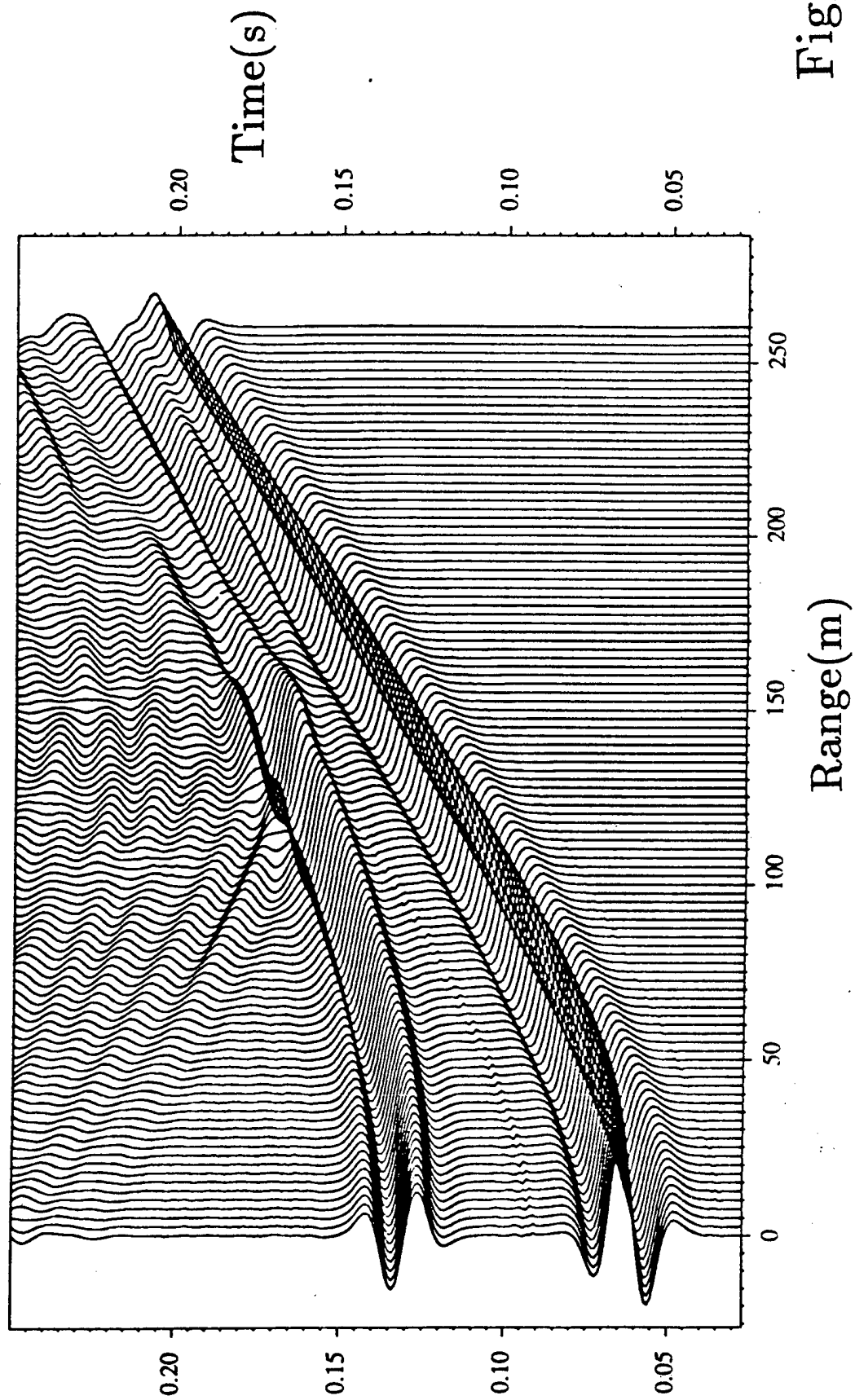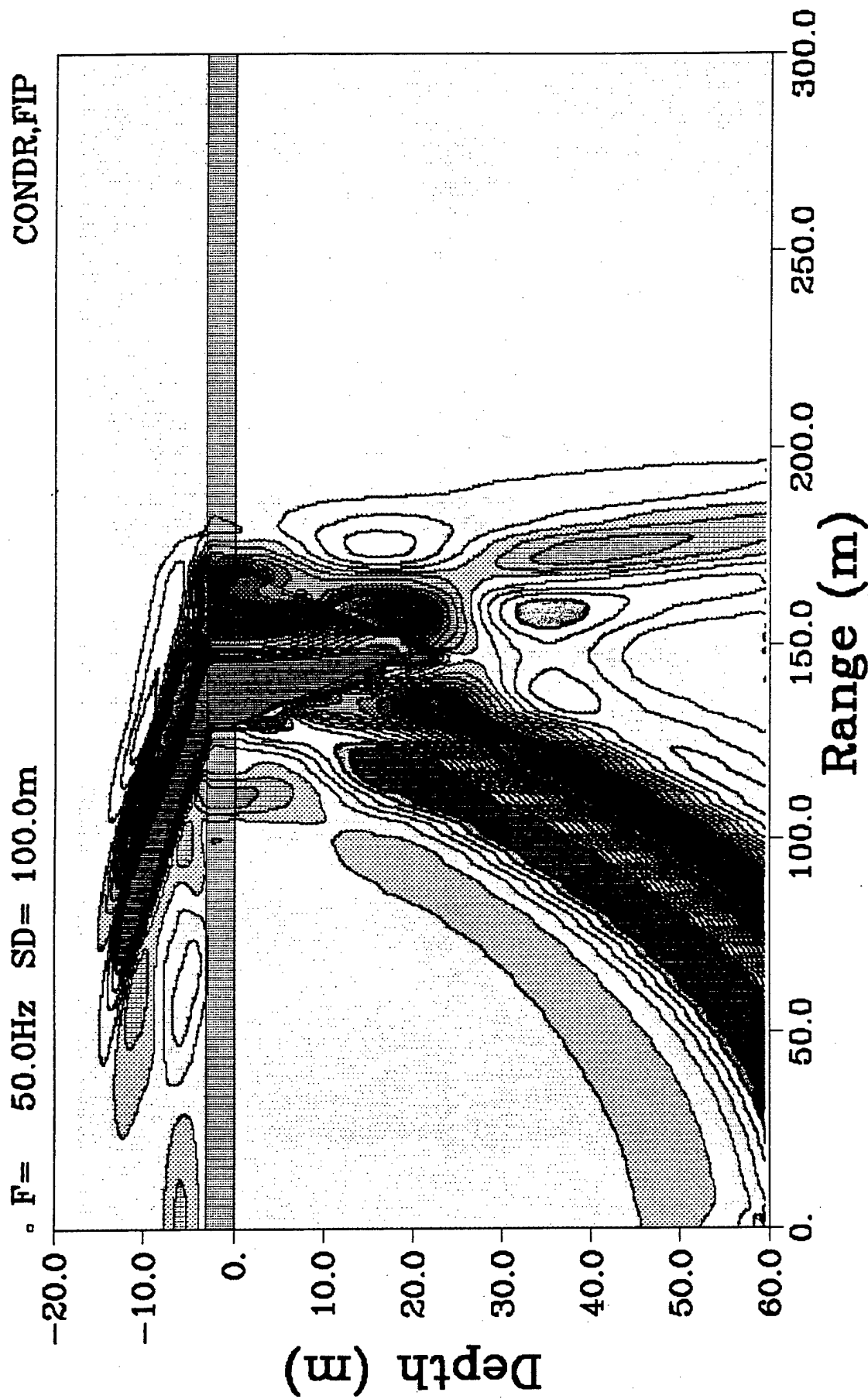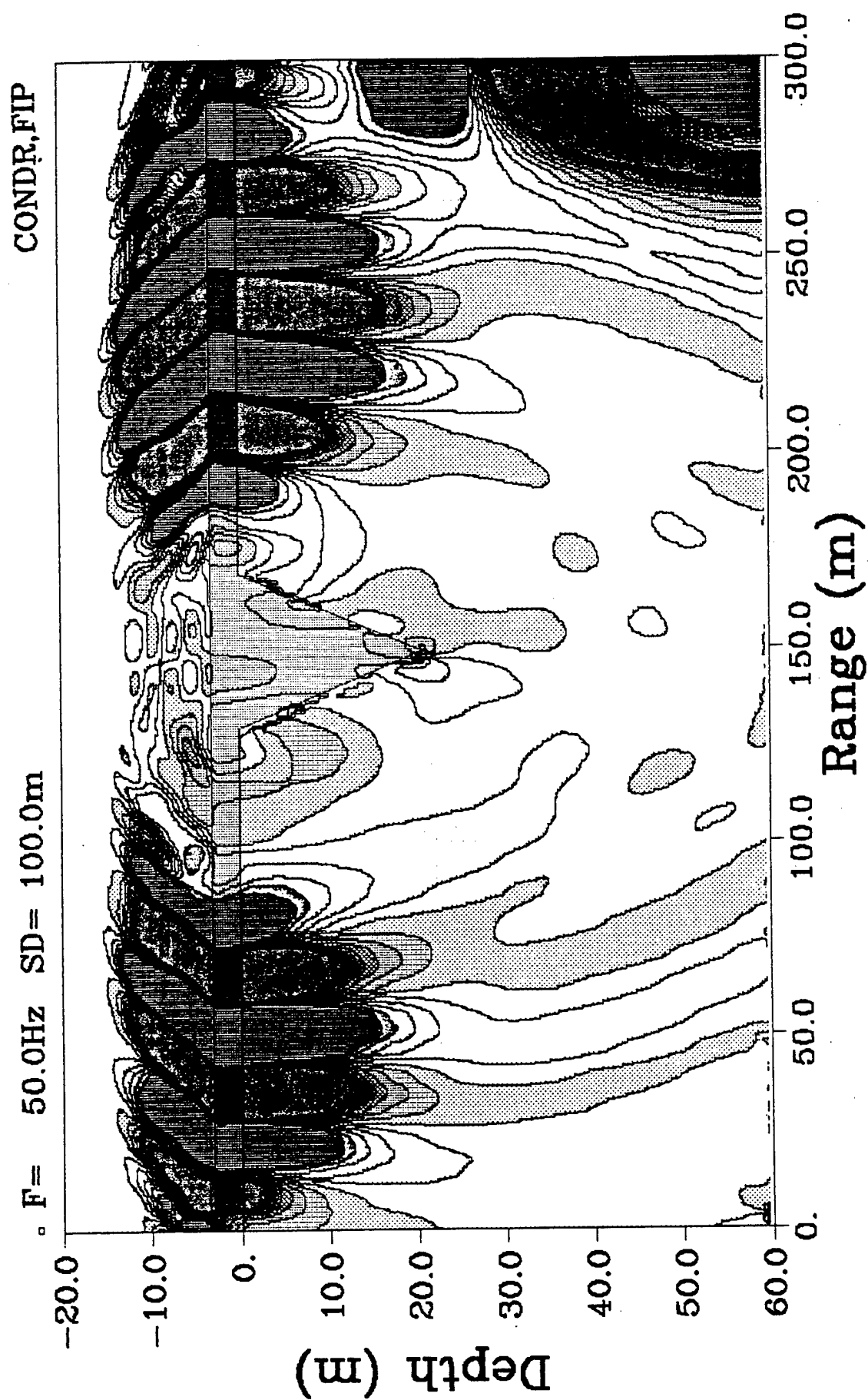
3m Ice with Keel, 0.25s, Vert

Fig. 9

117

Conclusions

- FD results are verified
- Elastic ice model is important

Fig. 10

Arctic Instrumentation Development
presented by Art Baggeroer, MIT

This presentation described the Arctic Remote Autonomous Measurement Platform(ARAMP), the Acoustic Sensor Tracking System (STS), and an Optical Disk Based Acquisition System(ODAS). The material presented for both the ARAMP and STS were described well in papers presented at the Instrumentation and Measurements in Polar Regions Workshop, 27-29 Jan 1988. These papers are included here since the distribution of the proceedings of that workshop was quite different from this workshop distribution.

The ODAS acquisition system has not as yet been documented formally. A draft paper was written by Keith von der Heydt(WHOI) in Sept 1987 after the first field test of a partially developed system. The objective of this new acquisition system was to maximize flexibility in the field by designing in a capability to swap bandwidth per channel recorded with the number of channels. The system was designed around an Optimem 1000 "write once-read many" optical disc drive. The optical disc was chosen to provide a 2 gigabyte/disc random access data collection(1987) capability with high potential for future improvements. A block diagram, Figure 1, illustrates the main components of the system.

The ODAS system has been developed into a forty channel system which became the main data collection equipment for MIT at the A-Camp during the CEAREX experiment. Its performance and current detailed configuration will be documented after the completion of CEAREX.

W.H.O.I. OPTICAL DISK BASED ACQUISITION SYSTEM
(ODAS)   1987

```
  ┌──────────────┐                    ┌──────────────┐
  │  GRAPHICS    │                    │   PRINTER    │
  │  TERMINAL    │                    │   PLOTTER    │
  └──────────────┘                    └──────────────┘
         │                                   │
         └──────────┐         ┌──────────────┘
                    │         │
         ┌──────────┴─────────┴──────────┐
         │  INTEL 310 - MSDOS            │
         │  8086 PROCESSOR               │
         │  1 MBYTE MEMORY               │
         │  20 MBYTE DISK                │
         │  FLOPPY DISK                  │        ┌──────────────┐
         │  MULTIBUS BACKPLANE           │        │ OPTICAL DISK │
         ├───────────────────────────────┤        │   2 GBYTE    │
         │                               │────────└──────────────┘
         │  NCR SCSI HOST                │   │
┌──────────────┐│      ADAPTER          │   │
│  TIME CODE   ││                       │   │    ┌──────────────┐
│  GENERATOR   ├┤                       │   │    │ OPTICAL DISK │
└──────────────┘├───────────────────────┤   └────│   2 GBYTE    │
      │         │                       │        └──────────────┘
┌──────────────┐│  GRA INTERFACE        │
│  RHUBIDIUM   ││  1 MBYTE BUFFER       │
│  OSCILLATOR  ├┤                       │
└──────────────┘└───────────┬───────────┘
                            │
                 ┌──────────┴───────────┐
                 │  GAIN RANGING        │
                 │  AMPLIFIERS/DIGITIZERS│
                 │  (GRA'S)             │
                 │                      │
                 │  'N'  CHANNELS       │
                 └──────────────────────┘
                    │ │ │ │  o o o o o o
```
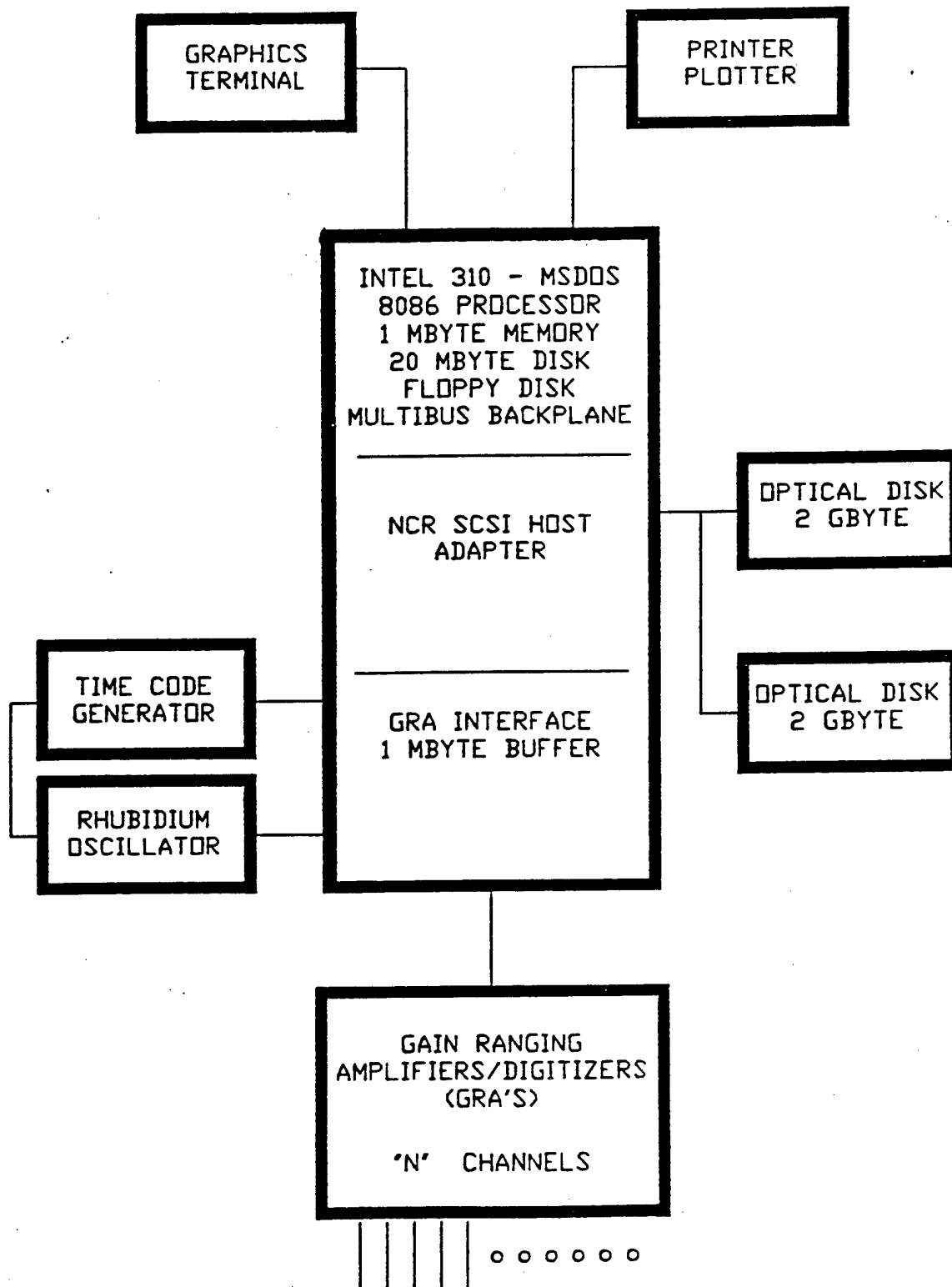
SIGNAL INPUTS

ACOUSTIC SENSOR TRACKING SYSTEM

Keith von der Heydt[*], Gregory L. Duckworth[**], Arthur B. Baggeroer[***]

ABSTRACT

Acoustic and geophysical experiments conducted from ice covered Arctic waters in summer of 1983, 1984, and the spring of 1987 have employed arrays of suspended hydrophones with intersensor spacing ranging from 25 meters to 15 km. Dynamic environments impose the difficulty of continuous real-time measurement of relative sensor position for use during subsequent coherent processing of array data. Data have been telemetered over broadband radio links for ranges greater than 1 kilometer and over cables for shorter ranges.

A system of hardware and software has been developed to measure and record sensor spacing so that relative location can be accurately estimated. The system consists of 5 reference sensors in the array field, each co-located with a source emitting 5 millisecond "pings" at a unique frequency approximately every 15 seconds. Signals from all array and reference sensors are telemetered to a set of receiving hardware which detects pings and computes time delays between all sensors and all sources. Delays are recorded every 30 seconds and used for real-time position estimates which can then be plotted. Offline processing is done to compute best estimates of sensor positions using local sound speed profile information. Relative location accuracies of +/- 2 meters can be obtained at ranges up to 15 km. Accuracy is limited in practice by acoustic path stability.

INTRODUCTION

Acoustic and geophysical experiments have been conducted in the Marginal Ice Zone (MIZ) between northeast Greenland and Svalbard (1983,1984) and north of Prudhoe Bay, Alaska (1987). High fidelity digital data, 250 Hz bandwidth per channel, have been recorded from arrays of hydrophones with intersensor ranges of 25 m to 15 km. Coherent processing of the recorded multichannel data requires a means of continuously monitoring and recording the relative location of all sensors in these arrays to accuracies of about 1/10 the shortest wavelength of interest. Conventional surveying techniques are usually not practical due to rates of floe motion, and the effort required to provide continous fixes for many sensors.

Borrowing ideas developed for the "STRAP" program conducted at N.O.S.C., by Morrison et al, an acoustic Sensor Tracking System (STS), comprised of hardware and software was developed. The "wet" part of the system consists of 5 reference sensors in the array field, each co-located with a source emitting 5 millisecond pings at a unique frequency approximately every 15 seconds, Figures 1 & 2. Signals from all source sensors and all array elements (receive sensors) are telemetered to a set of hardware which detects pings and

*Woods Hole Oceanographic Institution, Woods Hole MA 02543
**BBN, 70 Fawcett Street, Cambridge, MA 02238
***MIT,Building 5-204,77 Massachusetts Avenue, Cambridge, MA 02139

computes delays between all sources and all sensors. These delays, the basic measurement, are recorded by a small computer. Position estimates can be also be computed and displayed in real-time to assist with array maintenance. For use in processing array data, a suite of software routines has been written to convert the delay data to range, as a function of sound speed profile information, and compute and filter positions relative to a selected baseline.

In spring of 1987, STS was used during the ice camp based experiment, PRUDEX, north of Prudhoe, Alaska. One objective was to determine a practical upper limit of array size for which the current configuration of STS is useful for sensor localization in Arctic waters. A small hardwired X-shaped array with sensors at 25, 50 & 100 meters from an apex sensor was deployed. Additionally, sensors were deployed at ranges of about 4 km along the extensions of 2 array legs and at varying ranges up to 20 km. along the bisector of these 2 legs, Figure 3. Extensive measurements were made at ranges of 7, 10, & 15 km.

STS DESCRIPTION

Consider an array of hydrophones, random or otherwise, all at a common depth, Figure 1. At deployment time, 5 geometrically appropriate sites are selected as sources and are equipped with a "pinger" 1 meter above the hydrophone, Figure 2. The remaining sensors are receivers only. The sources are programmed to emit pings of 5 ms duration at fixed frequencies of 8,9,10,11, & 13 kHz. The sensors at the pinger sites are the "references". The STS electronics receives the acoustic signals from all sensors in the array. The pings received by source sensors at their own frequency provide reference emission times for all other source and receiver channels at that frequency. The STS electronics measures these times delays with 200 usec resolution between all sensors, including reciprocal delays between source units. On command, the set of most recently acquired delays are transmitted to a computer for storage.

The hardware and cardlevel software of this system have been described in detail by von der Heydt et al in [1]. Briefly, the system consists of an arbitrary number of identical cards in 1 or more chassis. Each card accepts any 2 channels from an array of sensors. The signals are expected to be broadband to the extent that the 8 to 13 khz range is intact. For any given channel, gain is applied to the signal, it is broadband-pass filtered, with rolloffs of 12 db/octave at 18 khz and 30 db/octave at 2 khz, and hard-limited,[3]. The clipped signal is applied to bandpass filters (BPF) at each of the frequencies in use, (normally 8,9,10,11 & 13 khz). The BPF bandwidths are nominally matched to the 200 Hz BW of pings emitted from the sources. Outputs from each are threshold detected and the resultant detections used by the on-board processor to compute time delays from all references.

HARDWARE ACCURACY

Measurements have been made with the hardware to characterize the accuracy with which detections will be made as a function of in-band signal-to-noise ratio (SNR) at the input to an STS channel. As used here, SNR is defined as the ratio of received ping energy to the spectral level of the ambient acoustic noise at the ping frequency:

$$SNR = Eo - S_n(f_p) \quad (dB) \qquad\qquad (1)$$

where:

$S_n(f_p)$ = (ambient noise spectral level) dB re 1 uPa/Hz @ ping freq
Eo = (received power level of CW tone @ ping freq) + 10 log(.005 sec)

Figure 4 shows a typical STS channel's characteristic detection accuracy vs. SNR. For example, the 90% bands indicate the range of delays that include 90% of all detections. The central solid line indicates the delay bin collecting the most detections during the test. The non-ideal detector design causes accuracy at high SNR to be limited to the carrier period. These tests were performed using a signal generated on the bench that approximated the ambient noise spectrum observed in Arctic Ocean regions, summed with a tone burst of 5 ms duration to provide the various SNR levels. The rms voltage level of the signal was near the middle of the dynamic range capability of the STS hardware. At different frequencies, these curves change slightly and the detection time offsets vary, but at a given frequency, all cards behave similarly. Using these curves, it can be estimated that a minimum of 26 dB SNR is needed to obtain accuracy of about +/- 1 meter.

As a point of reference, at the 20 dB SNR level, approximately 10% of these pings are not detected. If the time series of a "raw" signal at this SNR is observed, the pings are obscured by the noise level, i.e. the broadband SNR is near 0 dB. At 22 dB or greater in-band SNR, virtually all pings are detected, with the accuracy ranges indicated.

SOFTWARE

A set of programs has been developed to compute position estimates after STS data have been converted to horizontal range. This has been done post real-time using a tracking routine followed by a position filter. An arbitrary baseline consisting of 2 of the source sensors is selected, with absolute azimuth information being supplied independently. The tracker first solves for the locations of the source sensors and then uses these results to locate each of the receiver sensors. In both cases this is done by first eliminating outlier ranges with a minimum absolute value algorithm, followed by a least squares fit to converge on a set of relative positions for each set of range samples. A 2nd order Kalman filter is used to smooth the resultant positions based on a simple physical model depending on the conditions present during the experiment. The convergence characteristics and behavior of these programs have been described in detail by Duckworth [2].

PERFORMANCE LIMITATIONS

Conceptually, the STS is simple though +/- 2 meter accuracy can be achieved at ranges beyond a few kilometers only with considerable care given to certain facets of the system. The most difficult to control is the "path-to-range" correction based on the sound speed profile. This is especially true in complex temperature/salinity regimes common in near surface Arctic waters. The important practical issues are, in order of the degree to which they tend to limit performance:

1) Knowledge of the local sound speed profile
Clearly, the most troublesome problem encountered is that of path

instability due to multiple paths. With all other variables being fixed once delay measurements are taken, the accuracy with which sensors can be localized depends on the path-to-range correction that is applied. Figures 5 & 6 show a section of data taken during PRUDEX from 2 active sensors, showing the delays measured on reciprocal paths, (x axis = record #, y axis = time in seconds). Particularly from Figure 5 it's apparent that multiple paths are being received. Any path could conceivably provide a "good" horizontal range measurement if the path to measurement correspondence could be sorted out to permit the right correction. Referring to Figure 5, it's likely that the shortest times are for the deepest path with no under-ice reflections; that the next shortest times belong to a deep path with a reflection at 1 or both ends; and that the longest, most variable times result from shallow paths with under-ice reflections. The symptom of severe fading is that of few and inconsistent detections at ranges where they should be much more consistent based on a transmission loss estimate.

2) Array geometry

During the deployment phase of an experiment, STS sources are placed about an array to optimize accuracy of subsequent position estimates. In particularly dynamic regions such as the MIZ, often sensors must be redeployed in an attempt to maintain a useful array geometry. Since it is necessary to determine array azimuth independently, a source element is placed near the data collection site as the lower end of the array baseline. The top of the baseline is set with a second source element sufficiently distant to minimize large changes in the positions of other sensors as a function of small changes in position of the baseline sensors. A reliable method of continuously recording azimuth has not been established. When identifable array sensors are in sight, a sextant or theodolite has been used. The remaining source units are placed to assure a good set of reciprocal delay measurements between source sensors as well as good geometry for computing locations of receiver sensors. Problems occur when sensors move close to the baseline and delay measurements are not stable, causing "flips" from one side of the baseline to the other.

3) Data link fidelity and sensitivity

Typically, a radio link at sonobuoy carrier frequencies and bandwidths has been used. Despite efforts to improve its fidelity, dynamic range is still the greatest shortfall in performance of the link and must be considered when setting audio gain at the transmitter. A practical sensitivity level prior to the data link, for STS purposes is about -140 dBV re 1 uPa/Hz in the 8 to 13 khz band. In conjunction with the requirements of STS, the same link is used to recover absolute acoustic spectral levels to 10 kHz. Currently, about 80 dB amplitude range is possible at 15 km with about a 16 db shift downward of that range at 10 kHz with prewhitening. A pitfall with insufficient or improperly placed dynamic range in the link is that the RF noise floor can rise above the acoustic ambient noise floor in the vicinity of ping frequencies, effectively absorbing ping SNR equal to the difference between these 2 noise levels.

4) STS source power levels

The pinger power level is between 25 and 50 watts acoustic, (185 to 188 dB re 1 uPa). This level has been determined as much by what is cheap, small, has modest battery power requirements and uses standard, available, crystals, as by expected losses over 20 km.

PERFORMANCE ESTIMATES

All data shown in figures described herein are taken from 2 files acquired during the PRUDEX experiment. In Figures 5 & 6, the estimated SNR at the 2 receivers is considered. Though probably excessive, spherical spreading losses on the deep paths have been assumed:

$$SNR = SL - 20 \log(R) + 10 \log(T) - A - K - S_n(f_p) \qquad (2)$$

where:

SL = 185 dB re 1uPa @ 1 m	source level	
R = 12.5 km	8.65 sec * 1440 m/s	
T = .005 sec	ping duration	
A @8khz .8 dB/km	estimated attenuation due	
@9khz 1.0 dB/km	to absorption @ 0 degrees C.	
K = 5 db	RF noise floor -	
	acoustic noise floor	
	for 8 khz ref sensor link	
$S_n(f_p)$ = 40 dB re 1uPa/Hz	measured acoustic noise	
	floor @ 8-9 kHz	

The dynamic range limitation of the radio link affects the estimated SNR in this example. Signals received by the 8 khz source sensor had insufficient audio gain to bring the acoustic ambient noise in the 8-13khz region above the noise floor of the telemetry system. The earliest arrivals in Figure 5 often fade enough that the added loss due to link dynamic range precludes detection. In comparison, the reciprocal path to the 9 kHz source sensor, Figure 6 is more reliable. Spectral plots at these ranges, made in the field, show that the inadequate link dynamic range caused an effective loss of 4-8 dB in SNR in the 8 to 13 kHz band.

The figures shown above result in SNR's of 30 dB and 25 dB for the 8 kHz and 9 kHz sensors respectively. These estimates are probably low considering that spherical losses were assummed. In contrast, Figures 5 & 6 suggest somewhat higher losses on the faster paths than these computed SNR's indicate since often they are not detected. They also suggest that arrivals in the 8.68 to 8.69 sec range, contained more energy since they are never missed. The SNR estimates appear to be much higher than what the STS detectors received otherwise the pings would have been detected more reliably. Fading due to interference is the most plausible explanation.

At 15 km, the spherical spreading loss is 83.5 dB. Again, this is probably excessive as a realistic spreading loss, though numerous time series plots of pings from ranges up to 6 km have shown total losses that are within plus or minus a few dB of spherical plus absorption losses. Including absorption losses, the estimated SNR's for deep paths at the 5 frequencies is the following, (disregarding any problems with radio links, and assumming an observed ambient acoustic level of 37 dB):

8 khz	27	dB
9 khz	24	dB
9.5 khz	22.5	dB
11 khz	16	dB
13 khz	8	dB

These ratios show that detections made at 11 or 13 khz, spreading losses are something less than spherical. The most likely paths to be concerned with are the direct, the paths with one reflection at either the source or the receiver, the path with a reflection at both ends and possibly 1 or more of the paths that are near the surface with a few reflections. Difficult to quantify scattering losses become an issue with the latter.

During PRUDEX there was a paucity of consistent delays measured from 9 khz pings from all sensors at the 15 km range, suggesting an SNR less than 18-20 dB, despite what might be computed. Again, the only current explanation is fading due to interference. As might be expected, data from the 9 kHz sensor, shows significantly better reception at 9.5 khz than at 13 kHz possibly because of the increased absorption loss.

Figures 7,8, & 9, all at the same resolution in time, compare delay data from 3 dramatically different ranges, each showing use of a single stable path. Figure 7 shows delays measured between sensors at the ends of 2 of the hardwired array legs at 9.5 kHz. Disregarding actual sensor motion, it's reasonable to expect that with the 200 usec sample period of the STS processor, most detections would be at 1 or 2 different delays. Greater deviations are possibly watch circle motion. Figure 8, at a range of approximately 6.5 km, and 11 kHz shows essentially the same character. There are actually 2 points not shown on this scale that appeared to be slightly slower paths, but this is a case of a moderate range where a single path was clearly dominant. Figure 9, at about 12.6 km and 8 kHz shows more deviation, but is still very stable. The reciprocal paths in these 3 cases are similarly good, though other sensors at these ranges often have significantly less consistent delays. All 3 of these examples exhibit delay accuracies that would be expected if the STS detectors had receive levels given by an SNR computation as done earlier.

Much of the data taken during PRUDEX is somewhat more complex than depicted by Figures 8 & 9. Currently, the path-to-range correction is made using a raytracing routine to create a range-time table and assumes that segments of that table are linearly connected. Measured delays are then converted to the shortest range that corresponds with a given delay, i.e., the measured delay is assumed to be from the fastest path, which is not necessarily true at longer ranges.

Development of a method for a more accurate correction using information about a possible set of paths in use at any given range is in progress. Figures 10 & 11 show the estimated errors in x and y axes for the 9 kHz sensor at approximately 15 km from the apex sensor after a crude attempt at this type of correction. These estimates are generated by the tracking routine as it propagates the fitting error through the least squares solution. Figure 12 is the relative position computed using the same data.

CONCLUSIONS

As used in 1984, in the MIZ, STS sporadically provided relative position estimates for an array aperture up to 5 km, with accuracies of +/- 2 to 3 meters. Reasonable array geometry was difficult to maintain due to an extremely divergent ice field.

Using STS data taken during the PRUDEX experiment, it can be demonstrated that an array of hydrophone sensors in Arctic waters can be located at ranges up to 15 km. Under PRUDEX conditions, relative position accuracy of +/-1 to +/- 2 meters can be achieved at ranges up to about 12 km. while accuracy at 15 km, using current time-to-range conversion methods, is closer to +/- 3 meters. Location accuracy at this time is sufficient to allow coherent processing to about 50 Hz with sensors at 15 km. The development of a more sophisticated method of time-to-range conversion shows promise for improving accuracy at the more distant ranges.

The importance of good quality sound speed information in the vicinity of an STS array cannot be overemphasized. During PRUDEX, it was not possible to obtain local profiles. Sound speed data acquired coincident in time but at 30 miles distant has been used used to make path to range corrections. These profiles, in most cases show a maxima near the 60 meter sensor depth used during PRUDEX which might be responsible for some shadow zone effect at certain ranges. In the future, the sound speed profile should be measured just prior to sensor deployment so perhaps a more judicious selection of sensor depth can be made, in conjunction with other experimental requirements.

Certain aspects of STS could be improved. At the hardware level, the bandwidth prior to hardlimiting could be decreased and the transition bands made sharper as well. There has been a constraint to keep the hardware simple to make expansion cheap. Easily programmable switched capacitor filters might be used for the BPF's so that a wide variety of ping frequencies could be accommodated.

Software at the card level could be modified to more closely "window" the acceptance period for new reference pings and possibly data pings as well. This would eliminate most instances of a channel locking onto an erroneous reference time which has been observed on occasion.

The combination of 80 (or more) db dynamic range in the telemetry link coupled with careful positioning of that range with gain is needed. STS needs an effective sensor sensitivity of about -140 dBv re 1 uPa, to have a good probability of sufficient accuracy at 15 km with current source levels, and anticipated acoustic ambient levels.

ACKNOWLEDGMENTS

REFERENCES

1. von der Heydt,K., Duckworth,G.L., and Baggeroer, A.B., "Acoustic Array Sensor Tracking System",Proceedings of the IEEE Oceans '85 Conference,1985
2. Duckworth,G.L.,"A Robust Algorithm for Tracking of Drifting Acoustic Arrays in the Arctic",1987 Asilomar Conference Proceedings,1987.
3. Davenport,W.B.,Jr.,Signal-to-Noise Ratios in Band-Pass Limiters, Journal Applied Physics 24(6), pp 720-7, June 1953.

BATTERY POWERED
RF TELEMETRY
TRANSMITTERS →

ICEFLOE
2–4 m

60m

1m

PASSING SENSOR

REFERENCE SENSOR
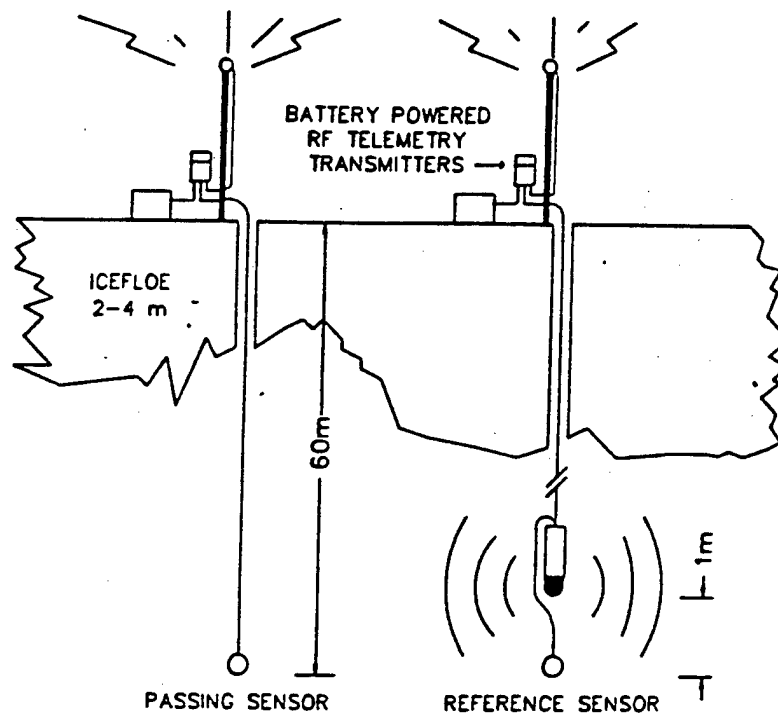
FIGURE 2

STS ARRAY CONFIGURATION
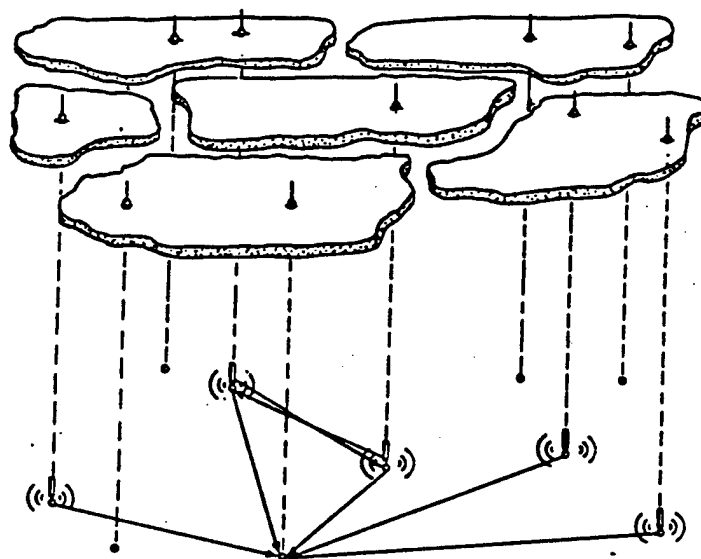
FIGURE 1
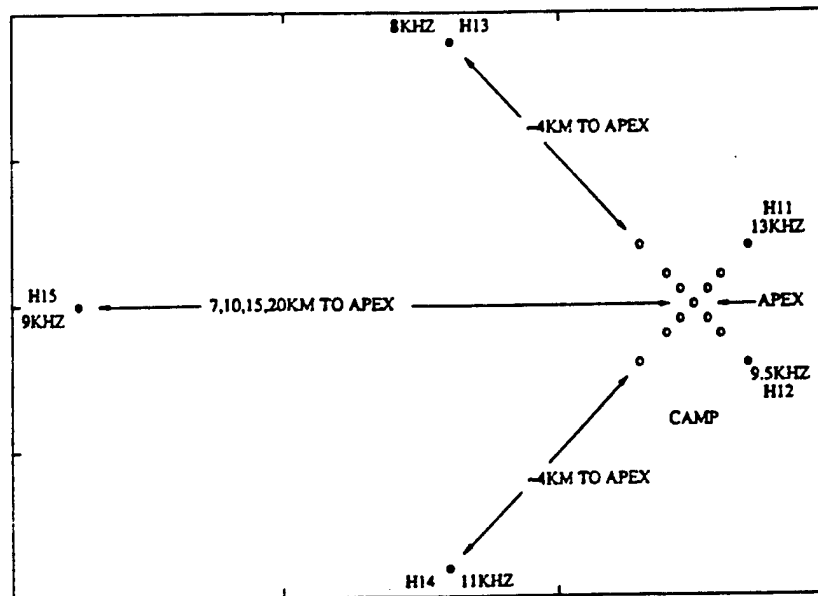
FIGURE 3. PRUDEX ACOUSTIC ARRAY GEOMETRY
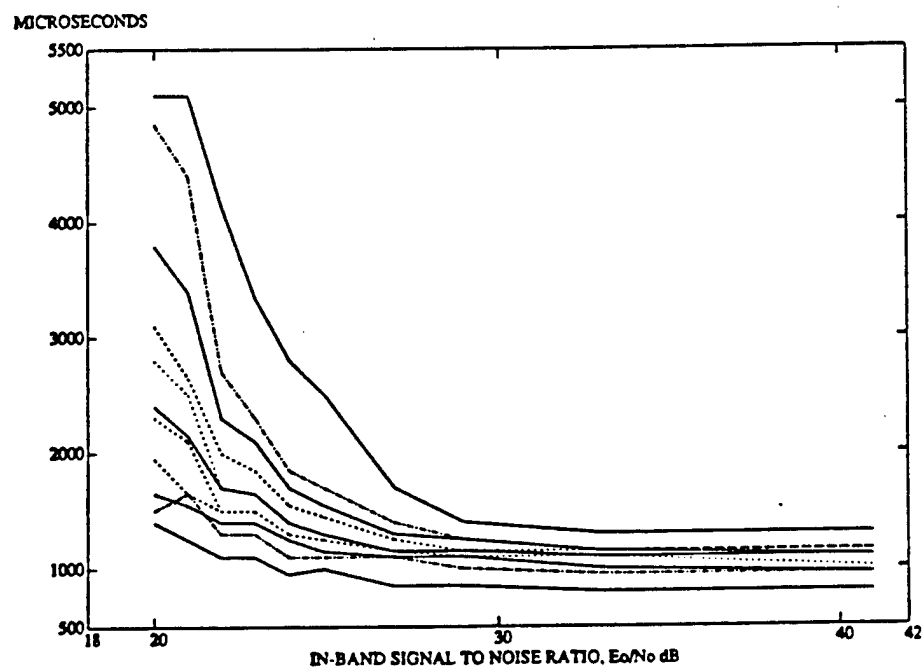
FIGURE 4. STS HARDWARE DETECTION DELAY VS SNR

SECONDS   STS DELAY DATA, UNCORRECTED, DAT.2.0, SENSOR H15

SAMPLES, 30 SECOND INTERVALS

FIGURE 6

SECONDS   STS DELAY DATA, UNCORRECTED, DAT.0.1, SENSOR H13

SAMPLES, 30 SECOND INTERVALS

FIGURE 5

130

SECONDS   STS DELAY DATA, UNCORRECTED, DAT.0.3, SENSOR H13

SAMPLES, 30 SECOND INTERVALS

FIGURE 8

SECONDS   STS DELAY DATA, UNCORRECTED, DAT.8.2, SENSOR H11

SAMPLES, 30 SECOND INTERVALS

FIGURE 7

131

RELATIVE LOCATION, UNFILTERED, PRUDEX 13B,138, SENSOR H15

FIGURE 12

STS DELAY DATA, UNCORRECTED, DAT.2.0, SENSOR H15

FIGURE 9

132

ERROR ESTIMATE, Y DIRECTION, SENSOR H15 @ 15 KM FROM APEX

SAMPLES, 30 SECOND INTERVALS

FIGURE 11

ERROR ESTIMATE, X DIRECTION, SENSOR H15 @ 15 KM FROM APEX

SAMPLES, 30 SECOND INTERVALS

FIGURE 10

133

AN ARCTIC REMOTE AUTONOMOUS MEASUREMENT PLATFORM

Kenneth E. Prada
Woods Hole Oceanographic Institution
Woods Hole, Massachusetts

and

Arthur B. Baggeroer
Massachusetts Institute of Technology
Cambridge, Massachusetts

ABSTRACT

Perpetual ice cover in the Arctic inhibits broad analysis of the region. Ice camps and research ships do not provide sufficient temporal and spatial coverage. Satellites expand the coverage, but only within the limits of on-board sensors. A multidisciplinary data collection tool is needed to expand coverage in ice covered regions.

The Arctic Remote Autonomous Measurement Platform (ARAMP) is a drifting ice or water borne platform to collect data from a variety of sensors, transmit selected results by Argos satellite, and store large data sets for later recovery or off-loading via RF telemetry. A typical sensor suite includes vector wind, barometric pressure, air temperature, humidity, compass, surface temperature, ice motion, broadband ambient noise, and upper ocean currents, temperature and conductivity. Optional sensors might measure ice thickness, ablation, thermal conductivity and solar radiation.

ARAMP is a four meter augmented spar buoy. A tower above supports an anemometer, meteorological sensors and antennas. A variable length cable below provides power and communications to underwater sensors. A three-axis accelerometer for ice motion measurements is inside the buoy. Data collection is controlled by a powerful microcomputer that performs intelligent data sampling, spectral analysis of ambient noise, telemetry, data compression, and internal storage.

INTRODUCTION

The Arctic is a critical region in which polar air, ice and water masses interact with the temperate ocean and climate systems. The processes which take place there profoundly influence hemispheric climate and have significant effect on naval and commercial operations. Some of the research interests in the Arctic involve:

- growth, propagation, and decay of ice-ocean eddies as affected by ice edge dynamical processes and their role in lateral heat transfer across the ice edge;
- changes in acoustic refraction and coherence via related changes in sound speed profiles due to fronts, ice-ocean eddies, and internal waves;
- intensification of ice cracking noise mechanisms as related to ice-ocean eddies, gravity waves, and presence of recently frozen thin ice;
- winter ice edge meteorology including mesoscale cyclogenesis (Arctic lows) as influenced by large temperature and water vapor contrast at the ice edge;

- morphology and dynamics of the ice field created by forcing of intense incoming gravity waves, winds and current.

These interests are part of studies in the Arctic environment which include acoustics, oceanography, meteorology, and ice and wave studies. The needs emphasize a strong interdependence between each of the research areas. Simultaneous spatial and temporal sampling of currents, water temperature, conductivity, vector winds, air pressure and humidity can provide valuable concurrent data for better understanding of the Arctic physical processes.

A key element of these studies is the ability to sample both environmental and ambient noise data concurrently at locations remote from a major ship or ice station. This capability can broadly expand spatial and temporal coverage while reducing the burden on ships and helicopters in obtaining measurements. It also can enhance the usefulness of data in expanding our understanding of the Arctic ice-ocean-air processes and their impact on acoustic ambient noise. It can allow data collection and analysis at times of the year when ships and ice camps cannot easily function. It also can provide for future autonomous instrumentation of various Arctic areas to fully replace the need for ships or ice camps and to provide extended temporal coverage that ships and camps cannot sustain without great cost and difficulty.

To accomplish these measurements a multi-sensor platform was needed that could perform the required measurements in the Arctic pack ice, the marginal ice zone and in open water. A prototype platform was built during 1986 and tested during March and April of 1987 as part of a field program north of Prudhoe Bay, Alaska. This report describes the prototype platform, its test results, and the platforms being produced for use in 1989 CEAREX field experiments.

THE ARAMP PLATFORM

The basic platform is a 14 foot (4.2 m) augmented spar buoy (figure 1). This configuration was selected to permit use in both ice and water. The spar is a rolled aluminum tube of 0.25 inch (6.35 mm) wall thickness with a tapered diameter. The upper 4 feet (1.2 m) has a constant diameter of 10 inches (254 mm). The remaining length has a linear taper with the diameter ranging from 10 inches (254 mm) at the top to 7.5 inches (190 mm) at the bottom. The taper facilitates easy removal of the spar from the ice.

A two-piece collar provides flotation. Each collar half is a hot molded sheet polyethylene shape filled with poured foam. The collar halves are bolted together on the spar prior to deployment. The plastic collars are light weight and less expensive than equivalent metal flotation collars.

A 10 foot (3 m) aluminum tower is mounted atop the buoy to provide support for meteorological sensors and telemetry antennas. The tower is designed for attachment of a meteorological package within the base of the tower frame. This positions the package weight at a lowest possible point and within the vertical axis of the buoy, thus maintaining optimum platform stability. An anemometer is attached at the tower top. Antennas for ARGOS and VHF telemetry are mounted on arms below the anemometer.

A data cable is suspended below the platform to provide mechanical support, power, and telemetry for attached sensor units. The cable is specially designed for this application (figure 2). It consists of a central RG-58A/U

coax with urethane jacket. This is surrounded by four #20 AWG conductors positioned in the four quadrants and supplemented with polyethylene fillers. A 30 mil urethane jacket separates the core wiring from the braided Kevlar strength member. The outer jacket is an abrasion resistant braided nylon with integral hair fairing stitched into and bonded to the nylon jacket. Outer diameter is 0.45 inches (11.5 mm) and design breaking strength is 1400 pounds (635 kg). Test breaking strength is greater than 4000 pounds (1814 kg). The cable is used in pre-cut lengths with an eye splice for the mechanical termination and Impulse series XS connectors for electrical termination.

The coaxial cable carries hydrophone signals and is chosen to support either a single hydrophone driving the cable at baseband or multiple hydrophones using analog or digital multiplexing techniques. The four single conductor wires are used as redundant pairs to concurrently carry power and digital data.

SENSORS

The prototype sensor suite has three sections, a meteorological package above the platform, internal accelerometers, and sensors attached to the suspended data cable The sensors are shown in block diagram in figure 3.

Meteorological sensors measure wind velocity and direction, air temperature, humidity, barometric pressure and compass. The package was acquired from Coastal Climate Company and contains an integral intelligent controller for sensor data acquisition and transmission to the platform controller.

An accelerometer unit is housed within ARAMP near the midpoint in its length. This unit, designed and built by Scott Polar Research Institute contains a triad of orthogonally mounted accelerometers with a compass. The accelerometers are mounted on a pendulum suspended from a set of damped gimbals, which ensure stability relative to the vertical and the limiting of pendulum resonance. Linear servo accelerometers are used and achieve resolutions to 8 micro g and accuracy to 32 micro g.

Sensors attached to the suspended cable include a current meter, temperature-pressure modules, and a single hydrophone. The hydrophone, with integral pre-amplifier and cable driver, is enclosed in a stainless steel rod cage. It is foam wrapped to reduce flow noise and is suspended in 'dead' silicon rubber compliant bands to decouple strum.

The current meter is the Smart Acoustic Current Meter (SACM) with tilt, pressure and conductivity options, produced by EG&G . Two factors influenced its selection. With support cage it fits easily through a ten inch ice hole and it is available in a configuration that supports cable telemetry of data.

Temperature and pressure measuring modules were designed and built at WHOI for attachment at selected points on the cable.

SENSOR COMMUNICATIONS

Most of the sensors are intelligent, i.e., they contain integral microcontrollers that, at the least, perform data sampling and telemetry. A standard communication protocol is used within ARAMP to interconnect sensors and platform controller. This is the ANSI/IEEE 997-1985 standard (1), the Serial ASCII Instrument Loop (SAIL). This protocol employs three different

physical layers within the ARAMP system. Communication with the meteorological package uses an open drain CMOS line. This path is short and the open drain line permits later connection of additional sensors within the platform. The suspended cable uses an FSK method that follows the Bell 202 standard, allowing half duplex data telemetry at 1200 Baud. This same FSK link is available at the top of the platform for connection to optional sensors mounted on, within, or through the ice separate from the platform. The third physical layer is a VHF-RF link that utilizes 1200 Baud FSK carrier modulation. The VHF link is used for remote platform control, local data telemetry, and as a location beacon.

PLATFORM ELECTRONICS

The platform electronics consists of several sections; controller, mass storage, analog front end, and telemetry.

Controller Section

The controller section consists of five circuit cards; processor, memory, modem, analog-to-digital converter, and power control.

The platform processor is an IBM-PC configured to occupy a single circuit card plugged into a standard IBM-PC bus. The card is commercially available populated with NMOS and TTL integrated circuits. Minor revisions and re-population with CMOS integrated circuits produce a processor system with the full potential of the IBM-PC in a low power version that is physically compatible with installation in tubular containers. This approach to the selection of a processor has resulted in the ability to design functional circuit boards that conform to the PC bus specifications, and can be tested in any compatible PC.

The memory card contains provisions for both EPROM and RAM. It also contains a UART for communication functions, a real-time clock, dead-man timer, and the interface to the mass storage section.

The analog-to-digital converter is a 12-bit CMOS device capable of 20 kilohertz sampling. There are provisions for 24 input channels. Eight of these channels are used to monitor internal parameters such as battery condition, temperature, etc. The remaining channels are for input from hydrophones and accelerometers. Four channels contain simultaneous sample/hold devices to maintain phase coherence between hydrophone and accelerometer signals. This card also contains circuitry to control gain and power in the analog front end section.

A power control card provides regulation and switching of required voltages for all internal electronics sections and the cable. The final card contains the FSK modem for cable communications.

Mass Storage

Two megabytes of mass storage are available using CMOS static RAM. This is an interim solution for mass storage and will be replaced or augmented for production units. It was, however, a quick and convenient method for prototype testing of ARAMP and allowed long term low temperature evaluations of alternate mass storage systems to proceed independently from ARAMP

fabrication and testing. Mass storage is used for high volume data sets such as noise and ice dynamics spectra.

Analog Front End

The analog section has amplification and filter functions for signals derived from the hydrophone and accelerometers. There are provisions for nine low frequency (5 to 250 Hz) channels and one high frequency (5 Hz to 10 kHz) channel. Each of the channels has independent power control. Gain is controlled from the A/D card in steps of 6 db over a range of 42 db. Filters are fifth order elliptic low pass types with attenuation of 60 db in the stop band and a 60 db/octave slope.

Telemetry

ARGOS telemetry is used for low volume data such as meteorological, temperature/pressure, and current values. Local telemetry is provided by a VHF transceiver operating in the 160 to 172 MHz region. A microcontroller provides an interface between the transceiver and the platform controller. The VHF control functions include transmitter keying, signal quality detection and data stream control.

SOFTWARE

There are three groups of software within ARAMP; resident monitor, tests and diagnostics, and operational functions. The monitor has a large number of functions that permit interactive debugging of system hardware and software. Further, the monitor contains DOS input/output emulation routines. The majority of ARAMP software is written in the 'C' language. The combined PC compatible hardware and DOS compatible high level language software permits the development and testing of complex functions and algorithms in the laboratory PC environment for later transfer to the ARAMP platform.

Test and diagnostic software enables interactive evaluation and calibration of all sensors and the mass storage system.

Operational software in the prototype was limited to functions designed to evaluate both short and long term acquisition and recording of data from each sensor. Development of the full suite of software required for long term data collection, recording and telemetry is an ongoing project for at least the next year. This software includes acoustic event detection, spectral analysis of both hydrophone and accelerometer ambient noise measurements, data type correlation, data compression and storage, high speed telemetry via VHF-RF, and ARGOS telemetry of routine low volume data sets.

DEPLOYMENT AND RECOVERY

Deployment and recovery are issues of great importance. A platform of this type is of small value if the logistics and complexity of use do not permit quick deployment and recovery. Helicopter payloads and handling by only two people are critical factors.

Two devices were designed to facilitate handling. A four legged frame with suspended chain fall was used to lower and raise the platform. The frame is 16 feet (4.9 m) high and is constructed of aluminum tubing. It is easily

assembled by inserting leg sections into the top framework. Sections are held in place by locking pins to eliminate the need to handle threaded fasteners in the Arctic cold.

A small winch with removable reels was fabricated to handle the suspended cable. Each reel contains a length of cable, mechanically and electrically terminated for attachment to an instrument or another cable section. The winch is positioned directly over the ice hole to simplify cable handling.

FIELD TESTS AND RESULTS

The prototype ARAMP was tested during a field experiment in the Arctic north of Prudhoe Bay during March and April of 1987. The tests were part of a larger engineering field program to test new systems for acoustic and geophysical data acquisition.

Deployment and recovery issues constituted a substantial portion of ARAMP testing. The cable deployment system worked well with the exception of the cable connectors. These exhibited consistent O-ring failures during assembly in the cold environment. Although the manufacturer had provided special low temperature O-rings, they deformed under assembly pressures and would not make good seals.

The physical size and weight of the fully assembled platform with tower and batteries is slightly larger and heavier than is practicable. While the camp deployments went smoothly, the two person limitation during helicopter supported deployments could prove difficult. Weight reduction also will ease helicopter payload to more reasonable levels.

All sensors worked well during deployment. There were no failures attributable to low temperature operation. Calibration and sensor drift issues have not been examined yet. The primary field issues involved successful deployment, recovery and operation of all system components. Calibration issues can be addressed in laboratory environmental chambers.

Software presented some major problems. These did not hinder proper and thorough tests of all sensors and systems. However, large volume concurrent data collection was not possible due to the software difficulties.

CHANGES AND IMPROVEMENTS

The experience gained from the prototype deployment and tests shows where changes are needed. Some particular areas for change involve the cable connectors, primary and secondary power systems, and the software needed for proper field operations.

The cable connectors are being replaced with a different design that eliminates O-ring use yet performs well in the cold. The new connectors are the XSG series from Impulse and offer easier assembly in the cold environment.

The platform will be reduced in length by at least one meter. This will reduce weight and handling problems, but will require thinner ice for deployment. Internal ballast will be removed and replaced with additional secondary batteries. This expands operational life while reducing overall weight. Platform stability should not be affected by the weight reduction.

139

The primary battery, a new salt water type tested separately during this field experiment, will be integrated with ARAMP to provide primary power. The secondary power regulation and control section will be redesigned to further improve regulation and efficiency. The design of special switching regulators effective at low temperatures is needed. Several commercial high efficiency switching regulators failed at the low temperatures used for testing in the laboratory.

The mass storage system, static RAM in the prototype, will be augmented with optical disk. Low density (120 megabytes per disk) optical disk drives and media have been successfully tested at extremely low temperatures (-30 C). The disk drives are available with direct support for the IBM-PC bus and, hence, are easily adapted to our processor system.

The telemetry section will be expanded to include a second VHF transmitter channel capable of at least 50 kiloBaud data transmission. This channel will provide for high speed data offloading. Competent error detection and correction techniques will be used to guarantee data integrity.

A substantial number of changes are underway for the processor hardware and sofware. Figure 4 shows a block diagram of the redesigned processor section. The processor will be fully DOS compatible and will execute the PCDOS operating system. A resident EPROM BIOS has been developed to support DOS compatibility. An improved memory section will provide 256 kilobytes of EPROM for use as a read-only disk for the PCDOS system. The 2-megabyte RAM mass storage will act as the system's "B" disk drive, and the optical disk will be a fully DOS compatible 'C' drive. These changes provide a greatly expanded ability to develop and test complex software without the need to accomodate those problems and limitations associated with the generation of ROMable code. Operational programs may be developed in any PCDOS compatible machine using a variety of high level languages, stored on removable optical disk media for transfer to and execution within the platform. Program size and complexity will no longer be limited to available EPROM space or a single unwieldy program. Different programs can be loaded from disk to accomodate changing conditions and sampling requirements. Programs stored on disk can also vary dependent on experiment needs and deployment sites and conditions.

ACKNOWLEDGEMENTS

REFERENCES

(1) ANSI/IEEE Standard 997-1985, Serial ASCII Instrumentation Loop (SAIL) Shipboard Data Communications, IEEE Publication SH09993, May 1985.
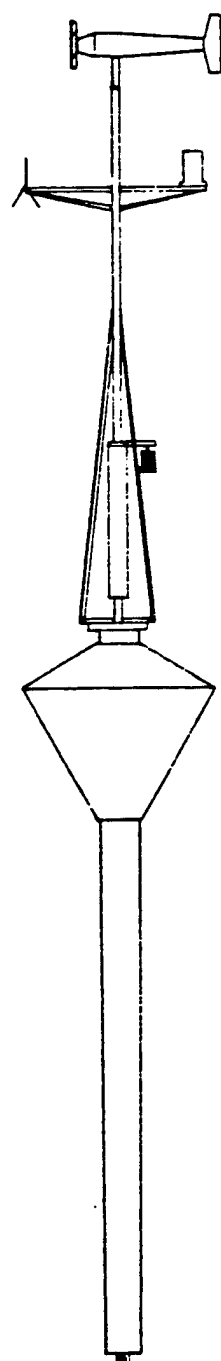
Anemometer

VHF Antenna
ARGOS PTT Antenna

Tower
Material: Aluminum Tubing
Length: 3.05 m

Meteorological Package
    – air pressure
    – air temperature
    – humidity
    – compass

Flotation
Material: Molded Sheet Polyethylene
         Foam Filled

Buoy
Type: Augmented spar
Material: Rolled Aluminum
Length: 4.25 m
Diameter: 190 mm / 254 mm
Taper: 63 mm / 3.05 m

ARAMP   Figure 1.   Basic Platform Outline Diagram

RG-58A/U COAX
20 AWG CONDUCTORS
POLYETHYLENE FILLERS

.195   .38 .400

.072

DACRON BRAID
WITH 3/4" HAIR FAIRING

POLYURETHANE JACKET

KEVLAR FOR CABLE BREAKING STRENGTH OF > 1400 lbs.
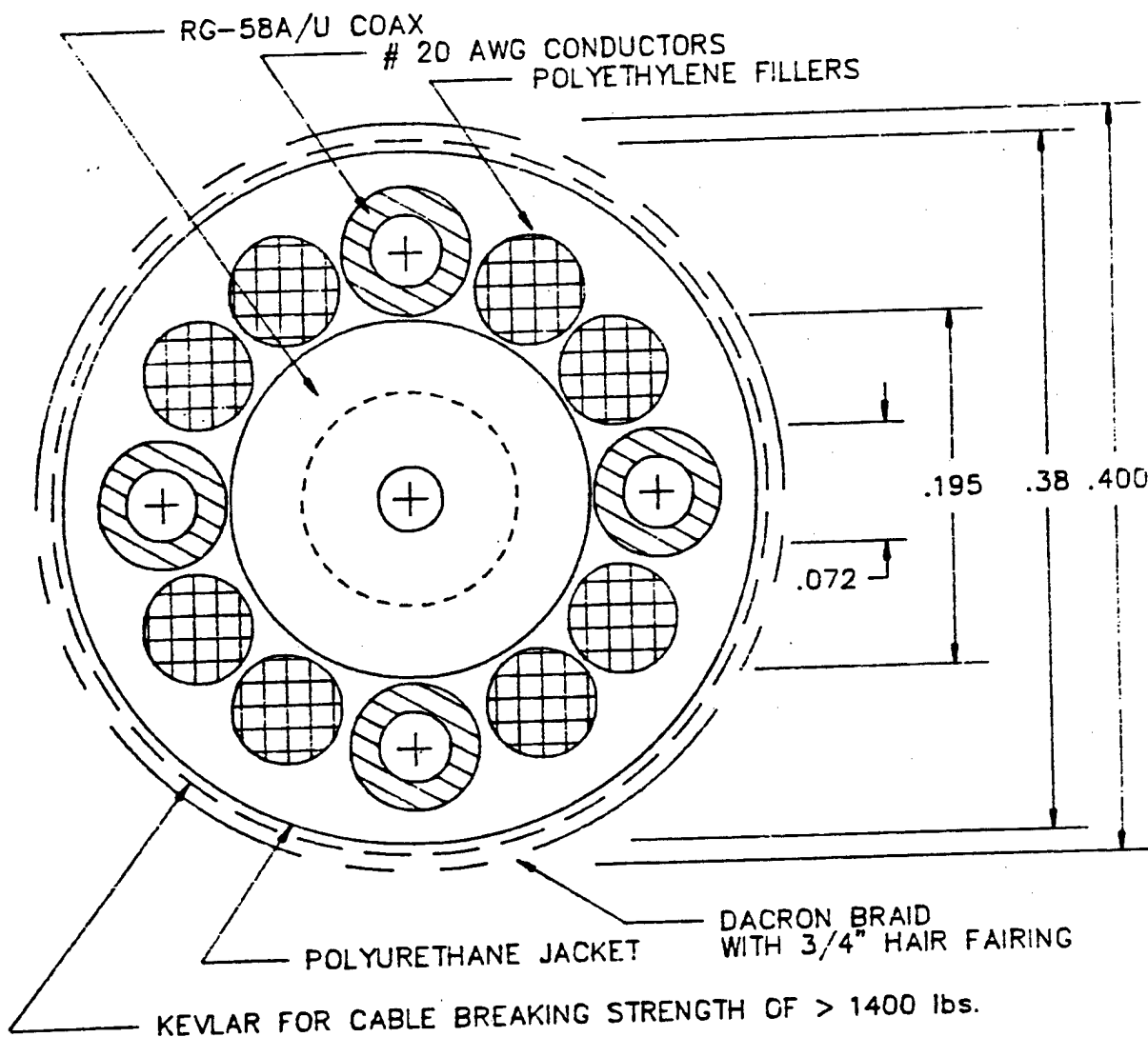
ARAMP   Figure 2.   Cable Outline Diagram

142
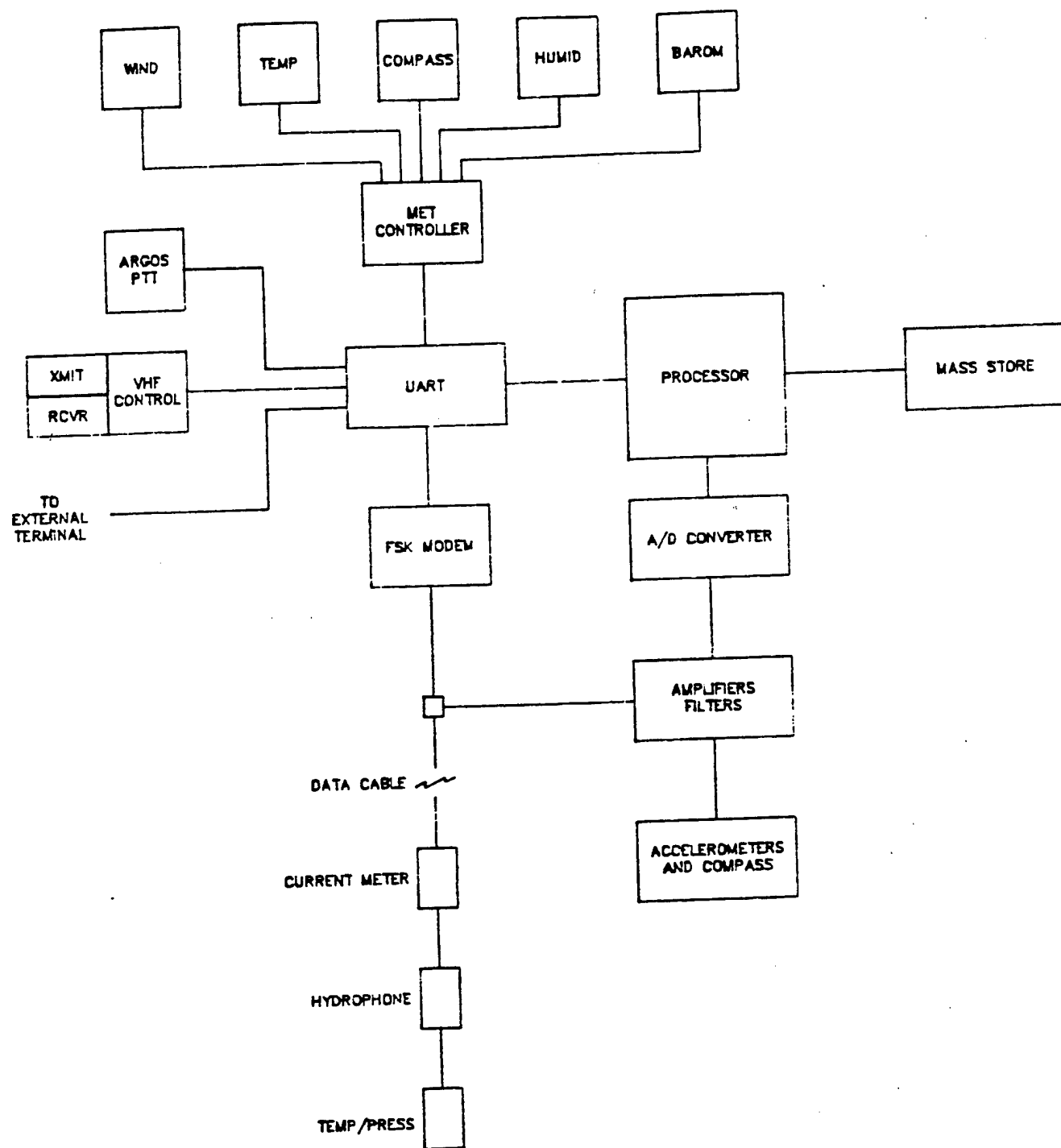
ARAMP   Figure 3.   Platform System Block Diagram
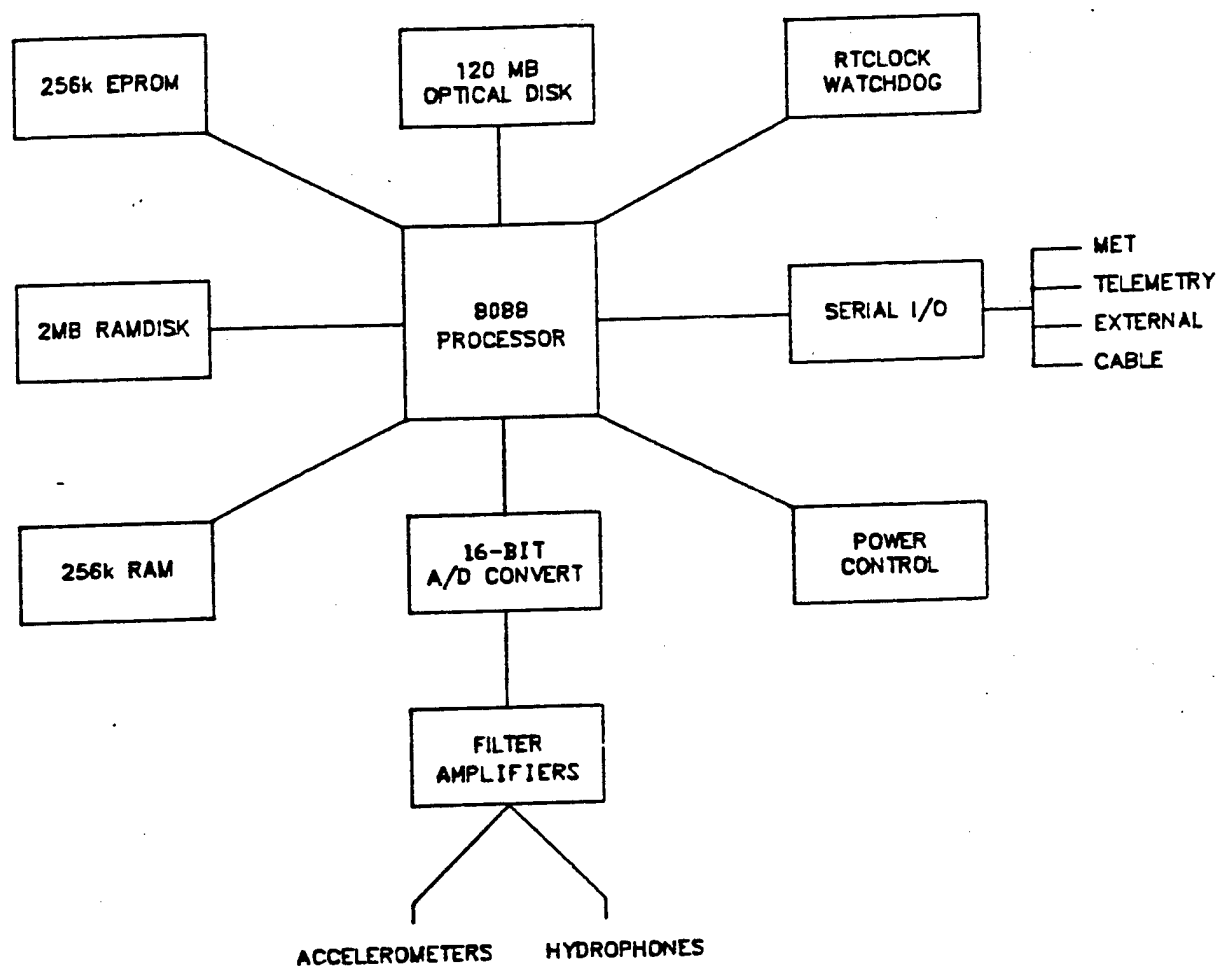
ARAMP   Figure 4.   Revised Processor Section Block Diagram

Methods for Measuring Arctic Ice Scattering Responses
and Precise Underice Configuration
by Terry Ewart and Eric Thorsos, APL,UW

The purpose of this presentation is to propose instrumentation designs that fit the requirements for future acoustic scattering experimental field efforts in the Arctic. The first design is for an acoustic source/receiver that would operate at 400 Hz with a conical beamwidth of 5 degrees(3dB down from axial) at a level near 240 dB re 1 a/1m.

The array consists of a circular array 20m in diameter with 61 elements. An ice deployment of the array is shown in Figure 1. Figure 2 shows a possible array of 61 elements(the actual configuration will be computed by optimization later). The transducers are fixed to a net that is held taut by four arms that fold up like an umbrella. The array will be launched with the net side of the array down as shown in Figure 3 where the array is in its fully collapsed position. Figure 4 shows the array in the partially erected position with the arms opening, and Figure 5 shows the array erected prior to tensioning the tilt and pan cables. Stress and drag analyses have been done with the conclusion that a maximum operating current would be 20cm/s at an operating depth of 300m with a reasonable ballast weight. The frame is constructed from 6 in. diameter 0.25 in. aluminum tubing. Tilt and pan is achieved by the cables shown in Figure 1.

The pattern as a function of the angle from axial in the vertical direction of the array in Figure 2 is shown in Figure 6. It is assumed that an additional 7 dB can be obtained by shading either geometrically or by adjustment of the number of elements in each ring. This would reduce the source level but produce sidelobes > 50 dB below the peak two-way transmission. Patterns at 10 degree intervals from the vertical were computed showing very little change in sidelobe variability. The array has 4 circular distributions of transducers and a central one. The array would be driven as a 2-terminal network, but split beams, 9 wires would be brought out for receive-mode to allow split beam processing. This allows better angle of incidence resolution in the data processing for backscattering(Ref. Jackson,et al, JASA 80(4), 1986).

An essential part of any scientific acoustic scattering experiment is the precise definition of the geometric shape that is being ensonified. A system has been devised that can provide extremely accurate 3-dimensional measurement of the underside of the Arctic ice canopy. It is called, Geodesic Underice Tramway System-GUTS. The system employs a set of three cable-coupled winches to maneuver acoustic field and ice mapping apparatus over a plane immediately below the ice. The cables are passed between holes using free swimming small vehicles to carry a lead line. Figure 7 provides a diagram of the system with blowups of the virtual mass that is coupled at very high tension(~3000 lb) to the winches and typical forward and backscatter illustrations. The instrument carrier above the virtual mass and the electronics package below are neutrally buoyant —+200 lb and -200 lb respectively. They are driven vertically with a small constant- tension drive on the vertical mass. The expected positioning accuracy of the system derives from an acoustic tracking system (shown in Fig 7). A computer(MASSCOMP 5500 as used in AATE) will provide the control logic. The ice sensors can be high frequency acoustic ice bottom surface mappers and also provide thickness by using a lower frequency. Nonlinear sonars have demonstrated excellent characteristics for such purposes(Wallerstadt,SAIC).
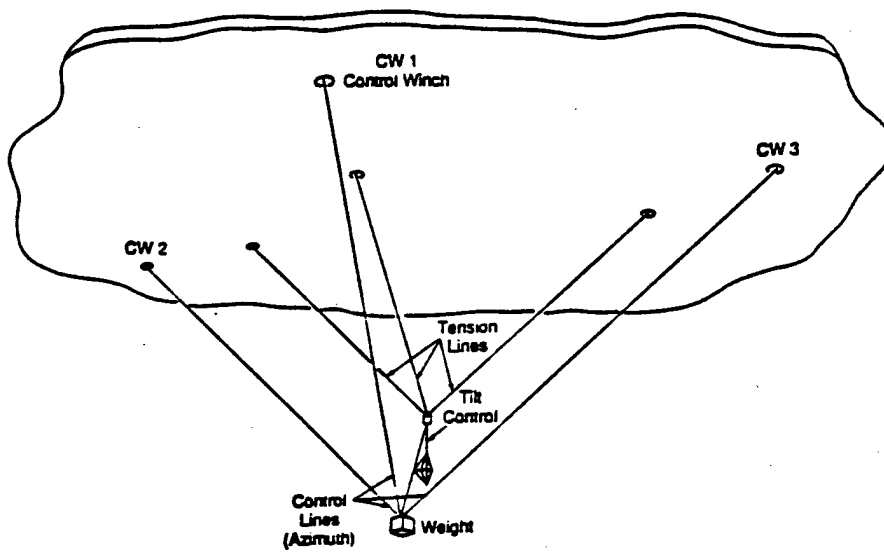
Figure 1. Array deployed for making under-ice scattering measurements

Figure 2   Tranducer Support Net Showing Transducer Placement

ICE
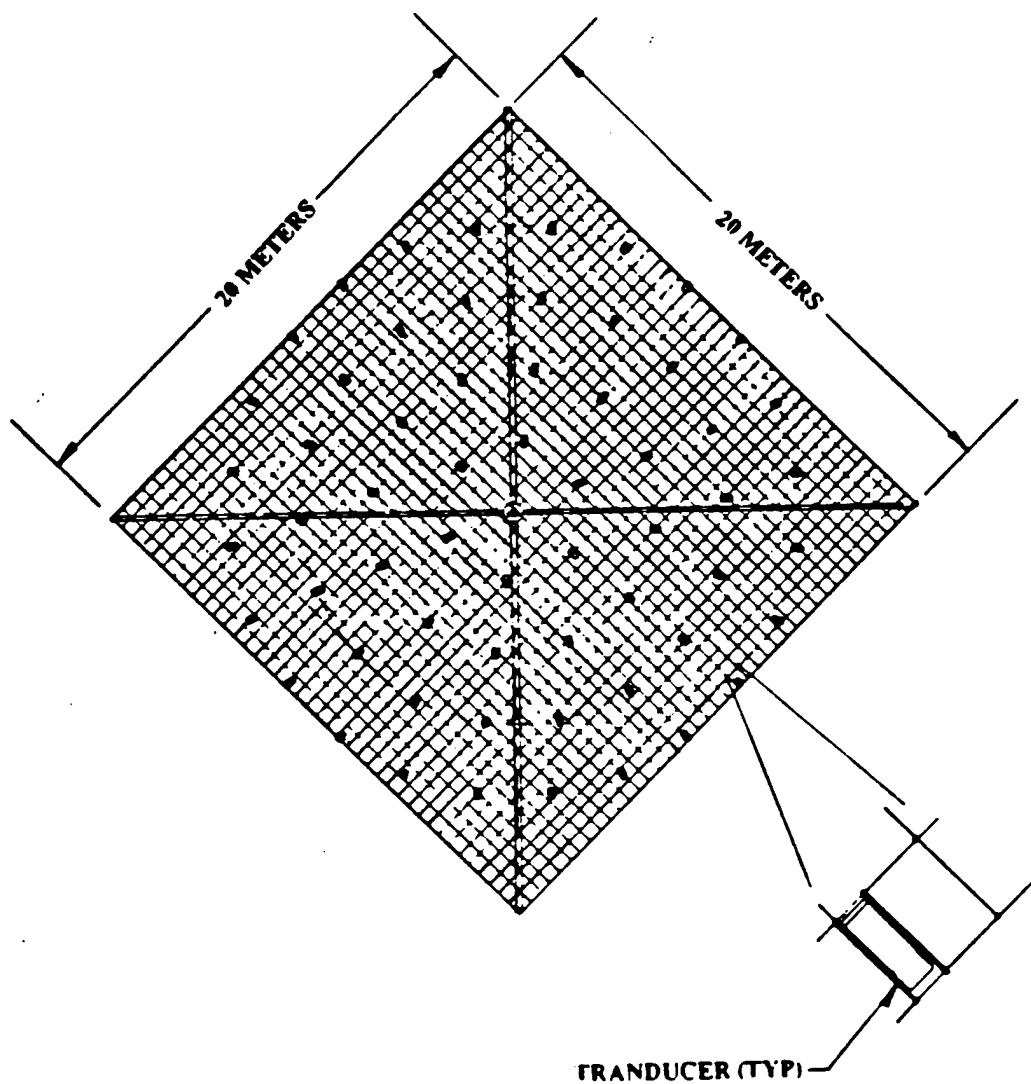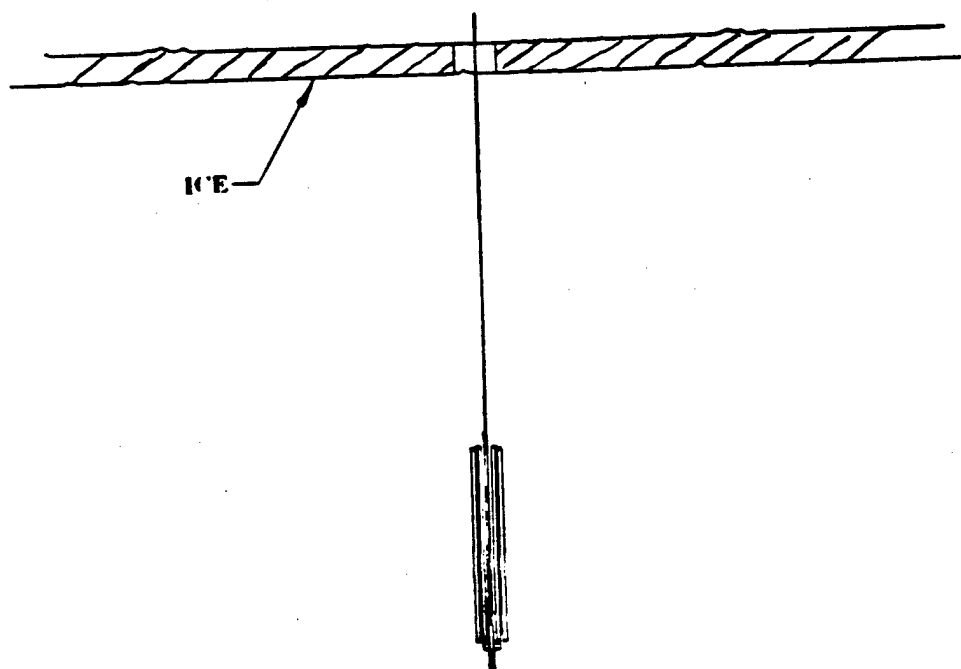
Figure 3   Array Frame in Collapsed Position

ICE

ALUMINUM FRAME WITH INTERNAL
CABLE TENSIONING MECHANISM

TENSIONING CABLES
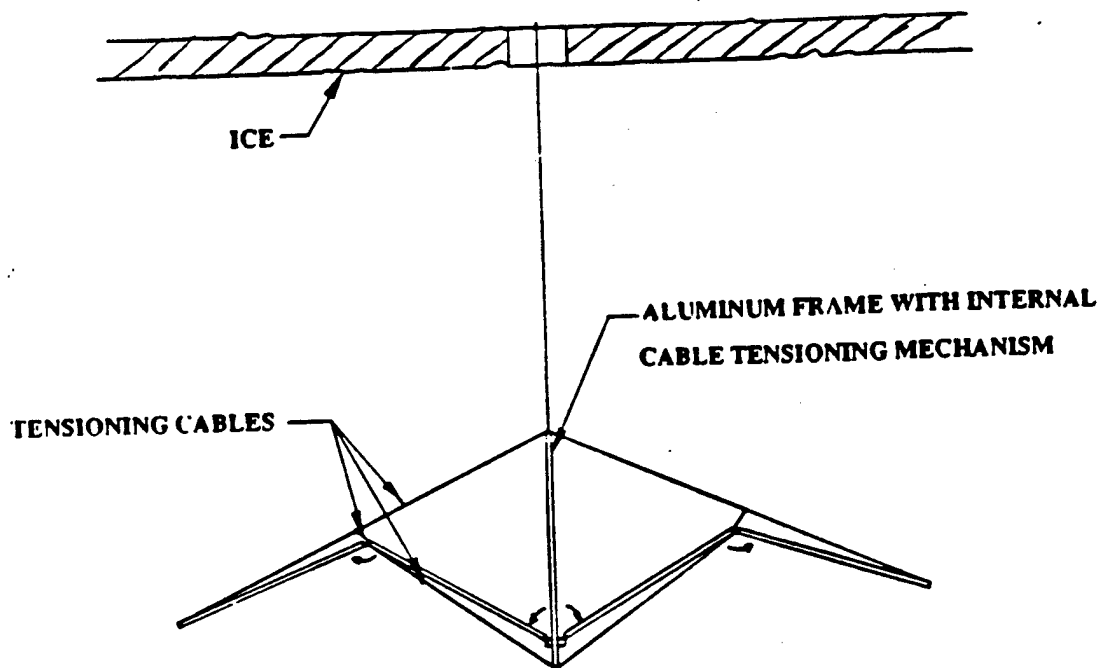
Figure 4   Array Frame Swinging Open

ICE
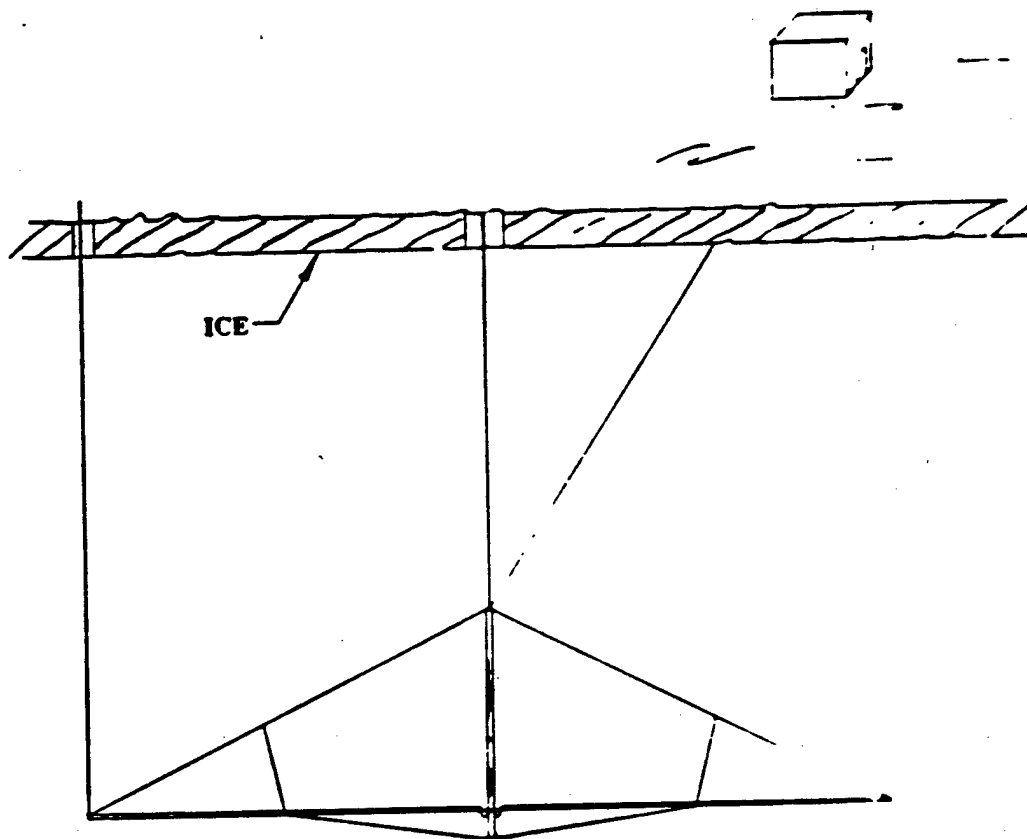
Figure 5   Array Frame Fully Extended
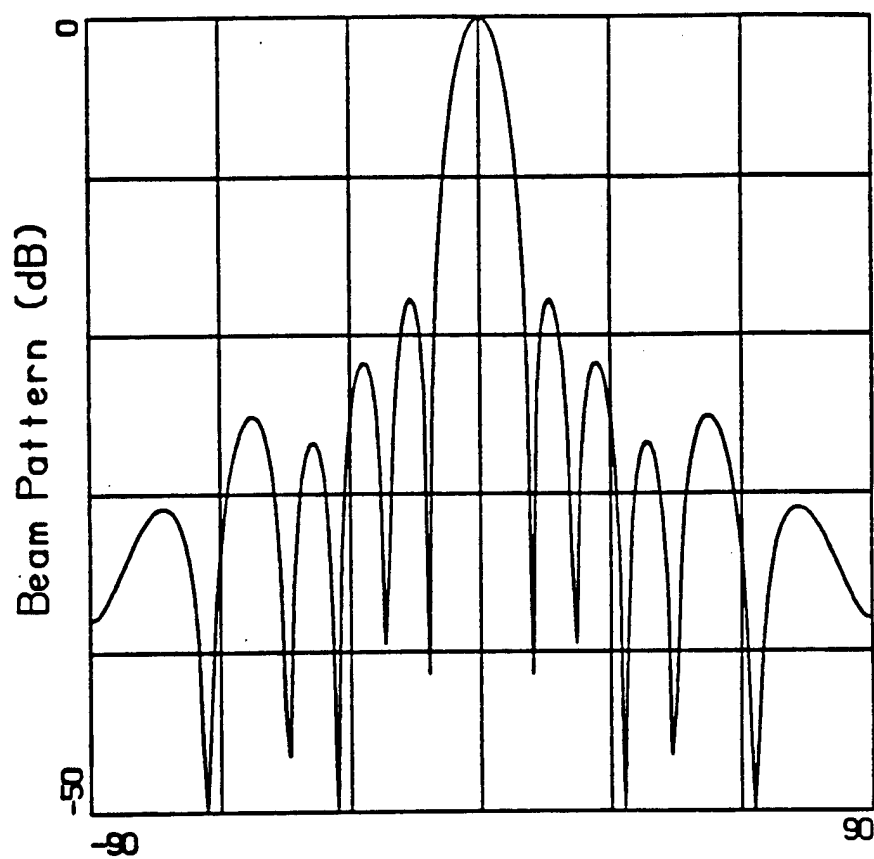
Figure 6   Pattern of the 61 element array

GUTS: Geodesic Underice
  Tramway System
GW: GUTS Winch
TR: Tracking Receiver
RA: Receiving Array
AT: Acoustic Transmitter
TF: Transmitted Footprint

GW (master)

RA

Ice Physics
Test Volume

TR3

Multi-year
Ice Canopy
(underside)

TR1

GW3

TF

TR2

GW2

AT

AT

GUTS
Ice Sensors

Virtual
Mass

GUTS
Electronics

Backscattering Geometry

TF

RA

AT

Forward Scattering Geometry

RA

TF

AT
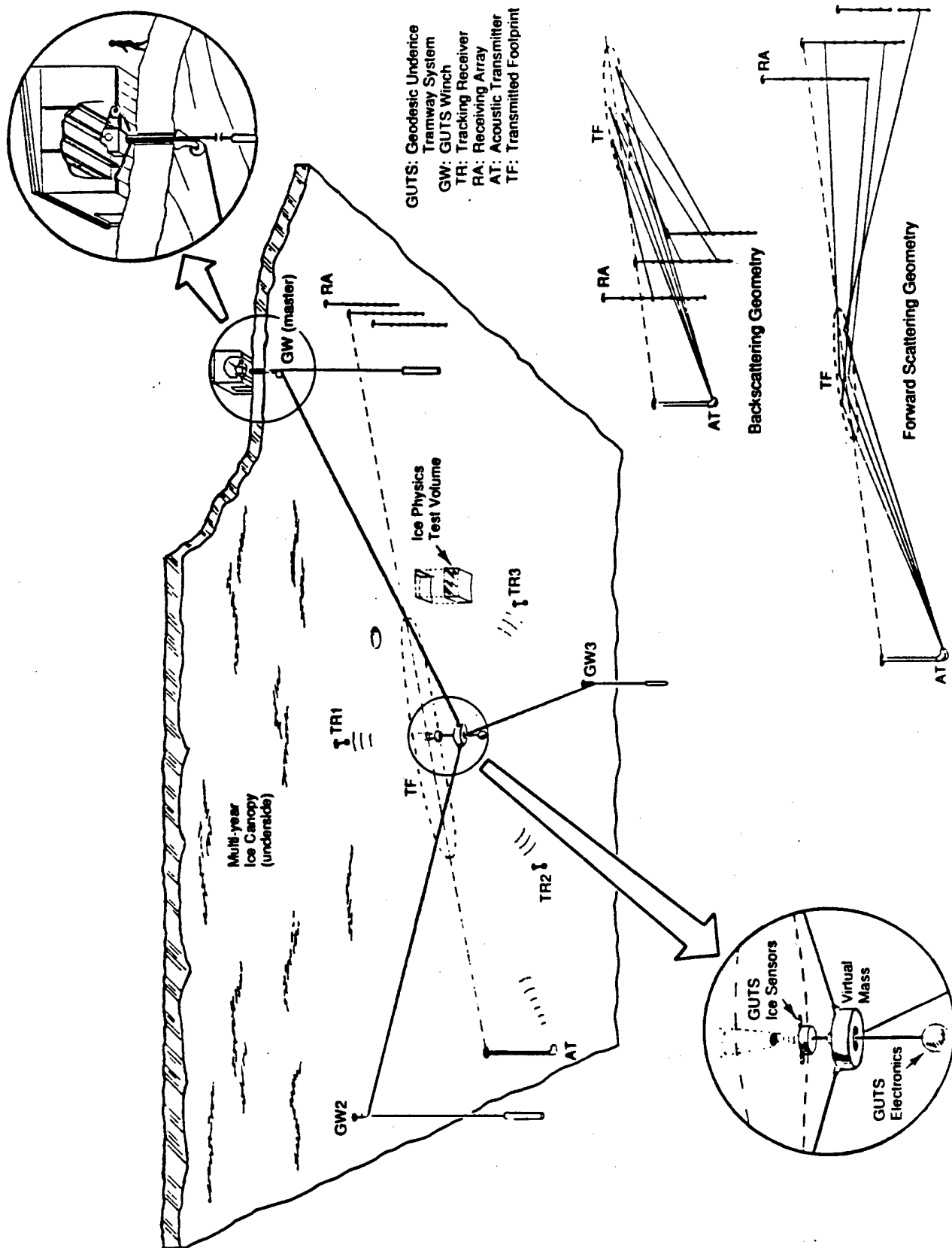
Figure 7 Deterministic ice scattering experiment (DISE).

152

Low Frequency Sea Surface Scattering

by Eric I. Thorsos

In a sonar system, sound scattered back to a receiver by the sea surface, sea bottom, and natural scatterers such as fish is a source of interference that can mask the sound scattered back from an object of interest. Such interference is commonly called reverberation. Our interest is focused on low frequency (50–500 Hz) reverberation due to sea surface scattering, where we are investigating reports that experimentally measured scattering levels are significantly enhanced compared with those predicted by scattering theory. A number of uncertainties cloud the issue. For example, in measuring surface scattering one must remove effects of propagation to and from the surface as well as effects of bottom and volume scattering. More uncertainties arise because predictions of scattering theory depend on the roughness of the surface, which is difficult to characterize quantitatively over the area contributing to the scattering. Differences between data and predictions can also arise if scattering theory is inaccurate, or if scattering mechanisms other than the rough sea surface are important. One such mechanism is scattering from bubbles near the sea surface. The importance of this phenomenon at high frequencies ($\geq 10\,\text{kHz}$) is generally recognized, but scattering from bubble plumes at low frequencies has only recently been considered a likely contributor.

Progress can be made in resolving these issues if the accuracy of scattering theory for the rough interface can be independently checked at low grazing angles. Work at APL funded by the Office of Naval Research addresses this issue by comparing scattering theory predictions with exact numerical predictions. The question is: Could the "enhanced" surface backscattering indicated by measurements arise because of

underprediction of rough surface scattering theory?

The standard model for predicting sea surface backscattering levels is the composite-roughness model.[1] Surface roughness is divided into small and large scales: the effects of small-scale roughness are treated with first-order perturbation theory; the effects of the large-scale roughness are treated using the Kirchhoff approximation. The composite-roughness model accounts for the fact that small-scale waves, which are the predominant mechanism for backscattering, ride on large-scale waves and thus can be tilted (which leads to a modest increase in backscattered level over that given by the small-scale roughness alone). However, the effects of multiple scattering due to large-scale waves are not included, and the consequences of this omission are most important at low grazing angles.

We can check the predictions of perturbation theory and the composite-roughness model through comparison with "exact" numerical results. To obtain the latter, we simplify the problem by considering scattering from a one-dimensional rough surface — that is, we allow the surface height to vary in one direction only. Although scattering from a one-dimensional rough surface does not have all the same properties as scattering from real two-dimensional rough surfaces, a good test of scattering theory can be made because it is unlikely that the dimensionality of the surface is critical to the validity of the theory. For our model, we use a roughness spectrum obtained from the Pierson-Moskowitz frequency spectrum for a fully developed sea. This model ignores nonlinear effects such as breaking waves; it is unlikely (though conceivable) that these effects could significantly change low-frequency scattering predictions. More recent and more accurate surface spectral models exist, but the Pierson-Moskowitz model is adequate for a test of surface scattering theory.

As an example, consider acoustic sea surface scattering at an incident grazing angle of 10°, a frequency of 200 Hz (acoustic wavelength λ = 7.5 m), and a wind speed of 20 m/s (39 knots). At this wind speed, the Pierson-Moskowitz surface model yields an rms waveheight h of about 2.2 m yielding kh = 1.83, where k is the acoustic wavenumber, $k = 2\pi/\lambda$. Because perturbation theory is based on a series expansion in powers of kh, we would expect it to be accurate for $kh \ll 1$. Conversely, we would not expect perturbation theory to work in the example given —normally, composite models would be used. However, we find by comparing with exact results that perturbation theory can indeed make accurate predictions when taken beyond lowest order. Exact predictions are found using an integral equation method[2] to find the scattered field for individual surface realizations, and a Monte Carlo method is used to find averaged quantities such as scattering strength.

For this example, Figure 1 compares the scattering strength for first-order perturbation theory with that for the exact integral equation method. The scattering angle varies from 0° to 180° for a fixed incident grazing angle of 10° (Figure 2). Thus a scattering angle of 10° corresponds to direct backscatter, and 170° corresponds to the specular direction. The integral equation result in Figure 1 is an average of 50 surface realizations; the fluctuations would become even smaller if more realizations were included. In this case, first-order perturbation theory is only about 3 dB low over a broad range of scattered angles. Usual practice is to attempt to make up this difference using the composite-roughness model.

In Figure 3, perturbation theory has been extended[3] beyond lowest order to include all contributions to the scattering strength up to fourth order in kh. There is now essentially perfect agreement with integral equation results, in spite of the large value of kh,

indicating that perturbation theory has a larger region of accuracy for sea surface scattering than previously thought. The composite-roughness prediction for backscattering (10°) is also shown in Figure 3 and is about 3 dB high compared with the other results. However, for a 20° incident grazing angle (not shown) the composite prediction is in very good agreement with the integral equation prediction. Thus, the composite model is basically accurate, except at the lowest grazing angles where its prediction is somewhat high. Further, there is no evidence of a major breakdown of scattering theory that might explain high experimentally measured values.

References

1. S.T. McDaniel, An examination of the composite-roughness scattering model, *J. Acoust. Soc. Am.* **73**, 1476–1486 (1983).

2. E.I. Thorsos, The validity of the Kirchhoff approximation for rough surface scattering using a Gaussian roughness spectrum, *J. Acoust. Soc. Am.* **83**, 78–92 (1988).

3. E.I. Thorsos and D.R. Jackson, The validity of the perturbation approximation for rough surface scattering using a Gaussian roughness spectrum, to be published in the *J. Acoust. Soc. Am.*
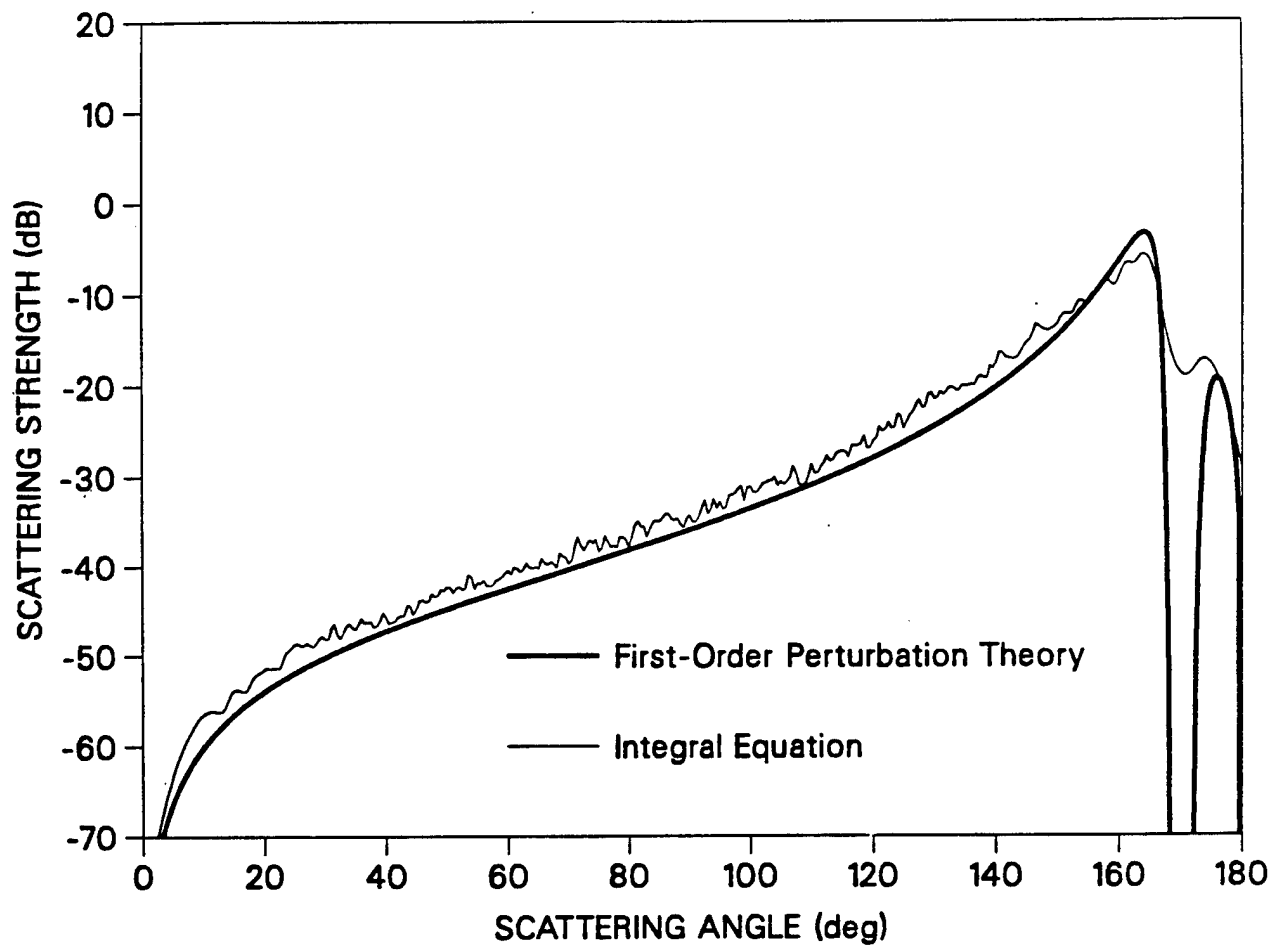
Figure 1. Scattering strength versus scattering angle for an incident grazing angle of 10° at an acoustic frequency of 200 Hz. A Pierson-Moskowitz surface model was used with a wind speed of 20 m/s (39 knots). The contribution from the reflected wave at 170° has not been included.
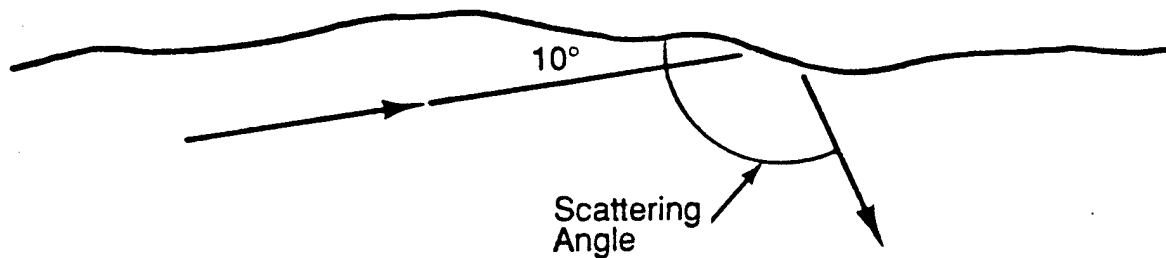
Figure 2. Sound is incident on the surface at a grazing angle of 10° and scatters into all angles from 0° to 180°. A scattering angle of 10° corresponds to direct (monostatic) backscatter.
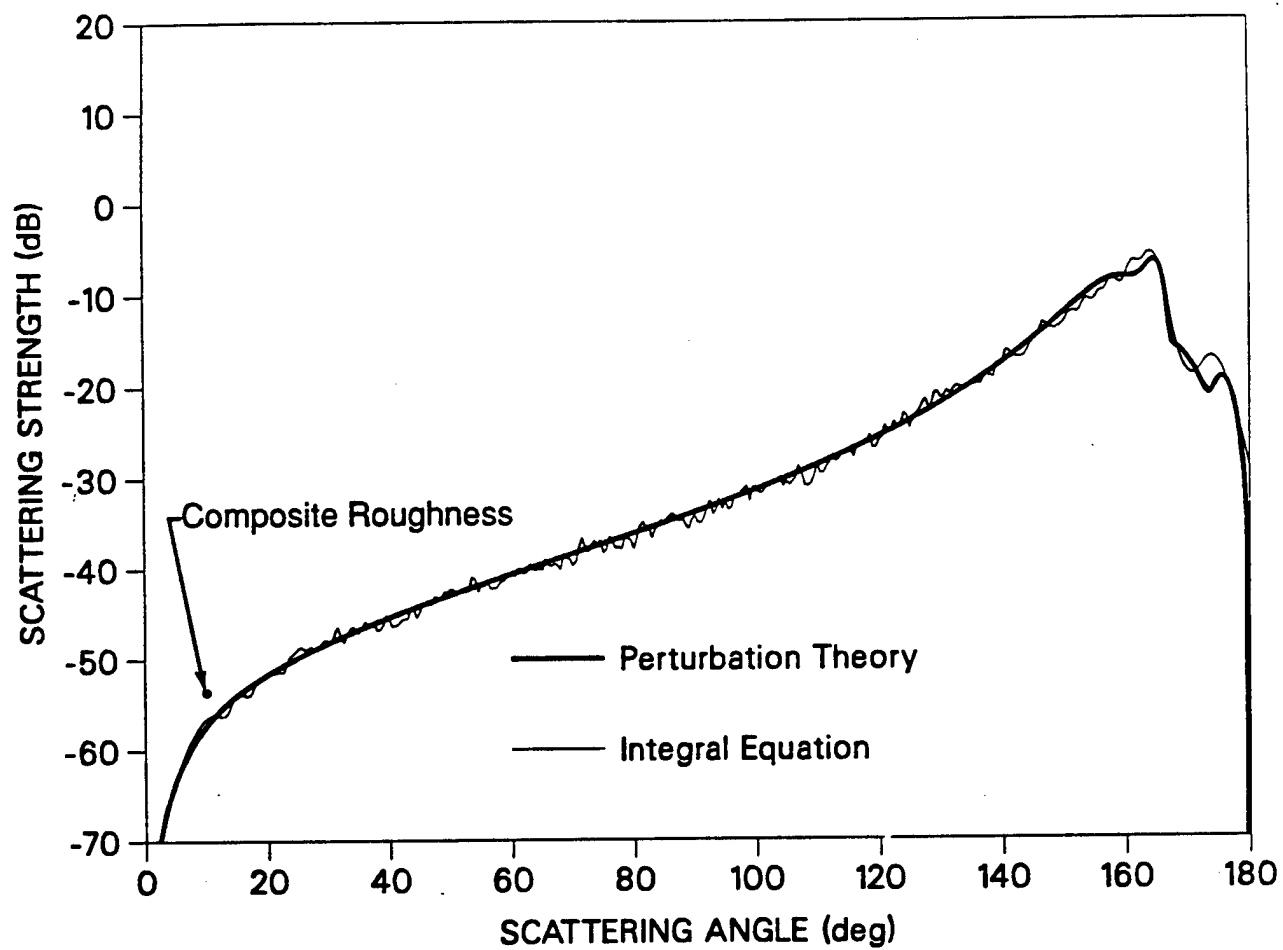
Figure 3. As in Figure 1, except perturbation theory has been calculated to higher order. The composite-roughness prediction is shown only for direct backscatter (10°).

Computer and Experimental Results on
Imaging Water Volume Velocity
presented by Nick Chotiros, ARL-UT

There are particles in the ocean , such as bubbles and biological debris, which can backscatter acoustic energy. In a previous design study, it was determined that the backscatter from a collection of particles could produce a detectable and unique acoustic signature. Since the particles are often passive riders, it should be feasible to track the movement of the water by using a sonar and a crosscorrelation method. The acoustic signature of scatterers and the operation of an acoustic tracker were simulated on a computer. A signal simulator generated a set of backscattered signals for a multibeam sonar system. The scatterers are ensonified with cw pings as their positions change in a way that duplicates normal ocean motion(translation and rotation). Crosscorrelating signals from successive pings produced a reasonable portrayal of water in irrotational translational motion. A small experimental sonar was constructed and tested in a laboratory tank and in the field. In the tank, the sonar was used to track the wall and a bubble stream. In the field, the sonar was used to track natural occurring bubbles.

Figures 1 & 2 are included to provide a conceptual picture of the project objectives. The project has had limited success in tracking any motion that is complicated by rotation. Interested readers are directed to the technical report, ARL-TR-89-4, "Experimental Study of Remote Sensing of Particle Motion by Crosscorrelation of Acoustic Backscatter", 7 Feb 1989.

WIND

WATER

FIELD
OF VIEW

SUBMERGED
UNIT

DATA
ACQUISITION

MOTION
PROCESSING

DISPLAY
PROCESSING

MOVING DISPLAY OF SURFACE
AND VOLUME MOTION
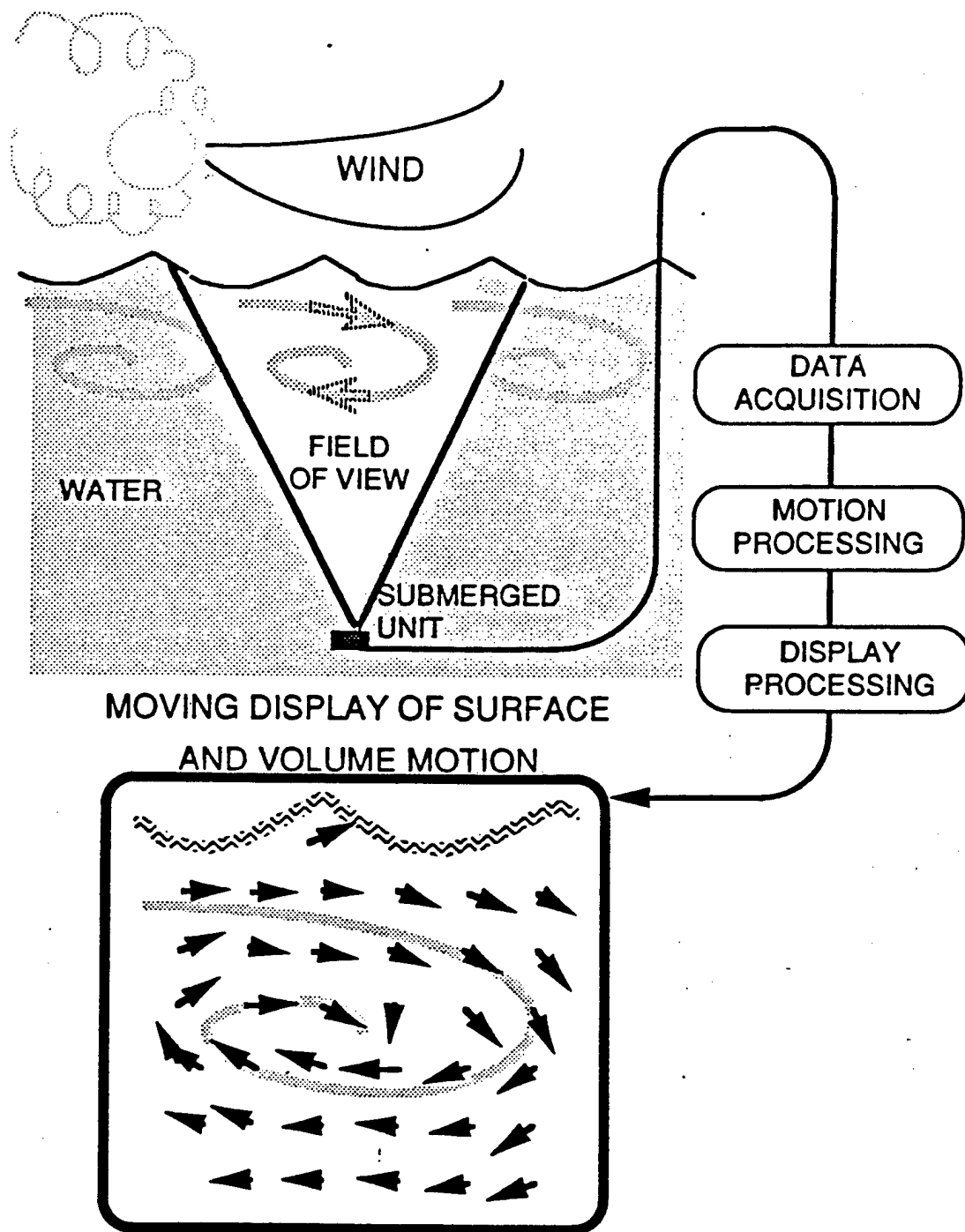
FIGURE 1

REMOTE SENSING SONAR CONCEPT
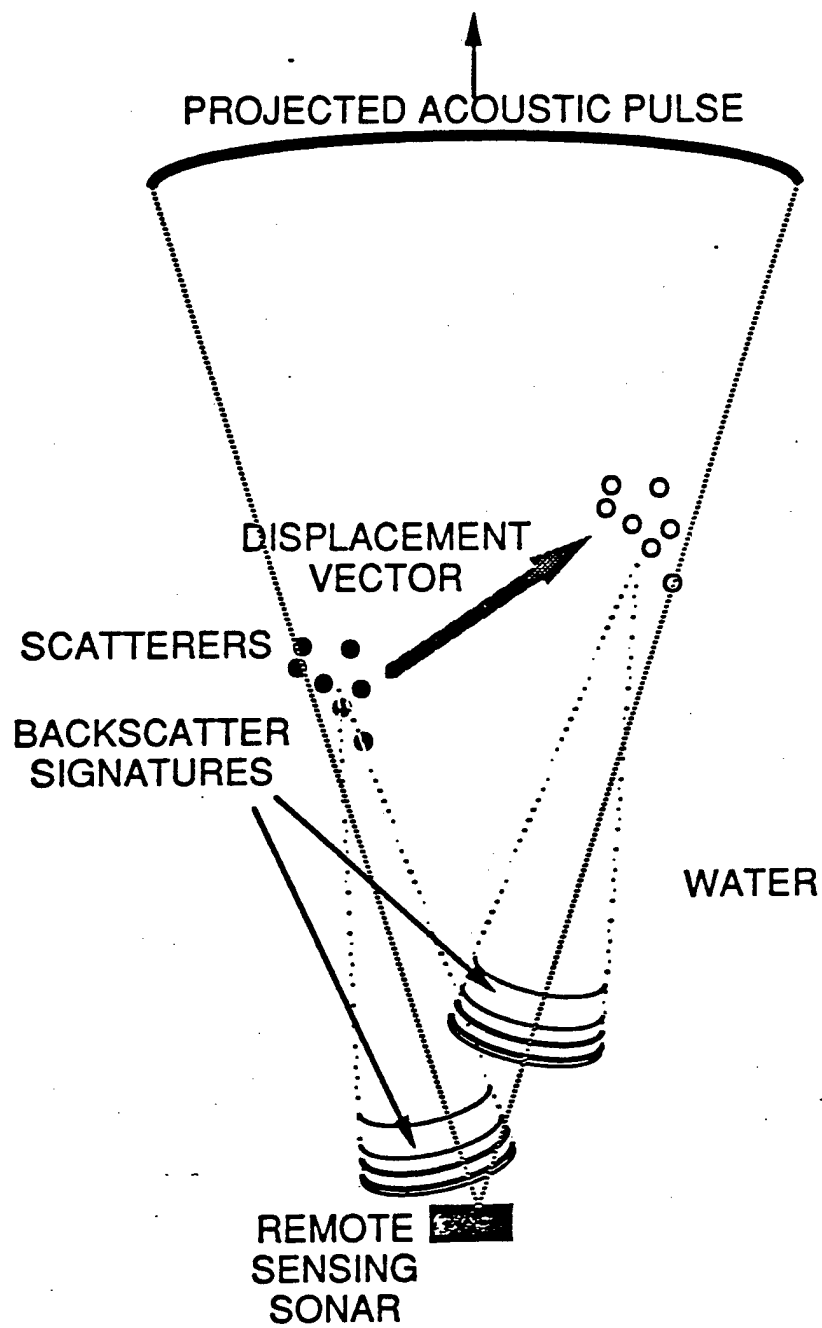
FIGURE 2

TRACKING SCATTERERS BY THEIR ACOUSTIC
SIGNATURES

Ice Physics
Presented by Max Coon, BDM

This presentation provided the attendees with preliminary results of the ice physics work conducted in the CEAREX Drift Phase. A paper presented at the "Instrumentation and Measurements in the Polar Regions" workshop is included to describe the project objectives and instrumentation.

The field efforts accomplished most of the objectives by collecting in-situ stress data and underwater ambient noise data simultaneously over a long period of time and during changing conditions. On the same scale, floe-to-floe deformations and ice mechanical properties were measured. In addition, for large-scale monitoring, ARGOS drifters operated in the field with position tracking being collected continuously.

The most striking first look result is the high correlation between stress level and ambient noise. As the stress increases, the ambient noise also increases. A nearby ridging event, documented by Coon et al.(1989), occurred such that both stress and noise data exist to compliment visual monitoring of the ridge dynamics . This data will be processed carefully to ensure that the propagation from the known ridging source to the omni hydrophone sensors is included to identify the potential of either shadowing or noise enhancement via multipath.

References

Coon, M.D. (1988) "Ice Monitoring During Cearex" in Instrumentation and Measurements in the Polar Regions Proceedings of a Workshop, January,1988, Monterey, California.

Coon, M.D., Lau,P.A., Bailey, S.H. and Taylor, B.J. (1989) "Observations of Ice Floe Stress in the Eastern Arctic" in Port and Ocean Engineering Under Arctic Conditions (POAC'89), Lulea, Sweden.

ICE MONITORING DURING CEAREX

Max D. Coon

The BDM Corporation
16300 Christensen Road, Bldg #3, Suite 315
Seattle WA, 98188

ABSTRACT

This paper presents a description of the ice measurements to be made during the Coordinated Eastern Arctic Experiment (CEAREX). There are two periods of measurements in CEAREX. Period I data collection will be made from a drifting ship and occurs from 20 September 1988 - 1 January 1989. Period II involves two ice camps scheduled for 15 March 1989 - 30 April 1989. CEAREX Period I is ideal for collection of ice data because: 1) a long time series of data can be obtained, 2) a ship drift will be from the interior to the edge, 3) the ship provides for transportation and power for many experiments, and 4) there will be an ice laboratory on the ship.

The ice measurements to be made in CEAREX are large-scale strain by independent buoys, small-scale strain by a laser or microwave ranger, small-scale stress by biaxial vibrating wire sensors, and flatjack sensors. In addition, ice methology and ice mechanical properties will be measured. The measurement will be made by many different organizations. The CEAREX plans call for the instrumentation of three floes near the ship.

This paper presents a description of the instrumentation to be used in the CEAREX ice program.

INTRODUCTION

CEAREX is designed to further understand the Fram Strait -- a 500 km strait between Greenland and Spitsbergen. This region is significant because the most important oceanic exchanges between the Central Arctic and the world ocean occur here. Annual mean horizontal transport estimates of sea ice mass and latent heat through Fram Strait are equivalent to the annual formation of a 30-cm layer of ice throughout the Central Arctic.

CEAREX is designed to understand a) the dynamics which govern the temporal and spatial distribution of observed variables in the region, and b) the role of intermediate (meso) and smaller scale processes on a seasonal basis. The CEAREX ice monitoring will be accomplished from a drifting ship scheduled to be frozen into the pack ice about 20 September 1988 at 83N, 30E and complete the drift to the ice edge by 1 January 1989.

An understanding of the ice dynamics in the Eastern Arctic is critical to meeting the objectives of CEAREX. The ship drift portion of CEAREX provides an ideal opportunity to study intrafloe stresses and interfloe deformation because of the time duration of the drift and because the ship will go from the interior of the ice pack to the edge.

BACKGROUND

A key objective of CEAREX is to understand the relationships between the mechanics of air-ice-ocean stress divergence and ambient noise generation from ice fracturing. An Ice Dynamics/Ambient Noise Program has been structured that addresses the critical issue to this understanding -- how the environmental driving forces of air and ocean stress cause fracturing of ice in floes and leads resulting in noise generation. This program attempts to develop an understanding of the relationship between small scale (1-4 km) stress-strain-noise generation, as illustrated in Figure 1, and the relationship between small and large scale (100-400 km) strain. Ultimately, it is desirable to develop the additional relationships that can predict noise generation using a limited number of environmental measurements.

The specific objectives of the CEAREX Ice program are to develop data sets that:

o   identify relationships between small and large scale (100-400 km) strain in pack ice.

o   identify the relationship between small scale (1-4 km) ice stress and strain to noise generation for both floe and lead ice.

o   develop force-deformation relationships that occur during ridge building between floes and relate ridge building to noise generation.

o   identify stress conditions of the floe ice at the time of floe ice fracturing and relate fracturing to noise generation.

To accomplish these objectives, field tests have been identified to be conducted in Period I.

The key in situ measurements to be made are:

o   Large-Scale Strain Measurements - seven aircraft-deployed data buoys which monitor position, surface air temperature, and atmospheric pressure will be arranged in two rings of 200 km and 25-40 km, respectively, from the ship.

o   Small-Scale Stress Measurements - twelve standard 8-inch flatjack stress sensors and four dataloggers are to be located near the ship: three sensors and one datalogger within 100 meters of the ship, and nine sensors and three dataloggers within 2-4 km of the ship on three multi-year floes.

o   Ambient Noise - three hydrophones with strum-suppression suspension and dataloggers will be located at 2, 4, and 6 km from the ship.

o   Ice Properties - Laboratory tests will be performed on small-size (2 inches in diameter, 6 inches in length) ice samples to determine the mechanical properties of both young sea ice and sprayed ice.

INSTRUMENTATION AND INSTALLATION

The drifting ship will initially be positioned such that the ice within a 2 to 4 km range of the ship is generally accessible. Several multi-year floes within this area will be heavily instrumented. In addition to the heavily instrumented floes, studies will be conducted at other selected locations within the area on first year ice and on leads as the opportunity arises (Figure 2). The measurement program is summarized in Table 1. The present plan for instrumentation and installation is given below.

Data Buoys

The ARGOS data buoys for the Period I CEAREX ice program will be air deployed by land-based aircraft. Because they will be deployed more than 25 km from the ship and there will be no helicopter available, the buoys will report position, surface air temperature, and atmospheric pressure through System ARGOS. The buoy chosen for this application is the parachute-deployable TIROS Arctic Drifter (TAD(A)). The buoy is designed for deployment onto ice from all aircraft commonly used in the Arctic; is constructed using a spherical, impact-resistant polycarbonate shell with foam insulation; and is powered with a lithium battery which can operate at temperatures to -50°C. The TIROS Arctic Drifter (TAD) is the successor to the Air Droppable RAMS (ADRAMS) buoy that was developed and successfully employed on AIDJEX. Position, surface air temperature, and atmospheric pressure data monitored by buoys will be transmitted via Service ARGOS to Seattle, Washington.

Stress Sensors

Three multi-year floes will be chosen for outfitting with stress measuring instrumenttion. At least two of the floes will be separated by young ice in anticipation of a ridging event. On each floe two stress measurement sites will be selected. At one site biaxial vibrating wire sensors will be placed at three vertical levels within the ice. At the second site three flatjack type sensors will be located at one vertical level. Data loggers will record stress sensor reading approximately every 15 minutes. Visits to the sites will be required every several days to download the data loggers and to service batteries.

The biaxial vibrating wire sensor is a steel cylinder shown in Figure 3. Principal ice stresses normal to the axis of the gauge are detemined by measuring the radial deformation of the cylinder wall in three directions. Three tensioned wires are set 120° from each other across the cylinder diameter (Fig. 3). The diametral deformation of the gauge in these three directions is determined by plucking each wire with a magnet/coil assembly and measuring the resonant frequency of the vibrating wires. A thermistor is also placed inside the cylinder to measure the gauge temperature. Both ends of the sensor are sealed to protect the wires and electronics from moisture.

One stress sensor being considered is the GEOTECH flatjack pressure sensor which is intended for use in ice (See Figure 4). The GEOTECH stress sensor is a fluid-filled, stainless-steel disk which is 8 inches in diameter. The unit is comprised of the sensor, a pressure transducer, and an adjustable fluid reservoir. This sensor has been used to measure pack ice forces by Croasdale et. al. (1987).

Floe Strain Sensors

Microwave transponders will be located on the floes with stress sensors such that the local ice strain field can be correlated with stress measurements. Two transponders (Del Norte or similar type system) will be located on each floe such that floe rotation can be determined. The use of this equipment has been described by Tucker et. al. (1980). The transponders will be interrogated by a computer-driven distance measuring unit on the ship. Direct range and range-loop measurements of position will be obtained every 15 minutes. The on-ice transponder units utilize batteries that will require charging or replacement at 5 to 7 day intervals. It is planned to place transponder units on at least two additional floes to better define the local strain field.

Hydrophones

The measurement of ambient noise beneath the ice will be made with hydrophones supported with strum-suppression suspension. The noise from the ship will pollute the natural ambient noise environment. The use of data from three hydrophones should make it possible to separate the ship noise from the ambient noise. The hydrophone units consist of hydrophones with strum-suppression suspension and a datalogger. An averaged spectral analysis up to 500 Hz will be performed on the ship with an IBM PC/AT.

ICE PROPERTIES MEASUREMENTS

The properties and morphology of the snow and ice within the local area of the ship will be studied on a continuing basis. The properties to be measured are listed in Table 1. An ice laboratory will be provided on the ship. The laboratory will be equipped with an ice load testing frame. Therefore, both in situ and laboratory tests will be performed.

Five sites will be instrumented for heat and mass balance studies. At least two of these sites will be on floes instrumented for the stress and strain measurements. The additional sites will be established on first-year and multi-year ice of a variety of thicknesses. Each of these sites will consist of a reference stake to measure mass changes at the surface, an acoustic thickness gauge to measure mass changes at the bottom of the ice, and a vertical string of thermistors to obtain temperature profiles in the ice and in the upper few meters of the water column. These sensors will be automatically interrogated every hour by datalogger. These sites will be visited at intervals of several days to download the dataloggers.

In addition to the detailed sites, hot wire thickness gauges will be located at about 20 other sites. Snow reference stakes will be collocated with the thickness gauges which will be selected to include ice of different types (first-year, multi-year and ridged). As the data are collected manually from these sites, they will be visited at 1 to 2 day intervals.

The mechanical properties test program is aimed at determining the compression strength and modulus of the ice with stress sensors installed. Also, finding the bending strength and modulus of the lead ice where ridge building events may occur. The compression tests and some of the bending tests will be conducted on the ship. Some of the bending tests will be conducted in situ. The compressive and bending strengths and modulus will be found as functions of ice temperatures and brine for young and multi-year ice.

CONCLUSION

The CEAREX ice monitoring program is intended to define the sea ice mechanical behavior resulting from interfloe interactions, to relate these measured forces to small scale ice physical and mechanical properties, and to achieve an understanding of the properties and processes of the ice cover during the transition from summer to autumn to winter conditions. In addition, the background noise generation of the fracturing and ridge building will be measured.

The CEAREX ice program will provide the first complete set of ice mechanics and ambient noise measurements. The data will be collected by proven instrumentation.

REFERENCES

Cox, G. F. N. and J. B. Johnson (1983) "Stress Measurements In Ice," U.S. Army Cold Region Research and Engineering Laboratory Research Report 83-23.

Johnson, J. B., G. F. N. Cox, and W. B. Tucker, (1985) "Kadluk Ice Stress Measurement Program," In Proceedings of the 8th International Conference on Port and Ocean Engineering Under Arctic Conditions, Nurssarssuaq, Greenland.

Tucker, W. B., W. F. Weeks, A. Kovacs, and J. A. Crow. (1980) "Nearshore Ice Motions at Prudhoe Bay, Alaska," Sea Ice Processes and Models, Ed. R. S. Pritchard, University of Washington, p 655.

Croasdale, K. R., G. Comfort, R. B. W. Graham, and E. L. Lewis (1987) "A Pilot Experiment to Measure Arctic Pack Ice Driving Forces," In Proceeding of the 9th International Conference on Port and Ocean Engineering Under Arctic Conditions, Fairbanks, Alaska.

TABLE I

SUMMARY OF MEASUREMENT PROGRAM

Measurement Component	Approx. No. Sites	Measurement Frequency	Method of Data Acquisition
Stress and Strain:			
Biaxial vibrating wires*	3	15 mins.	Data logger on site
Flatjack sensor*	3	15 mins.	Data logger on site
Del Norte transponder*	3-5	15 mins.	Computer on ship
Heat and Balance:			
Acoustic thickness gauges*	3-5	2-4 hours	Data logger on site
Vertical temperature profiles	3-5	2-4 hours	Data logger on site
Hot wire thickness gauges	20	1-2 days	Manual
Ice thickness surveys	-	5-7 days	Manual
Snow depth surveys	-	3-5 days	Manual
Ice Properties and Morphology:			
Morphology surveys	-	Daily	Manual
Ice coring*	5	1-2 days	Manual
Snow stratigraphy	5	1-2 days	Manual
Optical measurements*	5	2-4 days	Manual
Mechanical tests	-	Daily	Manual
Dielectric properties	-	2-4 days	Manual

*Denotes measurements to be made on the heavily instrumented floes.
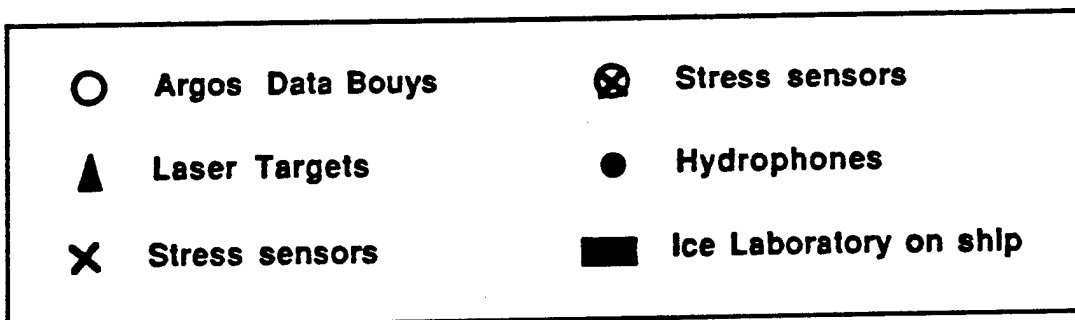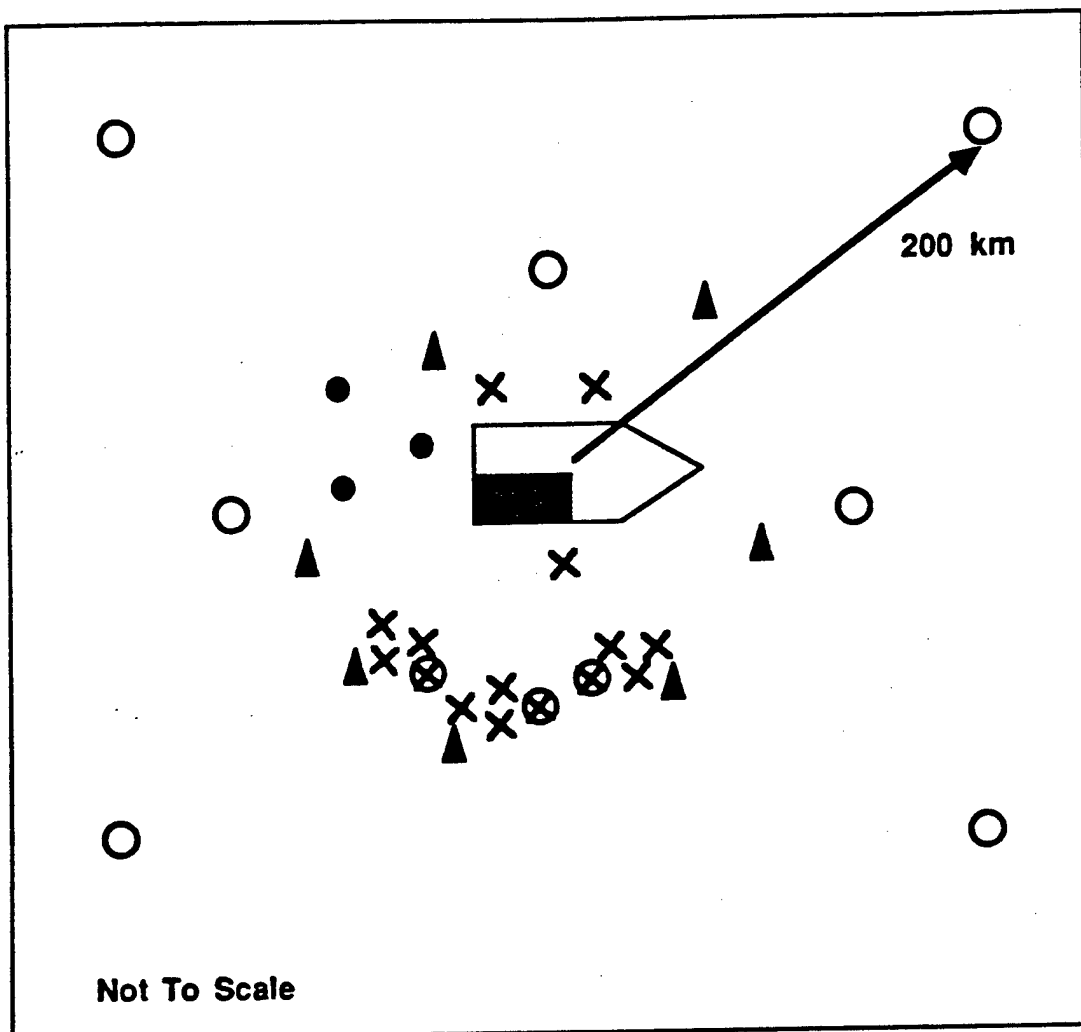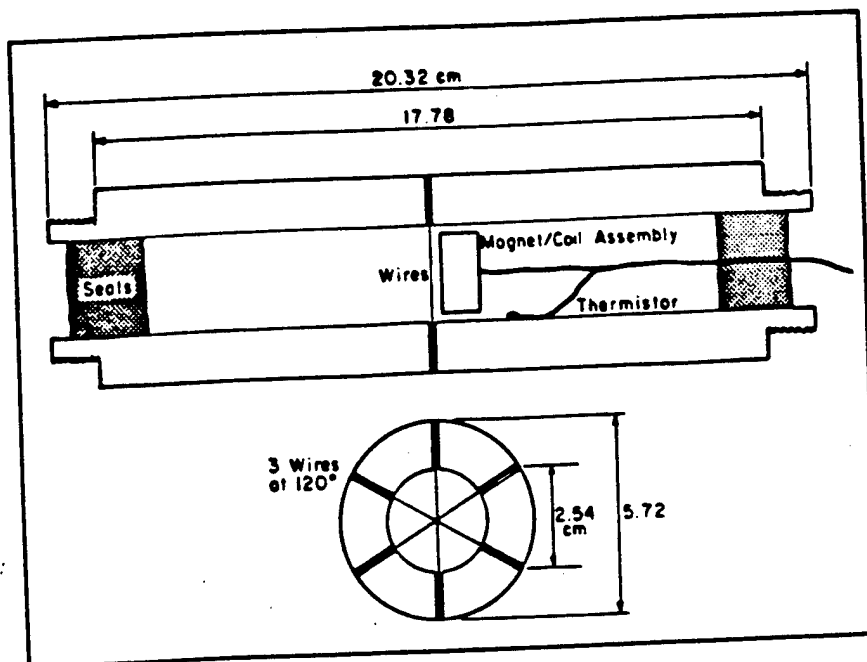
Figure 2. Test Site Layout for Period I

Figure 3.

Schematic of
Biaxial Ice
Stress Sensor
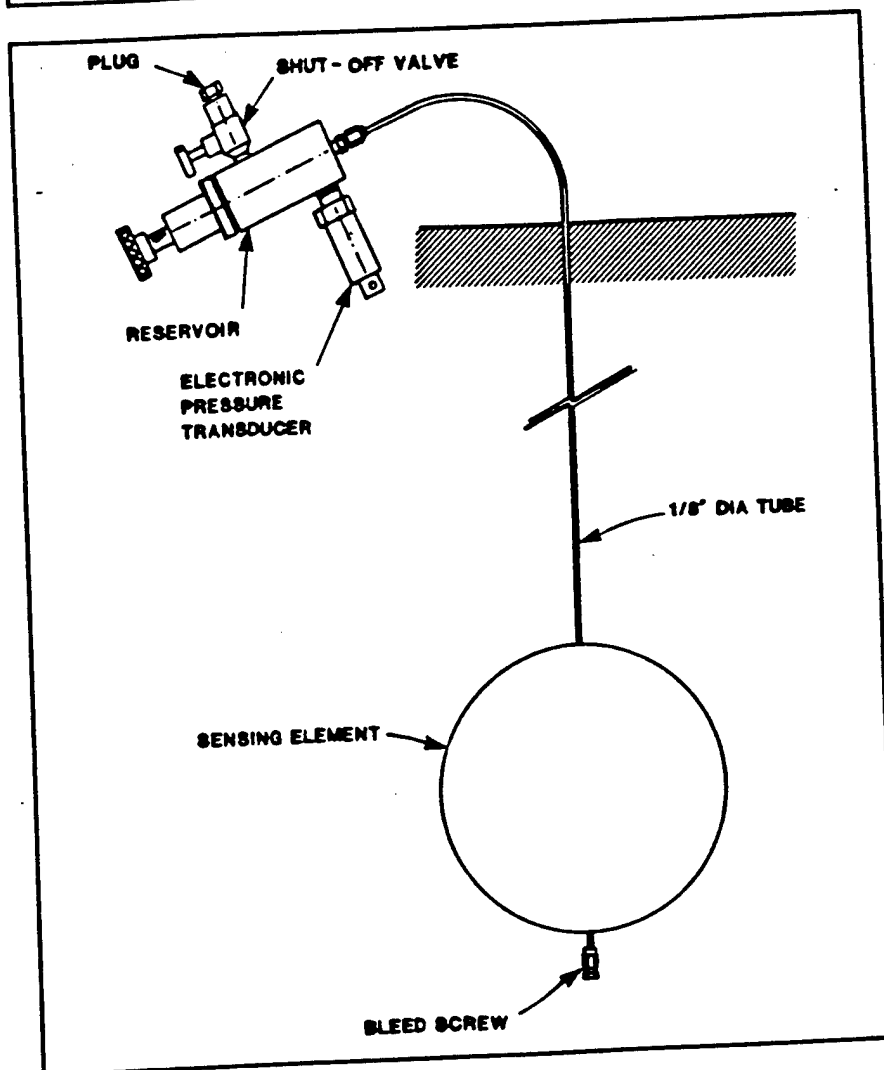
(Cox & Johnson,
1983)

Figure 4.

Schematic of
Flatjack Stress
Sensor

(Courtesy of
GEOTECH)

Future Experiments - Comparison Between Barents Sea
and Deep Water Central Arctic
Presented by Ira Dyer, MIT
(With many modifications and additions offered by the Workshop)

The viewpoint taken in this presentation was that the community might more readily address future field initiatives by comparing two possible Arctic field efforts: (1) Barents Sea shallow water; (2) Western Arctic deep water. The scientific issues that should be addressed at both are: (1) Event Physics and Ambient Noise (3-2000 Hz), (2) ULF (10E-3 - 1 Hz), (3) Ice Scattering (30-100 Hz) and (100-300 Hz), (4) Geophysics, and (5) Geologic and Oceanographic Support. The different assets and equipments required for each field area help to distinguish what can be accomplished; there was general agreement that the science research issues are worthy of pursuit.

The first issue (1) Event Physics and Ambient Noise takes on different scales at each of the two sites. At the deep waterWestern Arctic site, a scale of 500 km is required. At the same time, however, very high resolution is needed locally to identify, localize, and characterize eachice cracking event. Forcing functions(meteorology and oceanography) that result in ice strain, ice dynamics and ice fracturing or ridging events must be monitored over mesoscale areas. This leads to requirements for monitoring buoys. The number of ARAMP buoys needed for a deep water experiment is about 20, each fully capable of monitoring wind, ice drift, current, barometric pressure, air and water temperature, cloud cover, ice acceleration, water salinity, geographic position, and ambient acoustic noise. A horizontal acoustic array (2x2 km cross) and a 1km vertical array are needed to isolate and locate individual noise events. Synthetic Aperture Radar imagery (SAR) measured at 4 hour intervals is required to track precise ice motions. Stress sensors in the ice concentrated around the acoustic arrays are required to properly relate the individual ice events to ice stress buildup.

The same science issue can be examined in the Barents Sea area. In this shallow water regime, the higher propagation loss due to bottom interaction reduces the scale size of the experimental area to 30-40 km. The dynamic activity level of the environmental forcing and the ice dynamics makes it necessary to sample at a much closer spacing. The number of fully equipped buoys (ARAMP) would be 20-40 with precise positioning capabilities. The acoustic sensors required to isolate noise events would be nested free drifting vertical arrays(water surface to ocean bottom) that transmit data to an acoustically quiet drift ship. Ice imagery by SAR should be collected at 1 hour intervals.

The second issue, (2) ULF, is more a deep water problem since the shallow water duct will not support acoustic modes withsuch long wavelengths. In addition to the sensors needed for higher frequency noise measurements, both geophones and hydrophones(10E-3 - 1 Hz) should be implanted in both the ice and the bottom. The ideal sensing situation is a deep water site that has open water part of the year and is ice covered the rest of the year. This tests changes in the forcing functions as the natural environmental changes. A minimum of three sensors placed in a triangular configuration would be needed. Nested triangular arrays could produce a far more significant understanding of ULF properties and the physics causing them.

The third issue (3), Ice Scattering(30-100 Hz)in deep water, requires that roughness be surveyed to an accuracy of 1/2 meter, acoustic properties of the ice be measured insitu, and lead, crack, keel, and floe characteristics be gathered. Scattering (both forward and backward)

versus grazing angle and ice roughness should be measured, mode conversion of waterborne energy to ice plate waves be monitored with geophones, and long range propagation paths be excited and monitored systematically at 50 km intervals over a range of 500 km. Impulse measurements at ten stations(spaced equidistantly along the propagation path) to high resolution receiving arrays of hydrophones and geophones would provide the needed acoustic information to investigate scattering, and possibly the ice acoustic properties if sensors are deployed in tomographic configurations. The underice roughness(shape) should be obtained with a high resolution multibeam sonar coupled with a sidelooking sonar, thereby providing a very accurate elevation differential picture with extensive insight into the texture of the surface. A survey of the ice surface local to the array, and along the propagation path, is required to identify leads, cracks, and floe shapes. SAR coupled with local ground-truth to relate cracks to remote sensing is necessary.

A shallow water site would require the same information and methods except that only a 40x40 km square needs to be surveyed . The SAR support interval is no more than required for event physics in either deep or shallow water, but ground-truth is a requirement in both cases.

For the higher acoustic scattering frequencies (100-300 Hz), one needs to increase the resolution of the surveys, primarily of the underice topography, since the top ice surface can be well measured via optical imaging. The option of using acoustic sources that produce controlled steerable beams should be considered for isolating and investigating deterministic responses of special ice features, i.e. floe front/back edges, large cracks, new/old ice keels, various bottom types and features.

The fourth issue, (4) Geophysics, is important to acoustic coupling and transmission through the bottom. Both forward and inverse problems are of interest which, for the Arctic, typically are inverse. The procedures described for ice scattering will provide some bottom geophysics information, however, it is insufficient. Both the sound velocity profile and the layered structure and composition of the bottom are required to properly model the elastic response and properly address mode conversion, the propagation and attenuation of each elastic wave, and the conversion and retransmission into the water column. This information cannot be obtained directly by coring. The only practical method is to conduct both refraction and reflection seismic surveys. Refraction shots exploded at ranges up to 100 km would provide a description of the average crustal structure and its acoustic velocity. Reflection surveys at the deep water camp(at the arrays) using shots and an airgun would provide detailed upper sediment structure and relative layer velocities. The difference in requirements between a shallow and a deep water site is one of scale. The way one would do this in shallow water is to perform the measurement as the whole sensing area drifts under the influence of the environmental forces. This could easily provide a 300 mile path that delineates the importance of the bottom transmission paths, the variability due to glacial deposits and scouring, the reverberation levels versus the bottom properties, and the water column acoustic properties and variability. Performing this experiment is more difficult because the ice, in dynamic motion, continually changes the configuration of the acoustic array(s). But this is countered using acoustic positioning and computer software programs that were developed for the 1984 MIZEX experiment.

The last issue, (5) Geologic and Oceanographic Support, is required to tie the acoustic measurements to the physical world and to extend them to other areas that were not measured in the same detailed manner. The ideal oceanographic measurements would

define a dynamic mesoscale ocean model that could be used for predicting what the 3-D sound velocity profile over the experimental areas during the data collection. This is impossible to acquire via fixed moorings or drifting vertical lines unless the coherence of the oceanographic structures are very large, both spatially and temporally. The recommended solution for deep water mesoscale oceanographic monitoring is to use acoustic tomographic inversions with additional vertical sampling on ARAMP buoys and from expendables.

For the shallow water experiment, remote vehicles that sample in both the vertical and horizontal seem like the most plausible approach. With such vehicles, one has the potential of changing the sampling strategy as required to look at turbulence caused by high velocity ice motion or local bottom effects due to tidal flow over bottom forms. Appropriate oceanographic sampling could provide sufficient information to address important oceanographic research issues.

Geologic support for the deep water experiment is primarily to test uniformity, since abyssal plain deposits are expected to have very little change over large spatial dimensions. In shallow water, the geologic effort would be one of relating sediment types and structure to acoustic properties in a geoacoustic sense. The objective is to reach shallow water propagation/reverberation models that could predict more accurately using actual rather than estimated geologic information.

The presentation is summarized in an attached matrix for quick comparison among the various components. A strong protest was voiced by some at the Workshop against the magnitude of the proposed efforts, however, there is no avoiding a large effort if the purpose is to understand the relationships among all of the mechanisms. It was pointed out that a smaller effort could address ice scattering on a local deterministic basis in a much more controlled scientific manner. This viewpoint is understandable but must be put into perspective with what is needed overall in Arctic acoustics and oceanographic research.

The greatest value of a comprehensive experiment of the types presented here is that it allows the most importance parameters to be identified and quantified.

DESCRIPTION OF RESEARCH	EXPERIMENT WESTERN ARCTIC	EXPERIMENT BARENTS SEA
Event Physics and Ambient Noise 3Hz-2000Hz	Ice strain sensors 20 ARAMP Buoys GPS or ARGOS 500km scale coverage	Ice strain 20-40 ARAMP Buoys GPS or ARGOS 20-30km scale
	2X2km horizontal & 1km vertical arrays hardwired	Nested free drifting vertical arrays STS positioning & RF Data link to drift ship
	SAR imagery, 4hr interval	SAR imagery, 1hr interval
ULF 10E-3 - 1 Hz	Hydrophones and geophones on ice and bottom	Exploratory measurements on bottom over full year
Ice Scattering 30-100 Hz	Underice scattering with impulse source at each of 10 stations over 500km	Use impulse source in center of sensor distrbution
	Channel propagation over 10 sta. range e.g. 500 km	Channel propagation 3-5km grid size 30-40km scale
	Lead, keel, & crack statistics	floe statistics and characteristics
	Top/Bottom imagery SAR & sonar with 1/2m vertical resol	Top/Bottom imagery SAR & sonar with 1/2m vertical resol 1hr interval for SAR

Ice Scattering 100-300 Hz	Top/Bottom imagery SAR & sonar with 1/2m vertical resol	Top/Bottom imagery SAR & sonar with 1/2m vertical resol 1hr interval for SAR
	Underice scattering with impulse source at each of 10 stations over 250km	Use impulse source in center of sensor distrbution
	Lead, keel, & crack statistics	floe statistics and characteristics
	Channel propagation over 10 sta. range e.g. 250 km	Channel propagation 3-5km grid size 30-40km scale
Geophysics	Seismic Refraction with impulses from 100 km to hardwired arrays	
	Seismic reflection at ice camp with impulses /air gun	Seismic reflection at drift ship with air gun

Channel Properties; sound velocity profile in water and sediments,water dynamics, bathymetry, sedimentary column structure and acoustic properties

Horizontal uniformity of channel and bottom/subbottom properties at 0, 90, 180,and 270 degrees to arraysout to 500 km

N fixed(open water) or motion corrected(underice) sources and receivers with 40 ARAMP for sequential forward/backward experiments over 30km fixed range or 30km width swath along drift path

Detail bottom suveys(Multibeam or Seamarc) & 3.5 Khz subbottom profiler to confirm geologic structure and bathymetry

Oceanograhic synoptic data before/after and local measurements continuously during experiments

Acoustic Scattering from Arctic Air/Ice/Water Interfaces
Research Issues by Terry Ewart and Eric Thorsos

Scientific Objective: Achieve a relatively complete understanding
of the scattering of low frequency sound from the Arctic air/ice water interface

Background: Current theory treats the ice canopy in the Arctic as a simple attenuator at frequencies less than 30 Hz quite effectively. However, at higher frequencies it is treated less effectively as a geometric random roughness, or as Burke- Twersky half cylinder scatterers, triangular or trapezoidal prisms randomly distributed on a flat surface with heights matching spectral results obtained from submarine profiling. Although parameters can be adjusted to make theory and data match over broad frequencies on particular data sets, the methods break down versus location and changing time indicating that the models are lacking some important basic physics.

Technical Approach: Initiate a unified theoretical/ experimental approach that features a thorough deterministic characterization of the ice locally for a single interaction investigation, and a statistical mesoscale characterization of the ice properties for multiple interaction investigations; and numerical simulations and fundamental theory developments that can address the experimental situations for predictive/real result comparisons.

For the single interaction experiment, it is necessary to measure the ice geometry precisely (the method described by Ewart called Geodesic Underice Tramway System(GUTS), Figure 1 was recommended). The visco-elastic ice parameters (v_c, v_s, ρ) over the ensonified area on a grid scale fine enough to satisfy theoretic requirements must also be measured. Acquisition of similar information for the large scale experiment is required but will need the development of instrumentation that is currently not available. The possibility of obtaining the ice properties via holographic tomography would be considered.

The theoretical prediction development would extend current theory to predict forward and backscattered field using deterministic visco-elastic parameters as input for the single interaction case. This theory would include mode conversion to shear waves, surface waves, propagation/attenuation/reconversion to compressional water waves to quantify the significance of these occurrences. The long range development would incorporate the short range findings with a moments approach building from current developments by Uscinski. The numerical simulation capability would build on current efforts being developed by Ewart that capitalize on the parabolic equation marching method as applied to interactions with rough visco-elastic surfaces and /or finite element or finite difference approaches as are required.

Scientific Considerations: 1. For single interaction local experiment, a frequency of 400 Hz is recommended to allow the creation of a mechanically steerable single beam sonar that is practical in size and power with a wavelength that interacts strongly with the visco-elastic and geometric ice properties. Given the detailed ice properties, it is anticipated that the data gathered should scale to lower frequency acoustic interactions if the theory developed is correct. A potential pencil beam source/receiver is described in the

presentation by Ewart on pages ____. 2. The long range experiment would be conducted at lower frequencies with no emphasis on marginal ice zone conditions or ocean bottom interaction. Advances in theory, numerical methods and computer technology make it possible to incorporate complex ice configurations and visco-elastic properties to produce results to compare with experimental data.

Payoffs: By advancing from the local simple case to the more complex single and multiple interaction cases both experimentally and theoretically, it is possible to determine the validity of the theory and quantify the importance of the relevant parameters versus frequency, range, and ice properties.
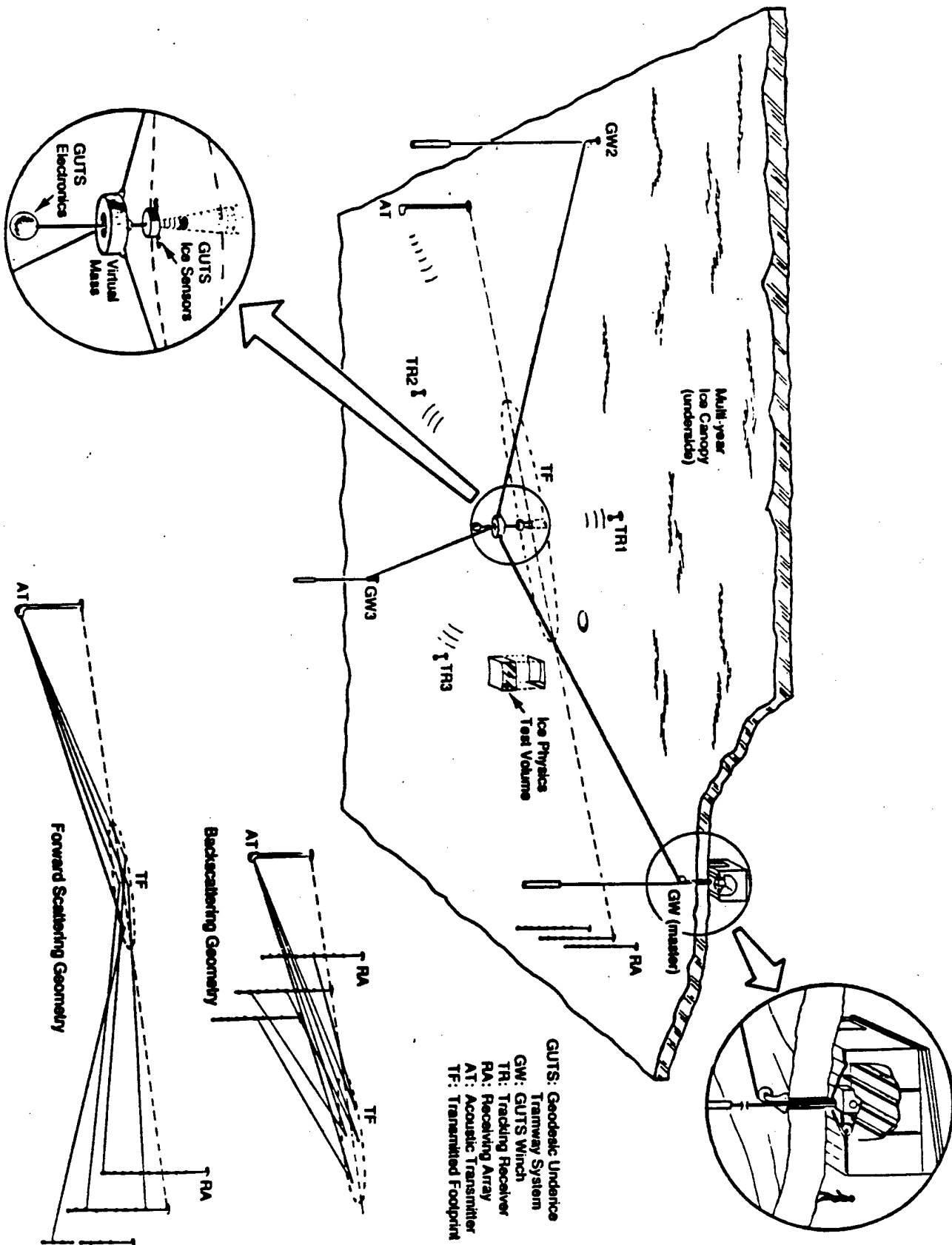
Figure 2. Deterministic ice scattering experiment (DISE).

Multi-year Ice Canopy (underside)

GUTS Electronics
Virtual Mass
GUTS Ice Sensors

GW2
AT
TR2
TF
TR1
GW3
TR3
Ice Physics Test Volume
GW (master)
RA

GUTS: Geodesic Underice Tramway System
GW: GUTS Winch
TR: Tracking Receiver
RA: Receiving Array
AT: Acoustic Transmitter
TF: Transmitted Footprint

AT
TF
RA
Backscattering Geometry

AT
TF
RA
Forward Scattering Geometry

20 METERS

20 METERS
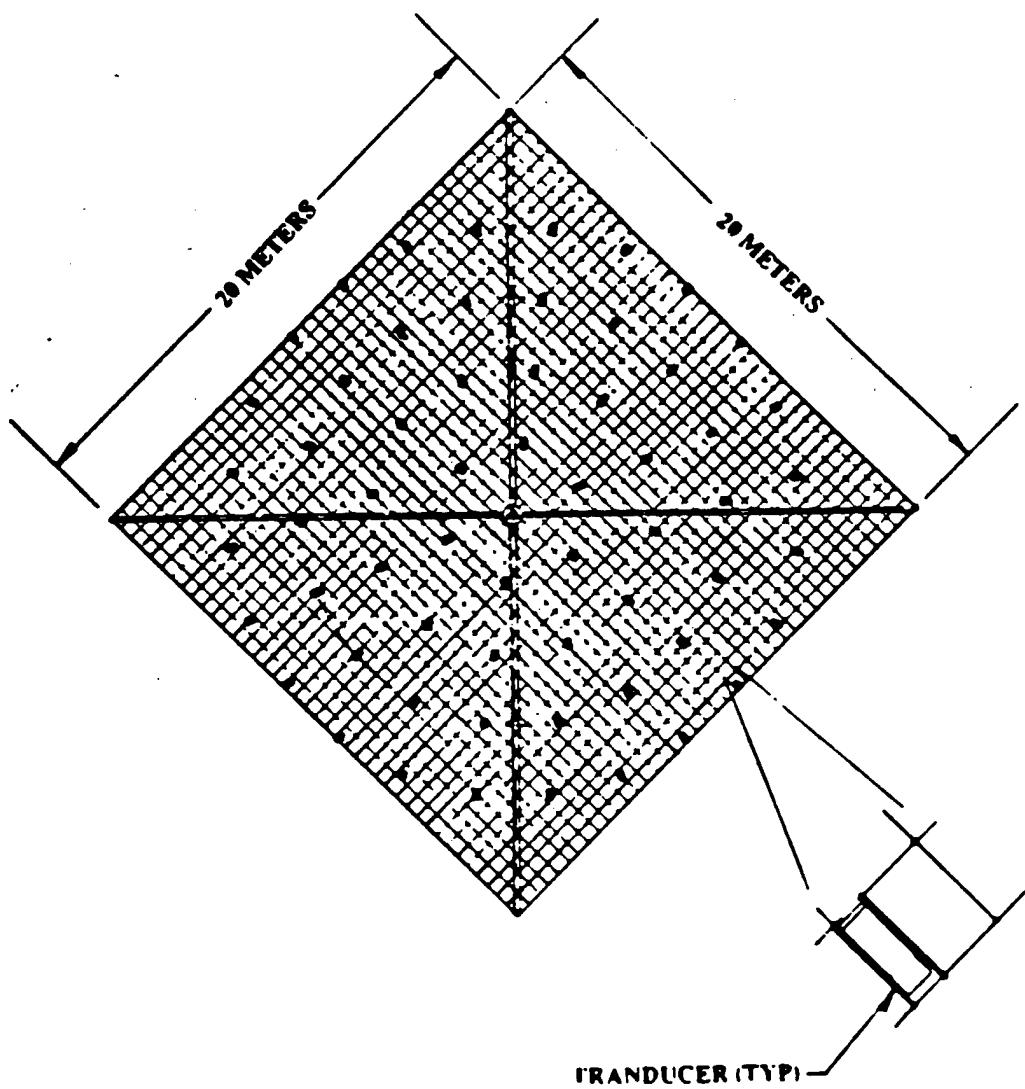
TRANDUCER (TYP)

Figure 2   Tranducer Support Net Showing Transducer Placement

Arctic VLF Propagation
Research Issues by Henrik Schmidt

Scientific Objective: Can elastic scattering effects explain excess acoustic transmission loss in the Arctic?

Background:

RAY TRACE
Arctic Ocean Propagation
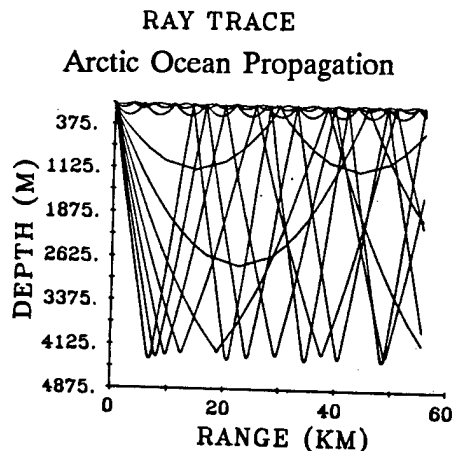
The Arctic Ocean is normally characterized as a bilinear sound velocity profile with the slowest sound speed at the surface and the change in sound speed gradient at the pycnocline. This propagation environment results in the creation of a half duct that has all sound rays upward refracting thereby interacting with the ice canopy. Data collected since the late 50's has shown attenuation/km in the VLF regime (10-100 Hz) to be much higher than open ocean values. The attenuation mechanisms that have been considered are bottom and water interaction, ice absorption, ice roughness, and sound coupling to the ice to form shear waves. Analyses done by Mellen, Nutall, Deavenport, and DiNapoli in 1985 indicate that rough surface scattering and ice absorption do not produce high enough levels to explain measured attenuation levels in the 10-100 Hz frequency ranges. Gruber compared Arctic measured data with Marsh-Mellon, Burke-Twersky, and Kuperman-Schmidt theories demonstrating that all gave different predictions none of which consistently agreed with measured data.
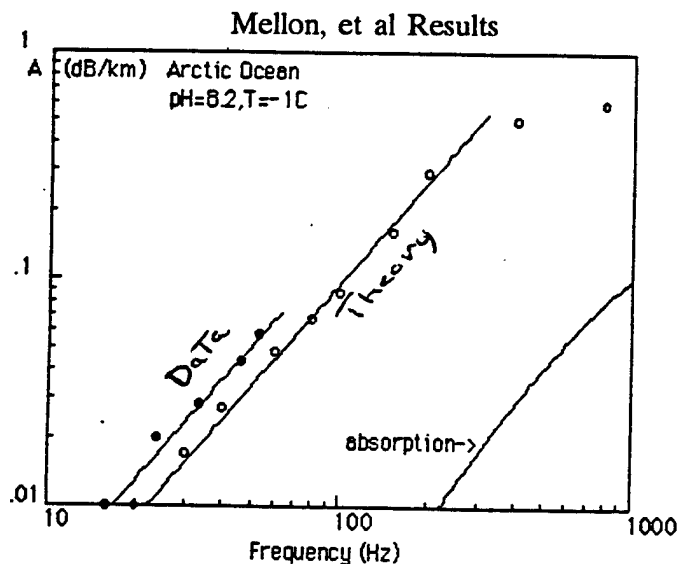
Figure 1: Arctic attenuation measurements.

Recent developments in theory using finite difference and perturbation approaches have shown that the inclusion of elastic properties and full wave acoustic propagation lead to additional scattering mechanisms.

Technical Approach: Conduct coordinated theoretical and experimental efforts.

Theory: Develop existing acoustic-elastic scattering theories to 2-d rough ice.

Deterministic:

* Finite Difference
* Integral Equation

Stochastic:

* Perturbation approaches
* Monte Carlo of finite difference and integral
  equation simulations

Predict forward and backscattered fields. Investigate effects of ice parameters: Cp, Cs, p, s, anisotropy, volume scattering, cracks, floe front/back edges, and keel scattering and mode conversion.

Experiment: Perform both a short and a long range experiment with extensive environmental support.

* Ice Parameters	Holographic tomography
	Direct measurements
	Matched field processing
* Ice Roughness	~500 Hz acoustic morphology
	ROV laser/acoustic morphology
	Satellite remote sensing

Short Range Scattering:

* Forward Scattering	Vertical arrays
* Backscattering	Horizontal arrays
	Geophone arrays

Long Range Propagation:

* Spectral composition	Vertical arrays
of coherent field	Horizontal arrays
* Scattered field	

Analysis: Deterministic modeling for short range and stochastic for long range experiments. The models would be initialized with the environmental data, the satellite remote sensing information, the ice physics and properties.

Noise Generation
Research Issues by James Lewis, SAIC

SCIENTIFIC OBJECTIVES

Develop an understanding of Arctic ambient noise events and episodes in terms of
environmental forcing functions, ice physical response, stress buildup and plastic deformation, ice
fracture, and plate vibration with noise radiation; i.e. wind/ice motion/stress buildup/ice
fracture/noise radiation, or temperature change/ice volume change/stress buildup/ice
fracture/noise radiation.

BACKGROUND

Development of relationships between environmental forcing and Arctic ambient noise
have been underway for the last ten years. Ira Dyer(MIT) has developed both a horizontal ice
sheet stress/noise and a tangential moment stress/noise model that produce high correlations
with ambient noise(JASA, May 1986) measured in the Central Arctic in April(70-84%). Jim
Lewis(SAIC) decomposed the ice dynamics as measured by field buoys(AIDJEX 75-76) into five
independent components i.e. translation, vorticity, divergence, normal deformation rate, and
shear deformation rate. These components were then correlated with the ambient noise pressure
to derive imperical relationships. Correlations of >70% were achieved with the most important
component being translation. Lewis then focused on noise episodes that had no correlation with
motion. He showed that a heat flux model with ice rheology and ice fracture radiation physics
could produce noise patterns similar to those that are not motion related. These efforts indicate
that a higher level of understanding is required if models are expected to produce high
correlation with field data. At the noise radiation end, it appears that the fundamentals of ice
fracture need to be better understood in order to determine if the sources are dipoles or higher
order, if the plate vibratory response upon stress release is the actual radiator, and if not, how
much radiation actually gets from the ice into the water column. On the other end of the
problem, it is necessary to know the distribution of events spatially and temporally versus forcing
functions. This means that one needs to know the ice dynamics(most important), the ice sheet
characteristics(strength, rheology, shape, snow coverage) and the atmospheric conditions that
control heat flux.

TECHNICAL APPROACH

The on-going ambient noise program(a portion of the Arctic Acoustics ARI) has
developed theories for both heat flux and motion induced stress to predict Arctic ambient noise
pressure levels under various environmental conditions. The recently completed CEAREX drift
ship project and the planned Acoustics camp Mar-Apr 89 ambient noise efforts will provide
new much more applicable data sets to unravel the relationships between ambient noise and
forcing functions. The plan for this RO would be to start by capitalizing upon the CEAREX
data. There are different sets of data that address heat flux and mesoscale ice dynamics. The
plan would be to test the thermal stress model with the ship drift data since ice temperature
profiles, long wave radiation conditions, omni-ambient noise, and ice stress measurements were
collected simultaneously. A number of buoys also provide some ice dynamics information. The

spring A-Camp data will provide synoptic meteorological and position information over a 200km area with omni-ambient noise information at the extremities and detailed ambient noise event(spatial monitoring with large vertical/horizontal array combination)at the center. Accelerometers at both extremities and the center will monitor floe bumping and plate vibration. This data is ideal for testing stress and ice dynamics models and for gaining new insights on event physics,i.e. crack formation and propagation. After the analysis of these data and the testing/improving of the current models, more controlled experiments should be planned and executed to resolve the ice event physics for both thermal and motion induced caused acoustic noise.

NAVAL NEED

The understanding of ambient noise is critical to obtaining maximum gain out of acoustic surveillance systems. The critical parameters are the amplitude, coherence, spatial distribution, and similarity to target signatures. Predictive models make it possible to develop better systems and to know what performance to expect both spatially and temporally.

Arctic ULF/VLF Noise Generation and Propagation
Research Issues by Adam Schultz

Scientific Objectives:

To delineate the physical processes responsible for the generation of acoustic ambient
noise in the frequency bands; ULF(.001-1 Hz) and VLF(1-50 Hz), and to understand the
propagation of such frequencies in all ocean environments.

Background:

In open oceans most ULF/VLF acoustic noise is attributed to ocean/wind stress coupling.
Other possible causes are shipping and seafloor elastic stress due to geologic processes.
Prominent features in the open ocean noise spectrum include a background red spectrum in the
VLF band with peaks centered at 8 seconds(double the wind/wave frequency) and an 18
dB/octave rolloff at higher frequencies. Microseisms are attributed to   nonlinear wave/wave
interactions. Below these, a low amplitude noise notch occurs. Due to the frequency band of
the noise and the few new sensors capable of making measurements, efforts to date have not
isolated the cause mechanisms of ULF noise below the microseism band. Two approaches are
viable. One is to reduce the number of mechanisms acting to produce the noise while the other
is to create a large enough array of sensors(noise and environmental parameters) to isolate the
relationships of cause and effect in both a spatial and temporal manner.

The temporal oceans seem to have microseism activity basin wide and there are internal
wave that average to a Garrett-Munk spectra over space and time. The Arctic Ocean area in
known to be different although not well defined. Insufficient measurements exist to quantify the
microseism level or distribution. Also, measurements of internal wave activity under the central
ice canopy indicate a level that is a factor of ten lower than the open ocean.

TECHNICAL APPROACH

Conduct a series of experiments that couple with those planned under the current ONR
1125G&G ARI on ULF. This new series would emphasize experiments in the Arctic Ocean that
start with the most beneign environment(total ice coverage), proceed to the marginal ice zone
and then to the Arctic open water. The scientific rational is simple. The ice prevents wind/ocean
direct coupling eliminating surface waves while simultaneously reducing internal ocean dynamics.
Initially, a simple triangular deployment of three ocean bottom ULF/VLF sensors deployed in
the central Beaufort Sea would determine if the noise spectra in the Arctic with its beneign
conditions has a radically different spectral amplitude. The proper way to conduct this
experiment is to have it embedded in a large scale meteorologic/ice dynamics experiment so that
the mesoscale forcing functions would be known. These measurements would be followed by
deployments in the marginal ice zone and then in Arctic areas that have the same open water
meteorlogic characteristics as the temporate oceans.Analysis of the Arctic data and comparison
with temporal open ocean data provides the most likely scientific approach for quantifying the
contributions to ULF/VLF produced by wave/wave interactions and internal waves.

NAVAL NEEDS

The knowledge of the ULF/VLF noise spectral amplitude in both a spatial and temporal sense in the Arctic is basic to using these frequency in ASW operations. Understanding of the relationships to environmental forcing is essential if a dynamic predictive model is planned for the future.

FUNDING

To be decided at ONR

MANAGEMENT

To be decided at ONR

Shallow Water Arctic Acoustics
Research Issues by George Frisk, WHOI

Scientific Objectives: To determine the dominant features of sound propagation in a shallow water(modal representation of sound field is suitable) Arctic environment and to relate them to oceanographic parameters.

Background: Both the forward and inverse problems are well understood for a Pekaris waveguide.

* Forward problem understood for a Pekeris waveguide with elastic plate instead of a pressure-release surface.

* Forward and inverse problems somewhat understood for Pekeris waveguide with inhomogeneous range independent and weakly range dependent bottom.

$$* S \underline{\rho_1, c_1}$$
$$\rho_2, c_2 > c_1$$

* Shallow water volume tomography somewhat understood

* Scattering from rough elastic boundaries somewhat understood.

* Scattering from ice edge somewhat understood

Technical Approach: Initiate the more realistic problem of shallow water Arctic acoustic s which encompasses all of the above problems. Sound propagation in range dependent rough elastic boundaries.

1. Extend and develop new forward and inverse methods to deal with more complex environments, especially modal based methods.

2. Select a natural laboratory(e.g. Barents Sea) where many investigators cantest their methods and where meanongful conclusions can be derived thriugh the   intercomparison of methods.

3. Make comprehensive measurements of ice, bottom, and physical oceanographic properties.

4. Conduct extensive narrowband and broadband acoustic measurements using real and synthetic horizontal and vertical arrays.

5. Determine the seasonal variability associated with above.

6. Capitalize on ROV technology for underice deployments.

Arctic Acoustics Science Plan
by Robert Obrochta, ONR

The logic followed in creating this science plan is that the issues that are most important to naval operations should determine which issues are addressed first and the emphasis(% of program) applied to each issue. In addition, the interdependence of the research issues which requires many to be addressed simultaneously will be discussed.

The most important Arctic acoustic research issue is to quantify acoustic coherence in the 10-400 Hz frequency range, determine the factors that degrade spatial and temporal limits, and understand the physical mechanisms and materials that control these factors such that a realistics physics model can be developed to predict propagation and scattering conditions and acoustic signal interactions with these conditions.

A considerable knowledge base exists relative to this issue. The important factors are the 3-D sound velocity structure and its fluctuations and the boundary conditions(roughness, acoustic impedence,elastic properties, heterogeniety, discontinuities, and structure). Past acoustic experiments indicate that the Central Arctic Ocean over the deep abyssal plains has a very stable sound velocity(relative to long wavelength sound, 10-100 Hz). Mixing appears to be controlled by the ice canopy motion. It stirs the upper water column with the deep keels and moves continuously limiting deep convection occurrences by saline brine expulsion as the salt water freezes in open leads. 2-D statistics of underside ice roughness are available from submarine data but very little knowledge exists on the 3-D shape of the ice/water interface or the effects this shape has on the acoustic signal interaction with the surface. The importance of cracks, keels, and ice floe edges has been investigated using ultrasonic modeling on plastic and glass plates, however, the occurrences of these features in the real Arctic environment and their effect on acoustic signal propagation, scattering, mode transformation, and attenuation, all of which effect coherence have not been quantified.

Both theoretical and experimental efforts are needed to understand acoustic coherence in the Arctic. Theoretically, the acoustic propagation models have to be made fully elastic with capabilities of computing 2-D rough surface interactions. Then advances in 3-D volume and surface treatment are needed. This will be pursued by improving both the finite difference and integral equation approaches. Simultaneously in a parallel development, methods for modeling acoustic signal interactions on a stochastic basis(perturbation approaches, Monte Carlo FD, IE, IFD, & PE) will be promoted. Theorists have to address the existance of cracks, keels and floe boundaries as discrete or stochastic scattering features.

Experimentally, the state of knowledge on coherence will be improved with the processing of the 1989 CEAREX A-Camp data. The data will have information from a horizontal array with a length greater than 20 km(previous limit was 2km) with recordings made continuously over long durations of time. To supplement the understanding of this data, a long vertical array at the center of the horizontal array will monitor the multipath structure and its temporal variations. Also, three thermistor strings located between the source(200 km away) and receiver will give a sparse indication of the sound velocity structure. A local(center of array area) picture of the reverberation from the underice surface will provide useful information on

the acoustic scattering that is occurring and affecting the receiving arrays. Synthetic Aperture Radar data will also provide additional knowledge that will indicate numbers of leads, keels, floe sizes, and possible ice thickness inferences. Processing of selective portions of this data is the highest priority in the Arctic Acoustics Research plan. It should demonstrate how temporal coherence on an individual element with no knowledge of conditions compares with temporal coherence that can be achieved with additional knowledge(multipath energy shifts due to sound velocity perturbation over the propagation path) which will be a product from the long vertical array. Spatial coherence can likewise be quantified with and without consideration of spatial knowledge of the sound velocity. Interaction with the ice canopy should be the next most important factor affecting acoustic coherence. Unfortunately, the CEAREX experiment lacks the level of knowledge desired for this research. Knowledge of the underice roughness, ice canopy structure, and acoustic properties are needed to understand local scattering effects that effect the receivers. The local reverberation data will provide an indication of where rough underice features are producing higher scattering effects but it can not be used in a quantitative way to provide roughness inputs to models or to resolve energy partitioning of signals propagated from the O-Camp because the geometric interactions will be different. The SAR data will help initialize stochastic models but it too is limited because the effects of the features it indicates are not known.

The experimental information available from CEAREX should be utilized to its limit to provide insight on future experimental and theoretical efforts. The accuracy to which one needs to know the 3-D sound velocity and its fluctuations and the ice canopy characteristics that effect acoustics may be important products of this research.

Future research on the issue of coherence should capitalize on CEAREX data for initializing future efforts. One of the main foci of effort should be on more detailed characterization of the ocean volume and elastic boundaries such that the effects of these properties on acoustic signal scattering/coupling/ attenuation/re-emission are understood and properly included in modeling efforts.

The Greenland Sea Tomography signals received on the MIT and NRL arrays offer a sparse data set that will show long range long term path stability. The arrival structure changes over both horizontal and vertical arrays provides the first information of this type to the research community.

The second priority science issue that affects the science plan is understanding Arctic acoustic ambient noise and being able to predict it from remotely sensed data(environmental measurements such as pressure, ice dynamics, concentration and deformation). Past efforts have considered ambient noise to be the result of ice breaking as stress levels exceed ice strength (Dyer,MIT), the acoustic output from ridging of weaker ice areas (Pritchard,IceCasting Inc), the result of ice canopy motion and deformation(Lewis,SAIC) and the result(1000 Hz) of heat flux created stress fractures(Lewis SAIC). Advances in this research area are critically linked to a better understanding of the individual noise creating events and their relationships to the forcing functions. Recent work at MIT(Dyer) and IOS(Farmer) using array processing has shown that ice cracks can be located and tracked during propagation. Dyer postulates that the low frequency noise spectral amplitude seen in the Arctic during spring can be attributed to the sum of individual events over space with the number of such events being directly proportional to the environmental forcing functions. CEAREX data again offers some insight to the validity of the various theories that have been postulated. The A-Camp data offers an ideal opportunity to

locate and track individual noise events with the large horizontal and vertical arrays. The monitoring of the forcing functions with remote buoys(ARAMPS) over a large footprint for a long time may be inadequate due to instrumentation malfunctions in the buoys. The tracking of Argos drifters should provide a reasonably good picture of the ice canopy motion, deformation and dynamics. This data must be examined for completeness and processed in situations where theory can be tested or better formulated from the information available. The SAR data and the acoustic propagation data will aid this analysis. The data collected on the drift ship phase of CEAREX offers a rather different set of conditions and information. This data set provides a limited amount of ice canopy stress level quantification and simultaneous omnidirectional single sensor noise level data. It is supplemented with ice temperature profile data and heat flux radiation data making it a good candidate for testing the heat flux model created by Lewis. Additional spatial information can be obtained by analyzing the data collected from NAVOCEANO'S ambient noise buoys that were deployed in a pattern near the drift ship. Due to the limited amount of environmental forcing data over a large spatial footprint in both the drift phase and A-Camp operational period, it is anticipated that the physics relationships between ambient noise levels and environmental forcing will remain ambiguous. Selected portions of data must be analyzed to determine the potential gain achievable in resolving noise cause/effect relationships.

Based on the above philosophy, the first year of the science plan should emphasize quantifying the usefulness of the CEAREX ambient noise data and supporting environmental data. If the environmental monitoring turns out to be insufficient to test the theoretic models, then the shortfall in instrumentation must be highlighted to initialize any future field effort.

The third priority in an Arctic Acoustic science plan is to improve our understanding of acoustic interaction with the Arctic Ocean boundaries; i.e. the ice and the ocean bottom. Since the ice is unique to the Arctic, this boundary is considered unique to Arctic acoustic research. It has already been stated above that ultrasonic modeling has demonstrated the need to quantify the existance and importance of ice discontinuities such as floe edges, keels, cracks, and physical property heterogeneities. In parallel with CEAREX data analyses, the planning and preparation for a major ice acoustic interaction thrust will begin. In order to address the acoustic interaction with the ice properly, it is necessary to find out how sensitive the acoustic coupling/ scattering is to sea ice characteristics including the physical shape, chemical composition and discontinuities such as cracks. This requires advances in both theory and experiment since past efforts have failed to include or quantify the effect of these factors.

Theoretically, two approaches should be pursued; stochastic and deterministic. Both have to be fully elastic allowing the existence of shear and surface waves with transformation at discontinuities. The stochastic approach is the easier to advance at this time since it can start with the theory developed for the ocean volume scattering. The deterministic approach may require finite element approaches until a sorting of factor importance allows the reduction of variables and less difficult approximations to produce more easily computed accurate solutions.

Experimentally, the effort is extremely difficult since the resolution required for parameter quantification is not well defined. First, a means of imaging the physical shape of the ice/water interface is needed. This should be done optically or with very high frequency acoustic signals to over resolve the surface shape. The next step is to interact controlled acoustic signals(using a broad band of frequencies) with this surface while measuring the physical and chemical properties of the ice. The measurements have to cover angles from normal to grazing

incidence and sensors have to gather both monostatic and bistatic information. Sensors are required within the ice and on both top and bottom surfaces to monitor the various wave properties, i.e. amplitude,velocity, attenuation, and modal conversion. This may sound like an impossible task but if the effort starts with the most simple conditions, sufficient understanding may be achieved to reduce the resolution requirements and address only those properties that have a large effect. The data collected has to be compared with the theoretic model predictions that are initialized with all the measured ice and ocean acoustic parameters.

The current plan is to propose a research option entitled "Ice Processes" that would contain: (1) Acoustic/Ice interaction, (2) Ice Mechanics/Ambient Noise, and (3) Remote Sensing, all of which mutually require overlapping field measurements to address the scientific issues. Ice Mechanics includes the environmental forcing of the ice canopy and its response, the strength of the ice as a function of ice properties, and the deformation and cracking of the ice with the associated acoustic energy emissions. A proper scientific approach to field measurements for these objectives requires a knowledge of the ice plate thickness, its physical properties and discontinuities, measurements of environmental forcing(meteorology and oceanography), ice cracking event location, stress measurements, heat flux monitoring, and ice cover density and dynamics. Remote sensing focuses primarily on the ice canopy electromagnetic emissions and responses to active signals. This research requires a detailed monitoring of the ice physical and chemical characteristics and an understanding of the rate of change of these properties with time and space. Also, the integration of these properties as resolution cell size changes should be addressed. It is easily seen that many research needs are common for the three portions of the proposed research option. What is even more interesting is that each portion also acts as supporting scientific input that aids the other. For instance, remote sensing (SAR) can provide precise ice canopy motion and distortion. Ice stress sensors can determine the strength of the ice when it breaks but acoustic hydrophone arrays are required to locate cracking events over large areas. Once located, new crack acoustic scattering cross sections can be measured to determine their significance. In general, the synergism of the research areas in the option strongly suggests that most of the field work required to do each portion would be nearly identical to that for all of them.

The research option will be proposed for a FY 92 start although work is already in progress preparing for it. Without the option funding, there is insufficient funds to mount a worthwhile comprehensive field experiment.

The fourth priority of the Arctic research plan is to address the acoustic bottom interaction in the shelf areas and the shallow seas. The physics involved with acoustic interaction with the water/seabed boundary should be addressed in the Special Research Program which excludes the Arctic area from its perview. If fully elastic theory that is capable of addressing extremely heterogeneous glacially altered surfaces is developed, then the focus of the effort required for the Arctic can be upon delineation of the ocean bottom acoustic parameters, i.e. types of sediments,layering, deformation from flat lying conditions. If not, then research on the acoustic interaction with the bottom environment that is unique to the Arctic is required. It is anticipated that some of the latter situations will occur due to the high probability of frozen gas hydrates, permafrost, and iceberg gouging(unusual geometrries).

The long range plan for this research area is to try to capitalize on the Norwegian long term efforts that have already taken place, that is, review their research results to determine if the bottom acoustic properties and geometric shape has been sufficiently defined to feed

192

theoretical elastic acoustic propagation models. Also, examine the oceanographic and ice dynamics models they are using that delineate the rate of change in the water volume and bottom surface acoustic parameters. If these prove adequate, then theoretic efforts can be initiated to quantify the variations and fluctuations in propagation loss and coherence that should occur in the shallow seas and shelf areas. It is anticipated that the state of knowledge available will not support research as advanced as proposed and that a field experiment that provides more specific site dependent data will be required. If this situation exists, then the proper approach is to perform a field experiment that capitalizes on the future Shelf Processes research option since this option would support measurements of the water column parameters and dynamics (including topographic roughness delineation) which are needed inputs for the acoustic research effort.

There are other important acoustic research topics that should be addressed in a timely manner but that are not as critically associated with other efforts. One such subject is ULF/VLF Arctic ambient noise. This research subject is unique because no data exists in the Central Arctic to delineate the noise levels. Also, the Arctic provides completely different noise causal conditions from other oceanic environments, that is, the ice canopy disallows water surface gravity waves and coastline surf(wave breaking) noises. It does, however, have an ice canopy that cracks with broadband emissions which haven't been examined in the ULF frequency range.

AGENDA

14 FEB 1989

0830 OBROCHTA   WELCOME!   Meeting Objectives

ACOUSTIC PROPAGATION, AMBIENT NOISE, CEAREX

0845 BAGGEROER - MIT, MF & LF Scientific/Naval Issues
                        PROPAGATION, CEAREX
                        Program and Accomplishments @ MIT

0930 DIACHOK/YANG - NRL, Program & Accomplishments

1000 CHAMUEL - SONOQUEST, Accomplishments

1030 BREAK

1045 EWART - APL/UW, Program & Accomplishments

1115 FLATTE - UC/SANTA CRUZ, Arctic Program and Accomplishments

1145 LYNCH - WHOI, Arctic Tomography Program & Accomplishments

1215 LUNCH

1315 DYER - MIT, Scientific/Naval Issues
                   AMBIENT NOISE, CEAREX
                   Program and Accomplishments @ MIT

1345 LEWIS - SAIC, Program and Accomplishments

1415 OBROCHTA - WORKSHOP
                   DEFINE CEAREX/TOMOGRAPHY DATA
                   PROCESSING/PROPAGATION, AMBIENT NOISE SCIENCE PLAN

1700 ADJOURN to LOCAL BAR

15 FEBRUARY 1989

ARCTIC ACOUSTIC/ICE INTERACTION

0830 JEZEK, STANTON - CRREL,WHOI, Ice Scattering & Absorption

0900 FRISK - WHOI, Ice Tomography Program

0930 BAGGEROER - MIT, Ice Acoustic Interactions

1000 PRADA - WHOI, Instrumentation Development for Arctic

1030 BREAK

1045 PINKEL - SIO, Scientific/Naval Issues
       Program and accomplishments at SIO

1115 CHOTIROS - ARL/UT, Imaging Ocean Dynamics Acoustically

1145 OBROCHTA - WORKSHOP
    DEFINE A THEORY, MODELLING SCIENCE PLAN

1230 LUNCH

1330 ARCTIC ACOUSTIC WORKSHOP

1500 PRIORITIZE RESEARCH TOPICS/EXPERIMENTS/INSTRUMENTATION
    DEFINE POTENTIAL RESEARCH OPTION

1700 ADJOURN

16 FEB 1989

0830 ARCTIC ACOUSTIC WORKSHOP
  Draft proposed five year research plan and research option

1230 FINISHED

LIST OF ATTENDEES

NAME	AFFILIATION	TEL. NO.
Baggeroer, Art	MIT	617-253-4336
Bordley, Thomas	NRL	202-767-2196
Chamuel, Jacques	Sonoquest, MA	617-239-0554
Chotiros, Nick	ARL:UTX	512-835-3512
Coon, Max	BDM, WA	206-246-2100
Curtin, Thomas	ONR	202-696-4118
Denner, Warren	SAIC	408-649-5242
DeSanto, John	CO Sch. of Mines	303-273-3036
Diachok, Orest	NRL	202-767-3359
Dyer, Ira	MIT	617-253-6824
Ewart, Terry	U of WA/APL	206-543-1327
Fricke, J. Robert	MIT	
Frisk, George	WHOI	508-548-1400
Hug, Ed	NUSC/NL	203-440-6698
Jacobsen, Randy	ONR	202-696-4121
Jezek, Ken	CRREL	603-646-4596
Keenan, Ruth	SAIC	508-477-8450
Lewis, James	SAIC	409-846-7756
Lynch, Jim	WHOI	508-548-1400
Obrochta, Bob	ONR	202-696-4118
Rajan, S.	WHOI	508-548-1400
Schmidt, Henrik	MIT	617-253-5727
Schultz, Adam	U of WA	206-543-6043
Stanton, Tim	WHOI	508-548-1400
Stickler, David	NJIT	201-596-3499
Yang, T. C.	NRL	202-767-2579
Zhou, J. X.	Georgia Tech	404-894-6793